XX(101580.1)

CINVESTAV
Centro de Investigación y de Estudios Avanzados del IPN
Unidad Guadalajara de Ingeniería Avanzada

CINVESTAV
I P N
ADQUISICION
DE LIBROS

Control Discreto De Modos Deslizantes De Un Motor De Inducción

TESIS QUE PRESENTA

JORGE RIVERA DOMINGUEZ

PARA OBTENER EL GRADO DE
MAESTRO EN CIENCIAS

EN LA ESPECIALIDAD DE
INGENIERÍA ELÉCTRICA

Guadalajara, Jalisco, Diciembre de 2001.

CINVESTAV I.P.N.
SECCION DE INFORMACION
Y DOCUMENTACION

CLASIF.:
ADQUIS.: TESIS-2002
FECHA: 6-agosto-02
PROCED: Ser B. dl

CINVESTAV
Centro de Investigación y de Estudios Avanzados del IPN
Unidad Guadalajara de Ingeniería Avanzada

Discrete-time sliding mode control of an induction motor

Thesis presented by

JORGE RIVERA DOMINGUEZ

To obtain the degree of

MAESTRO EN CIENCIAS

In the speciality of

INGENIERÍA ELÉCTRICA

Guadalajara, Jalisco. December 2001.

Control Discreto De Modos Deslizantes De Un Motor De Inducción

Tesis de Maestría en Ciencias
Ingeniería Eléctrica

Por:

Jorge Rivera Dominguez

Ingeniero en Electrónica opción en Sistemas Digitales
Instituto Tecnológico del Mar en Mazatlán
1994-1999

Becario del CONACYT, expediente No.**143914**

Directores de Tesis

Dr. Alexander Loukianov
Dr. José Manuel Cañedo Castañeda

CINVESTAV del IPN Unidad Guadalajara, Noviembre de 2001.

Discrete-time sliding mode control of an induction motor

Master of Science Thesis
Electrical Engineering

By:

Jorge Rivera Dominguez

Ingeniero en Electrónica opción en Sistemas Digitales
Instituto Tecnológico del Mar en Mazatlán
1994-1999

Scholarship granted by CONACYT, expedient No.**143914**

Thesis advisors:

Dr. Alexander Loukianov
Dr. José Manuel Cañedo Castañeda

CINVESTAV del IPN Unidad Guadalajara. December 2001

Dedico este trabajo de tesis a mi familia:

Nadia Yasmin Flores Ortiz

Karla Georgina Rivera Dominguez

Ma. Longina Flores Mancillas

Ma. Elenena Rivera Flores

Prof. Jorge Rivera Flores

A ellos les agradezco todo el apoyo incondicional que me brindaron en todo momento.

Agradezco al CONACYT por la gran labor que realizan con todos nosotros, que deseamos superarnos cada día más.

Agradezco de misma forma a mis asesores: Dr. Alexander G. Loukianov y Dr. José Manuel Cañedo Castañeda por su asesoramiento incondicional.

Igualmente hago mención de mi agradecimiento a mis sinodales por dedicarle tiempo de revisión a mi trabajo.

Resumen

Se diseña un control de modos deslizantes en tiempo discreto para sistemas discretos no lineales, también se desarrolló la técnica del control por bloques para sistemas discretos no lineales, y un observador de orden reducido fue desarrollado para sistemas discretos electromecánicos no lineales. Todas estas técnicas son aplicadas al modelo discreto no lineal de un motor de inducción que se encontró aquí, que posee dinámicas eléctricas y mecánicas, en donde el par de carga se considera una perturbación desconocida. Con mediciones completas de los estados, se satisfacen objetivos de seguimiento de la velocidad del rotor y de la amplitud del flujo magnético del rotor, en donde la carga desconocida no afecta la regulación de la velocidad. Luego, es implementado un observador de orden reducido en donde las mediciones de velocidad y de corriente se emplean para estimar el par de carga y los flujos que son muy difíciles de medir. El método propuesto tiene un diseño y procedimiento de estabilidad de análisis directos, conservando una estructura simple de la ley de control. Las simulaciones predicen que el sistema es robusto con respecto a varios tipos de pares de carga. Las respuestas de velocidad y de amplitud del flujo del rotor a las referencias de entrada se desempeñaron muy bien. Estas referencias tienen una dinámica lineal de segundo orden con constantes de tiempo que pueden ser elegidas por el usuario del motor. Se consideran los aspectos prácticos para una futura implementación digital de la ley de control, incluyendo los sensores de velocidad y corrientes, el acondicionamiento de señales, la transformación de la corriente al marco de referencia estacionario, PWM y módulos inversores, los cuales fueron vistos con detalle. Los resultados experimentales se dejan como trabajo futuro.

Summary

A discrete-time sliding mode control was developed for discrete-time nonlinear systems, also, a block control technique was developed for discrete-time nonlinear systems and a reduced order observer was developed for discrete-time nonlinear electromechanical systems . All of these techniques were applied to a nonlinear discrete-time induction motor model developed here, with both electrical and mechanical dynamics, where the load torque is considered as unknown parameter. With full state measurements, both rotor speed and rotor flux amplitude tracking objectives are satisfied, where the unknown load does not affect the speed regulation. Then, a reduced order observer is implemented where speed measurements help to estimate the load torque and current measurements provide the estimation for the unreachable fluxes. The proposed approach has a straightforward design and stability analysis procedure, keeping the control law structure simple. The simulations predict the system to be robust with respect to several external load torques. Responses to speed and rotor magnetic flux amplitude reference input which have a second order linear dynamics with time constants that may be chosen by the user of the electric drive performed well. Practical aspects for a future digital implementation of the control law are considered, topics like current and speed sensors, signal conditioning, current transformation to the fixed reference frame, PWM, inverter modules are viewed in detail. Experimental results are left for future work.

Contents

1 Introduction 5

2 Induction motor modelling 9

2.1 *Introduction* 9

2.2 *Representation of an induction motor* 9

2.2.1 Introduction 9

2.2.2 Energy relationships 10

2.2.3 Induction motor construction 11

2.2.4 Voltage equations 17

2.2.5 Transformation to a rotating frame 24

2.2.6 Stator and rotor equations transformed into an arbitrary reference frame 27

2.2.7 Torque equation 30

2.2.8 Stationary reference frame model ($\alpha - \beta$ model) 33

2.3 *Discretization of the continuos-time induction motor model* 38

3 Theoretical tools 47

3.1 *Introduction* 47

3.2 *Exosystems* 47

3.3 *Discrete-time sliding mode* 51

3.4 *Block control technique* 64

3.4.1 Block control form 65

3.4.2 Linearization transformation 66

3.4.3 Control design 70

3.4.3.1 Sliding mode control design 71
3.5 *Nonlinear observers* 74

4 Application 77
4.1 *Introduction* 77
4.2 *Discrete-time sliding mode with block control* 80
4.2.1 Master control law 80
4.2.2 Slave control law 85
4.2.3 Sliding mode control 88
4.2.3.1 Sliding mode control as a continuous function of states 88
4.2.3.2 Sliding mode control as a discontinuous function of states 90
4.3 *Reduced order observer* 91

5 Results 97
5.1 *Introduction* 97
5.2 *Control law simulations* 97
5.2.1 Continuos sliding mode simulations 98
5.2.2 Discontinuous sliding mode simulations 105
5.3 *Observer simulations* 107

6 Practical aspects for a real time future implementation 109
6.1 *Introduction* 109
6.2 *Sensors* 110
6.2.1 Speed sensor 110

6.2.2 Current sensor 111
6.3 *Signal conditioning* 112
6.4 *Current transformation* 114
6.5 *Pulse Width Modulation* 115
6.6 *Inverter* 117

7 Conclusions and future work 123
7.1 *Conclusions* 123
7.2 *Future work* 125

References 127

Chapter one

Introduction

Induction motor is one of the most widely used actuator for industrial applications because of its reliability, ruggedness and relatively low cost. The control of induction motor systems is challenging, since the dynamical system is multivariable, coupled, and highly nonlinear. A classical technique for induction motor control is field-oriented control [14]; which involves nonlinear state transformation and feedback for asymptotic decoupling of the rotor speed and rotor flux, combining linear control methods such as PID control. More recently, various nonlinear control design approaches have been applied to the induction motor control problem to improve its performance, like adaptive control [7]-[5], that is used for parameter uncertainties in the system. Among many works in this increasingly active research area we may cite input-output linearization [7], backstepping [13], passivity [11], adaptive input-output linearization [7], and sliding modes [5]-[16]-[17]. All of these approaches are mostly based on the continuous-time model of the plant, and for practical implementation in a digital device, is necessary to discretize the continuous controller.

The most recent works on the control of induction motor with sliding modes are found in [5] and [17]. This works are based on continuous-time sliding mode control. The algorithms are programmed on a digital processor for implementation where the differential equations are numerically integrated by Euler's explicit method in order of minimizing the computational burden as stated in [17]. This has the disadvantage of not exactly implement the desired continuos-time control law.

The major difference between continuos-time sliding mode control and the other control techniques mentioned above for the induction motor, is that sliding modes results in a discontinuous control law that is applied directly to the driver (inverter) of the motor, and in the other techniques, the control law results in continuos control law, that is applied to the driver of the motor through a PWM. Adding a PWM requires more external electronic circuits or software, where the real control law is modified.

This work is based on a digital sliding mode [16] with a block control aided design approach to achieve rotor speed and rotor flux amplitude tracking objectives in the fixed

reference frame model. The uncertainty accounted for is an unknown load torque. A novel block control scheme is intended for discrete-time systems combined with a novel digital sliding mode controller implementation. The reason for using a digital or discrete-time sliding mode control technique is to avoid the use of PWM and the easy of implementation on a digital device of the difference equations that appear in the control law, avoiding numerical integration.

The highlights of this work can be stated as follows. It is developed a discrete-time sliding mode and block control technique for nonlinear systems. A nonlinear observer for electric machinery was also developed for discrete-time systems. All of these contributions are applied to the induction motor.

This work consists of seven chapters. *Chapter one* was a short review of the common induction motor control techniques available today. It was also established the control approach that will be developed to accomplish the rotor speed and rotor flux amplitude tracking objectives by means of digital techniques for a readily implementation. *Chapter two* deals with the induction motor system model differential equations that are transformed to the fixed reference frame in order to eliminate the time dependency that appear in the original equations [9]. Then, the continuous-time equations are discretized in order to obtain a discrete-time version of the plant. This model will serve to obtain the discrete-time controller in a subsequent chapter. *Chapter three* discusses basic control theoretical tools such as exosystems; these systems provide the reference signals to be tracked by the plant. The principles of sliding mode control techniques [15] are shown for continuos-time systems, where the control design consist of two steps: step one is to choose a sliding surface where all the state trajectories are heading to; and step two is to apply the well known sliding mode control. These principles are then developed for discrete-time systems, obtaining a discrete-time sliding mode control. Then, the block control technique is developed for discrete-time nonlinear systems, this technique consists of a step-by-step coordinate transformation where the desired dynamics of the transformed system is proposed in each step, and the last step results in the control law. This technique will be useful in obtaining a sliding mode surface. Due to the non-observable fluxes, we need the basics for discrete-time observers, and here are developed for nonlinear electromechanical discrete-time systems. *Chapter four* contains the contributions of this research work,

dealing with the application of the theoretical tools developed in chapter three to the discrete-time model obtained in chapter two. With the help of the block control technique, continuos and discontinuous discrete-time sliding mode controls are developed, and their differences are analyzed. Then, discrete-time observers are implemented for load and fluxes estimation. *Chapter five* shows us the simulations for both controls and for different references and load signals. Also, observer simulations are shown. *Chapter six* can be considered as a background for a future implementation, taking into consideration all the practical aspects to implement the control law in a digital device. Speed and current sensors are featured as source devices. They measure the variables needed to obtain our control objectives. But this signals needs special treatment in order to be manipulated by a digital device, all this is seen in the sub-chapter 6.3 titled 'Signal conditioning' Since the measured currents are not referred to fixed reference frame, these currents need to be transformed to that frame. The Pulse Width Modulation process is introduced for a continuos control implementation. Finally we introduce the inverter. This device is the responsible for driving the motor, and is fed by a set of pulses coming out of the PWM or directly of the discontinuous control law. *Chapter seven* extracts all the theoretical results from the previous chapters, and proposes future research for this work.

Chapter two

Induction motor modelling

2.1 INTRODUCTION

This chapter deals with typical construction and basic concepts of the induction motor [3]. Voltage and torque equations are established in a *state-space* realization, which represent the induction motor in operation [9]. Due to the inductance angular dependency, the induction motor is a time-variant system, therefore a change of variables is needed in order to avoid this dependency. This transformation is computed with respect to spinning reference frames of the machine, that could go from non-spinning (stationary reference frame) to arbitrary spinning (arbitrary reference frame). The induction motor model is discretized, and in a subsequent chapter a discrete-time control-law is developed for a fast and easy computer based system implementation.

2.2 REPRESENTATION OF AN INDUCTION MOTOR

2.2.1 Introduction

This section begins with the basic concepts about energy conversion for electromechanical systems, then, basic induction motor construction methods and concepts are shown. We deal with reference frame for transforming equations, which can eliminate parameter time dependency. These concepts are applied in order to find the induction motor mathematical model in the stationary reference frame. Moreover, the induction motor model shows us that the transformation process yields a two-phase model, where the control law is designed (once discretized), and then with a backward transformation we transform the two-phase control law into a three-phase one, which is applied to the induction machine.

2.2.2 Energy relationships

An electromechanical system is made up an electric system, a mechanical system and a coupling one in which both of them interact. Electromagnetic fields and/or electrostatic ones can give the interaction. These fields are reciprocal in each system, being the transferring energy from one system to another the result of such interactions. Both coupling fields can co-exist, and the entire system can count with any number of electrical and mechanical systems. Figure 2.1 shows an electromechanical system, i.e. an electric system, a mechanical system and a coupling one.

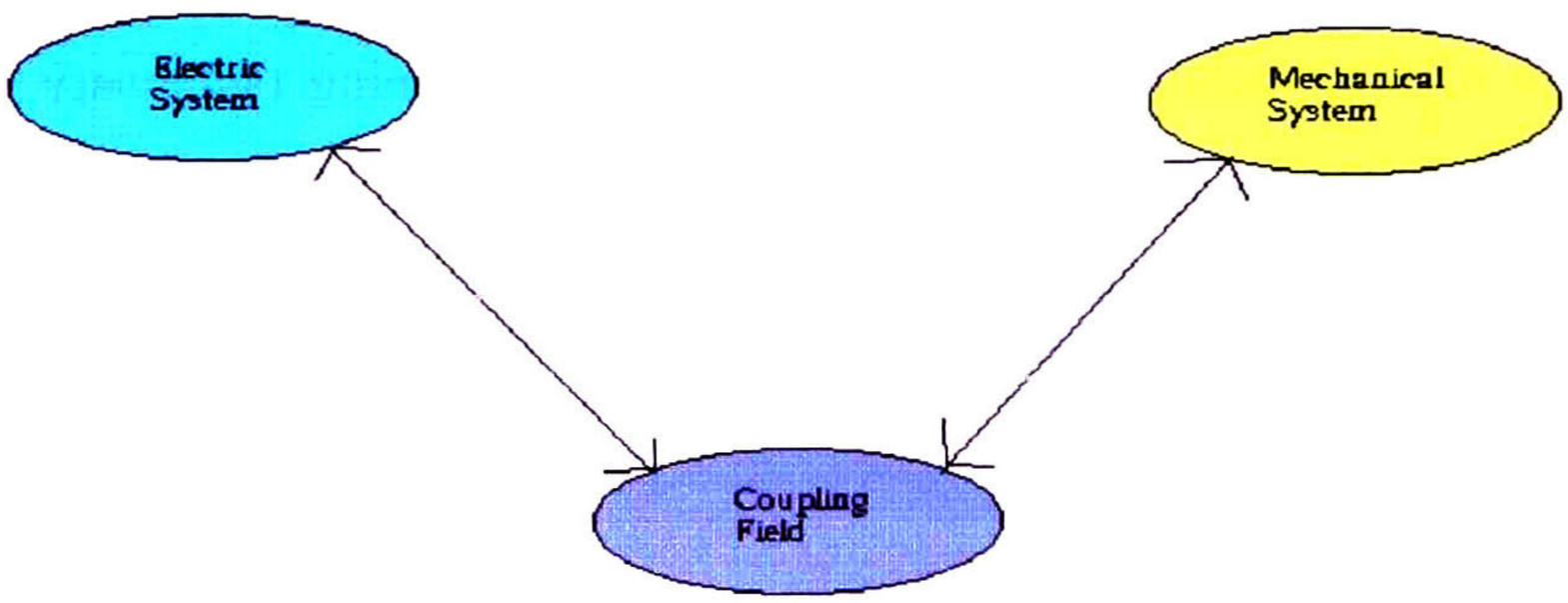

Figure 2.1. Electromechanical system

Defining W_E as the total of energy given by an electric source, W_M the total of energy given by a mechanical source, then an energy distribution can be expressed as

$$\begin{aligned} W_E &= W_e + W_{eL} + W_{eS} \\ W_M &= W_m + W_{mL} + W_{mS} \end{aligned} \qquad (2.2.2.1)$$

where W_{eS} is the stored energy in electric or magnetic field form, which is not coupled to the mechanical system. W_{eL} is the heat related lost energy in the electrical system. W_e is the transfer energy to the coupling field from the electrical system. W_{mS} is the store energy

by the mechanical impetus, W_{mL} is the heat related lost energy related in the mechanical system and W_m is the transferred energy to the coupling field. The supplied energy is assumed positive in any source.

If we set W_F as the total energy transferred to the coupling field, then

$$W_F = W_f + W_{fL} \tag{2.2.2.2}$$

where W_f is the stored energy in the coupling field and W_{fL} is the lost energy in heat form inside the coupling field. The electromechanical system obeys the energy conservative law, so, the total store energy is

$$\begin{aligned} W_f + W_{fL} &= W_e + W_M \\ W_f + W_{fL} &= (W_E - W_{eL} - W_{eS}) + (W_M - W_{mL} - W_{mS}) \end{aligned} \tag{2.2.2.3}$$

If the lost energy inside the coupling field is not considered, then the equation (2.2.2.3) reduces to

$$W_f = W_e + W_M \tag{2.2.2.4}$$

In the process of energy conversion we conclude that the conversion from one system to another is independent of the lost energy of each system, the stored energy in both systems and the lost energy inside the coupling field.

2.2.3 Induction motor construction

As a general overview, induction machines have their field current supplied by magnetic induction in its excitation windings; their armature windings are placed in the stator and their excitation windings in the rotor. A three-phase current systems in the armature windings produce a spinning magnetic field, which interacts with the rotor magnetic field producing a torque in the shaft of the machine.

We begin with the stator construction that is quite complicated [3]. The stator has several coils in each phase, which are inside the gaps located in the interior surface. It is very common that each coil is an independent unit, with several spirals insulated one from each other and the entire set insulated from the stator. The voltage delivered by one spiral is too small and to get a considerable voltage, then, several spirals are needed. This extensive number of spirals is divided in several coils that are equally space-placed along the stator surface gaps.

With the exception of very small machines, the stator coils usually are distributed shaping *double layer windings* as illustrated in Figure 2.2.

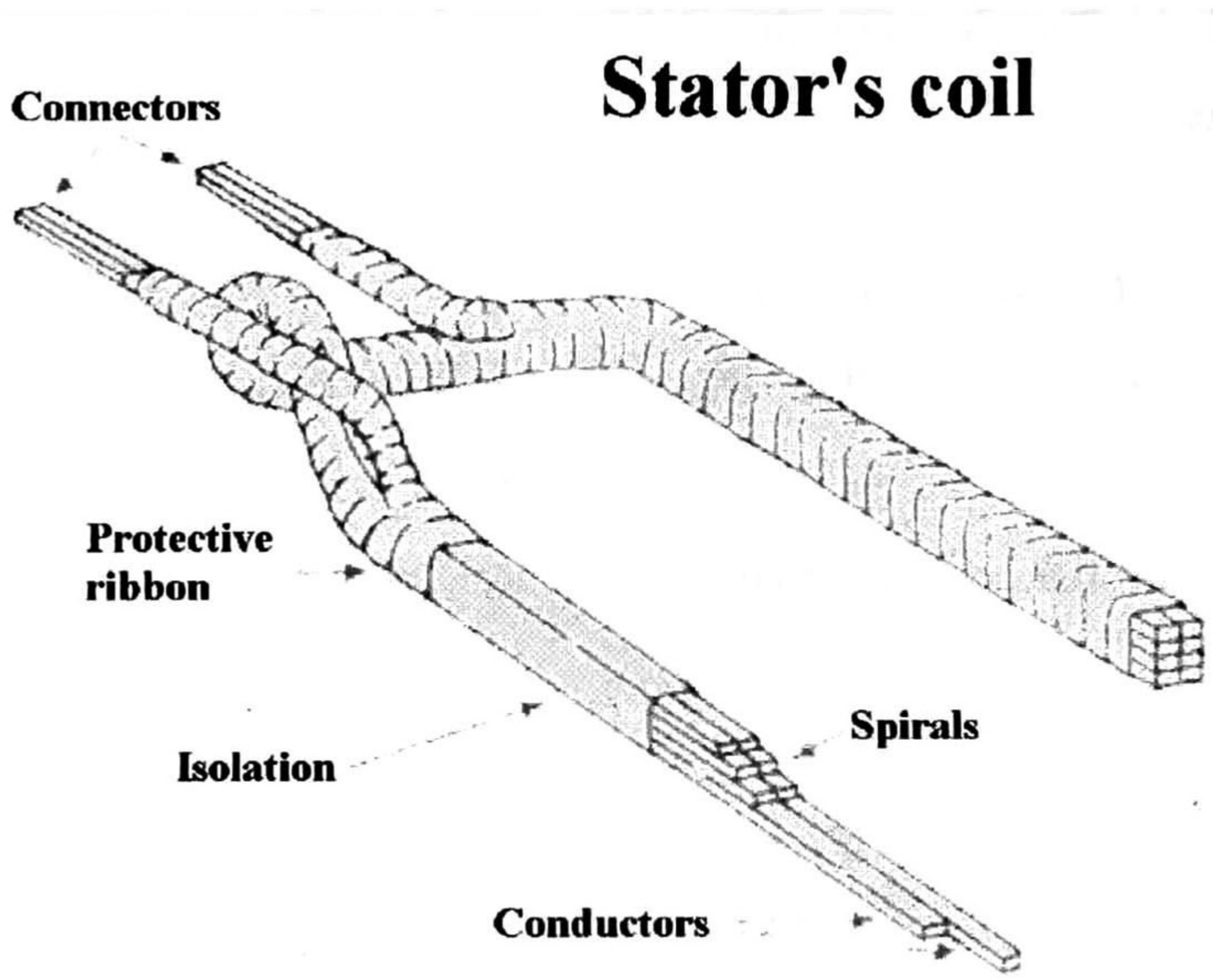

Figure 2.2. Typical coil of a stator induction motor.

The double layer windings are easier to construct (less gaps are needed for a given number of coils) and their connections between their coil terminals are quite easy rather than one layer winding. Therefore, its manufacture is less expensive. Figure 2.3 shows two pictures of stator coils, and Figure 2.4 shows a stator of a two-pole machine.

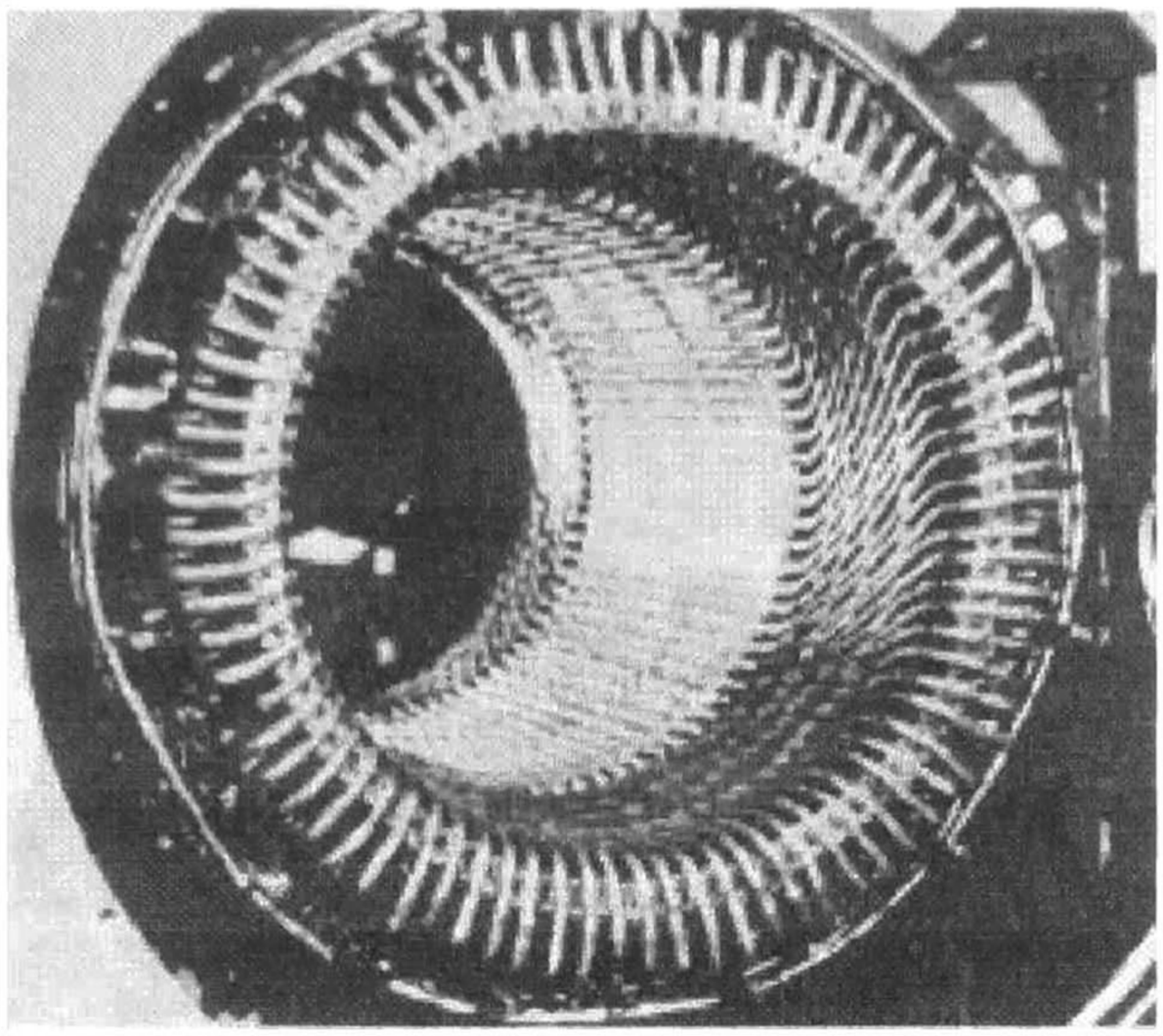

(a)

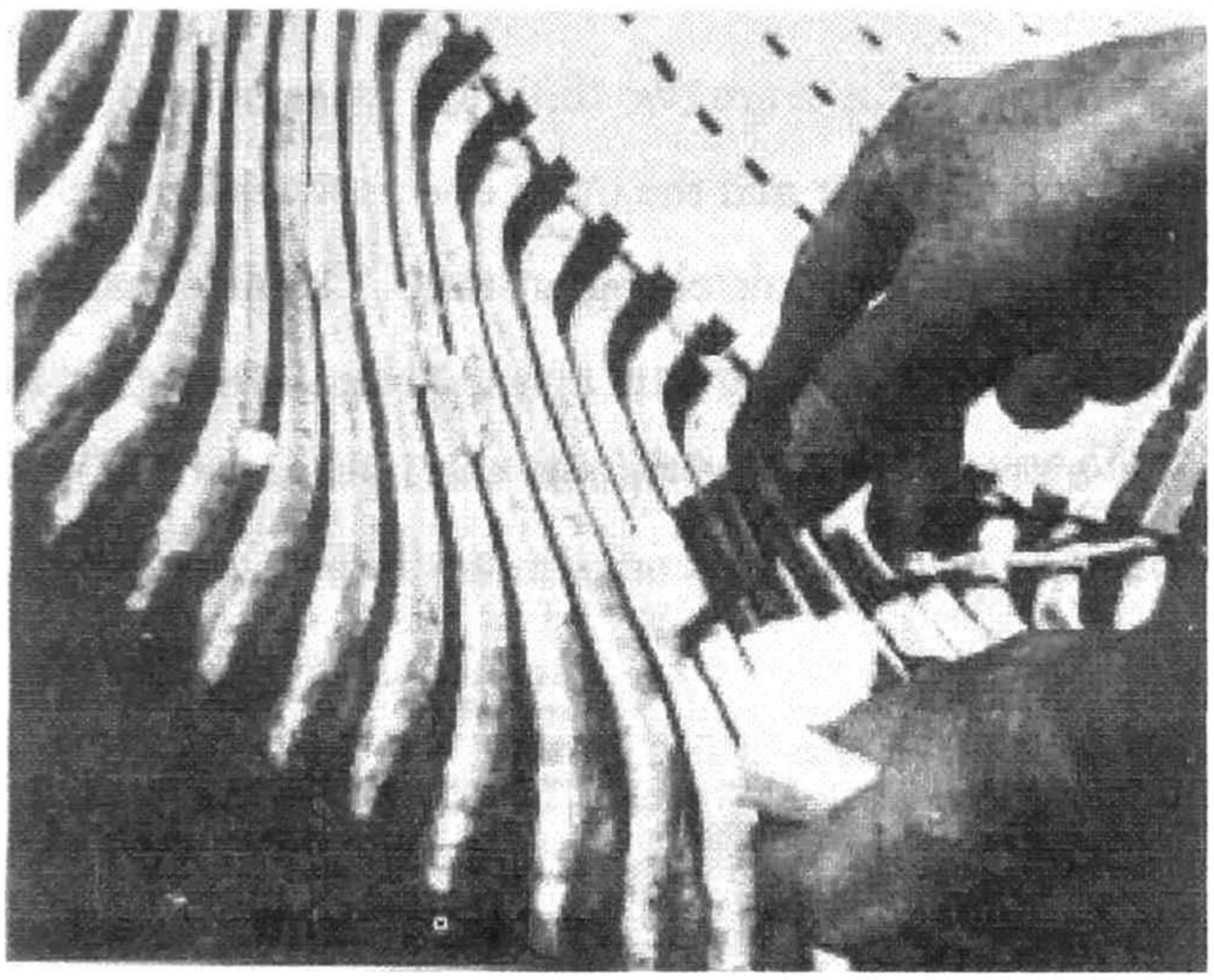

(b)

Figure 2.3. (a) The stator with its pre-shaped coils view. (b) Detailed view of the terminals of the stator coils. Note that one coil side is in a less deep part of a gap and the other side in the deepest part. This arrangement lets the making of the coils in a uniform way to be placed then in the stator gaps.

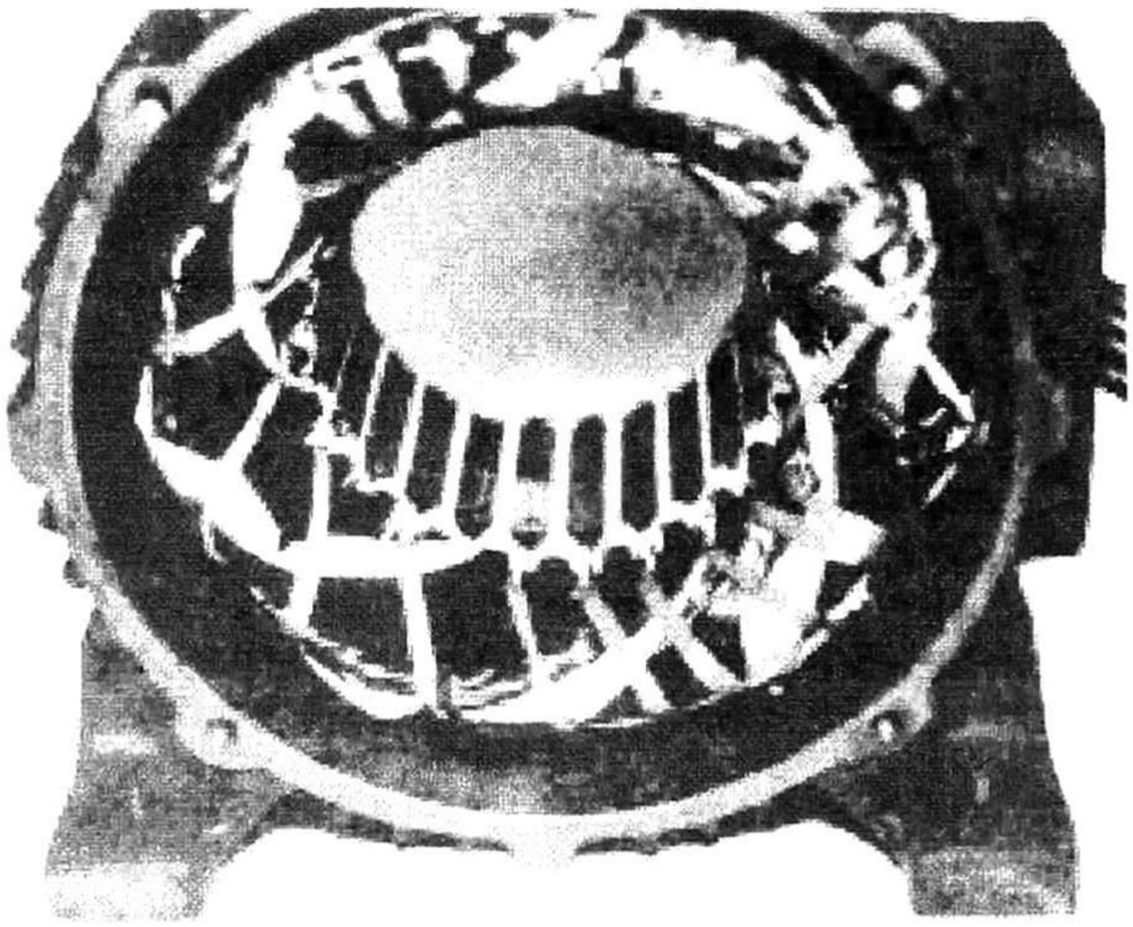

Figure 2.4. Common stator of an induction motor with its windings.

Now let's see the rotor; there are two different types of rotor for an induction motor, one is known as *squirrel cage rotor* and the other one as *wound rotor*.

Figures 2.5 and 2.6 shows squirrel cage rotors. A squirrel cage rotor of an induction motor consists of a series of conducting bars arranged inside the gaps located at the surface of the rotor with its extremes in short-circuit through *rings*. This design is known as squirrel cage rotor because its conductors are similar to the cages where squirrels play.

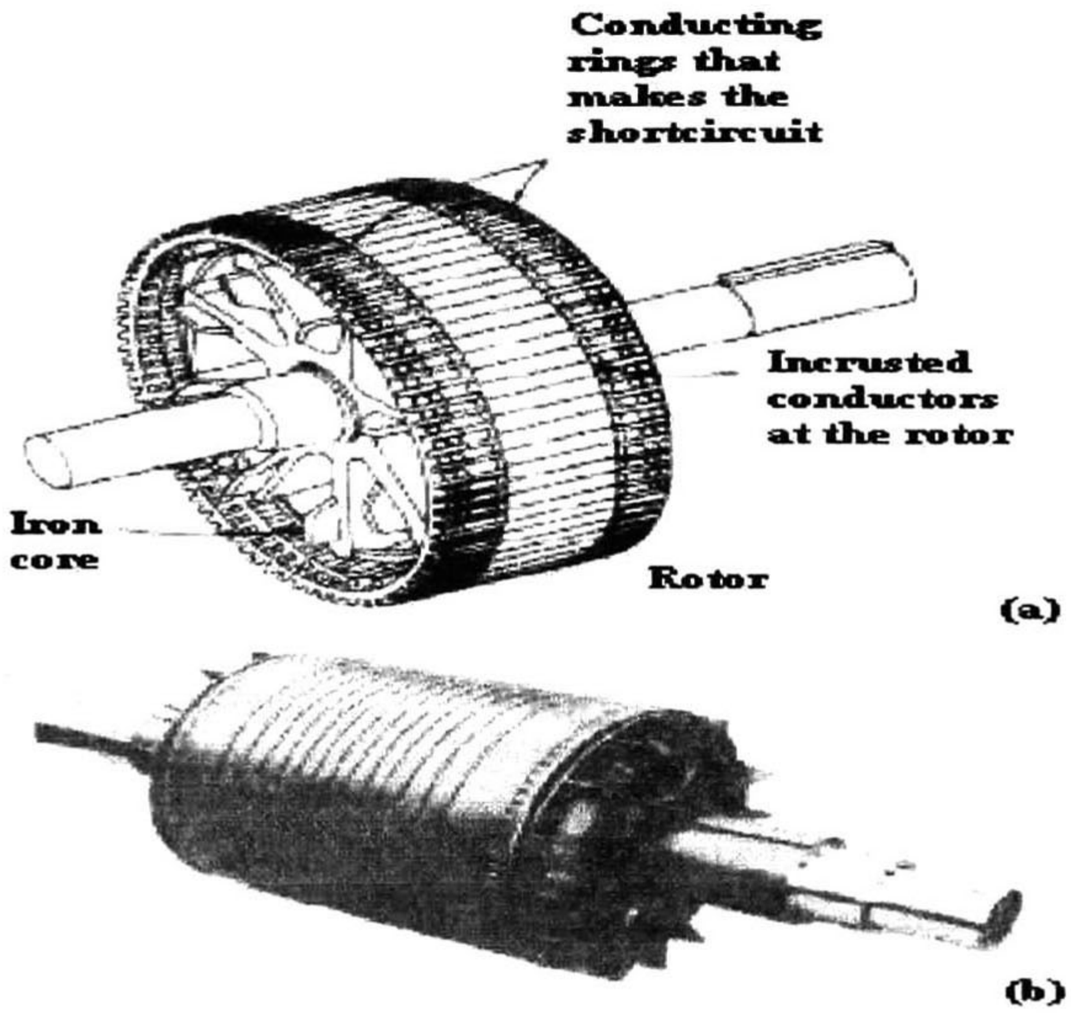

Figure 2.5. (a) Squirrel cage rotor. (b) Typical squirrel cage rotor.

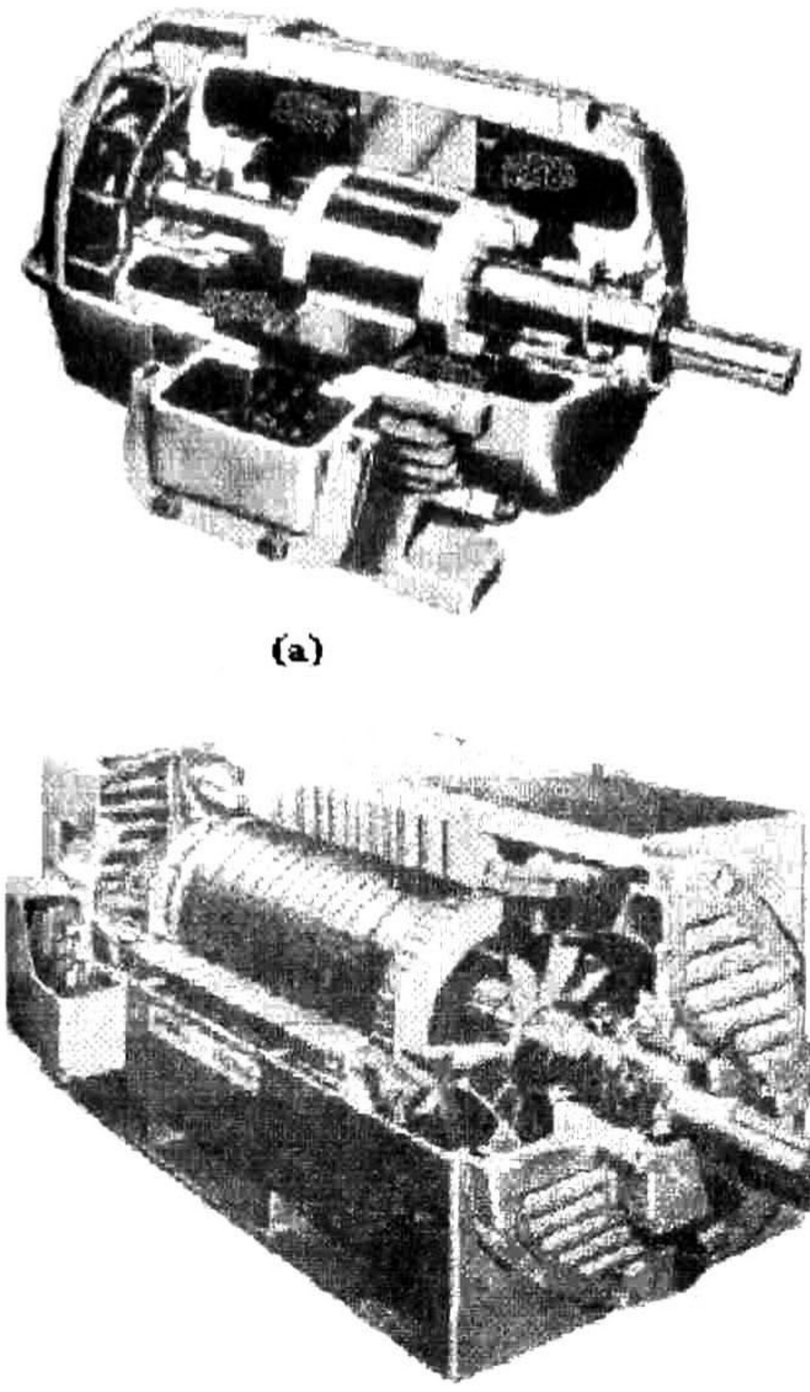

(a)

(b)

Figure 2.6. (a) An inside view of a typical small squirrel cage rotor of an induction motor. (b) An inside view of a typical large squirrel cage rotor of an induction motor.

The other kind of rotor is the wound rotor, and it has a complete three-phase winding that is a kind of mirror image reflection of the stator winding. The three winding phases of this rotor are usually connected in **Y**, and their extremes are connected to some slightly touching rings mounted in the shaft. The rotor windings can be short-circuited through a set of brushes that slightly touch the rings. External resistances can be inserted in the rotor circuit, due to the fact that the rotor currents are available in wound rotor induction motors through brushes. This fact enables us to modify the motor torque-velocity characteristics. Figure 2.7 shows a wound rotor, and Figure 2.8 shows a complete wound rotor induction motor.

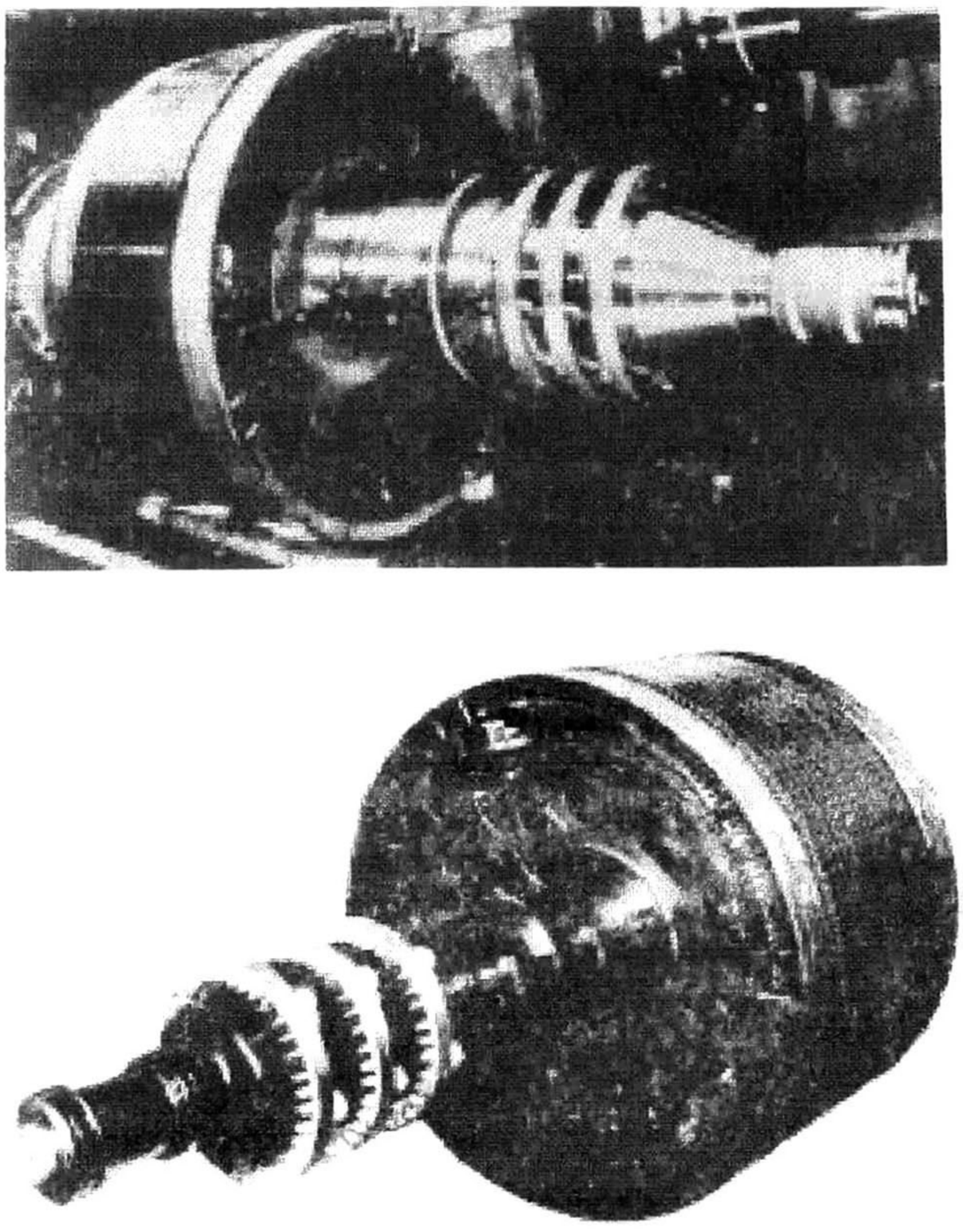

Figure 2.7. A typical wound rotor for induction motor. Slightly touching rings and bars that connect the rotor with such rings can be appreciated.

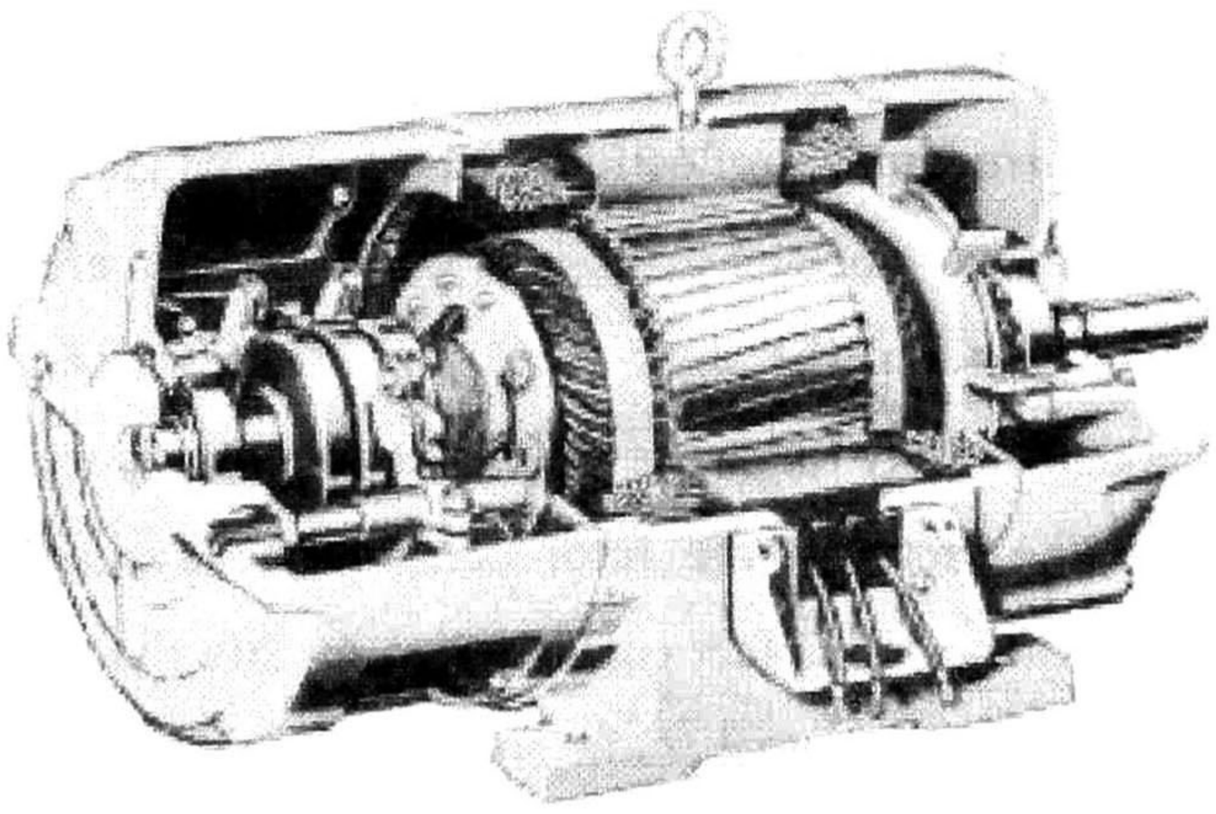

Figure 2.8. An inside view of a wound rotor induction motor. Brushes and slightly touching rings can be seen. We can also see the rotor-winding slope to eliminate the gap harmonics.

2.2.4 Voltage equations

To calculate the state equations of the idealized three-phase induction machine, we will assume the winding configuration shown in Figure 2.9 [9]. In this case the winding placement is only conceptually shown with the centerline of the equivalent inductors directed along the magnetic axis of the windings. Again an elementary two-pole machine is considered. 'Balanced' three phase windings are assumed for both the stator and the rotor. That is, all three windings designated as the *as*, *bs* and *cs* windings are assumed to have the same number of effective turns, N_S, and the same resistance R_S; and the *bs* and *cs* windings are symmetrically displaced from the *as* winding by $\pm 120^{\circ}$. The subscript 's' is used to denote that these windings are *stator* or *stationary* windings. The rotor windings are similarly arranged but have N_r turns and resistance R_r. These windings are designated by *ar*, *br* and *cr*, where the second subscript reminds us that these three windings are *rotor* or *rotating* windings.

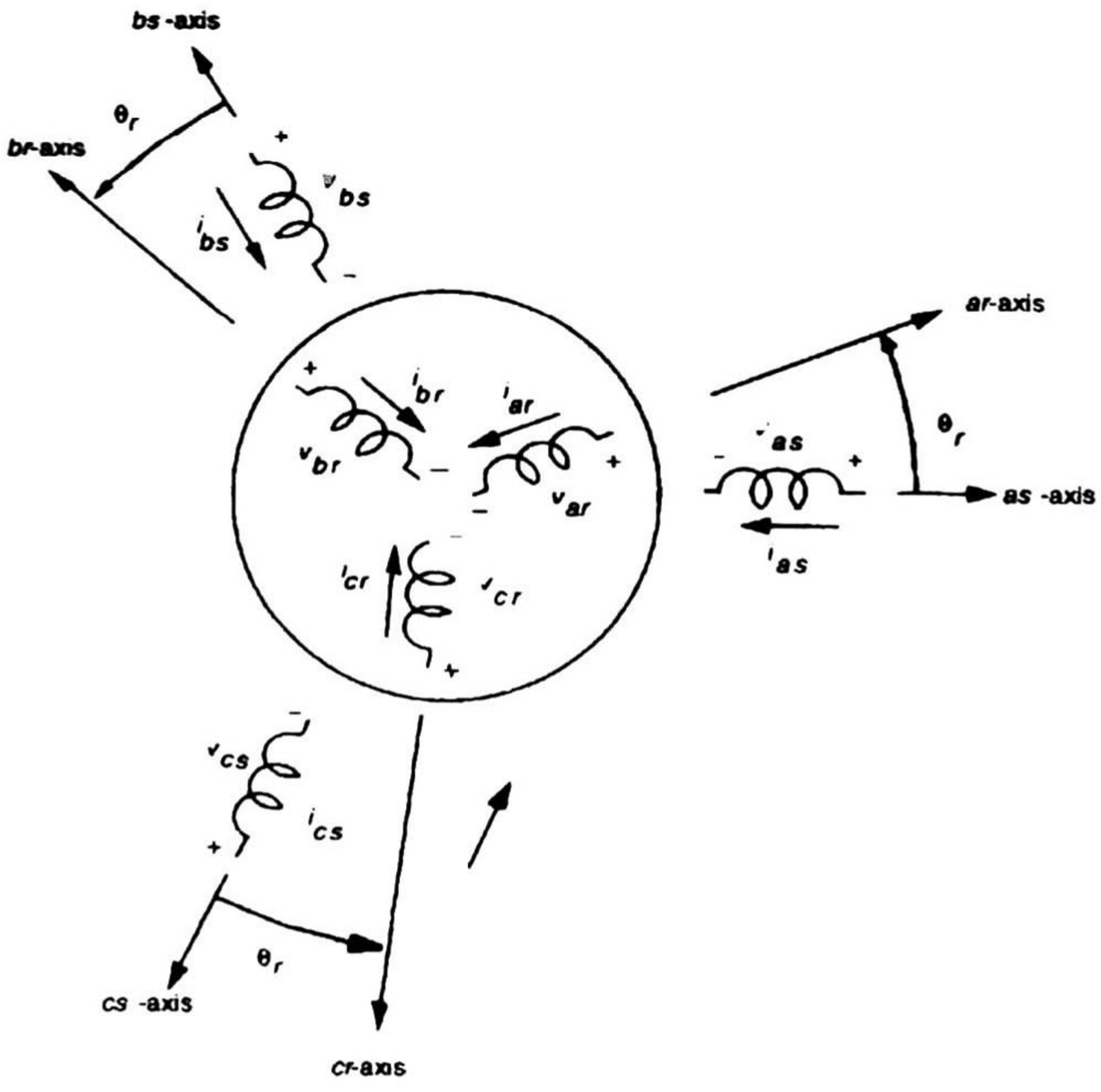

Figure 2.9. Induction motor windings.

The self-inductance of the stator phase *as* is denoted by L_{am}. The subscript m is used to denote the fact that this inductance is a *magnetizing* inductance. That is, it is associated with flux lines which cross the air gap and link rotor as well as stator windings. In general, it is necessary to add a relatively small, but important, leakage term to L_{am} to account for leakage flux. This term accounts for flux lines that do not cross the gap but instead close with the stator slot itself (slot leakage), in the air gap (belt and harmonic leakage) and at the ends of the machine (end winding leakage). Hence, the total self-inductance of phase *as* can be expressed as

$$L_{asas} = L_{ls} + L_{am} \tag{2.2.4.1}$$

Since the windings of the *bs* and *cs* phases are identical to phase *as*, it is clear that the magnetizing inductances of these windings are the same as phase *as* so that, also

$$L_{bsbs} = L_{ls} + L_{bm}$$

$$L_{cascs} = L_{ls} + L_{cm} \tag{2.2.4.2}$$

It is apparent that L_{am}, L_{bm} and L_{cm} are equal making the self-inductances also equal. It is therefore useful to denote the stator magnetizing inductance by L_{ms}, so that

$$L_{asas} = L_{bsbs} = L_{\mathrm{csc}\,s} = L_{ls} + L_{ms} \tag{2.2.4.3}$$

The mutual inductances between phases *as* and *bs*, *bs* and *cs*, and *cs* and *as* are equal to minus one half of the magnetizing inductance

$$L_{asbs} = L_{bscs} = L_{csas} = \frac{-L_{ms}}{2} \tag{2.2.4.4}$$

Let us now turn to the mutual coupling between the stator and the rotor windings. Referring to Figure 2.9, the rotor phase *ar* is displaced from the stator phase *as* by the

electrical angle θ_r where θ_r is in this case a variable. Similarly, the rotor phases *br* and *cr* are displaced from *bs* and *cs* respectively by θ_r. Hence, the corresponding mutual inductances between the phase of the stator and rotor are defined as follows in terms of the magnetizing inductance of the stator

$$L_{asar} = L_{bsbr} = L_{\mathrm{csc}\,r} = \frac{N_r}{N_S} L_{ms} \cos(\theta_r) \qquad (2.2.4.5)$$

The angle between the *as* and *br* phases is $\theta_r + \frac{2\pi}{3}$, so that

$$L_{asbr} = L_{bscr} = L_{csar} = \frac{N_r}{N_S} L_{ms} \cos\left(\theta_r + \frac{2\pi}{3}\right) \qquad (2.2.4.6)$$

Finally, the stator phase *as* is displaced from the rotor *cr* phase by the angle $\theta_r - \frac{2\pi}{3}$

Therefore

$$L_{ascr} = L_{bsar} = L_{csbr} = \frac{N_r}{N_S} L_{ms} \cos\left(\theta_r - \frac{2\pi}{3}\right) \qquad (2.2.4.7)$$

The self-inductances of the rotor are equal, and have the same basic form of the self-inductances of the stator, again in terms of the magnetizing inductance of the stator

$$L_{arar} = L_{brbr} = L_{crcr} = L_{lr} + \left(\frac{N_r}{N_s}\right)^2 L_{ms} \qquad (2.2.4.8)$$

where L_{lr} is the rotor leakage.

The mutual inductances between phases, that is, *ar* and *br*, *br* and *cr*, and *cr* and *ar* are defined as follows in terms of the magnetizing inductance of the stator

$$L_{arbr} = L_{brcr} = L_{crar} = -\left(\frac{N_r}{N_s}\right)^2 \frac{L_{ms}}{2} \qquad (2.2.4.9)$$

Once known the inductive parameters of the induction motor, the stator and rotor voltage equations are obtained applying Kirchoff's voltage law to diagram in Figure 2.9. The obtained equations are

$$\begin{aligned} v_{as} &= R_s i_{as} + \frac{d\psi_{as}}{dt} \\ v_{bs} &= R_s i_{bs} + \frac{d\psi_{bs}}{dt} \\ v_{cs} &= R_s i_{cs} + \frac{d\psi_{cs}}{dt} \\ v_{ar} &= R_r i_{ar} + \frac{d\psi_{ar}}{dt} \\ v_{br} &= R_r i_{br} + \frac{d\psi_{br}}{dt} \\ v_{cr} &= R_r i_{cr} + \frac{d\psi_{cr}}{dt} \end{aligned} \qquad (2.2.4.10)$$

where ψ_{xy} are the linkage fluxes, and are defined in the following form

$$\begin{aligned} \psi_{as} &= L_{asas} i_{as} + L_{asbs} i_{bs} + L_{ascs} i_{cs} + L_{asar} i_{ar} + L_{asbr} i_{br} + L_{ascr} i_{cr} \\ \psi_{bs} &= L_{bsas} i_{as} + L_{bsbs} i_{bs} + L_{bscs} i_{cs} + L_{bsar} i_{ar} + L_{bsbr} i_{br} + L_{bscr} i_{cr} \\ \psi_{cs} &= L_{csas} i_{as} + L_{csbs} i_{bs} + L_{\mathrm{csc}\,s} i_{cs} + L_{csar} i_{ar} + L_{csbr} i_{br} + L_{\mathrm{csc}\,r} i_{cr} \\ \psi_{ar} &= L_{aras} i_{as} + L_{arbs} i_{bs} + L_{arcs} i_{cs} + L_{arar} i_{ar} + L_{arbr} i_{br} + L_{arcr} i_{cr} \\ \psi_{br} &= L_{bras} i_{as} + L_{brbs} i_{bs} + L_{brcs} i_{cs} + L_{brar} i_{ar} + L_{brbr} i_{br} + L_{brcr} i_{cr} \\ \psi_{cr} &= L_{cras} i_{as} + L_{crbs} i_{bs} + L_{crcs} i_{cs} + L_{crar} i_{ar} + L_{crbr} i_{br} + L_{crcr} i_{cr} \end{aligned} \qquad (2.2.4.11)$$

As can be appreciated, the voltage equations are quite complicated, due to the time dependency of the mutual inductances. That justifies that a transformation is needed in order to eliminate this time dependency. For better handling of the above equations, we introduce a matrix representation

$$\begin{aligned}
\mathbf{V}_{abcs} &= R_s \mathbf{I}_{abcs} + \frac{d\boldsymbol{\Psi}_{abcs}}{dt} \\
\mathbf{V}_{abcr} &= R_r \mathbf{I}_{abcr} + \frac{d\boldsymbol{\Psi}_{abcr}}{dt} \\
\boldsymbol{\Psi}_{abcs} &= \mathbf{L}_{ss} \mathbf{I}_{abcs} + \mathbf{L}_{sr} \mathbf{I}_{abcr} \\
\boldsymbol{\Psi}_{abcr} &= \mathbf{L}_{sr}^{T} \mathbf{I}_{abcs} + \mathbf{L}_{rr} \mathbf{I}_{abcr}
\end{aligned} \tag{2.2.4.12}$$

where

$$\mathbf{f}_{abcx} = \begin{bmatrix} f_{ax} \\ f_{bx} \\ f_{cx} \end{bmatrix} \tag{2.2.4.13}$$

the symbol **f** is used to represent any of the three phase circuit variables such a voltage, current or flux linkage and the subscript **x** is used to represent stator or rotor variables.

$$\mathbf{L}_{ss} = \begin{bmatrix} L_{ls} + L_{ms} & -\frac{1}{2}L_{ms} & -\frac{1}{2}L_{ms} \\ -\frac{1}{2}L_{ms} & L_{ls} + L_{ms} & -\frac{1}{2}L_{ms} \\ -\frac{1}{2}L_{ms} & -\frac{1}{2}L_{ms} & L_{ls} + L_{ms} \end{bmatrix}$$

$$\mathbf{L}_{sr} = \frac{N_r}{N_s} L_{ms} \begin{bmatrix} \cos(\theta_r) & \cos(\theta_r + \frac{2\pi}{3}) & \cos(\theta_r - \frac{2\pi}{3}) \\ \cos(\theta_r - \frac{2\pi}{3}) & \cos(\theta_r) & \cos(\theta_r + \frac{2\pi}{3}) \\ \cos(\theta_r + \frac{2\pi}{3}) & \cos(\theta_r - \frac{2\pi}{3}) & \cos(\theta_r) \end{bmatrix}$$

$$\mathbf{L}_{rr} = \begin{bmatrix} L_{lr} + \left(\frac{N_r}{N_s}\right)^2 L_{ms} & -\frac{1}{2}\left(\frac{N_r}{N_s}\right)^2 L_{ms} & -\frac{1}{2}\left(\frac{N_r}{N_s}\right)^2 L_{ms} \\ -\frac{1}{2}\left(\frac{N_r}{N_s}\right)^2 L_{ms} & L_{lr} + \left(\frac{N_r}{N_s}\right)^2 L_{ms} & -\frac{1}{2}\left(\frac{N_r}{N_s}\right)^2 L_{ms} \\ -\frac{1}{2}\left(\frac{N_r}{N_s}\right)^2 L_{ms} & -\frac{1}{2}\left(\frac{N_r}{N_s}\right)^2 L_{ms} & L_{lr} + \left(\frac{N_r}{N_s}\right)^2 L_{ms} \end{bmatrix} \tag{2.2.4.14}$$

It is rather apparent that the turns ratio $\frac{N_S}{N_r}$ causes these matrices and equations to be needlessly cumbersome. The appearance of the turns ratio is of course, not unexpected since the induction motor is simply another type of coupled magnetic circuit and is related to the transformer. In fact we can view the induction motor as equivalent to a transformer with a short circuited and rotating secondary. We can get rid of the explicit dependence of these expressions on the turns ratio by referring the rotor circuits to the stator in much the same manner as utilized for a transformer. Equations in (2.2.4.12) can be manipulated to form

$$\mathbf{V}_{abcs} = R_s\mathbf{I}_{abcs} + \frac{d\boldsymbol{\Psi}_{abcs}}{dt}$$

$$\left(\frac{N_S}{N_r}\right)\mathbf{V}_{abcr} = \left(\frac{N_S}{N_r}\right)^2 R_r\left(\frac{N_r}{N_S}\right)\mathbf{I}_{abcr} + \frac{d\left(\frac{N_S}{N_r}\right)\boldsymbol{\Psi}_{abcr}}{dt}$$

$$\boldsymbol{\Psi}_{abcs} = \mathbf{L}_{ss}\mathbf{I}_{abcs} + L_{ms}\begin{bmatrix} \cos(\theta_r) & \cos(\theta_r + \frac{2\pi}{3}) & \cos(\theta_r - \frac{2\pi}{3}) \\ \cos(\theta_r - \frac{2\pi}{3}) & \cos(\theta_r) & \cos(\theta_r + \frac{2\pi}{3}) \\ \cos(\theta_r + \frac{2\pi}{3}) & \cos(\theta_r - \frac{2\pi}{3}) & \cos(\theta_r) \end{bmatrix}\left[\left(\frac{N_r}{N_S}\right)\mathbf{I}_{abcr}\right]$$

$$\left(\frac{N_S}{N_r}\right)\boldsymbol{\Psi}_{abcr} = L_{ms}\begin{bmatrix} \cos(\theta_r) & \cos(\theta_r + \frac{2\pi}{3}) & \cos(\theta_r - \frac{2\pi}{3}) \\ \cos(\theta_r - \frac{2\pi}{3}) & \cos(\theta_r) & \cos(\theta_r + \frac{2\pi}{3}) \\ \cos(\theta_r + \frac{2\pi}{3}) & \cos(\theta_r - \frac{2\pi}{3}) & \cos(\theta_r) \end{bmatrix}^{\mathbf{T}}\mathbf{I}_{abcs} +$$

$$+\begin{bmatrix} \left(\frac{N_r}{N_s}\right)^2 L_{lr} + L_{ms} & -\frac{1}{2}L_{ms} & -\frac{1}{2}L_{ms} \\ -\frac{1}{2}L_{ms} & \left(\frac{N_r}{N_s}\right)^2 L_{lr} + L_{ms} & -\frac{1}{2}L_{ms} \\ -\frac{1}{2}L_{ms} & -\frac{1}{2}L_{ms} & \left(\frac{N_r}{N_s}\right)^2 L_{lr} + L_{ms} \end{bmatrix}\left[\left(\frac{N_r}{N_S}\right)\mathbf{I}_{abcr}\right] \qquad (2.2.4.5)$$

We now define the primed variables and matrices

$$\left(\frac{N_S}{N_r}\right)\mathbf{V}_{abcr} = \mathbf{V}'_{abcr}$$

$$\left(\frac{N_S}{N_r}\right)\mathbf{\Psi}_{abcr} = \mathbf{\Psi}'_{abcr}$$

$$\left(\frac{N_r}{N_S}\right)\mathbf{I}_{abcr} = \mathbf{I}'_{abcr}$$

$$\left(\frac{N_S}{N_r}\right)^2 R_r = R'_r$$

$$\left(\frac{N_S}{N_r}\right)^2 L_{lr} = L'_{lr}$$

$$L'_{sr} = L_{ms}\begin{bmatrix} \cos(\theta_r) & \cos(\theta_r + \frac{2\pi}{3}) & \cos(\theta_r - \frac{2\pi}{3}) \\ \cos(\theta_r - \frac{2\pi}{3}) & \cos(\theta_r) & \cos(\theta_r + \frac{2\pi}{3}) \\ \cos(\theta_r + \frac{2\pi}{3}) & \cos(\theta_r - \frac{2\pi}{3}) & \cos(\theta_r) \end{bmatrix}$$

$$L'_{rr} = \begin{bmatrix} \left(\frac{N_r}{N_s}\right)^2 L_{lr} + L_{ms} & -\frac{1}{2}L_{ms} & -\frac{1}{2}L_{ms} \\ -\frac{1}{2}L_{ms} & \left(\frac{N_r}{N_s}\right)^2 L_{lr} + L_{ms} & -\frac{1}{2}L_{ms} \\ -\frac{1}{2}L_{ms} & -\frac{1}{2}L_{ms} & \left(\frac{N_r}{N_s}\right)^2 L_{lr} + L_{ms} \end{bmatrix} \qquad (2.2.4.16)$$

Combining the above results, the equations for stator and rotor circuits finally becomes

$$\begin{aligned} \mathbf{V}_{abcs} &= R_s\mathbf{I}_{abcs} + \frac{d\mathbf{\Psi}_{abcs}}{dt} \\ \mathbf{V}'_{abcr} &= R'_r\mathbf{I}'_{abcr} + \frac{d\mathbf{\Psi}'_{abcr}}{dt} \\ \mathbf{\Psi}_{abcs} &= \mathbf{L}_{ss}\mathbf{I}_{abcs} + \mathbf{L}'_{sr}\mathbf{I}'_{abcr} \\ \mathbf{\Psi}'_{abcr} &= \mathbf{L}'^{T}_{sr}\mathbf{I}_{abcs} + \mathbf{L}'_{rr}\mathbf{I}'_{abcr} \end{aligned} \qquad (2.2.4.17)$$

2.2.5 Transformation to a rotating reference frame

The aforementioned coupling between the stator and rotor circuits can essentially be eliminated, if the stator and rotor equations are referred to a common frame of reference. This common frame of reference can be non-rotating in which case it is associated with the stator and is called the *stator* or *stationary* reference. Alternative the d,q axis can be made to rotate with the same angular velocity as the rotor circuits, and is termed the *rotor* reference frame.

Consider for example, a rotating set of d,q axis as defined by Figure 2.10. Figure 2.10 also shows reference axis corresponding to the magnetic axis of the three-phase stator and three phase rotor circuits. Variables along the a,b and c stator axis can be referred to the d and q axis by the expressions

$$\begin{aligned} f_{ds} &= \frac{2}{3}\left[f_{as}\cos(\theta) + f_{bs}\cos\left(\theta - \frac{2\pi}{3}\right) + f_{cs}\cos\left(\theta + \frac{2\pi}{3}\right)\right] \\ f_{qs} &= \frac{2}{3}\left[- f_{as}sin(\theta) - f_{bs}sin\left(\theta - \frac{2\pi}{3}\right) - f_{cs}sin\left(\theta + \frac{2\pi}{3}\right)\right] \end{aligned} \qquad (2.2.5.1)$$

where the symbol f is used again to represent any of the three phase circuit variables such a voltage, current or flux linkage. It should be noted that the coefficient $\frac{2}{3}$ in these two equations is somewhat arbitrary. The choice of $\frac{2}{3}$ is usually selected so as to maintain the same modulus of the voltage and current signals for sinusoidal steady state. Since there are three phases, then in general, it is necessary to define a third new variable to obtain a unique transformation. This third new variable is typically defined as the *zero sequence component*

$$f_{0s} = \frac{1}{3}[f_{as} + f_{bs} + f_{cs}] \qquad (2.2.5.2)$$

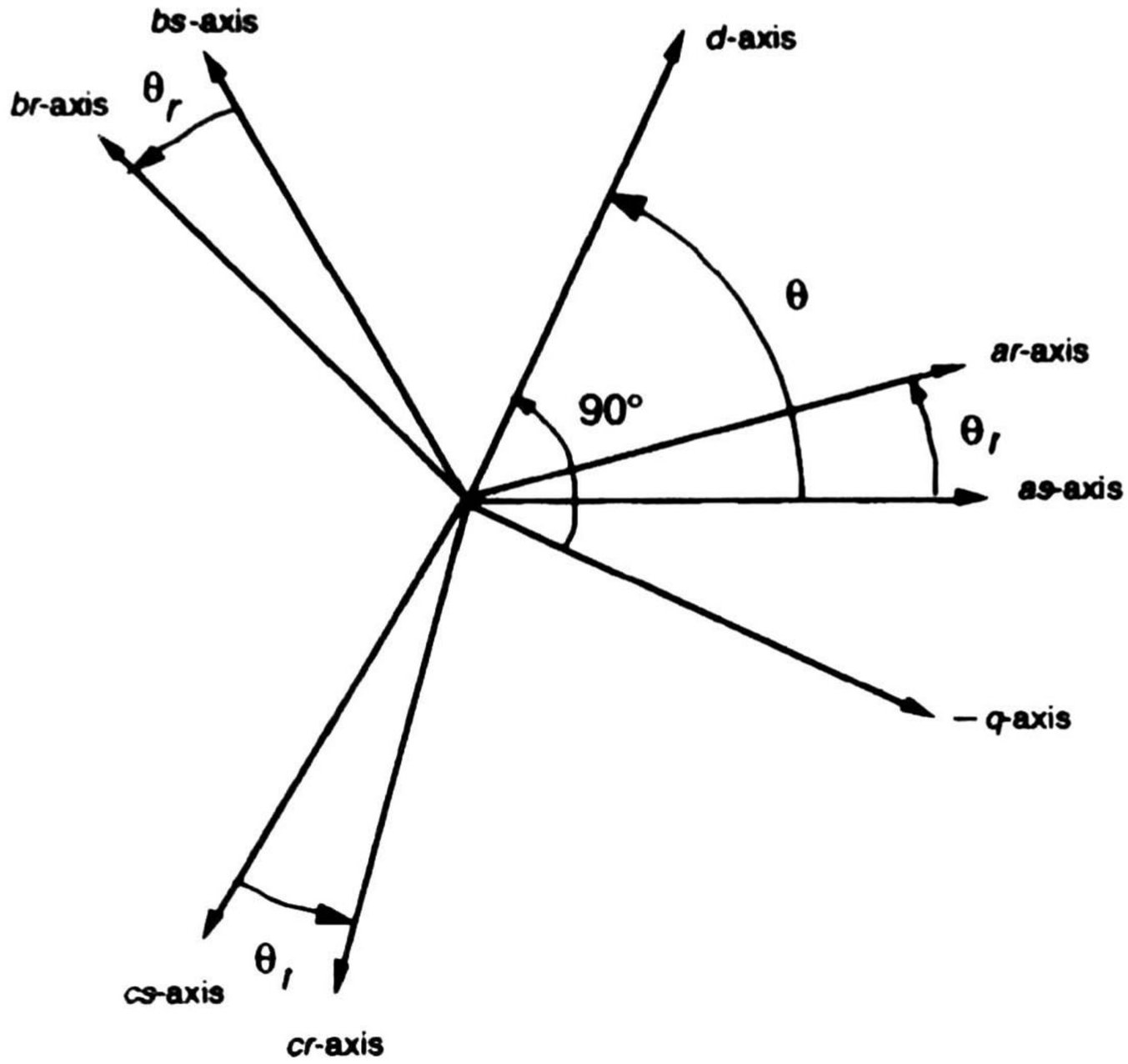

Figure 2.10. Location of the rotating *d,q* axis relative to the magnetic axis of the stator and rotor phases.

In this context the use of the symbol *0* in the subscript of the new variable is used to designate a zero component *normal* to the *d,q* plane.

In practical applications, the machine is connected either in Δ or in $\mathbf{Y}$, thus, the three stator currents sum to zero. As a result, the other significant three phase variables such as phase voltages, the stator flux linkages and rotor currents also sum to zero. Hence, it is necessary to concern oneself only with projections on the *d,q* plane.

From (2.2.5.1) and (2.2.5.2) we obtain a matrix denoted by $\mathbf{K}_s$, that converts the aforementioned vector $\mathbf{f}_{abcs}$ into the vector $\mathbf{f}_{dq0s}$. Such operation is shown by,

$$\mathbf{f}_{dq0s} = \mathbf{K}_s \mathbf{f}_{abcs} \tag{2.2.5.3}$$

where the matrix $\mathbf{K}_s$ is as follows

$$\mathbf{K}_s = \frac{2}{3}\begin{bmatrix} \cos(\theta) & \cos(\theta - \frac{2\pi}{3}) & \cos(\theta + \frac{2\pi}{3}) \\ -\sin(\theta) & -\sin(\theta - \frac{2\pi}{3}) & -\sin(\theta + \frac{2\pi}{3}) \\ \frac{1}{2} & \frac{1}{2} & \frac{1}{2} \end{bmatrix} \qquad (2.2.5.4)$$

the inverse of this matrix is

$$\mathbf{K}_s^{-1} = \begin{bmatrix} \cos(\theta) & -\sin(\theta) & 1 \\ \cos(\theta - \frac{2\pi}{3}) & -\sin(\theta - \frac{2\pi}{3}) & 1 \\ \cos(\theta + \frac{2\pi}{3}) & -\sin(\theta + \frac{2\pi}{3}) & 1 \end{bmatrix} \qquad (2.2.5.5)$$

where the angular displacement between the *d* and *as* axis is denoted by θ as shown in Figure 2.10.

Let us now turn to the variables of the rotor and transform them into *d,q* variables. We observe from Figure 2.10 that the angular displacement between the *d* and *ar* axis is $\theta - \theta_r$, and denoting this displacement by β, we obtain a matrix by direct replacement of β instead of θ in (2.2.5.4). Such transformation is as follows,

$$\mathbf{f}_{dq0r} = \mathbf{K}_r \mathbf{f}_{abcr} \qquad (2.2.5.6)$$

where the matrix $\mathbf{K}_r$ is as follows

$$\mathbf{K}_r = \frac{2}{3}\begin{bmatrix} \cos(\beta) & \cos(\beta - \frac{2\pi}{3}) & \cos(\beta + \frac{2\pi}{3}) \\ -\sin(\beta) & -\sin(\beta - \frac{2\pi}{3}) & -\sin(\beta + \frac{2\pi}{3}) \\ \frac{1}{2} & \frac{1}{2} & \frac{1}{2} \end{bmatrix} \qquad (2.2.5.7)$$

and the inverse of this matrix is

$$\mathbf{K}_r^{-1} = \begin{bmatrix} \cos(\beta) & -\sin(\beta) & 1 \\ \cos(\beta - \frac{2\pi}{3}) & -\sin(\beta - \frac{2\pi}{3}) & 1 \\ \cos(\beta + \frac{2\pi}{3}) & -\sin(\beta + \frac{2\pi}{3}) & 1 \end{bmatrix} \tag{2.2.5.8}$$

2.2.6 Stator and rotor equations transformed into an arbitrary reference frame

Let us proceed with the stator voltage equation, transforming it into an arbitrary spinning reference frame, i.e.

$$\frac{d\theta}{dt} = \omega \tag{2.2.6.1}$$

Transforming the stator voltage equation appearing in (2.2.4.17), we obtain the following

$$\begin{aligned} \mathbf{V}_{dq0s} &= \mathbf{K}_s \mathbf{V}_{abcs} \\ \mathbf{V}_{dq0s} &= \mathbf{K}_s (R_s \mathbf{I}_{abcs} + \frac{d\boldsymbol{\Psi}_{abcs}}{dt}) \\ \mathbf{V}_{dq0s} &= R_s \mathbf{K}_s \mathbf{I}_{abcs} + \mathbf{K}_s \frac{d\boldsymbol{\Psi}_{abcs}}{dt} \end{aligned} \tag{2.2.6.2}$$

using the following facts

$$\begin{aligned} \mathbf{I}_{abcs} &= \mathbf{K}_s^{-1} \mathbf{I}_{dq0s} \\ \boldsymbol{\Psi}_{abcs} &= \mathbf{K}_s^{-1} \boldsymbol{\Psi}_{dq0s} \end{aligned} \tag{2.2.6.3}$$

and replacing it in (2.2.6.2), yields the following equation

$$\mathbf{V}_{dq0s} = \mathbf{R}_s\mathbf{I}_{dq0s} + \mathbf{K}_s\frac{d\mathbf{K}_s^{-1}}{dt}\boldsymbol{\Psi}_{dq0s} + \frac{d\boldsymbol{\Psi}_{dq0s}}{dt} \qquad (2.2.6.4)$$

Computing separately the derivative of $\mathbf{K}_s^{-1}$ in (2.2.6.4), we obtain,

$$\frac{d\mathbf{K}_s^{-1}}{dt} = \omega\begin{bmatrix} -sin(\theta) & -\cos(\theta) & 0 \\ -sin(\theta-\frac{2\pi}{3}) & -\cos(\theta-\frac{2\pi}{3}) & 0 \\ -sin(\theta+\frac{2\pi}{3}) & -\cos(\theta+\frac{2\pi}{3}) & 0 \end{bmatrix} \qquad (2.2.6.5)$$

Then we have

$$\mathbf{K}_s\frac{d\mathbf{K}_s^{-1}}{dt} = \omega\begin{bmatrix} 0 & -1 & 0 \\ 1 & 0 & 0 \\ 0 & 0 & 0 \end{bmatrix} \qquad (2.2.6.6)$$

We define the matrix $\mathbf{D}$ as follows

$$\mathbf{D} = \begin{bmatrix} 0 & -1 & 0 \\ 1 & 0 & 0 \\ 0 & 0 & 0 \end{bmatrix} \qquad (2.2.6.7)$$

and finally putting all together

$$\mathbf{V}_{dq0s} = R_s\mathbf{I}_{dq0s} + \omega\mathbf{D}\boldsymbol{\Psi}_{dq0s} + \frac{d\boldsymbol{\Psi}_{dq0s}}{dt} \qquad (2.2.6.8)$$

Proceeding similarly with the rotor voltage equation, we transform it to an arbitrary reference frame, i.e.

$$\frac{d\beta}{dt} = \omega - \omega_r \tag{2.2.6.9}$$

Then, we start from the following equation

$$\mathbf{V}'_{dq0r} = \mathbf{K}_r \mathbf{V}'_{abcr} \tag{2.2.6.10}$$

and with some computations that finally yields

$$\mathbf{V}'_{dq0r} = R'_r \mathbf{I}'_{dq0r} + (\omega - \omega_r)\mathbf{D}\boldsymbol{\Psi}'_{dq0r} + \frac{d\boldsymbol{\Psi}'_{dq0r}}{dt} \tag{2.2.6.11}$$

We continue the transformation process with the flux linkage, when proceeding in the same way we obtain the following equations

$$\begin{aligned} \boldsymbol{\Psi}_{dq0s} &= \mathbf{K}_s \mathbf{L}_s \mathbf{K}_s^{-1} \mathbf{I}_{dq0s} + \mathbf{K}_s \mathbf{L}'_{sr} \mathbf{K}_r^{-1} \mathbf{I}'_{dq0r} \\ \boldsymbol{\Psi}'_{dq0r} &= \mathbf{K}_r \mathbf{L}'^{T}_{sr} \mathbf{K}_s^{-1} \mathbf{I}_{dq0s} + \mathbf{K}_r \mathbf{L}'_{rr} \mathbf{K}_r^{-1} \mathbf{I}'_{dq0r} \end{aligned} \tag{2.2.6.12}$$

where each operation is as follows

$$\mathbf{K}_s \mathbf{L}_{ss} \mathbf{K}_s^{-1} = \begin{bmatrix} L_{ls} + \frac{3}{2} L_{ms} & 0 & 0 \\ 0 & L_{ls} + \frac{3}{2} L_{ms} & 0 \\ 0 & 0 & L_{ls} \end{bmatrix} \tag{2.2.6.13}$$

$$\mathbf{K}_s\mathbf{L}_{sr}\mathbf{K}_r^{-1} = \mathbf{K}_r\mathbf{L}_{sr}^T\mathbf{K}_s^{-1} = \begin{bmatrix} \frac{3}{2}L_{ms} & 0 & 0 \\ 0 & \frac{3}{2}L_{ms} & 0 \\ 0 & 0 & 0 \end{bmatrix}$$

$$\mathbf{K}_r\mathbf{L}'_{rr}\mathbf{K}_r^{-1} = \begin{bmatrix} L'_{lr} + \frac{3}{2}L_{ms} & 0 & 0 \\ 0 & L'_{lr} + \frac{3}{2}L_{ms} & 0 \\ 0 & 0 & L'_{lr} \end{bmatrix} \qquad (2.2.6.14)$$

Defining the matrix elements for sake of simplicity

$$\begin{aligned} L_s &= L_{ls} + M \\ L_r &= L'_{lr} + M \end{aligned} \qquad (2.2.6.15)$$

where

$$M = \frac{3}{2}L_{ms} \qquad (2.2.6.16)$$

2.2.7 Torque equation

Up to this point we have treated the induction machine as simply an interesting type of coupled magnetic circuit and the electromechanical properties of this device so far has been ignore. It is now time to consider where the energy goes that passes into the machine via the stator and rotor terminals.

The power flow into the induction motor in terms of the newly defined $d,q,0$ variables must now be examined. The power flowing into an n phase induction machine is clearly the instantaneous product of the voltages across and currents through the n phases of the machine. In this work the machine is assumed to have three stator and three rotor phases, the power into the machine can be written as

$$\mathbf{P}_e = \frac{3}{2}\left[\mathbf{V}_{dq0s}\mathbf{I}^T_{dq0s} + \mathbf{V}'_{dq0r}\mathbf{I}'^T_{dq0r}\right] \tag{2.2.7.1}$$

Replacing the voltage equations that are shown in (2.2.6.8) and (2.2.6.11) into (2.2.7.1)

$$\begin{aligned}\mathbf{P}_e = \frac{3}{2}\left[R_s\mathbf{I}_{dq0s} + \omega\mathbf{D}\boldsymbol{\Psi}_{dq0s} + \frac{d\boldsymbol{\Psi}_{dq0s}}{dt}\right]\mathbf{I}^T_{dq0s} + \\ \frac{3}{2}\left[R'_r\mathbf{I}'_{dq0r} + (\omega-\omega_r)\mathbf{D}\boldsymbol{\Psi}'_{dq0r} + \frac{d\boldsymbol{\Psi}'_{dq0r}}{dt}\right]\mathbf{I}'^T_{dq0r}\end{aligned} \tag{2.2.7.2}$$

It is interesting to observe that the power into the d,q circuits is calculated in a slightly different fashion to that in the actual circuits of the machine due to the appearance of the $\frac{3}{2}$ factor. This is a direct result of the $\frac{2}{3}$ factor that we selected as the proportionality constant between the a,b,c and d,q variables.

The right hand expression in (2.2.7.2) can be arranged in the form

Power lost in conductors **Time rate of change of stored energy**

$$\begin{aligned}P_e = \frac{3}{2}\left[R_s\left|\mathbf{I}_{dq0s}\right|^2 + R'_r\left|\mathbf{I}'_{dq0r}\right|^2\right] + \frac{3}{2}\left[\frac{d\boldsymbol{\Psi}_{dq0s}}{dt}\mathbf{I}^T_{dq0s} + \frac{d\boldsymbol{\Psi}'_{dq0r}}{dt}\mathbf{I}'^T_{dq0r}\right] + \\ \frac{3}{2}\left[\omega\mathbf{D}\boldsymbol{\Psi}_{dq0s}\mathbf{I}^T_{dq0s} + (\omega-\omega_r)\mathbf{D}\boldsymbol{\Psi}'_{dq0r}\mathbf{I}'^T_{dq0r}\right]\end{aligned} \tag{2.2.7.3}$$

Energy conversion term

Hence, the electrical power into the terminals of the machine can be segregated into three terms. The first term clearly accounts for the power dissipated in the stator and rotor resistances. The second term corresponds to the time rate of change of the magnetic energy stored in the inductances of the machine. Since the remaining power must be going somewhere, it is natural to suspect that the third term account for energy conversion, that is the power being converted from electrical to mechanical form. Let us call this term P_{CONV}, the electromechanical output power.

With some computations it is easy to obtain the following expression from (2.2.7.3)

$$P_{CONV} = \frac{3}{2}\omega_r M\left(I_{qs}I'_{dr} - I_{ds}I'_{qr}\right) \tag{2.2.7.4}$$

An important expression for (2.2.7.4) can be obtained if equations in (2.2.6.12) are solved for rotor current rather than stator current, whereupon

$$\begin{aligned} I'_{dr} &= \frac{1}{L_r}\psi'_{dr} - \frac{M}{L_r}I_{ds} \\ I'_{qr} &= \frac{1}{L_r}\psi'_{qr} - \frac{M}{L_r}I_{qs} \end{aligned} \tag{2.2.7.5}$$

Substituting (2.2.7.5) into equation (2.2.7.4) yields

$$P_{CONV} = \frac{3}{2}\omega_r M\left(I_{qs}\psi'_{dr} - I_{ds}\psi'_{qr}\right) \tag{2.2.7.6}$$

The electrical angular velocity of the equivalent two pole machine, ω_r, is related to the actual mechanical speed by the pole pairs, i.e.

$$\omega_r = n_p\omega_{rm} \tag{2.2.7.7}$$

where n_p is the number of poles and ω_{rm} is the mechanical speed in radians per second. Since rotational mechanical power is defined as the product of speed times torque impressed on the shaft of the machine can be expressed as

$$T_e = \frac{3}{2}\frac{Mn_p}{L_r}\left(I_{qs}\psi'_{dr} - I_{ds}\psi'_{qr}\right) \tag{2.2.7.8}$$

In addition to the equations describing the electrical behavior of the machine, more equations are, of course, necessary to describe its electromechanical behavior. In its simplest form, the electromechanical behavior is described by

$$T_e = J\frac{d\omega_{rm}}{dt} + T_L \qquad (2.2.7.9)$$

where ω_{rm} is the mechanical angular velocity of the rotor in rad/s and T_L is the load torque which may itself be described by additional differential or algebraic equations. Solving equation (2.2.7.9) and substituting (2.2.7.8) yields

$$\frac{d\omega_{rm}}{dt} = \frac{3}{2}\frac{Mn_p}{JL_r}\left(I_{qs}\psi'_{dr} - I_{ds}\psi'_{qr}\right) - \frac{1}{J}T_L \qquad (2.2.7.10)$$

2.2.8 Stationary reference frame model ($\alpha - \beta$ model)

There are four reference frames commonly used

- Stationary reference frame ($\omega = 0$).
- Fixed rotor reference frame ($\omega = \omega_r$).
- Reference frame that rotates at a synchronal velocity ($\omega = \omega_e$).
- Reference frame that rotates at rotor flux velocity ($\omega = \omega_{rf}$).

The voltage equations can be obtained from the arbitrary reference frame voltage equations shown in (2.2.6.8) and (2.2.6.11), by replacing the right value of ω.

The most convenient reference frame is dictated by the machine operational conditions, i.e., if the voltages are discontinuous or unbalanced, and the voltages that feed the rotor are balanced or are zero, then, the stationary reference frame can be used in this case. If the voltages that fed the rotor are unbalanced and the voltages in the stator are in balance, then is convenient the fixed rotor reference frame. The reference frame that rotates

synchronously it is useful when analyzing transient and stability dynamics in high power systems, and also when the frequency is free adjusted and the stator voltages are a set of sinusoidal balanced waves.

So, the best case that fits this work is the stationary reference frame ($\omega = 0$), due to the discontinuous voltages that will feed the stator. We show again the voltage equations in the arbitrary reference frame

$$\mathbf{V}_{dq0s} = R_s\mathbf{I}_{dq0s} + \omega\mathbf{D}\boldsymbol{\Psi}_{dq0s} + \frac{d\boldsymbol{\Psi}_{dq0s}}{dt}$$
$$\mathbf{V}'_{dq0r} = R'_r\mathbf{I}'_{dq0r} + (\omega - \omega_r)\mathbf{D}\boldsymbol{\Psi}'_{dq0r} + \frac{d\boldsymbol{\Psi}'_{dq0r}}{dt} \qquad (2.2.8.1)$$

Expanding these equations and substituting $\omega = 0$, yields

$$v_{ds} = R_s i_{ds} + \frac{d\psi_{ds}}{dt}$$
$$v_{qs} = R_s i_{qs} + \frac{d\psi_{qs}}{dt}$$
$$v_{0s} = R_s i_{0s} + \frac{d\psi_{0s}}{dt} \qquad (2.2.8.2)$$

$$v'_{dr} = R'_r i_{dr} + \omega_r\psi'_{qr} + \frac{d\psi'_{dr}}{dt}$$
$$v'_{qr} = R'_r i_{qr} - \omega_r\psi'_{dr} + \frac{d\psi'_{qr}}{dt}$$
$$v'_{0r} = R'_r i_{0r} + \frac{d\psi'_{0r}}{dt}$$

Due to the short-circuited rotor circuits, their voltages are zero, that is, $v'_{dr} = v'_{qr} = v'_{0r} = 0$, moreover if we consider a balanced system we can omit the $0s$ and $0r$ variables, due to its null contribution. So far we have considered a two-pole machine, in order to manipulate any quantity of pole pairs, we introduce again the variable n_p as in

(2.2.7.7), or in other words, we substitute the electrical angular velocity of the equivalent two pole machine, ω_r, by $\omega_r = n_p\omega_{rm}$

$$v_{ds} = R_s i_{ds} + \frac{d\psi_{ds}}{dt}$$
$$v_{qs} = R_s i_{qs} + \frac{d\psi_{qs}}{dt}$$
(2.2.8.3)
$$v'_{dr} = R'_r i'_{dr} + n_p\omega_{rm}\psi'_{qr} + \frac{d\psi'_{dr}}{dt}$$
$$v'_{qr} = R'_r i'_{qr} - n_p\omega_{rm}\psi'_{dr} + \frac{d\psi'_{qr}}{dt}$$

Proceeding in the same way, and omitting the $0s$ and $0r$ variables, we show the flux linkage equations

$$\psi_{ds} = L_s i_{ds} + Mi'_{dr}$$
$$\psi_{qs} = L_s i_{qs} + Mi'_{qr}$$
(2.2.8.4)
$$\psi'_{dr} = Mi_{ds} + L_r i'_{dr}$$
$$\psi'_{qr} = Mi_{qs} + L_r i'_{qr}$$

If we take the derivative of the first equation of (2.2.8.4) and then substitute it in the first equation of (2.2.8.3), yields

$$v_{ds} = R_s i_{ds} + L_s \frac{di_{ds}}{dt} + M\frac{di'_{dr}}{dt} \qquad (2.2.8.5)$$

and isolating i'_{dr} from the third equation of (2.2.8.4) and replace its derivative into equation (2.2.8.5), yielding to

$$v_{ds} = R_s i_{ds} + \left(L_s - \frac{M^2}{L_r} \right) \frac{di_{ds}}{dt} + \frac{M}{L_r} \frac{d\psi'_{dr}}{dt} \qquad (2.2.8.6)$$

Proceeding in the same way, we manipulate the second equation of (2.2.8.3), obtaining the following voltage equation

$$v_{qs} = R_s i_{qs} + \left(L_s - \frac{M^2}{L_r} \right) \frac{di_{qs}}{dt} + \frac{M}{L_r} \frac{d\psi'_{qr}}{dt} \qquad (2.2.8.7)$$

Isolating i'_{dr} from the third equation of (2.2.8.4) and then substitute it in the third equation of (2.2.8.3), yields

$$0 = R'_r \left(\frac{1}{L_r} \psi'_{dr} - \frac{M}{L_r} i_{ds} \right) + \frac{d\psi'_{dr}}{dt} + n_p \omega_{rm} \psi'_{qr} \qquad (2.2.8.8)$$

solving for $\frac{d\psi'_{dr}}{dt}$, results in

$$\frac{d\psi'_{dr}}{dt} = -\frac{R'_r}{L_r} \psi'_{dr} - n_p \omega_{rm} \psi'_{qr} + \frac{R_r M}{L_r} i_{ds} \qquad (2.2.8.9)$$

and continuing in the same way, starting from the fourth equation of (2.2.8.4) and (2.2.8.3), we obtain $\frac{d\psi'_{qr}}{dt}$, as follows

$$\frac{d\psi'_{qr}}{dt} = -\frac{R'_r}{L_r} \psi'_{qr} + n_p \omega_{rm} \psi'_{dr} + \frac{R_r M}{L_r} i_{qs} \qquad (2.2.8.10)$$

Substituting (2.2.8.9) and (2.2.8.10) into (2.2.8.6) and (2.2.8.7) respectively, and solving for $\frac{di_{ds}}{dt}$ and $\frac{di_{qs}}{dt}$, yields

$$\frac{di_{ds}}{dt} = \frac{R_r' M}{L_r(L_s L_r - M^2)}\psi'_{dr} + \frac{n_p M}{L_s L_r - M^2}\omega_{rm}\psi'_{qr} - \frac{R_s L_r^2 + R_r' M^2}{L_r(L_s L_r - M^2)} i_{ds} + \frac{L_r}{L_s L_r - M^2} v_{ds}$$

$$\frac{di_{qs}}{dt} = \frac{R_r' M}{L_r(L_s L_r - M^2)}\psi'_{qr} - \frac{n_p M}{L_s L_r - M^2}\omega_{rm}\psi'_{dr} - \frac{R_s L_r^2 + R_r' M^2}{L_r(L_s L_r - M^2)} i_{qs} + \frac{L_r}{L_s L_r - M^2} v_{qs} \qquad (2.2.11)$$

Finally, putting the torque and voltage equations together, and changing the notation in order to distinguish a stationary reference frame model, we name this model as usual in literature as "$\alpha - \beta$ model" We change voltage v by u, the index d and q by α and β respectively, and we omit the stator an rotor indexes because it is well known that voltages and currents are with respect to stator and the angular velocity and fluxes are with respect to rotor. We also omit the primed variables; it is known that are to respect to the stator.

$$\frac{d\omega}{dt} = \frac{3}{2}\frac{n_p M}{J L_r}\left(\psi_\alpha i_\beta - \psi_\beta i_\alpha\right) - \frac{1}{J} T_L$$

$$\frac{d\psi_\alpha}{dt} = -\frac{R_r}{L_r}\psi_\alpha - n_p \omega \psi_\beta + \frac{R_r M}{L_r} i_\alpha$$

$$\frac{d\psi_\beta}{dt} = -\frac{R_r}{L_r}\psi_\beta + n_p \omega \psi_\alpha + \frac{R_r M}{L_r} i_\beta$$

$$\frac{di_\alpha}{dt} = \frac{R_r M}{L_r(L_s L_r - M^2)}\psi_\alpha + \frac{n_p M}{L_s L_r - M^2}\omega\psi_\beta - \frac{R_s L_r^2 + R_r M^2}{L_r(L_s L_r - M^2)} i_\alpha + \frac{L_r}{L_s L_r - M^2} u_\alpha$$

$$\frac{di_\beta}{dt} = \frac{R_r M}{L_r(L_s L_r - M^2)}\psi_\beta - \frac{n_p M}{L_s L_r - M^2}\omega\psi_\alpha - \frac{R_s L_r^2 + R_r M^2}{L_r(L_s L_r - M^2)} i_\beta + \frac{L_r}{L_s L_r - M^2} u_\beta$$

This system is the one to be discretized, where we will design and apply the control law in discrete-time.

2.3 DISCRETIZATION OF THE CONTINUOS-TIME INDUCTION MOTOR MODEL

In this section we develop another representation of the induction motor model, called *discrete-time* induction motor model. The states of discrete-time systems are defined only at discrete instants of time. For example, a digital computer reads and prints out data that are the values of variables at discrete instant of time; hence it is a discrete-time system. A continuos-time system can also be modeled as a discrete-time system if its responses are of interest or measurable only at certain instants of time. This is the case of this work, because, we will read or print out data at discrete instants of time in a digital computer as just mentioned above.

Under the assumptions of equal mutual inductance and a linear magnetic circuit, a fifth-order induction motor continuos-time model, which includes both the electrical and mechanical dynamics, is given as

$$\begin{aligned}
\frac{d\omega}{dt} &= \mu\left(\psi_\alpha i_\beta - \psi_\beta i_\alpha\right) - \frac{T_L}{J} \\
\frac{d\psi_\alpha}{dt} &= -\alpha\psi_\alpha - n_p\omega\psi_\beta + \alpha M i_\alpha \\
\frac{d\psi_\beta}{dt} &= -\alpha\psi_\beta + n_p\omega\psi_\alpha + \alpha M i_\beta \\
\frac{di_\alpha}{dt} &= \alpha\beta\psi_\alpha + n_p\beta\omega\psi_\beta - \gamma i_\alpha + \frac{1}{\sigma}u_\alpha \\
\frac{di_\beta}{dt} &= \alpha\beta\psi_\beta - n_p\beta\omega\psi_\alpha - \gamma i_\beta + \frac{1}{\sigma}u_\beta
\end{aligned} \tag{2.3.1}$$

where

$$\begin{aligned}
\alpha &= \frac{R_r}{L_r} = \frac{1}{T_r} \qquad \gamma = \frac{M^2 R_r}{\sigma L_r^2} + \frac{Rs}{\sigma} \qquad \sigma = L_s - \frac{M^2}{L_r} \\
\beta &= \frac{M}{\sigma L_r} \qquad\qquad\qquad\qquad \mu = \frac{3}{2}\frac{Mn_p}{JL_r}
\end{aligned} \tag{2.3.2}$$

To face the problem of discretization of the continuos time-model, we need to found the solutions of the fifth-order system equations, but this is a difficult task. To overcome this problem we divide this model in a current-fed induction motor third-order model, where the current inputs are considered as pseudo-inputs, and a second-order subsystem that only models the currents of the stator with voltages as inputs. The current-fed model will be exactly discretized by solving the set of differential equations and the other subsystem will be discretized by a first-order Taylor series.

We present the current-fed induction motor third-order model

$$\begin{aligned}
\frac{d\omega}{dt} &= \mu\left(\psi_\alpha i_\beta - \psi_\beta i_\alpha\right) - \frac{T_L}{J} \\
\frac{d\psi_\alpha}{dt} &= -\alpha\psi_\alpha - n_p\omega\psi_\beta + \alpha M i_\alpha \\
\frac{d\psi_\beta}{dt} &= -\alpha\psi_\beta + n_p\omega\psi_\alpha + \alpha M i_\beta
\end{aligned} \tag{2.3.3}$$

To simplify notation, we define the following matrices

$$\begin{aligned}
\boldsymbol{\Psi} &= \begin{bmatrix} \psi_\alpha \\ \psi_\beta \end{bmatrix} \\
\mathbf{I} &= \begin{bmatrix} i_\alpha \\ i_\beta \end{bmatrix} \\
\mathfrak{I} &= \begin{bmatrix} 0 & -1 \\ 1 & 0 \end{bmatrix}
\end{aligned} \tag{2.3.4}$$

yielding the following simplified third-order model version

$$\begin{aligned}
\frac{d\omega}{dt} &= \mu\mathbf{I}^{\mathrm{T}}\mathfrak{I}\boldsymbol{\Psi} - \frac{T_L}{J} \\
\frac{d\boldsymbol{\Psi}}{dt} &= -\alpha\boldsymbol{\Psi} + n_p\omega\mathfrak{I}\boldsymbol{\Psi} + \alpha M\mathbf{I}
\end{aligned} \tag{2.3.5}$$

Founding a solution to the third-order model is quite complicated, but making use of the following globally defined change of coordinates [10]

$$\mathbf{Y} = e^{-n_p\theta\mathfrak{I}}\mathbf{\Psi} \qquad \mathbf{X} = e^{-n_p\theta\mathfrak{I}}\mathbf{I} \tag{2.3.6}$$

where θ is the rotor angular displacement, that is,

$$\dot{\theta} = \omega \tag{2.3.7}$$

the exponential factor that appears in (2.3.6) it is a rotational matrix that rotates with the actual mechanical speed

$$e^{-n_p\theta\mathfrak{I}} = \begin{bmatrix} \cos(n_p\theta) & sin(n_p\theta) \\ -sin(n_p\theta) & \cos(n_p\theta) \end{bmatrix} \tag{2.3.8}$$

applying the last transformation to the system (2.3.5) yields the following bilinear model that can be easily solved

$$\begin{aligned} \frac{d\omega}{dt} &= \mu\mathbf{X}^T\mathfrak{I}\mathbf{Y} - \frac{T_L}{J} \\ \frac{d\mathbf{Y}}{dt} &= -\alpha\mathbf{Y} + \alpha M\mathbf{X} \end{aligned} \tag{2.3.9}$$

where the transformed current $\mathbf{X}$ can be considered as an input [1] in the third-order model or a pseudo-input in the fifth-order model. In spite of the simplicity of the model, this is not an obvious fact that can be exactly discretized, and is possible only due to the particular form of the bilinear term in (2.3.9).

Founding a solution to (2.3.9) involves integral operations, where we suppose that the controls are applied in a piecewise constant fashion so that control is constant over the integration interval $[kT,(k+1)T)$, $k = 0,1,2,\ldots$, where $T > 0$ is the *sampling time* or the time between data (the super-index T over any vector it means the transpose of that vector).

We start by solving the second differential equation in (2.3.9)

$$\frac{d\mathbf{Y}}{dt} + \alpha\mathbf{Y} = \alpha M\mathbf{X} \tag{2.3.10}$$

we can easily see that an integral factor of this differential equation is

$$e^{\alpha t} \tag{2.3.11}$$

multiplying the differential equation in (2.3.10) by the integral factor in (2.3.11)

$$e^{\alpha t}\frac{d\mathbf{Y}}{dt} + \alpha e^{\alpha t}\mathbf{Y} = \alpha M e^{\alpha t}\mathbf{X} \tag{2.3.12}$$

simplifying and solving (2.3.12), considering that input $\mathbf{X}$ is always constant during the integration interval time

$$\mathbf{Y}(t) = e^{-\alpha t}\mathbf{Y}(0) + M(1 - e^{-\alpha t})\mathbf{X} \tag{2.3.13}$$

Let us turn to the electromechanical equation; solving it, yields to

$$\begin{aligned} \frac{d\omega}{dt} &= \mu\mathbf{X}^{\mathrm{T}}\Im\mathbf{Y} - \frac{T_L}{J} \\ d\omega &= \mu\mathbf{X}^{\mathrm{T}}\Im\mathbf{Y}dt - \frac{T_L}{J}dt \\ \omega(t) &= \omega(0) + \mu\mathbf{X}^{\mathrm{T}}\Im\int_0^t \mathbf{Y}(s)ds - \frac{T_L}{J}(t-0) \end{aligned} \tag{2.3.14}$$

Solving the last integral of (2.3.14) separately, where s is a dummy integration variable

$$\begin{aligned}\int_0^t \mathbf{Y}(s)ds &= \mathbf{Y}(0)\int_0^t e^{-\alpha s}ds + M\mathbf{X}\int_0^t ds - M\mathbf{X}\int_0^t e^{-\alpha s}ds \\ \int_0^t \mathbf{Y}(s)ds &= -\frac{\mathbf{Y}(0)}{\alpha}\left[e^{-\alpha t}-1\right]+M\mathbf{X}t-\frac{M\mathbf{X}}{\alpha}\left[e^{-\alpha t}-1\right]\end{aligned} \tag{2.3.15}$$

and using the skew-symmetry of $\mathfrak{I}$

$$\mathbf{X}^T\mathfrak{I}\mathbf{X}=0 \tag{2.3.16}$$

we can assure that

$$\mu\mathbf{X}^{\mathrm{T}}\mathfrak{I}\int_0^t \mathbf{Y}(s)ds = \frac{\mu}{\alpha}\left(1-e^{-\alpha t}\right)\mathbf{X}^{\mathrm{T}}\mathfrak{I}\mathbf{Y}(0) \tag{2.3.17}$$

to finally yield

$$\omega(t)=\omega(0)+\frac{\mu}{\alpha}\left(1-e^{-\alpha t}\right)\mathbf{X}^{\mathrm{T}}\mathfrak{I}\mathbf{Y}(0)-\frac{Tl}{J}(t-0) \tag{2.3.18}$$

Solution to system (2.3.9) were found from an initial time $t_0=0$ to an arbitrary time t, but in order to change the solution of (2.3.9) equally to the same steps of the discrete control input [1], we define time t as $t=t_1=T$

$$\begin{aligned}\omega(t_1)&=\omega(t_0)+\frac{\mu}{\alpha}\left(1-e^{-\alpha T}\right)\mathbf{X}^T(t_0)\mathfrak{I}\mathbf{Y}(t_0)-\frac{T_L}{J}T \\ \mathbf{Y}(t_1)&=e^{-\alpha T}\mathbf{Y}(t_0)+M\left[1-e^{-\alpha T}\right]\mathbf{X}(t_0)\end{aligned} \tag{2.3.19}$$

Noting that, only with initial conditions at time $t_0=0$ we know the states at time t_1. We can use the state equations in (2.3.19) as recursive equations, that is, taking as initial conditions the states just founded at time t_1, we found the states at time t_2, so, any discrete

time instant can be known only with the previous information. In a general form, the initial time is kT and the states are found in a $(k+1)T$ time. This is the way that it is implemented in a digital computer.

Defining a common notation [12]

$$\mathbf{X}_K \equiv \mathbf{X}(kT) \tag{2.3.20}$$

Making use of the new notation, we finally have

$$\begin{aligned} \omega_{k+1} &= \omega_k + \frac{\mu}{\alpha}\left(1 - e^{-\alpha T}\right)\mathbf{X}_k^T \Im \mathbf{Y}_k - \frac{T_{Lk}}{J}T \\ \mathbf{Y}_{k+1} &= e^{-\alpha T}\mathbf{Y}_k + M\left[1 - e^{-\alpha T}\right]\mathbf{X}_k \end{aligned} \tag{2.3.21}$$

This system is a discrete-time version of the transformed one, where it only takes values at time instants multiples of T To take this system to the original states, we need to make a backward transformation with the following change of coordinates

$$\mathbf{\Psi} = e^{n_p \theta \Im}\mathbf{Y} \quad \mathbf{I} = e^{n_p \theta \Im}\mathbf{X} \tag{2.3.22}$$

With some computations, we yield to

$$\begin{aligned} \omega_{k+1} &= \omega_k + \frac{\mu}{\alpha}\left(1 - e^{-\alpha T}\right)M\left(i_k^\beta \psi_k^\alpha - i_k^\alpha \psi_k^\beta\right) - \left(\frac{T}{J}\right)T_{Lk} \\ \psi_{k+1}^\alpha &= \cos\left(n_p \theta_{k+1}\right)\rho_1 - sin\left(n_p \theta_{k+1}\right)\rho_2 \\ \psi_{k+1}^\beta &= sin\left(n_p \theta_{k+1}\right)\rho_1 + \cos\left(n_p \theta_{k+1}\right)\rho_2 \end{aligned} \tag{2.3.23}$$

where

$$\begin{aligned} \rho_1 &= a\left(\cos(n_p\theta_k)\psi_k^\alpha + sin(n_p\theta_k)\psi_k^\beta\right) + (1-a)M\left(\cos(n_p\theta_k)i_k^\alpha + sin(n_p\theta_k)i_k^\beta\right) \\ \rho_2 &= a\left(\cos(n_p\theta_k)\psi_k^\beta - sin(n_p\theta_k)\psi_k^\alpha\right) + (1-a)M\left(\cos(n_p\theta_k)i_k^\beta - sin(n_p\theta_k)i_k^\alpha\right) \end{aligned} \tag{2.3.24}$$

To obtain the rotor position θ we proceed in the same way, i.e. to solve the equation, describe it with the right notation, and make a backward change of coordinates

$$\frac{d\theta}{dt} = \omega$$
$$d\theta = \omega dt$$
$$\theta(t) - \theta(0) = \int_0^t \omega(s)ds$$
$$\theta(t) = \theta(0) + \omega(0)\int_0^t ds + \frac{\mu}{\alpha}\int_0^t \left(1 - e^{-\alpha s}\right)ds\,\mathbf{X}^T \Im\mathbf{Y}(0) - \frac{T_L}{J}\int_0^t sds$$
$$= \theta(0) + \omega(0)t + \frac{\mu}{\alpha}\left[t + \frac{1}{\alpha}\left(e^{-\alpha t} - 1\right)\right]\mathbf{X}^T \Im\mathbf{Y}(0) - \frac{T_{Lk}}{2J}t^2$$
$$\theta_{k+1} = \theta_k + \omega_k T + \frac{\mu}{\alpha}\left[T - \frac{1}{\alpha}\left(1 - e^{-\alpha T}\right)\right]\mathbf{X}_k^T \Im\mathbf{Y}_k - \frac{T_{Lk}}{2J}T^2$$
$$= \theta_k + \omega_k T + \frac{\mu}{\alpha}\left[T - \frac{1}{\alpha}\left(1 - e^{-\alpha T}\right)\right]M\left(i_k^\beta \psi_k^\alpha - i_k^\alpha \psi_k^\beta\right) - \frac{T_{Lk}}{2J}T^2$$

We have exactly discretize the current-fed induction motor third-order model, but there are left two dynamical equations (current differential equations) to discretize, that are discretized by a first order Taylor series [4]

$$\begin{aligned} i_{k+1}^\alpha &= i_k^\alpha + (\alpha\beta\psi_k^\alpha + n_p\beta\omega_k\psi_k^\beta - \gamma i_k^\alpha + \frac{1}{\sigma}u_k^\alpha)T \\ i_{k+1}^\beta &= i_k^\beta + (\alpha\beta\psi_k^\beta - n_p\beta\omega_k\psi_k^\alpha - \gamma i_k^\beta + \frac{1}{\sigma}u_k^\beta)T \end{aligned} \tag{2.3.25}$$

If we define the following variables

$$\begin{aligned} \varphi_k^\alpha &= i_k^\alpha + \alpha\beta T\psi_k^\alpha + n_p\beta T\omega_k\psi_k^\beta - \gamma T i_k^\alpha \\ \varphi_k^\beta &= i_k^\beta + \alpha\beta T\psi_k^\beta - n_p\beta T\omega_k\psi_k^\alpha - \gamma T i_k^\beta \end{aligned} \tag{2.3.26}$$

Using the new defined variables, we realize a compact description of the current dynamical equations in (2.3.25)

$$i_{k+1}^{\alpha} = \varphi_k^{\alpha} + \frac{T}{\sigma} u_k^{\alpha}$$
$$i_{k+1}^{\beta} = \varphi_k^{\beta} + \frac{T}{\sigma} u_k^{\beta} \qquad (2.3.27)$$

Finally, putting all together, we feature the discrete-time version of the induction motor model

$$\omega_{k+1} = \omega_k + \frac{\mu}{\alpha}(1-a)M\left(i_k^{\beta}\psi_k^{\alpha} - i_k^{\alpha}\psi_k^{\beta}\right) - \left(\frac{T}{J}\right)T_{Lk}$$
$$\psi_{k+1}^{\alpha} = \cos\left(n_p\theta_{k+1}\right)\rho_1 - sin\left(n_p\theta_{k+1}\right)\rho_2$$
$$\psi_{k+1}^{\beta} = sin\left(n_p\theta_{k+1}\right)\rho_1 + \cos\left(n_p\theta_{k+1}\right)\rho_2$$
$$i_{k+1}^{\alpha} = \varphi_k^{\alpha} + \frac{T}{\sigma} u_k^{\alpha}$$
$$i_{k+1}^{\beta} = \varphi_k^{\beta} + \frac{T}{\sigma} u_k^{\beta}$$
$$\theta_{k+1} = \theta_k + \omega_k T + \frac{\mu}{\alpha}\left[T - \frac{1}{\alpha}(1-a)\right]M(i_k^{\beta}\psi_k^{\alpha} - i_k^{\alpha}\psi_k^{\beta}) - \frac{T_{Lk}}{2J}T^2$$

where

$$\rho_1 = a\left(\cos(n_p\theta_k)\psi_k^{\alpha} + sin(n_p\theta_k)\psi_k^{\beta}\right) + (1-a)M\left(\cos(n_p\theta_k)i_k^{\alpha} + sin(n_p\theta_k)i_k^{\beta}\right)$$
$$\rho_2 = a\left(\cos(n_p\theta_k)\psi_k^{\beta} - sin(n_p\theta_k)\psi_k^{\alpha}\right) + (1-a)M\left(\cos(n_p\theta_k)i_k^{\beta} - sin(n_p\theta_k)i_k^{\alpha}\right)$$

$$\varphi_k^{\alpha} = i_k^{\alpha} + \alpha\beta T\psi_k^{\alpha} + n_p\beta T\omega_k\psi_k^{\beta} - \gamma T i_k^{\alpha}$$
$$\varphi_k^{\beta} = i_k^{\beta} + \alpha\beta T\psi_k^{\beta} - n_p\beta T\omega_k\psi_k^{\alpha} - \gamma T i_k^{\beta}$$

$$\alpha = \frac{R_r}{L_r} \qquad \gamma = \frac{M^2 R_r}{\sigma L_r^2} + \frac{Rs}{\sigma} \qquad \sigma = L_s - \frac{M^2}{L_r}$$
$$\beta = \frac{M}{\sigma L_r} \qquad a = e^{-\alpha T} \qquad \mu = \frac{Mn_p}{JL_r}$$

Figure 2.11 confronts continuos-time and discrete-time open-loop simulations, where the speed is in $\frac{rad}{\sec}$, voltages are in *volts*, currents in *amperes* and *fluxes* are in wb^2; all these states are with respect to the α component.

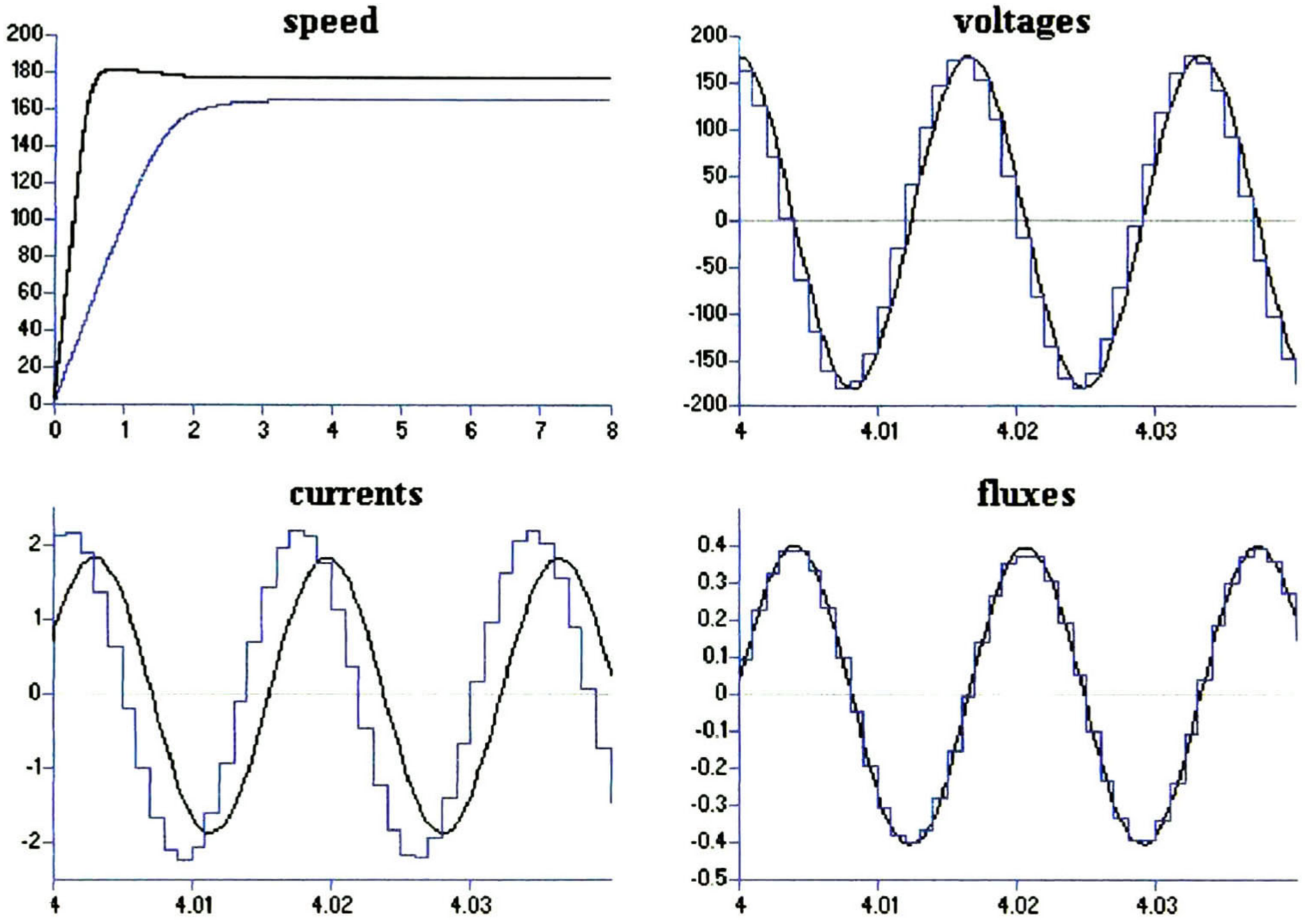

Figure 2.11. Continuos states (___) versus discrete states (___).

Note that the discrete signals track the continuous signals with a considerable amount of error. The reason of this error is that the current equations are numerically integrated using Euler (first-order Taylor series). The control appears in the current equations, it means that the error introduced by Euler's method is satisfied the matching condition, and therefore it can be eliminated by the control action .

Chapter three

Theoretical tools

3.1 INTRODUCTION

This chapter introduces the mathematical control tools that are needed to accomplish the control objectives. Since the output variables are to be controlled; they are required to track a reference signal provided by exosystems [7], such exosystems are treated here, even load is considered as an exosystem for simulations proposes. Then, general concepts for sliding mode control are shown, and are developed to the discrete-time domain [16] where the control is calculated. Another important issue to deal with, is the so-called block control technique [16], this technique is developed for nonlinear discrete-time systems and is useful to transform the system into a tracking error linear one, where a sliding surface is drawn for sliding mode control. And finally, a section is devoted for state estimation due to the unreachable fluxes and the difficult to measure load; where an observer is developed for discrete-time nonlinear electromechanical systems.

3.2 EXOSYSTEMS

Reference signals represent the desired output behavior of the induction motor, and disturbances (load) affecting the motor as well, these signals are generated from external systems called exosystems. Figure 3.1 shows a generic time response of a second-order reference signal, where K represents the desired amplitude and $1/\omega_n$ is the time constant.

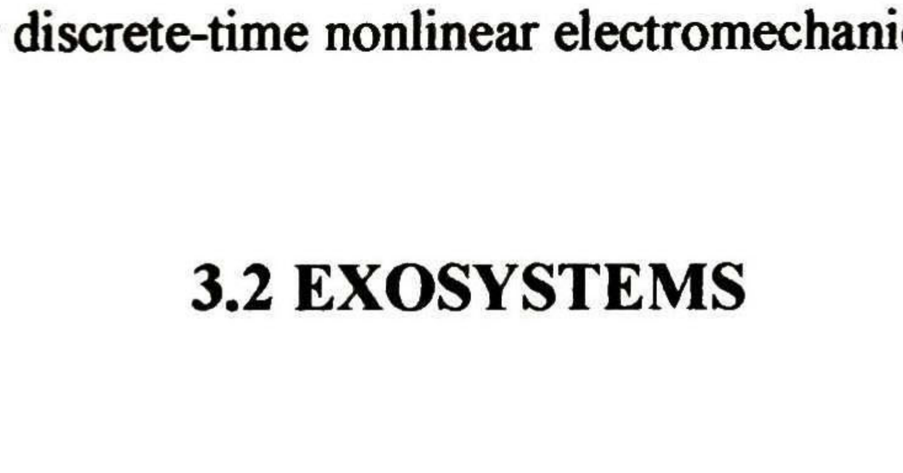

Figure 3.1. Graph from the second order exosystem.

Note that the final value is reached close to $5/\omega_n$ seconds, according to the fact that the steady state is reached in about five time constants. This reference signal is used in velocity and flux amplitude tracking and is generated by the following continuos-time second-order exosystem

$$\begin{bmatrix} \frac{d\omega^1}{dt} \\ \frac{d\omega^2}{dt} \end{bmatrix} = \begin{bmatrix} 0 & 1 \\ -\omega_n{}^2 & -2\omega_n \end{bmatrix} \begin{bmatrix} \omega^1 \\ \omega^2 \end{bmatrix} + \begin{bmatrix} 0 \\ \omega_n^2 \end{bmatrix} u \tag{3.2.1}$$

where ω^1 is the reference signal, and the input u corresponds directly to the desired K amplitude. Now we show this model in matrix form

$$\frac{d\boldsymbol{\omega}}{dt} = \mathbf{A}_c\boldsymbol{\omega} + \mathbf{B}_c u \tag{3.2.2}$$

A discrete-time representation of (3.2.2) with sampling time T is as follows

$$\boldsymbol{\omega}_{k+1} = \mathbf{A}_d\boldsymbol{\omega}_k + \mathbf{B}_d u_k \tag{3.2.3}$$

where

$$\begin{aligned} \mathbf{A}_d = \boldsymbol{\Phi}_c(T) = e^{\mathbf{A}_c T} &= \mathcal{L}^{-1}\left\{(\mathbf{sI} - \mathbf{A}_c)^{-1}\right\}_{t=T} \\ &= \mathcal{L}^{-1}\left\{\begin{bmatrix} \frac{s+2\omega_n}{(s+\omega_n)^2} & \frac{1}{(s+\omega_n)^2} \\ \frac{-\omega_n^2}{(s+\omega_n)^2} & \frac{s}{(s+\omega_n)^2} \end{bmatrix}\right\}_{t=T} \\ &= \begin{bmatrix} e^{-\omega_n T}(1+\omega_n T) & Te^{-\omega_n T} \\ -\omega_n^2 Te^{-\omega n T} & e^{-\omega n T}(1-\omega_n T) \end{bmatrix} \end{aligned} \tag{3.2.4}$$

$$\begin{aligned} \mathbf{B}_d = \int_0^T \boldsymbol{\Phi}_c(v)\mathbf{B}_c dv &= \int_0^T \begin{bmatrix} ve^{-\omega_n v}\omega_n^2 \\ e^{-\omega_n v}(1-\omega n)\omega_n^2 \end{bmatrix} dv \\ &= \begin{bmatrix} 1-\omega_n Te^{-\omega_n T} & -e^{-\omega_n T} \\ \omega_n^2 Te^{-\omega_n T} \end{bmatrix} \end{aligned}$$

Now, Figure 3.2 shows a generic time response of a sinusoidal reference signal.

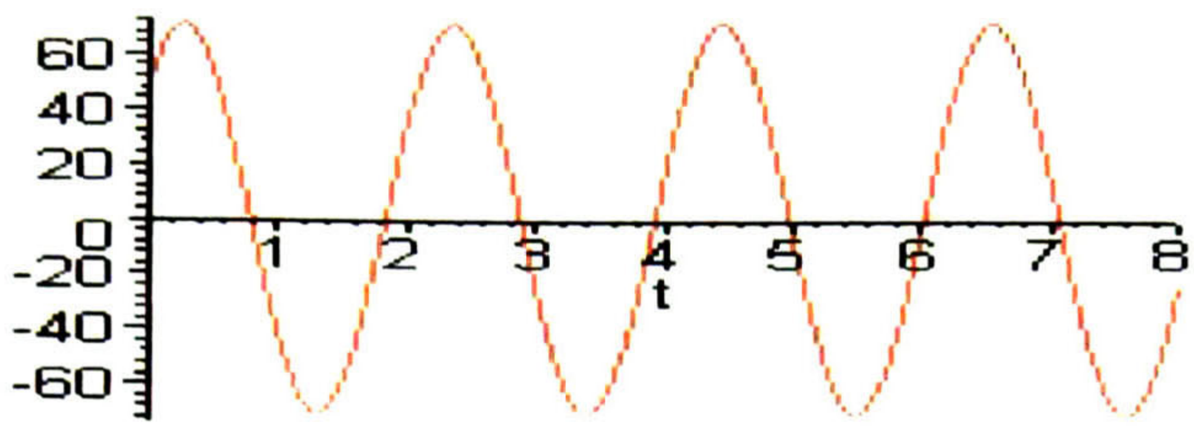

Figure 3.2. Sinusoidal reference graph.

This reference signal is used in velocity tracking only, and is generated by the following continuos-time exosystem:

$$\begin{bmatrix} \frac{d\omega^1}{dt} \\ \frac{d\omega^2}{dt} \end{bmatrix} = \begin{bmatrix} 0 & v \\ -v & 0 \end{bmatrix} \begin{bmatrix} \omega^1 \\ \omega^2 \end{bmatrix} \tag{2.3.5}$$

where v is the desired frequency in $rad/\sec$. Now we show this model in matrix form

$$\dot{\boldsymbol{\omega}} = \mathbf{A}_c \boldsymbol{\omega} \tag{2.3.6}$$

A discrete-time representation of (2.3.6) is given as

$$\boldsymbol{\omega}_{k+1} = \mathbf{A}_d \boldsymbol{\omega}_k \tag{2.3.7}$$

where

$$\begin{aligned} \mathbf{A}_d = \boldsymbol{\Phi}_c(T) &= e^{\mathbf{A}_c T} = \mathcal{L}^{-1}\left\{(\mathbf{sI} - \mathbf{A}_c)^{-1}\right\}_{t=T} \\ &= \mathcal{L}^{-1}\left\{\begin{bmatrix} \frac{s}{s^2+v^2} & \frac{v}{s^2+v^2} \\ \frac{-v}{s^2+v^2} & \frac{s}{s^2+v^2} \end{bmatrix}\right\}_{t=T} \\ &= \begin{bmatrix} \cos(vT) & sin(vT) \\ -sin(vT) & \cos(vT) \end{bmatrix} \end{aligned} \tag{2.3.8}$$

where ω_k^1 is the reference signal, T is the sampling period. If we choose equal initial conditions $\left(\omega_k^1(0) = \omega_k^2(0)\right)$, then the amplitude of the signal will be $\sqrt{2}\omega_k^1(0)$, with v as the frequency.

The load torque is always considered constant, but a first-order exosystem will represent this load. The load is generated by the following exosystem

$$\dot{T}_L = -\frac{1}{\tau}T_L + \frac{1}{\tau}u \tag{2.3.9}$$

It is easy to see that a solution (considering u constant in the integral period time) to (2.3.9) is

$$T_L(t) = e^{\frac{-1}{\tau}t}T_L(0) + \left[1 - e^{\frac{-1}{\tau}t}\right]u \tag{2.3.10}$$

Now, from (2.3.10), the discrete-time model is obtained in a straightforward manner

$$T_{Lk+1} = e^{\frac{-1}{\tau}T}T_{Lk} + \left[1 - e^{\frac{-1}{\tau}T}\right]u_k \tag{2.3.11}$$

where τ is the time constant and u_k is the desired constant level. Figure 3.3 shows a typical response of this system

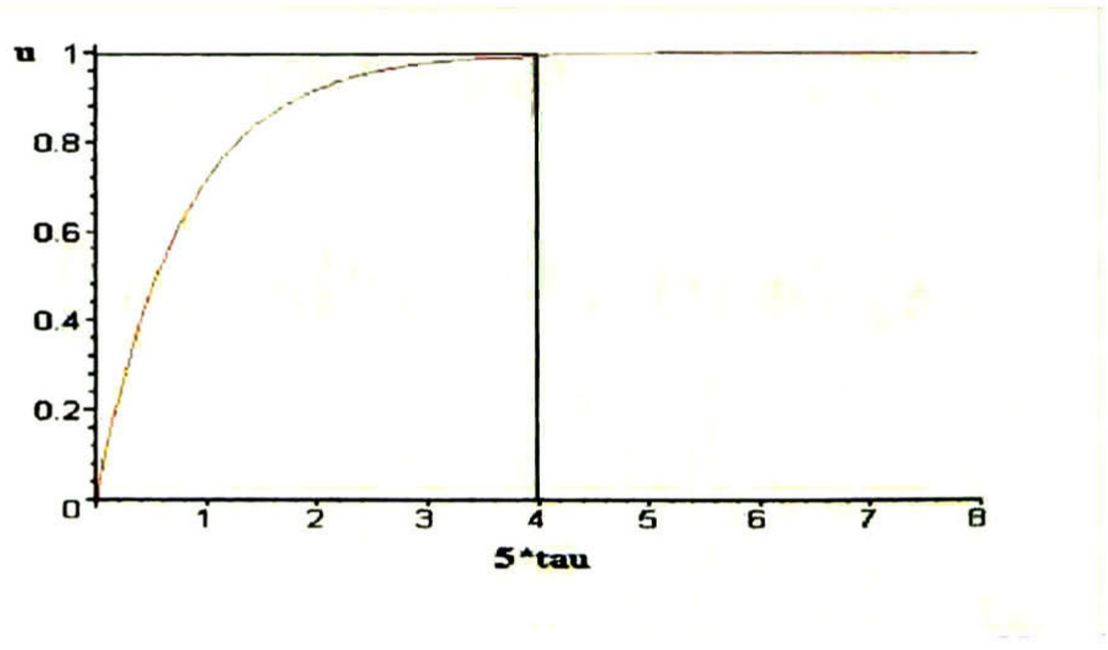

Figure 3.3. Load affecting the motor.

It can be simulated a square-shape load signal, generated from the sinusoidal exosystem, just taking the sign of the output. For a more realistic load signal, we can add noise to the output of the exosystem load. Figure 3.4 shows an example.

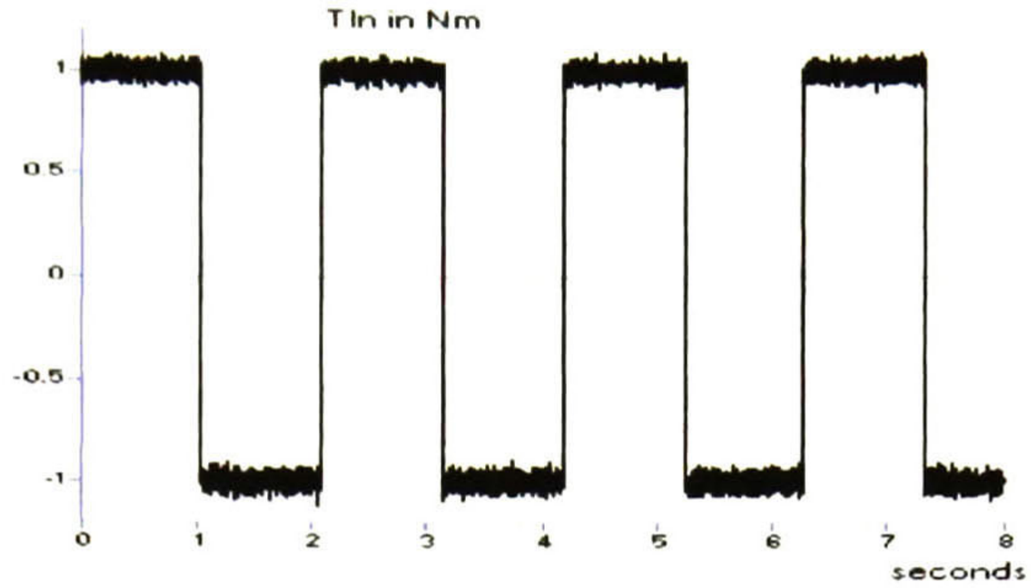

Figure 3.4. Square-shape load with white noise added.

3.3 DISCRETE-TIME SLIDING MODE

The term `*sliding mode control*' first appeared in the context of *variable-structure* systems. Soon sliding modes became the principal operational mode for this class of control systems. Practically all design methods for variable-structure systems are based on deliberate introduction of sliding modes which have played, and are still playing, an exceptional role both in theoretical developments and in practical applications.

A variable structure system consists of a set of continuous subsystems with a proper switching logic. The resulting control action is a discontinuous function of the system states, disturbances, and reference inputs. In the course of the entire history of the automatic control theory development, the intensity of discontinuous control investigation has been maintained at a sufficiently high level. Particularly during the early stage, *relay* or *on-off*, or *bang-bang* regulator, ranked highly for the design of feedback control systems. The reason was twofold: ease of implementation, and efficiency of control hardware.

The term "variable structure control" arises because the "controller structure" around the plant is intentionally changed by some external influence to obtain a desired plant behavior or response.

Since sliding mode control is quite similar in operation to the classical on-off control [8], it will be of interest to investigate this old technique.

When operating with an on-off control, the final corrective device only has two positions or operative states. For this reason, the on-off control is also known as a *two-position* control. If the error signal is positive then the controller will position the final corrective device to a desired position. If the error signal is negative then the controller will position the final corrective device to the other position. The on-off control can conveniently be seen as (considering as a corrective final device) a coil operated valve. When a coil operates the valve, this is open or close all the way. So, a coil operated valve match perfectly in an on-off control system. Figure 3.5(a) shows a position graph of the final corrective device (aperture percentage of the valve) for an ideal on-off control. This Figure considers the temperature as the variable to be controlled with a set point of $120°F$ As can be seen, if the measured temperature value is less than $120°F$ even for a small amount, the valve is set 100% open. If the measured temperature value is great than $120°F$ even for a small amount, the valve is set 0% open, or completely close.

Figure 3.5(b) shows a typical graph of the temperature measured versus time, with the valve position versus the same time axis. We observe that the real temperature value tends to oscillate about the set point. This is a universal characteristic of the on-off control. This particular graph shows an overshoot of $4°F$ in the positive direction and an overshoot of $4°F$ in the negative direction. These values have been taking randomly. The real overshoot depends on the nature of the system and could be different in the negative and positive directions.

We will see later in the following chapter, that the control task reduces to a current control problem. It is well known in the industry that, when the electrical current is the manipulated variable in a closed-loop control system, the final corrective device is of the switching type. This fits perfectly in this work due to the switching control signals obtained, and that are applied to switching devices like the drive of a motor (inverter), as we will see later.

Implementation of a continuous controller in a system with discontinuous inputs (inverter) generally requires PWM, whereas direct implementation of sliding mode control avoids PWM. This justifies the choice of a sliding mode control for an induction motor.

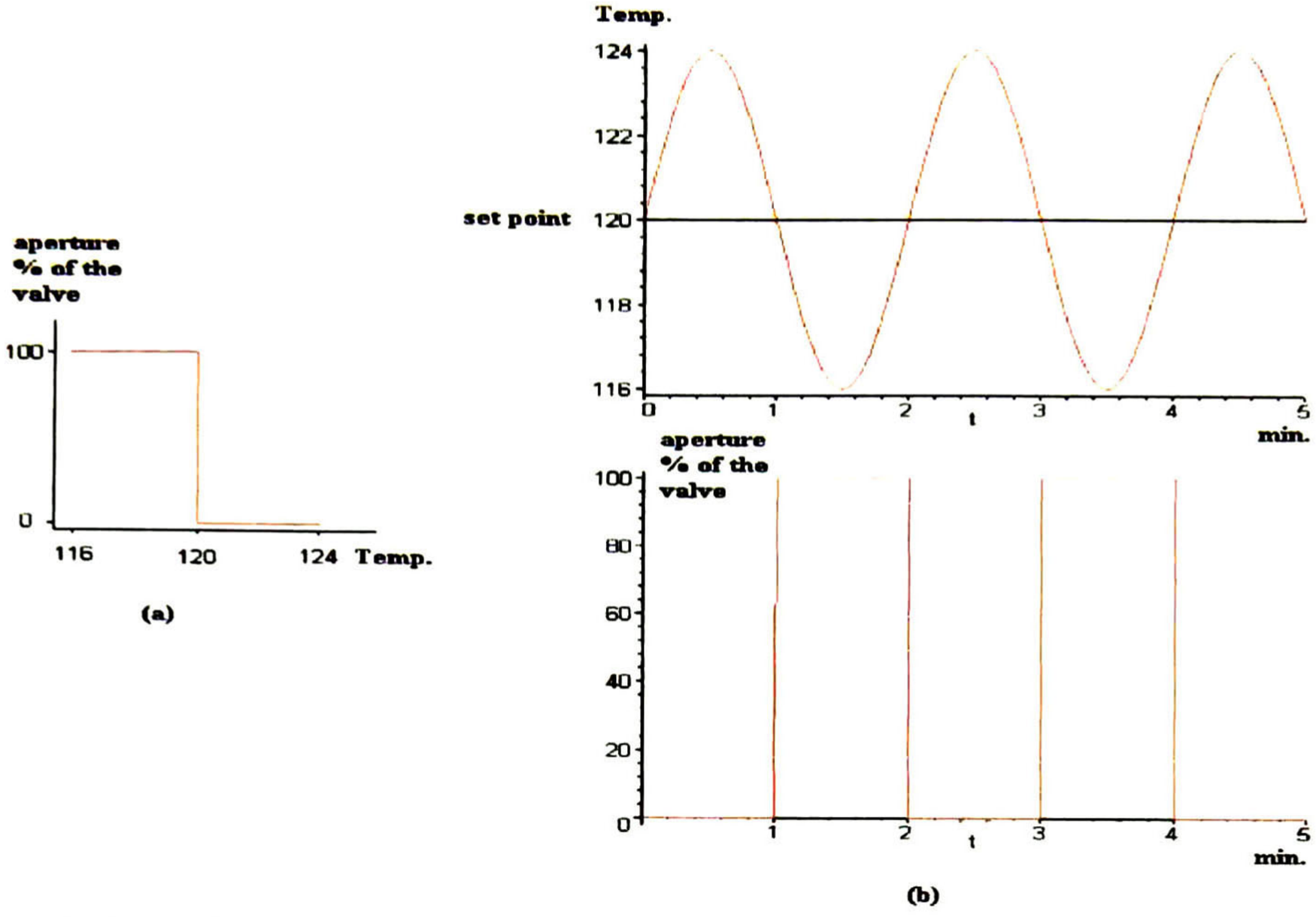

Figure 3.5. (a) Valve position versus measured temperature with a set point of $120°F$.

(b) Real measured temperature versus time and valve aperture versus time.

We shall first specify the class of discontinuous control systems to be considered. The discontinuous control in this class of systems are prescribed prior to the stages of criterion selection and design, unlike, for example, in optimal control where the need for stepwise control arises in the solution of a variational problem. Consider the nonlinear system

$$\begin{aligned} \dot{\mathbf{x}} &= \mathbf{f}(\mathbf{x},\mathbf{u},\mathbf{t}) \\ \mathbf{x} &\in \mathbf{R}^n, \mathbf{u} \in \mathbf{R}^m \end{aligned} \tag{3.3.1}$$

A control design for the system (3.3.1) consists of two steps. First, the surface $\mathbf{s} = \mathbf{0}$ in the state space

$$\mathbf{s}^T = (\mathbf{s}_1,\ldots,\mathbf{s}_m) = \mathbf{0} \tag{3.3.2}$$

where the control experience discontinuities.

And then the continuos control functions $u_i^+(\mathbf{x},t)$ and $u_i^-(\mathbf{x},t)$, beyond the discontinuity surfaces are selected

$$u_i = \begin{cases} u_i^+(\mathbf{x},t) & if \quad s_i(\mathbf{x}) \geq 0 \\ u_i^-(\mathbf{x},t) & if \quad s_i(\mathbf{x}) < 0 \end{cases} \qquad i = 1,...m \tag{3.3.3}$$

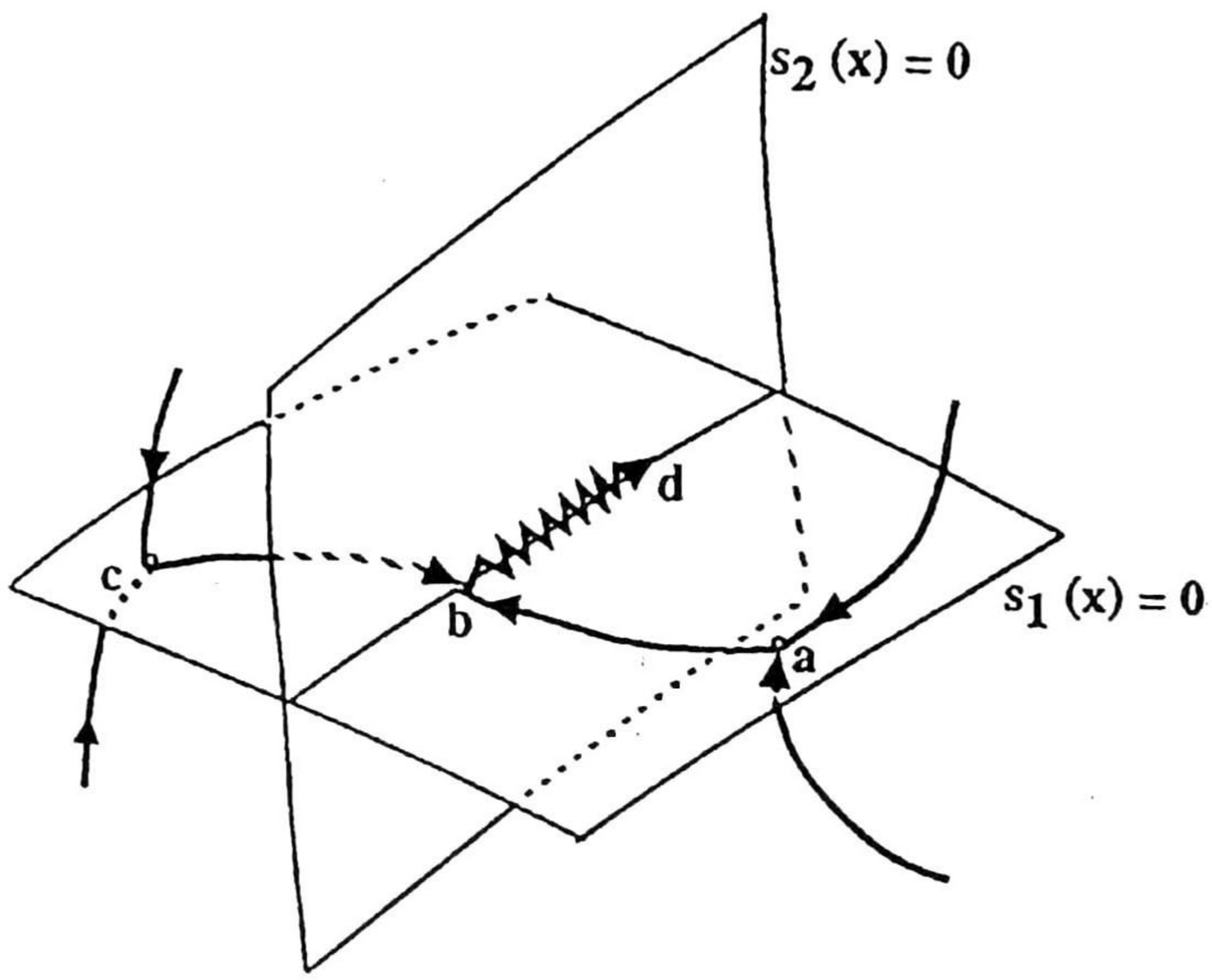

Figure 3.6. State trajectories.

Due to the discontinuity, the state velocity vectors may be directed towards one of the surface, and sliding mode occurs along it (arcs a-b and c-b in Figure 3.6) can arise also along their intersections (arc b-d).

We will clarify all of the above concepts with a numerical example. Consider the state space model

$$\begin{bmatrix} \dot{x}_1 \\ \dot{x}_2 \end{bmatrix} = \begin{bmatrix} 0 & 1 \\ 1 & 2 \end{bmatrix} \begin{bmatrix} x_1 \\ x_2 \end{bmatrix} + \begin{bmatrix} 0 \\ 1 \end{bmatrix} u \tag{3.3.4}$$

Under the variable structure control law

$$u = kx_1 \tag{3.3.5}$$

Where k can be "2" or "-3". This system has two linear structures, one for each k. When $k = -3$, the system has complex eigenvalues and with $k = 2$ the system has real eigenvalues. When switching to $k = -3$, the feedback produces an unstable free motion [6] (unstable focus) satisfying

$$\begin{bmatrix} \dot{x}_1 \\ \dot{x}_2 \end{bmatrix} = \begin{bmatrix} 0 & 1 \\ -2 & 2 \end{bmatrix} \begin{bmatrix} x_1 \\ x_2 \end{bmatrix} \tag{3.3.6}$$

as shown in Figure 3.7.

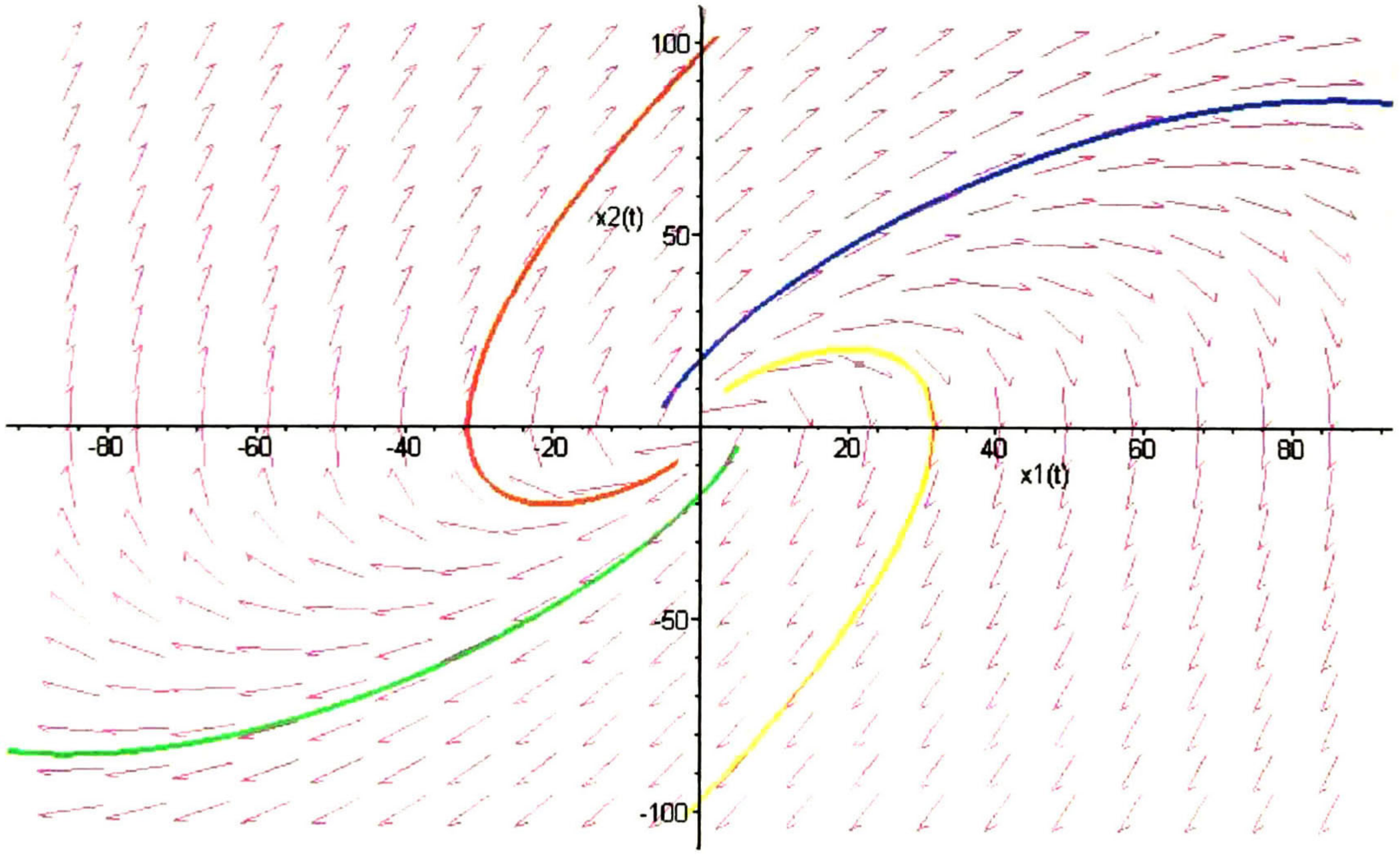

Figure 3.7. Phase portrait of system (3.3.6).

When switching to $k = 2$, the feedback becomes positive and the free motion of the system satisfies

$$\begin{bmatrix} \dot{x}_1 \\ \dot{x}_2 \end{bmatrix} = \begin{bmatrix} 0 & 1 \\ 3 & 2 \end{bmatrix} \begin{bmatrix} x_1 \\ x_2 \end{bmatrix} \tag{3.3.7}$$

The unstable equilibrium point (0,0) is now a saddle point [6] with asymptotes $x_2 = 3x_1$ and $x_2 = -x_1$, as shown in Figure 3.8.

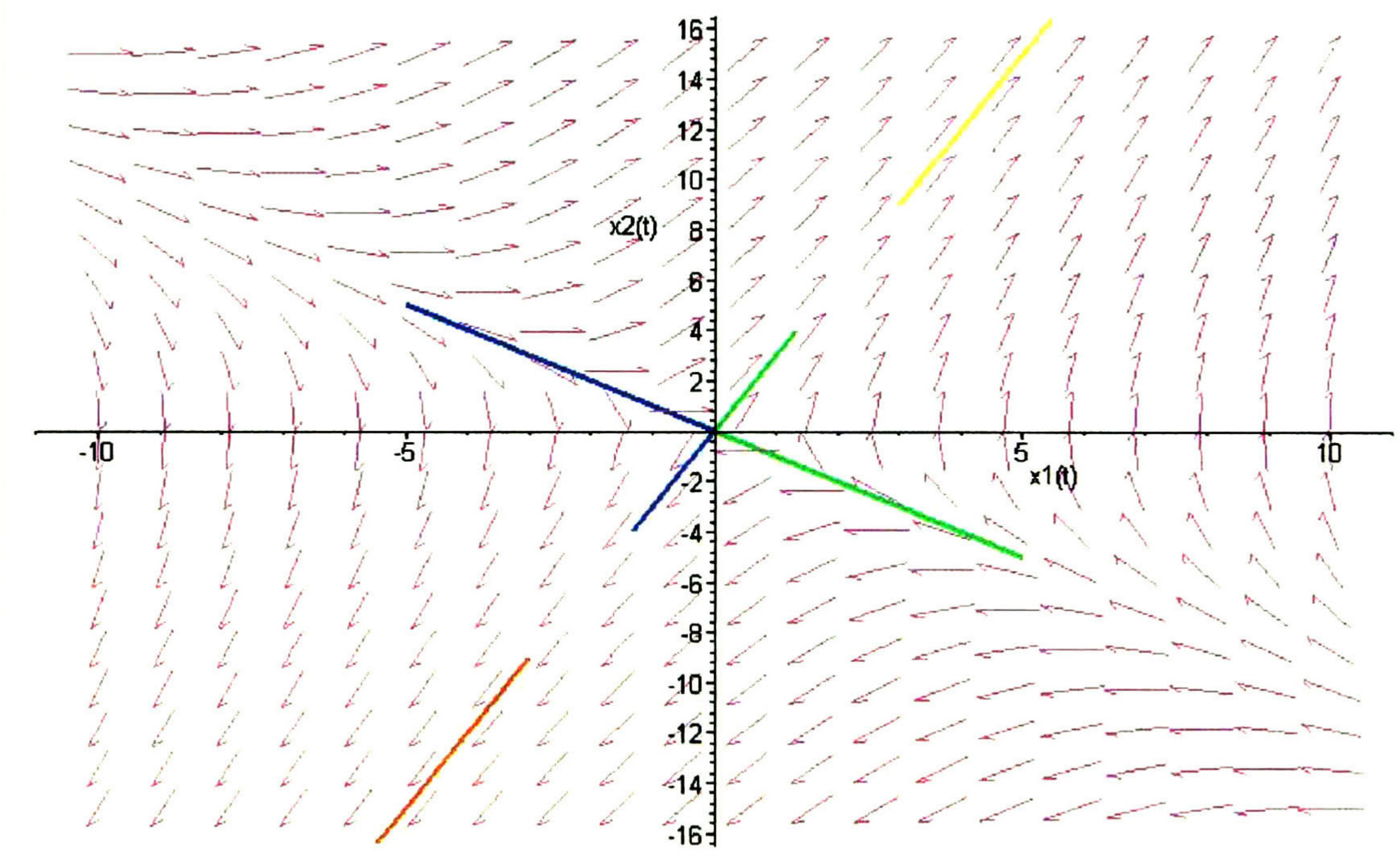

Figure 3.8. Phase portrait of system (3.3.7).

Switching is not selected randomly of course. It occurs with respect to a sliding or switching surface, generally denoted as $s = 0$. To illustrate this notion, consider the surface defined as $s = c_1 x_1 + x_2 = 0$ with $c_1 > 0$. If the feedback is switched according to

$$k = \begin{cases} -3 & \text{if} \quad s_1(x_1, x_2)x_1 \geq 0 \\ 2 & \text{if} \quad s_1(x_1, x_2)x_1 < 0 \end{cases} \tag{3.3.8}$$

this behavior is illustrated in the phase portrait plot of Figure 3.9

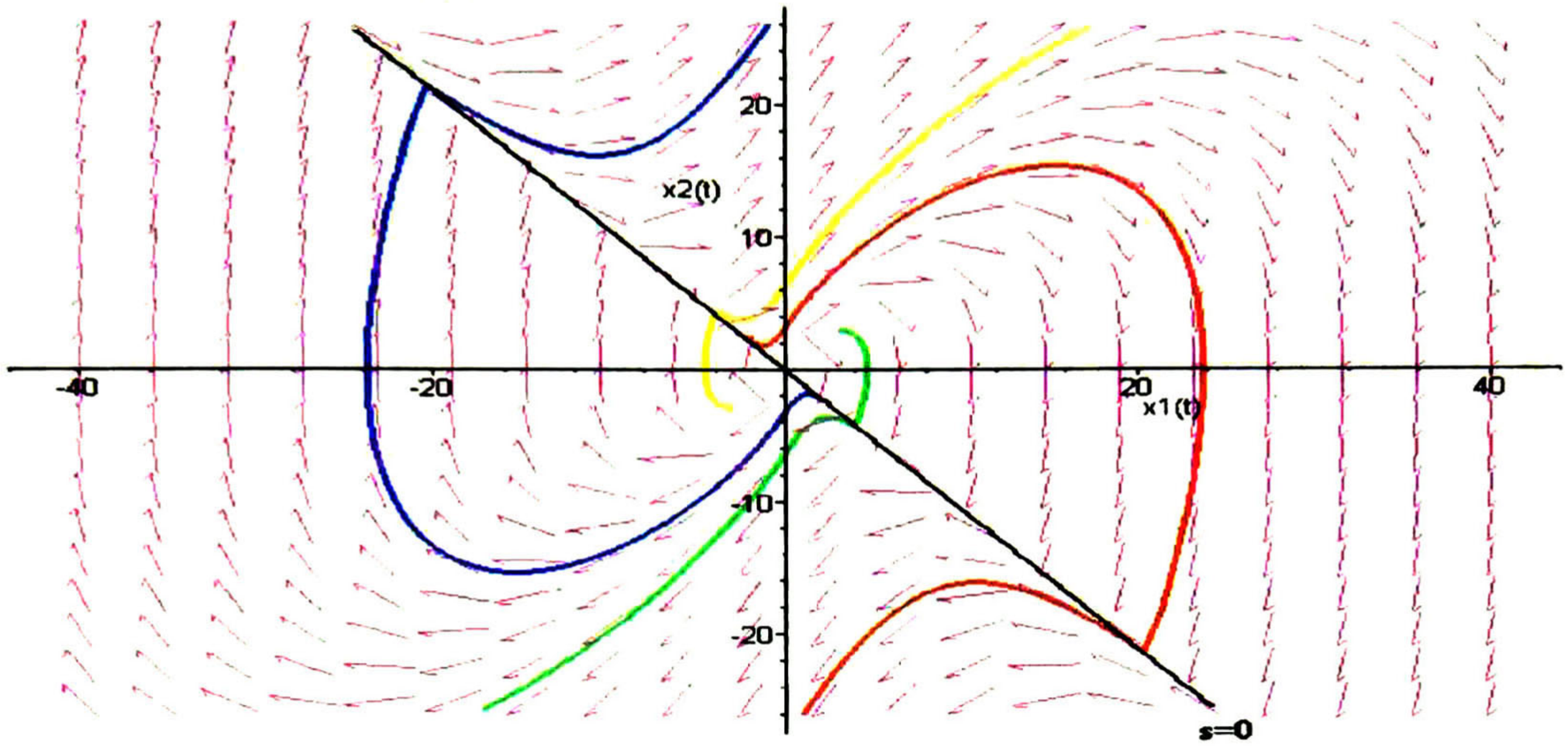

Figure 3.9. Phase portrait when $c_1 > 0$.

Note that this is an unstable system. All state trajectories intercept the surface but are not able to remain on it. On the other hand, if we select $c_1 < 1$, then, the state trajectories remain on the surface because all the velocity vectors always point towards the origin through the surface. Figure 3.10 illustrates this phenomenon.

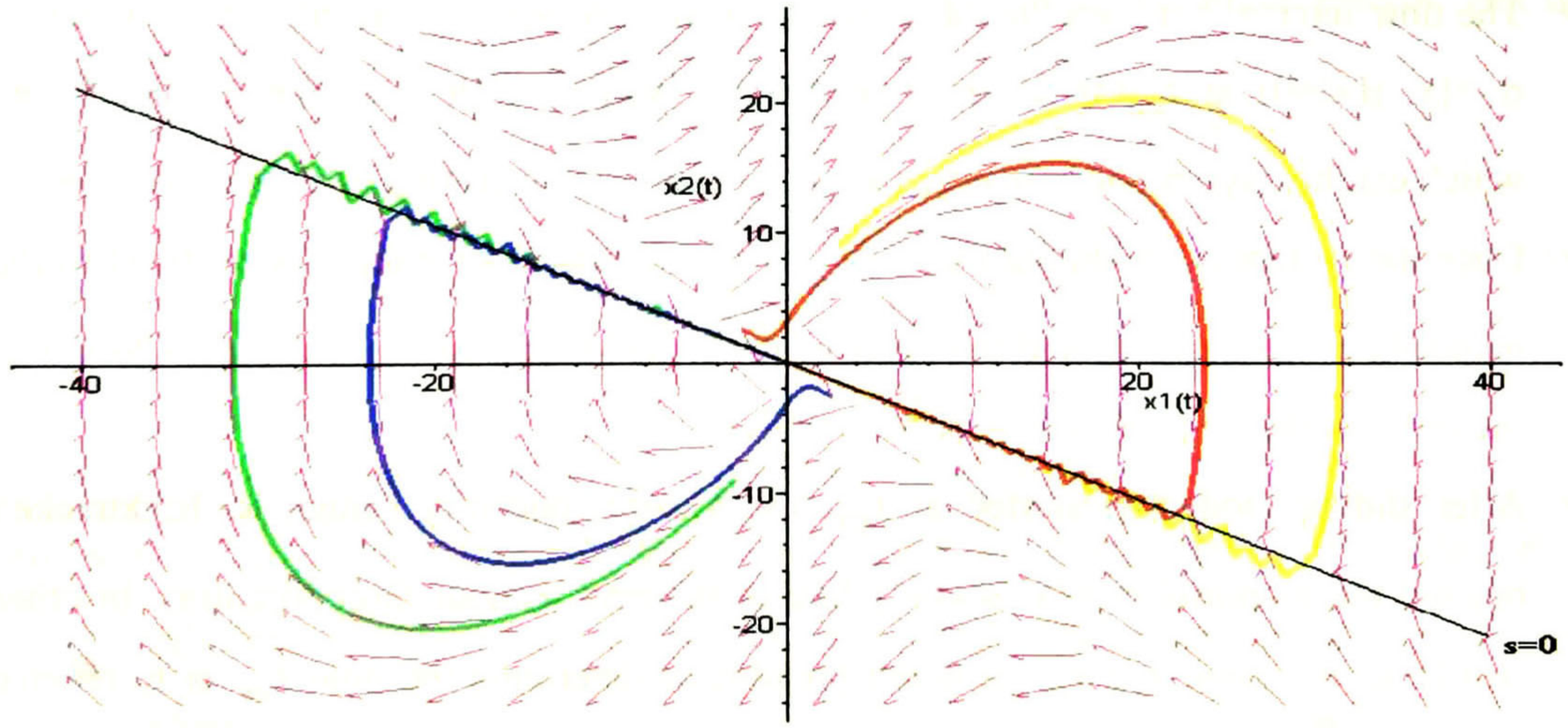

Figure 3.10. Phase portrait when $c_1 < 0$

As suggested by Figures 3.9 and 3.10, different choices of switching surfaces produce radically different system responses. The riches of variable structure control come from this ability to choose various controller structures at different point in time. The above example also illustrates an important notion in VSC. For the switching surface of Figure 3.6, once the state trajectory intercepts the surface it remains on the surface for all subsequent time. This property of remaining on the switching surfaces once intercepted is called a sliding mode. A sliding mode will exist for a system if in the vicinity of the switching surface, the state velocity vector (the derivative of the state vector) is directed toward the surface.

Insuring the existence of a sliding mode on the switching surface is a key necessity in VSC design. Designing the proper surface is the complementary key problem. Thus VSC design breaks down into two major phases. The first is the construction of the switching surface so that the original system or plant restricted to the surface responds in the desired manner. The second phase entails the development of the switching control law (i.e., appropriate switched control gains) which satisfies the set of "sufficient conditions" for the existence and reachability of a sliding mode.

Before developing the concept of discrete–time sliding mode, let us revisit the properties of sliding mode in continuos-time systems with ideal discontinuous control from an engineering viewpoint. The following observations characterize the nature of sliding mode systems:

- The time interval between the initial point t=0 and the reaching of the sliding manifold $\sigma = \{x: s(x)=0\}$ at t_{sm} is finite, in contrast to systems with a continuos control law, which exhibit asymptotic convergence to any manifold consisting of state trajectories.
- Once the system is 'in sliding mode' $\forall\ t \geq t_{sm}$, its trajectory motion is confined to the manifold $\sigma = \{x: s(x)=0\}$ and the order of the closed-loop system dynamics is less than the order of the original uncontrolled system.
- After sliding mode has started at t_{sm}, the system trajectory cannot be backtracked beyond the manifold $\sigma = \{x: s(x)=0\}$ like in systems without discontinuities. In other words, at any point $t_0 \geq t_{sm}$, it is not possible to determine the time t_{sm} or to reverse calculate the trajectory $t_0 < t_{sm}$ based on the information of the system state at t_0.

Now we are going to examine a first-order example system modeled in continuos-time as

$$\dot{x}(t) = g(t) + u(t) \tag{3.3.9}$$

with state $x(t)$, bounded dynamics $|g(t)| \leq g_b$ and control input $u(t)$. To enforce sliding mode on the manifold

$$\sigma = \{x : x(t) = 0\} \tag{3.3.10}$$

a discontinuous control law may be designed as

$$u(t) = -u_0 sign(x(t)) \tag{3.3.11}$$

with available control resources $u_0 > g_b$. The usual Lyapunov-based stability analysis examines

$$V = \frac{1}{2}x^2(t) \tag{3.3.12}$$

Taking the derivative of (3.3.12) along the state trajectories of the given system with the discontinuous control (3.3.11), yields to

$$\begin{aligned} \dot{V}(t) &= x(t)(g(t)) - u_0 sign(x(t))) \\ \dot{V}(t) &\leq |x(t)|(g_b - u_0) \end{aligned} \tag{3.3.13}$$

which testifies the convergence of the state vectors toward the manifold within finite time. An example trajectory is shown in Figure 3.11 with $g(t) = sin(t)$ and $u_0 = 2$, starting from initial conditions $x(t = 0) = 3$. At $t_{sm} = 2.256$ sec, the system reaches the sliding manifold $x = 0$. Thereafter, the motion trajectory is invariantly confined to the manifold via discontinuously switching control, illustrated by a black rectangle in the lower diagram of Figure 3.11.

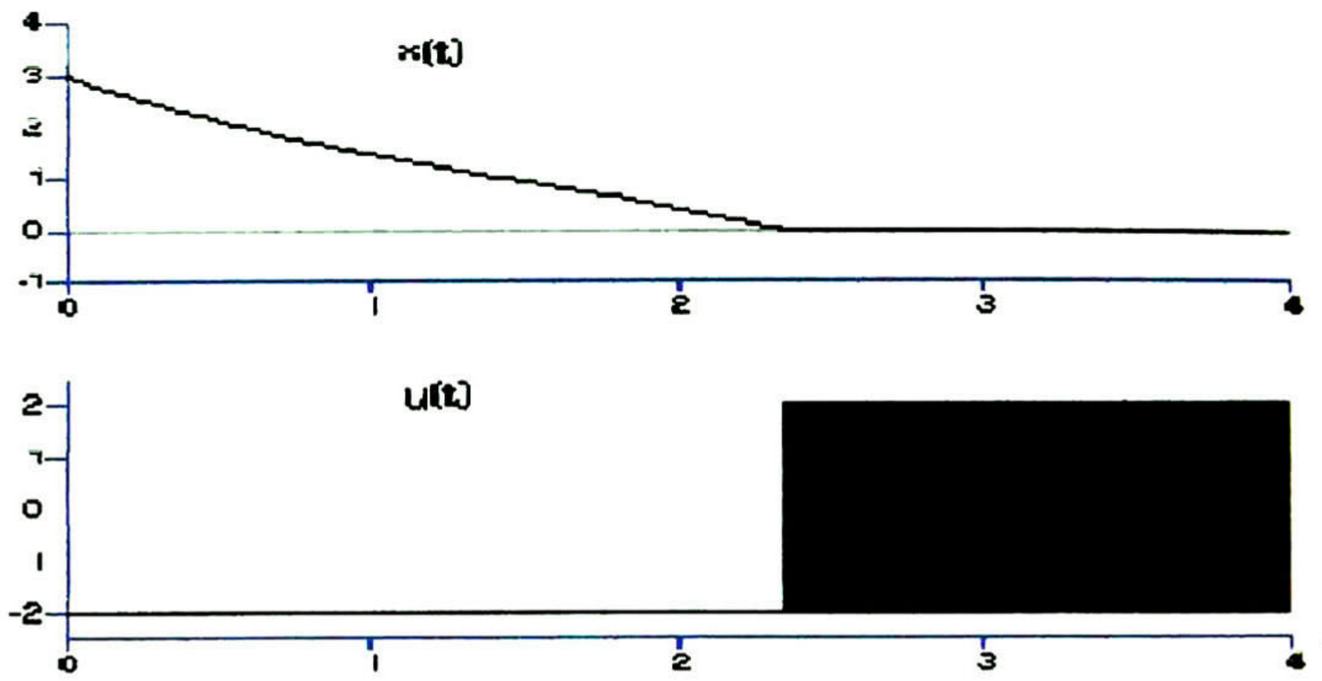

Figure 3.11. Ideal sliding mode in the first-order example achieved via direct analogue implementation of a discontinuous control law with infinitely fast switching.

A direct discrete implementation with sampling time Δt would result in

$$\begin{aligned} x_{k+1} &= x_k + (g_k + u_k)\Delta t \\ u_k &= -u_o sign(x_k) \\ k &= 1,2,\ldots \end{aligned} \tag{3.3.14}$$

where the subscript k denotes the sampling points, e.g. the system state x_k at time $t_k = k\Delta t$. The motion trajectory may not reach the manifold $x = 0$ since control u_k is only calculated at the sampling points k, i.e. the switching frequency is limited by the sampling rate $1/\Delta t$. During the sampling interval Δt, the control is constant and the system behaves like an open-loop system.

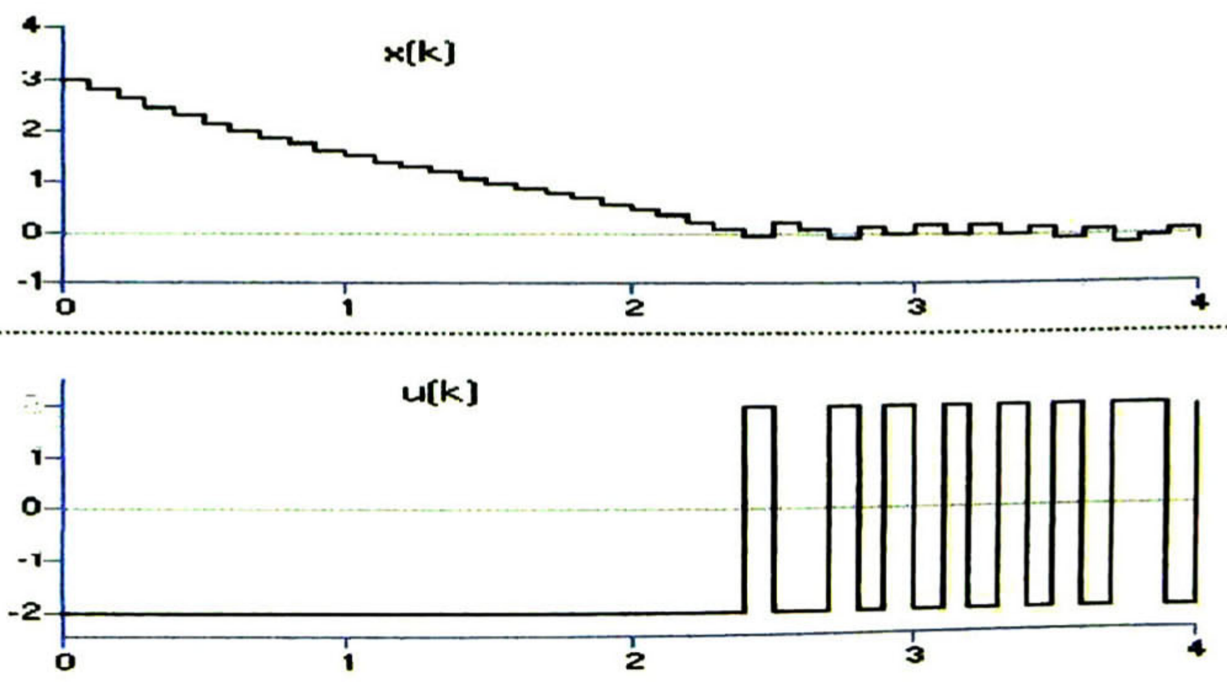

Figure 3.12. Direct implementation of sliding mode control in discrete time.

The example with exaggerated sampling time Δt=0.1s, as depicted in Figure 3.12, illustrates the need to develop a discrete-time sliding mode algorithm rather than implementing the continuos-time version. Note that increasing the sampling rate decreases the amplitude of the discretization chatter and increases its frequency, but may not eliminate this discrete-time phenomenon unless $\Delta t \to 0$. Moreover, the sampling rate of a control system should correspond to the fastest dynamics of the system instead of 'wasting' computational power for the sake of the control algorithm.

To obtain a discrete-time sliding mode just like in continuos-time we first make the following observations. During both time intervals before and after reaching the sliding manifold, the state trajectories are continuous functions of time, and the relation between two values of the state at the ends of a finite time interval $t = [t_0, t_0 + \Delta t]$ may be found by solving (3.3.1) as

$$\mathbf{x}(t_0 + \Delta t) = \mathbf{F}(\mathbf{x}(t_0)) \tag{3.3.15}$$

where $\mathbf{F}(\mathbf{x}(t))$ is a continuous function as well. When derived for each sampling point $t_k = k\Delta t, k = 1,2,...,$ equation (3.3.15) is nothing but the discrete-time representation of the continuous-time prototype (3.3.9), i.e.

$$\mathbf{x}_{k+1} = \mathbf{F}(\mathbf{x}_k) \;\; ; \;\; \mathbf{x}_k \equiv \mathbf{x}(k\Delta t) \tag{3.3.16}$$

Starting from time t_{sm}, the state trajectory belongs to the sliding manifold with $\mathbf{s}(\mathbf{x}(t)) = \mathbf{0}$, or for some $k_{sm} \geq \frac{t_{sm}}{\Delta t}$,

$$\mathbf{s}(\mathbf{x}_k) = 0 \quad (\forall k \geq k_{sm}) \tag{3.3.17}$$

It seems reasonable to call this motion 'sliding mode in discrete-time' or 'discrete-time sliding mode' Note that the right-hand side of the motion equation of the system with discrete-time sliding mode is a continuous state function.

So far, we have generated a discrete-time description of a continuous-time sliding mode system. The next step is to derive a discrete-time control law, which may generate sliding mode in a discrete-time system. Suppose that for any constant control input $\mathbf{u}$ and any initial condition $\mathbf{x}(0)$, the solution to (3.3.1) may be found in closed form, i.e.

$$\mathbf{x}(t) = \mathbf{F}(\mathbf{x}(0), \mathbf{u}) \tag{3.3.18}$$

Now also assume that control $\mathbf{u}$ may be chosen arbitrarily. With the help of (3.3.18), follow the procedure below:

1. At time $t = 0$ select constant control $\mathbf{u}(\mathbf{x}(t = 0), \Delta t)$ for a given time interval Δt such that $\mathbf{s}(\mathbf{x}(t = \Delta t)) = \mathbf{0}$.
2. At time $t = \Delta t$ find constant control $\mathbf{u}(\mathbf{x}(t = \Delta t), \Delta t)$ such that $\mathbf{s}(\mathbf{x}(t = 2\Delta t)) = 0$
3. In general, for each $k = 0,1,2,...,$ at $t = k\Delta t$ choose constant $\mathbf{u}(\mathbf{x}_k, \Delta t)$ such that $\mathbf{s}(\mathbf{x}_{k+1}) = \mathbf{0}$.

In other words, at each sampling point *k*, select $\mathbf{u}_k$ such that, this control input is constant during the next sampling interval Δt, and will achieve $\mathbf{s}(\mathbf{x}_{k+1}) = \mathbf{0}$ at the next sampling point (k+1). During the sampling interval, state $\mathbf{x}(k\Delta t < t < (k+1)\Delta t)$ may not belong to the manifold, i.e. $\mathbf{s}(\mathbf{x}(t)) \neq \mathbf{0}$ is possible for $k\Delta t < t < (k+1)\Delta t$ However, the discrete-time system

$$\begin{aligned} \mathbf{x}_{k+1} &= \mathbf{F}(\mathbf{x}_k, \mathbf{u}_k) \\ \mathbf{u}_k &= \mathbf{u}(\mathbf{x}_k) \end{aligned} \tag{3.3.19}$$

hits the sliding manifold at each sampling point, i.e. $\mathbf{s}(\mathbf{x}_{k+1}) = \mathbf{0}$ $\forall k = 0,1,2,...,$ is fulfilled.

By analogy with continuous-time systems, the control law $\mathbf{u}_k$ that yields motion in the manifold $\mathbf{s} = \mathbf{0}$ will be called 'equivalent control' or represented by $\mathbf{u}_{keq}$. Equivalent control theory may be found in Utkin (1993) [15].

Since $\mathbf{F}(\mathbf{x}(0),\mathbf{u})$ tends to $\mathbf{x}(0)$ as $\Delta t \to 0$, the function $\mathbf{u}(\mathbf{x}(0),\Delta t)$ may exceed the available control resources u_0. As a result, the control resources should bound the control by u_0, to finally yield

$$\mathbf{u}_k = \begin{cases} \mathbf{u}_{keq} & for \quad \|\mathbf{u}_{keq}\| \le u_0 \\ u_0 \dfrac{\mathbf{u}_{keq}}{\|\mathbf{u}_{keq}\|} & for \quad \|\mathbf{u}_{keq}\| > u_0 \end{cases} \tag{3.3.20}$$

Continuing with the first-order system (3.3.9), instead of discontinuous control (3.3.14), control u_k adopt the form of (3.3.20) for scalar case

$$u_k = \begin{cases} u_{keq} & for \quad |u_{keq}| \le u_0 \\ u_0 \dfrac{u_{keq}}{|u_{keq}|} & for \quad |u_{keq}| > u_0 \end{cases} \tag{3.3.21}$$

where u_{keq} is calculated as

$$\begin{aligned} s_{k+1} &= x_{k+1} = x_k + (g_k + u_{k_{eq}})\Delta t = 0 \\ u_{keq} &= -\frac{1}{\Delta t} x_k - g_k \end{aligned} \tag{3.3.22}$$

As a result, the bounded control ($u_0 = 2$) shown in the lower diagram of Figure 3.13 steers state x_k to zero only after a finite number of steps k_{sm}. Thus the manifold is reached after a finite time interval $t_{sm} = k_{sm}\Delta t$ and thereafter the state x_k remains on the manifold. In analogy to continuos-time systems, this motion may be called 'discrete-time sliding mode'

The first-order example clarifies the definition of the term 'discrete-time sliding mode' introduced by Utkin (1999) [16] for an arbitrary finite-dimensional discrete-time system.

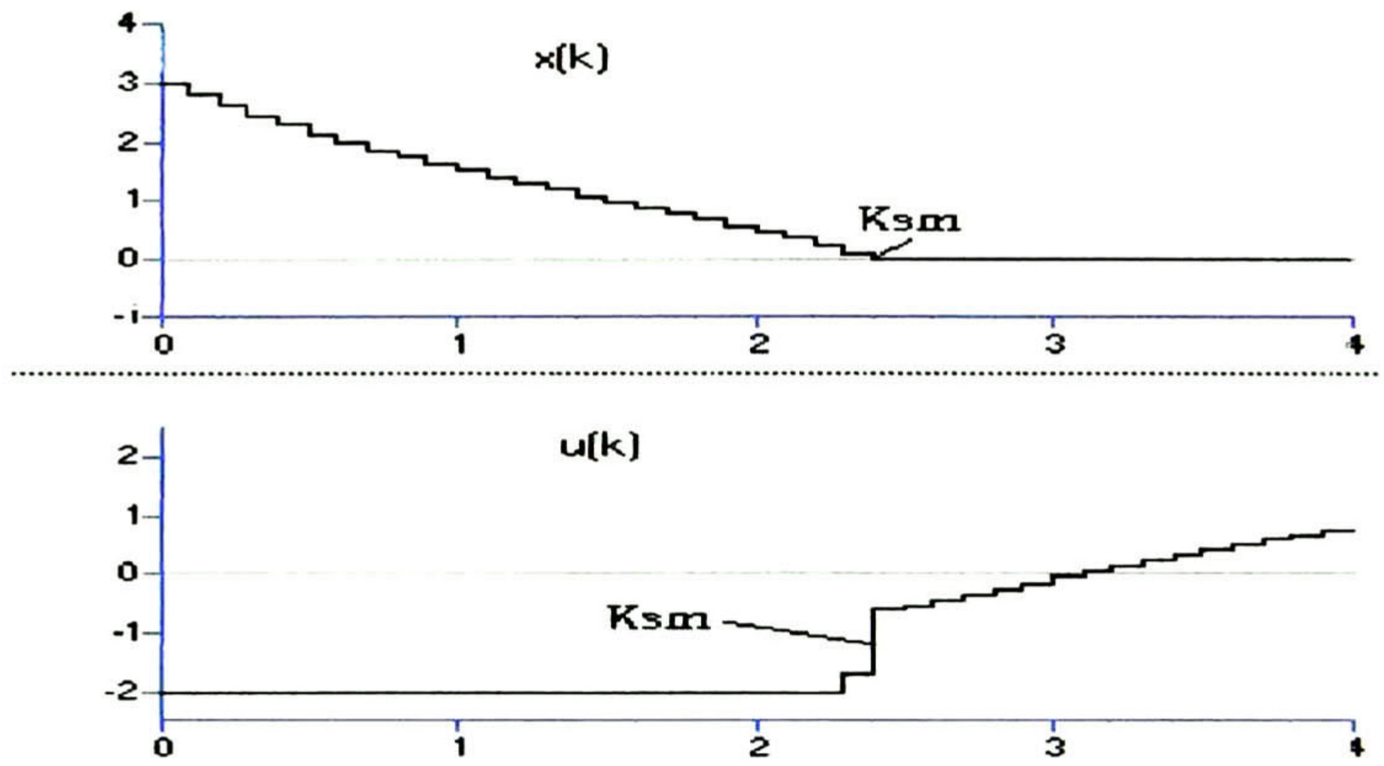

Figure 3.13. Proper implementation of sliding mode control in discrete-time.

3.4 BLOCK CONTROL TECHNIQUE

Consider a nonlinear MIMO perturbed system

$$\begin{aligned} \mathbf{x}_{k+1} &= \mathbf{f}(\mathbf{x}_k) + \mathbf{B}(\mathbf{x}_k)\mathbf{u}_k + \mathbf{d}(\boldsymbol{\omega}_k) \\ \mathbf{y}_k &= \mathbf{h}(\mathbf{x}_k) \end{aligned} \tag{3.4.1}$$

where $\mathbf{x}_k \in \mathbf{R}^n, \mathbf{u}_k \in \mathbf{R}^m, \mathbf{y}_k \in \mathbf{R}^m$ and $\boldsymbol{\omega}_k \in \mathbf{R}^m$; the known perturbation term $\mathbf{d}(\boldsymbol{\omega}_k)$ could result from modelling errors, aging or uncertainties and disturbances which exist in any realistic problem. In a typical situation, we do not know $\boldsymbol{\omega}_k$, but we will consider that is generated from a known exosystem

$$\boldsymbol{\omega}_{k+1} = \mathbf{S}(\boldsymbol{\omega}_k) \tag{3.4.2}$$

Since reference signals are generated by exosystems, system (3.4.2) is considered to generate these signals as well.

3.4.1 Block control form

We present a *Block Controllable Form (BCF)* MIMO system

$$\begin{aligned}
&\mathbf{x}_{k+1}^1 = \mathbf{f}_1(\mathbf{x}_k^1) + \mathbf{B}_1(\mathbf{x}_k^1)\mathbf{x}_k^2 + \mathbf{d}_1(\boldsymbol{\omega}_k)\\
&\mathbf{x}_{k+1}^2 = \mathbf{f}_2(\mathbf{x}_k^1,\mathbf{x}_k^2) + \mathbf{B}_2(\mathbf{x}_k^1,\mathbf{x}_k^2)\mathbf{x}_k^3 + \mathbf{d}_2(\boldsymbol{\omega}_k)\\
&\vdots\\
&\mathbf{x}_{k+1}^i = \mathbf{f}_i(\mathbf{x}_k^1,...,\mathbf{x}_k^i) + \mathbf{B}_i(\mathbf{x}_k^1,...,\mathbf{x}_k^i)\mathbf{x}_k^{i+1} + \mathbf{d}_i(\boldsymbol{\omega}_k)\\
&\vdots\\
&\mathbf{x}_{k+1}^r = \mathbf{f}_r(\mathbf{x}_k^1,...,\mathbf{x}_k^r) + \mathbf{B}_r(\mathbf{x}_k^1,...,\mathbf{x}_k^r)\mathbf{u}_k + \mathbf{d}_r(\boldsymbol{\omega}_k)\\
&(i = 3,...,n-1)\\
&\mathbf{y}_k = \mathbf{x}_k^1
\end{aligned} \qquad (3.4.1.1)$$

$$\mathbf{x}_k \in \mathbf{R}^n, \mathbf{u}_k \in \mathbf{R}^m, \mathbf{y}_k \in \mathbf{R}^m, \boldsymbol{\omega}_k \in \mathbf{R}^m$$

where $\mathbf{x}_k = \begin{bmatrix}\mathbf{x}_k^1 & \cdots & \mathbf{x}_k^r\end{bmatrix}^T, \mathbf{x}_j \in R^{n_j}$, and the set of numbers $(n_1,\ldots,n_r)$ define the structure of system (4.3.1.1) as

$$n_1 \le n_2 \le \ldots \le n_r \le m \qquad (3.4.1.2)$$

with the following assumptions:

1. The $\mathbf{B}_j$ matrix has full row rank

$$rank(\mathbf{B}_j) = n_j \quad \forall \mathbf{x} \in \mathbf{R}^n \quad j = 1,\ldots r \qquad (3.4.1.3)$$

with

$$\sum_{j=1}^{r} n_j = n \tag{3.4.1.4}$$

2. The matrix $\mathbf{B}_j$ is bounded

$$\left|\mathbf{B}_j(\mathbf{x}_k^1,\ldots,\mathbf{x}_k^i)\right| \le \beta_i \tag{3.4.1.5}$$

3.4.2 Linearization transformation

In this work, the system (3.4.1.1) will be considered with the following structure:

$$n_1 = n_2 = \ldots = n_r = m \tag{3.4.2.1}$$

We start by defining a new variable, $\mathbf{z}_k^1$, but there are two different ways of defining it depending on the control objectives. If the control objective is that the output $\mathbf{y}_k$ (or state vector $\mathbf{x}_k^1$) can track a desired signal $\mathbf{x}_k^{1\,d}(\boldsymbol{\omega}_k)$ generated by exosystem (3.4.2), then $\mathbf{z}_k^1$ is defined as

$$\mathbf{z}_k^1 = \mathbf{x}_k^1 - \mathbf{x}_k^{1\,d} \tag{3.4.2.2}$$

But, if the control objective is to drive the output toward zero, then $\mathbf{z}_k^1$ is defined as

$$\mathbf{z}_k^1 = \mathbf{x}_k^1 \tag{3.4.2.3}$$

we note that the later is a particular one of (3.4.2.2) where $\mathbf{x}_k^{1\,d}(\boldsymbol{\omega}_k) = \mathbf{0}$, and that we are looking for a unique objective in both cases, that the state $\mathbf{z}_k^1$ tends asymptotically or in

finite time to zero. So, the block control design procedure consist of step-by-step construction of a transformed system with the states

$$\mathbf{z}_k^j = \mathbf{x}_k^j - \mathbf{x}_k^{j^d}, \qquad j = 1,\ldots,r \tag{3.4.2.4}$$

where $\mathbf{x}_k^{j^d}$ is the desired value of $\mathbf{x}_k^j$, which will be defined by a step-step transformation.

Once defined the new first variable (3.4.2.2), we continue with taking one step ahead of that variable

$$\mathbf{z}_{k+1}^1 = \mathbf{f}_1(\mathbf{x}_k^1) + \mathbf{B}_1(\mathbf{x}_k^1)\mathbf{x}_k^2 + \bar{\mathbf{d}}_1(\omega_k) \tag{3.4.2.5}$$

where

$$\bar{\mathbf{d}}_1(\omega_k) = \mathbf{d}_1(\omega_k) - \mathbf{x}_{k+1}^{1^d}(\omega_k) \tag{3.4.2.6}$$

The equation (3.4.2.5) is considered as a block with state $\mathbf{z}_k^1$; and the state $\mathbf{x}_k^2$ handled as a control for this block, must be selected as a function of the state vector $\mathbf{x}_k^1$ in order to shape the desired dynamics of this perturbated block. This task can be solved because of the condition (3.4.1.5), anticipating the desired dynamic of this block as follows

$$\mathbf{z}_{k+1}^1 = \mathbf{f}_1(\mathbf{x}_k^1) + \mathbf{B}_1(\mathbf{x}_k^1)\mathbf{x}_k^2 + \bar{\mathbf{d}}_1(\omega_k) = \mathbf{K}_1\mathbf{z}_k^1 \tag{3.4.2.7}$$

where $\mathbf{K}_1 = diag\{k_{11},\cdots,k_{1m}\}$ and has the following bound,

$$|k_{1q}| < 1 \quad q = 1,\ldots,m \tag{3.4.2.8}$$

to assure stability of (3.4.2.7). From (3.4.2.7), $\mathbf{x}_k^2$ is calculated as

$$\mathbf{x}_k^2 = \left[\mathbf{B}_1(\mathbf{x}_k^1)\right]^{-1}\left(\mathbf{K}_1\mathbf{z}_k^1 - \mathbf{f}_1(\mathbf{x}_k^1) - \bar{\mathbf{d}}_1(\boldsymbol{\omega}_k)\right) \qquad (3.4.2.9)$$

Note that the value of the state $\mathbf{x}_k^2$ (3.4.2.9) is not equal to the real value of the state $\mathbf{x}_k^2$, instead, represents the desired behavior of $\mathbf{x}_k^2$ that will drive the first block to the desired dynamics. In order to avoid confusions we redefine this desired value of $\mathbf{x}_k^2$ as $\mathbf{x}_k^{2^d}$, so, equation (3.4.2.9) is redefined as

$$\mathbf{x}_k^{2^d} = \left[\mathbf{B}_1(\mathbf{x}_k^1)\right]^{-1}\left(\mathbf{K}_1\mathbf{z}_k^1 - \mathbf{f}_1(\mathbf{x}_k^1) - \bar{\mathbf{d}}_1(\boldsymbol{\omega}_k)\right) \qquad (3.4.2.10)$$

Proceeding in the same way, we define a second new variable, $\mathbf{z}_k^2$ as follows

$$\mathbf{z}_k^2 = \mathbf{x}_k^2 - \mathbf{x}_k^{2^d} \qquad (3.4.2.11)$$

Taking one step ahead

$$\begin{aligned}\mathbf{z}_{k+1}^2 &= \mathbf{x}_{k+1}^2 - \mathbf{x}_{k+1}^{2^d} \\ &= \mathbf{f}_2(\mathbf{x}_k^1, \mathbf{x}_k^2) + \mathbf{B}_2(\mathbf{x}_k^1, \mathbf{x}_k^2)\mathbf{x}_k^3 + \mathbf{d}_2\boldsymbol{\omega}_k - \mathbf{x}_{k+1}^{2^d}\end{aligned} \qquad (3.4.2.12)$$

we propose the desired dynamic for this block

$$\mathbf{z}_{k+1}^2 = \mathbf{f}_2(\mathbf{x}_k^1, \mathbf{x}_k^2) + \mathbf{B}_2(\mathbf{x}_k^1, \mathbf{x}_k^2)\mathbf{x}_k^3 + \mathbf{D}_2\boldsymbol{\omega}_k - \mathbf{x}_{k+1}^{2^d} = \mathbf{K}_2\mathbf{z}_k^2 \qquad (3.4.2.13)$$

where $\mathbf{K}_2 = diag\{k_{21}, \cdots, k_{2m}\}$, with

$$|k_{2q}| < 1 \quad q = 1, \ldots, m \qquad (3.4.2.14)$$

From (3.4.2.13), $\mathbf{x}_k^{3^d}$ is calculated as

$$\mathbf{x}_k^{3\,d} = \left[\mathbf{B}_2(\mathbf{x}_k^1, \mathbf{x}_k^2)\right]^{-1}\left(\mathbf{K}_2\mathbf{z}_k^2 - \mathbf{f}_2(\mathbf{x}_k^1, \mathbf{x}_k^2) + \mathbf{x}_{k+1}^{2\,d} - \mathbf{d}_2\boldsymbol{\omega}_k\right) \qquad (3.4.2.15)$$

and so on.

At the last step, the known variable is $\mathbf{x}_k^{r\,d}$, and the last new variable $\mathbf{z}_k^r$ is defined as

$$\mathbf{z}_k^r = \mathbf{x}_k^r - \mathbf{x}_k^{r\,d} \qquad (3.4.2.16)$$

As usually, taking one step ahead

$$\mathbf{z}_{k+1}^r = \mathbf{f}_r(\mathbf{x}_k^1,\ldots,\mathbf{x}_k^r) + \mathbf{B}_r(\mathbf{x}_k^1,\ldots,\mathbf{x}_k^r)\mathbf{u}_k + \mathbf{d}_r\boldsymbol{\omega}_k - \mathbf{x}_{k+1}^{r\,d} \qquad (3.4.2.17)$$

The new $\mathbf{z}_k^j$ variables compound a nonlinear transformation of the state variables defined as

$$\begin{aligned}
\mathbf{z}_k^1 &= \mathbf{x}_k^1 - \mathbf{x}_k^{1\,d} = \varphi_1(\mathbf{x}_k^1, \mathbf{x}_k^{1\,d}, \boldsymbol{\omega}_k)\\
\mathbf{z}_k^2 &= \mathbf{x}_k^2 - \left[\mathbf{B}_1(\mathbf{x}_k^1)\right]^{-1}\left(\mathbf{K}_1\mathbf{z}_k^1 - \mathbf{f}_1(\mathbf{x}_k^1) - \bar{\mathbf{d}}_1(\boldsymbol{\omega}_k)\right) = \varphi_2(\mathbf{x}_k^1, \mathbf{x}_k^2, \boldsymbol{\omega}_k)\\
\mathbf{z}_k^3 &= \mathbf{x}_k^3 - \left[\mathbf{B}_2(\mathbf{x}_k^1, \mathbf{x}_k^2)\right]^{-1}\left(\mathbf{K}_2\mathbf{z}_k^2 - \mathbf{f}_2(\mathbf{x}_k^1, \mathbf{x}_k^2) + \mathbf{x}_{k+1}^{2\,d} - \mathbf{d}_2\boldsymbol{\omega}_k\right) = \varphi_3(\mathbf{x}_k^1, \mathbf{x}_k^2, \mathbf{x}_k^3, \boldsymbol{\omega}_k) \qquad (3.4.2.18)\\
&\vdots\\
\mathbf{z}_k^r &= \mathbf{x}_k^r - \mathbf{x}_k^{r\,d} = \varphi_r(\mathbf{x}_k^1, \mathbf{x}_k^2, \ldots, \mathbf{x}_k^r, \boldsymbol{\omega}_k)
\end{aligned}$$

in this way, we found the diffeomorphic transformation

$$\mathbf{z}_k = \varphi(\mathbf{x}_k, \boldsymbol{\omega}_k) \quad \varphi = (\varphi_1, \ldots, \varphi_r)^T \qquad (3.4.2.19)$$

that simplifies (3.4.1.1)the original system to the following form

$$\begin{aligned}
\mathbf{z}_{k+1}^{1} &= \mathbf{K}_1\mathbf{z}_k^1 + \mathbf{B}_1\mathbf{z}_k^2 \\
\mathbf{z}_{k+1}^{2} &= \mathbf{K}_2\mathbf{z}_k^2 + \mathbf{B}_2\mathbf{z}_k^3 \\
&\vdots \\
\mathbf{z}_{k+1}^{r-1} &= \mathbf{K}_{r-1}\mathbf{z}_k^{r-1} + \mathbf{B}_{r-1}\mathbf{z}_k^r \\
\mathbf{z}_{k+1}^{r} &= \mathbf{f}_r(\mathbf{x}_k^1,....,\mathbf{x}_k^r) + \mathbf{B}_r(\mathbf{x}_k^1,....,\mathbf{x}_k^r)\mathbf{u}_k + \mathbf{d}_r\omega_k - \mathbf{x}_{k+1}^{r\,d}
\end{aligned} \tag{3.4.2.20}$$

3.4.3 Control design

Adding the desired dynamic to equation (3.4.2.17)

$$\mathbf{z}_{k+1}^{r} = \mathbf{f}_r(\mathbf{x}_k^1,....,\mathbf{x}_k^r) + \mathbf{B}_r(\mathbf{x}_k^1,....,\mathbf{x}_k^r)\mathbf{u}_k + \mathbf{d}_r\omega_k - \mathbf{x}_{k+1}^{r\,d} = \mathbf{K}_r\mathbf{z}_k^r \tag{3.4.3.1}$$

the control $\mathbf{u}_k$ is chosen of the form

$$\mathbf{u}_k = \left[\mathbf{B}_r(\mathbf{x}_k^1,...,\mathbf{x}_k^r)\right]^{-1}\left(\mathbf{K}_r\mathbf{z}_k^r - \mathbf{f}_r(\mathbf{x}_k^1,...,\mathbf{x}_k^r) + \mathbf{x}_{k+1}^{r\,d} - \mathbf{d}_r\omega_k^r\right) \tag{3.4.3.2}$$

This control law is a continuous function of states and will shape the last block dynamics as

$$\mathbf{z}_{k+1}^{r} = \mathbf{K}_r\mathbf{z}_k^r \tag{3.4.3.3}$$

where $\mathbf{K}_r = diag\{k_{r1},\cdots,k_{rm}\}$, and each element has the following bound, in order to assure stability $|k_{rq}| < 1 \quad q = 1,\ldots,m$. With this condition, the state $\mathbf{z}_k^r$ tends asymptotically to zero, i.e.

$$\begin{aligned}
&\lim(\mathbf{z}_k^r) = \mathbf{0} \Rightarrow \mathbf{x}_k^r = \mathbf{x}_k^{r\,d} \\
&k \to \infty
\end{aligned} \tag{3.4.3.4}$$

This means that $\mathbf{x}_k^r$ (the pseudo-control for the *r-1* block) has reached the desired value $\mathbf{x}_k^{r\,d}$, then the (*r-1*) block under the condition (3.4.1.5) will have a similar dynamics to (3.4.3.3):

$$\mathbf{z}_{k+1}^{r-1} = \mathbf{K}_{r-1}\mathbf{z}_k^{r-1} \tag{3.4.3.5}$$

Again, the vector state $\mathbf{z}_k^{r-1}$ will tends asymptotically to zero, i.e.

$$\lim(\mathbf{z}_k^{r-1}) = \mathbf{0} \Rightarrow \mathbf{x}_k^{r-1} = \mathbf{x}_k^{r-1^d} \qquad k \to \infty \tag{3.4.3.6}$$

and so on. In the last case, i.e., the first block, we will have that $\mathbf{x}_k^2 = \mathbf{x}_k^{2^d}$, i.e., $\mathbf{x}_k^2$ has reached the desired form $\mathbf{x}_k^{2^d}$, modeling the first block dynamics under the condition (3.4.1.5)

$$\mathbf{z}_{k+1}^1 = \mathbf{K}_1\mathbf{z}_k^1 \tag{3.4.3.7}$$

then, the tracking error $\mathbf{z}_k^1$ will tend asymptotically to zero, implying that $\mathbf{x}_k^1 = \mathbf{x}_k^{1\,d}$ and accomplishing in that way the original control tracking objectives.

3.4.3.1 Sliding mode control design

For a sliding mode control implementation in the case the control resources are bounded

$$\|\mathbf{u}_k\| \le u_0 \tag{3.4.3.1.1}$$

we need a surface and a control law that will drive the states toward the surface. The natural choice of $\mathbf{S}_k = \mathbf{0}$, is

$$\mathbf{S}_k = \mathbf{z}_k^r = \mathbf{x}_k^r - \mathbf{x}_k^{r\,d} = \varphi_r(\mathbf{x}_k^1, \mathbf{x}_k^2, \ldots, \mathbf{x}_k^r, \boldsymbol{\omega}_k) = \mathbf{0}$$

Then system (3.4.2.18) will have the following form:

$$\begin{aligned}
\mathbf{z}_{k+1}^1 &= \mathbf{K}_1 \mathbf{z}_k^1 + \mathbf{B}_1 \mathbf{z}_k^2 \\
\mathbf{z}_{k+1}^2 &= \mathbf{K}_2 \mathbf{z}_k^2 + \mathbf{B}_2 \mathbf{z}_k^3 \\
&\vdots \qquad\qquad (3.4.3.1.2) \\
\mathbf{z}_{k+1}^{r-1} &= \mathbf{K}_{r-1} \mathbf{z}_k^{r-1} + \mathbf{B}_{r-1} \mathbf{z}_k^r \\
\mathbf{S}_{k+1} &= \mathbf{f}_r(\mathbf{x}_k^1, \ldots, \mathbf{x}_k^r) + \mathbf{B}_r(\mathbf{x}_k^1, \ldots, \mathbf{x}_k^r)\mathbf{u}_k + \mathbf{d}_r \boldsymbol{\omega}_k - \mathbf{x}_{k+1}^{r\,d}
\end{aligned}$$

Taking in the account (3.4.3.1.1) the control $\mathbf{u}_k$ can be selected of the form

$$\mathbf{u}_k = \begin{cases} \mathbf{u}_{keq} & for \quad \|\mathbf{u}_{keq}\| \le u_0 \\ u_0 \dfrac{\mathbf{u}_{keq}}{\|\mathbf{u}_{keq}\|} & for \quad \|\mathbf{u}_{keq}\| > u_0 \end{cases} \qquad (3.4.3.1.3)$$

where the equivalent control is calculated from $\mathbf{S}_{k+1} = \mathbf{0}$ as

$$\mathbf{u}_{keq} = \left[\mathbf{B}_r(\mathbf{x}_k^1, \ldots, \mathbf{x}_k^r)\right]^{-1} \left(-\mathbf{f}_r(\mathbf{x}_k^1, \ldots, \mathbf{x}_k^r) + \mathbf{x}_{k+1}^{r\,d} - \mathbf{d}_r \boldsymbol{\omega}_k^r \right) \qquad (3.4.3.1.4)$$

A stability analysis will prove that the closed-loop system motion over the surface $\mathbf{S}_k = \mathbf{0}$, is stable. Let us represent the surface as

$$\mathbf{S}_{k+1} = \mathbf{S}_k - \mathbf{x}_k^r + \mathbf{x}_k^{r\,d} + \mathbf{f}_r(\mathbf{x}_k^1, \ldots, \mathbf{x}_k^r) + \mathbf{B}_r(\mathbf{x}_k^1, \ldots, \mathbf{x}_k^r)\mathbf{u}_k + \mathbf{d}_r \boldsymbol{\omega}_k - \mathbf{x}_{k+1}^{r\,d} \qquad (3.4.3.1.5)$$

Satisfying $\mathbf{S}_{k+1} - \mathbf{S}_k \le \mathbf{0}$, that is $\mathbf{S}_k$ decreases to zero, when $\|\mathbf{u}_{keq}\| \le u_0$ will be provided by the following condition:

$$\left\| \mathbf{B}_r^{-1} \left(\mathbf{f}_r + \mathbf{d}_r \boldsymbol{\omega}_k - \mathbf{x}_k^r + {\mathbf{x}_k^r}^d - {\mathbf{x}_{k+1}^r}^d \right) \right\| \leq u_0 \qquad (3.4.3.1.6)$$

Let us analyze when $\|\mathbf{u}_{keq}\| > u_0$. Replacing $\mathbf{u}_k = u_0 \dfrac{\mathbf{u}_{keq}}{\|\mathbf{u}_{keq}\|}$ in (3.4.3.1.5), it can be easily seen that

$$\mathbf{S}_{k+1} = \left(\mathbf{S}_k - \mathbf{x}_k^r + \mathbf{f}_r + \mathbf{d}_r \boldsymbol{\omega}_k + {\mathbf{x}_k^r}^d - {\mathbf{x}_{k+1}^r}^d \right) \left(1 - \frac{u_0}{\|u_{keq}\|} \right) \qquad (3.4.3.1.7)$$

Handling (3.4.3.1.7), we obtain

$$\mathbf{S}_{k+1} = \left(\mathbf{S}_k - \mathbf{x}_k^r + \mathbf{f}_r + \mathbf{d}_r \boldsymbol{\omega}_k + {\mathbf{x}_k^r}^d - {\mathbf{x}_{k+1}^r}^d \right) \left(1 - \frac{u_0}{\|u_{keq}\|} \right)$$

$$\|\mathbf{S}_{k+1}\| \leq \|\mathbf{S}_k\| + \left\| \mathbf{f}_r + \mathbf{d}_r \boldsymbol{\omega}_k - \mathbf{x}_k^r + {\mathbf{x}_k^r}^d - {\mathbf{x}_{k+1}^r}^d \right\| - \frac{u_0}{\|\mathbf{B}_r^{-1}\|} \qquad (3.4.3.1.8)$$

$$\|\mathbf{S}_{k+1}\| < \|\mathbf{S}_k\|$$

Hence $\|\mathbf{S}_k\|$ decreases monotonically to zero in a finite number of steps and then a discrete-time sliding mode will take place. The transformed system (3.4.3.1.2) of order n, reduces its order to $n - n_r$, under the condition (3.4.1.5)

$$\begin{aligned} \mathbf{z}_{k+1}^1 &= \mathbf{K}_1 \mathbf{z}_k^1 + \mathbf{B}_1 \mathbf{z}_k^2 \\ \mathbf{z}_{k+1}^2 &= \mathbf{K}_2 \mathbf{z}_k^2 + \mathbf{B}_2 \mathbf{z}_k^3 \\ &\vdots \\ \mathbf{z}_{k+1}^{r-1} &= \mathbf{K}_{r-1} \mathbf{z}_k^{r-1} \end{aligned} \qquad (3.4.3.1.9)$$

where the matrix $\mathbf{K}_l \quad l = 1,\ldots,r-1$ has the desired eigenvalues. The system (3.4.3.1.9) represents the dynamical sliding mode equations.

3.5 NONLINEAR OBSERVER

It is not very common that all the states of any system can be measured. Therefore it is of interest to determine the states of a system from available measurements and a model. Consider a class of nonlinear systems that fit into electromechanical systems

$$\begin{aligned}\mathbf{y}_{k+1}^1 &= \mathbf{f}_k^1(\mathbf{y}_k^1, \mathbf{y}_k^2, \mathbf{x}_k) + \mathbf{D}\boldsymbol{\omega}_k \\ \mathbf{y}_{k+1}^2 &= \mathbf{f}_k^2(\mathbf{y}_k^1, \mathbf{y}_k^2, \mathbf{x}_k) + \mathbf{B}\mathbf{u}_k \\ \mathbf{x}_{k+1} &= \mathbf{f}_k^3(\mathbf{y}_k^2, \mathbf{x}_k)\end{aligned} \tag{3.5.1}$$

where $\mathbf{y}_k^1 = (y_k^{1,1}, \ldots, y_k^{1,m})^T$ and $\mathbf{y}_k^2 = (y_k^{2,1}, \ldots, y_k^{2,m})^T$ are measurable vector state variables, and $\mathbf{x}_k = (x_k^{1,1}, \ldots, x_k^{1,m})$ is a non-measurable vector state variable, $\mathbf{u}_k \in \mathbf{R}^m$, matrix $\mathbf{B}$ and $\mathbf{D}$ are constant and $\boldsymbol{\omega}_k$ is a perturbation generated by an exosystem such as

$$\boldsymbol{\omega}_{k+1} = \mathbf{S}\boldsymbol{\omega}_k \tag{3.5.2}$$

The problem is thus to estimate the non-measurable state $\mathbf{x}_k$ and perturbation $\boldsymbol{\omega}_k$. Assume that the measurable and the non-measurable variables in $\mathbf{f}_k^1$ and $\mathbf{f}_k^3$ are separated as

$$\begin{aligned}\mathbf{f}_k^1(\mathbf{y}_k^1, \mathbf{y}_k^2, \mathbf{x}_k) &= \mathbf{f}_k^{1,1}(\mathbf{y}_k^1, \mathbf{y}_k^2) + \sum_{i=1}^{m} y_k^{2,1}\mathbf{A}_{1,i}\mathbf{x}_k \\ \mathbf{f}_k^3(\mathbf{y}_k^2, \mathbf{x}_k) &= \mathbf{A}_3\mathbf{x}_k + \mathbf{f}_k^{3,3}(\mathbf{y}_k^1, \mathbf{y}_k^2)\end{aligned} \tag{3.5.3}$$

Replacing (3.5.3) in (3.5.1) yields

$$\begin{aligned}\mathbf{y}_{k+1}^1 &= \mathbf{f}_k^{1,1}(\mathbf{y}_k^1, \mathbf{y}_k^2) + \sum_{i=1}^{m} y_k^{2,1}\mathbf{A}_{1,i}\mathbf{x}_k + \mathbf{D}\boldsymbol{\omega}_k \\ \mathbf{y}_{k+1}^2 &= \mathbf{f}_k^2(\mathbf{y}_k^1, \mathbf{y}_k^2, \mathbf{x}_k) + \mathbf{B}\mathbf{u}_k \\ \mathbf{x}_{k+1} &= \mathbf{A}_3\mathbf{x}_k + \mathbf{f}_k^{3,3}(\mathbf{y}_k^1, \mathbf{y}_k^2)\end{aligned} \tag{3.5.4}$$

For this system we need the following assumptions

A.1 The system (3.5.4) is input-to-state stable [6].

A.2 The pair $\left\{\begin{bmatrix} 0 & \mathbf{D} \\ 0 & \mathbf{S} \end{bmatrix}, \begin{bmatrix} \mathbf{I} & 0 \end{bmatrix}\right\}$ is observable.

A.3 The matrix is $\mathbf{A}_3$ is Hurwitz.

It can be noted that system (3.5.4) represents the general dynamics of electrical motors, where

- The vector $\mathbf{y}_k^1$ represents measurable mechanical variables as position and speed.
- The vector $\mathbf{y}_k^2$ represents measurable current variables as stator currents.
- The vector $\mathbf{x}_k$ represents non-measurable rotor flux variables.

Consider the system (3.5.3). Let us assume that the state vector $\mathbf{x}_k$ and the perturbation vector $\boldsymbol{\omega}_k$ are to be estimated by the state vector $\hat{\mathbf{x}}_k$ and by the perturbation vector $\hat{\boldsymbol{\omega}}_k$ respectively; yielding to the observer model as

$$\begin{aligned} \hat{\mathbf{y}}_{k+1}^1 &= \mathbf{f}_k^{1,1}(\mathbf{y}_k^1, \mathbf{y}_k^2) + \sum_{i=1}^{m} y_k^{2,1} \mathbf{A}_{1,i} \hat{\mathbf{x}}_k + \mathbf{D}\hat{\boldsymbol{\omega}}_k + \mathbf{L}_1(\mathbf{y}_k^1 - \hat{\mathbf{y}}_k^1) \\ \hat{\boldsymbol{\omega}}_{k+1} &= \mathbf{S}\hat{\boldsymbol{\omega}}_k + \mathbf{L}_2(\mathbf{y}_k^1 - \hat{\mathbf{y}}_k^1) \\ \hat{\mathbf{x}}_{k+1} &= \mathbf{A}_3\hat{\mathbf{x}}_k + \mathbf{f}_k^{3,3}(\mathbf{y}_k^1, \mathbf{y}_k^2) \end{aligned} \tag{3.5.5}$$

where $\mathbf{L}_1$ and $\mathbf{L}_2$ are the observer gain matrices. To determine these matrices, we introduce the reconstruction errors

$$\begin{aligned} \mathbf{e}_k^{y^1} &= \mathbf{y}_k^1 - \hat{\mathbf{y}}_k^1 \\ \mathbf{e}_k^{\omega} &= \boldsymbol{\omega}_k - \hat{\boldsymbol{\omega}}_k \\ \mathbf{e}_k^{x} &= \mathbf{x}_k - \hat{\mathbf{x}}_k \end{aligned} \tag{3.5.6}$$

The dynamical error equations are obtained from (3.5.4) and (3.5.5) of the form

$$\begin{bmatrix} \mathbf{e}_{k+1}^{y^1} \\ \mathbf{e}_{k+1}^{\omega} \end{bmatrix} = \begin{bmatrix} -\mathbf{L}_1 & \mathbf{D} \\ -\mathbf{L}_2 & \mathbf{S} \end{bmatrix} \begin{bmatrix} \mathbf{e}_k^{y^1} \\ \mathbf{e}_k^{\omega} \end{bmatrix} + \mathbf{f}_k^d \qquad (3.5.7)$$

$$\mathbf{e}_{k+1}^{x} = \mathbf{A}_3 \mathbf{e}_k^{x}$$

where $\mathbf{f}_k^d = \sum_{i=1}^{m} y_k^{2,1} \mathbf{A}_{1,i} e_k^x$. Since by assumption A.3, matrix $\mathbf{A}_3$ is Hurwitz, the vector error $\mathbf{e}_k^x$ tends asymptotically to zero, implying that $\mathbf{x}_k = \hat{\mathbf{x}}_k$. By assumption A.1 the functions $y_k^{2,1}$ are bounded, therefore, $\mathbf{f}_k^d = \sum_{i=1}^{m} y_k^{2,1} \mathbf{A}_{1,i} e_k^x = 0$ Hence the dynamical error equations (3.5.7) will reduce to

$$\begin{bmatrix} \mathbf{e}_{k+1}^{y^1} \\ \mathbf{e}_{k+1}^{\omega} \end{bmatrix} = \begin{bmatrix} -\mathbf{L}_1 & \mathbf{D} \\ -\mathbf{L}_2 & \mathbf{S} \end{bmatrix} \begin{bmatrix} \mathbf{e}_k^{y^1} \\ \mathbf{e}_k^{\omega} \end{bmatrix} \qquad (3.5.8)$$

By assumption A.2, there exists matrices $\mathbf{L}_1$ and $\mathbf{L}_2$ such that $\begin{bmatrix} -\mathbf{L}_1 & \mathbf{D} \\ -\mathbf{L}_2 & \mathbf{S} \end{bmatrix}$ is Hurwitz. Hence the error vector $(\mathbf{e}_k^{y^1}, \mathbf{e}_k^{\omega})^T$ will converge to zero

Chapter four

Application

4.1 INTRODUCTION

This section contains the contributions of this work, controlling the rotor magnetic flux magnitude and speed. Given full state measurements, the control objectives are to develop velocity and flux amplitude tracking for the electromechanical dynamics found in the discrete-time induction motor model, using block control and discrete-time sliding mode techniques. Then a reduced order observer will be developed for the induction motor, where rotor speed and current measurements provide the unreachable fluxes and load torque.

Figure 4.1 shows the overall control system. This control system has a hierarchical structure, comprising an inner and an outer loop where a speed and flux controller or *master control law* (outer loop) responds to the speed and rotor flux magnitude demands, and issues stator current demands to a current controller or *slave control law* (inner loop).

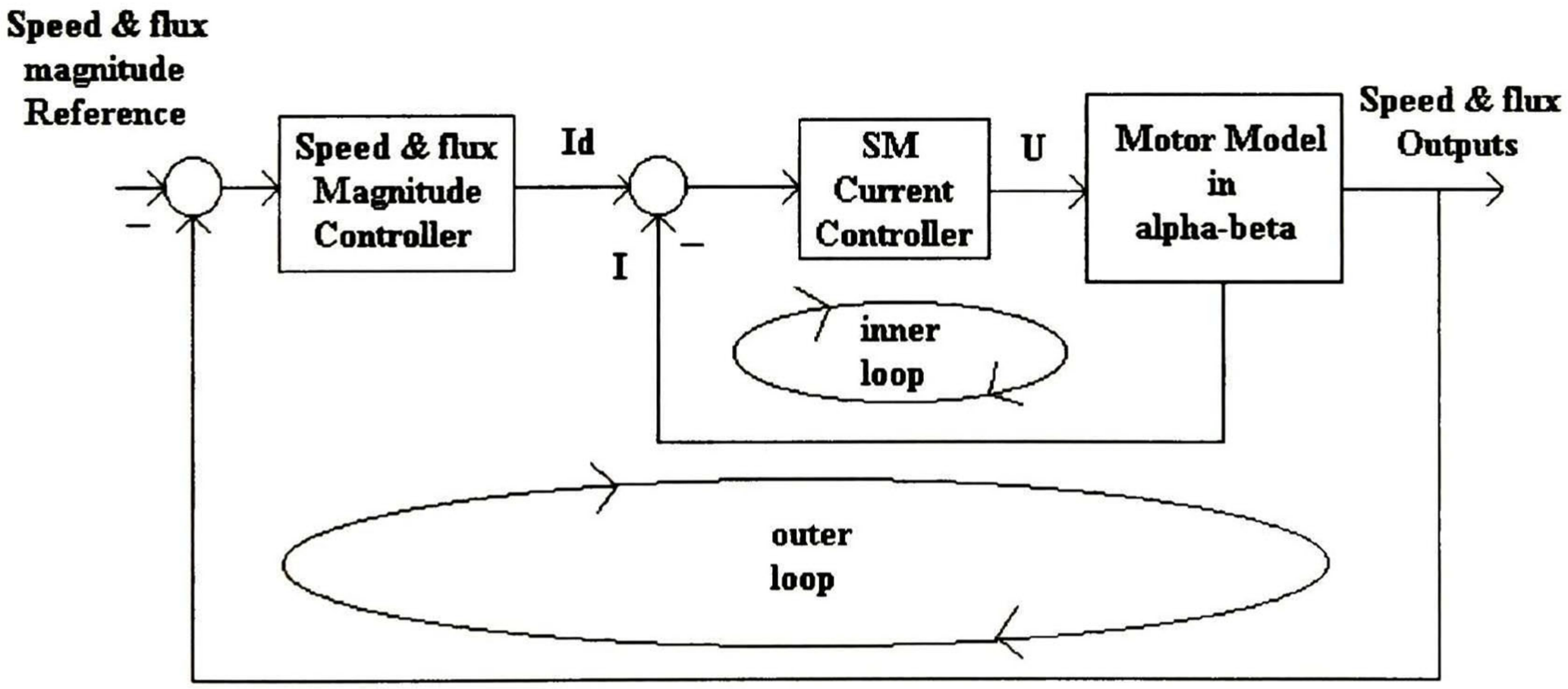

Figure 4.1. Block diagram of the control system.

The control law synthesis is carried out in two distinct stages as just mentioned. First, it is assumed that the control law operates ideally so, the current vector, $\mathbf{i}$, exactly follows the demanded current, $\mathbf{i}^d$ Then, $\mathbf{i}^d$ is the control vector of the master control law, which is formulated to control the rotor speed, according to a second order dynamics (exosystem) with a prescribed time constant or frequency. In this process, an extra degree of freedom becomes apparent allowing the rotor flux magnitude to be independently controlled as part of the master control law, also with second order dynamics and a prescribed time constant. Second, the slave control law is formulated as a simple robust discrete-time sliding mode control law of the switched type. This operates with phase current measurements in a similar way to the conventional hysteresis current controller but does not require the hysteresis element since software implementation is assumed where the maximum switching frequency of the power electronics is automatically equal to the iteration frequency of the digital processor.

For the sliding mode control design, we use the discrete-time dynamic model of the induction motor found in chapter two

$$
\begin{aligned}
\omega_{k+1} &= \omega_k + \frac{\mu}{\alpha}(1-a)M\left(i_k^{\beta}\psi_k^{\alpha} - i_k^{\alpha}\psi_k^{\beta}\right) - \left(\frac{T}{J}\right)T_{Lk} \\
\psi_{k+1}^{\alpha} &= \cos\left(n_p\theta_{k+1}\right)\rho_1 - sin\left(n_p\theta_{k+1}\right)\rho_2 \\
\psi_{k+1}^{\beta} &= sin\left(n_p\theta_{k+1}\right)\rho_1 + \cos\left(n_p\theta_{k+1}\right)\rho_2 \\
i_{k+1}^{\alpha} &= i_k^{\alpha} + (\alpha\beta\psi_k^{\alpha} + n_p\beta\omega_k\psi_k^{\beta} - \gamma i_k^{\alpha} + \frac{1}{\sigma}u_k^{\alpha})T \\
i_{k+1}^{\beta} &= i_k^{\beta} + (\alpha\beta\psi_k^{\beta} - n_p\beta\omega_k\psi_k^{\alpha} - \gamma i_k^{\beta} + \frac{1}{\sigma}u_k^{\beta})T \\
\theta_{k+1} &= \theta_k + \omega_k T + \frac{\mu}{\alpha}\left[T - \frac{1}{\alpha}(1-a)\right]M(i_k^{\beta}\psi_k^{\alpha} - i_k^{\alpha}\psi_k^{\beta}) - \frac{T_{Lk}}{2J}T^2
\end{aligned}
\qquad (4.1.1)
$$

where

$$
\begin{aligned}
\rho_1 &= a\left(\cos\left(n_p\theta_k\right)\psi_k^{\alpha} + sin\left(n_p\theta_k\right)\psi_k^{\beta}\right) + (1-a)M\left(\cos\left(n_p\theta_k\right)i_k^{\alpha} + sin\left(n_p\theta_k\right)i_k^{\beta}\right) \\
\rho_2 &= a\left(\cos\left(n_p\theta_k\right)\psi_k^{\beta} - sin\left(n_p\theta_k\right)\psi_k^{\alpha}\right) + (1-a)M\left(\cos\left(n_p\theta_k\right)i_k^{\beta} - sin\left(n_p\theta_k\right)i_k^{\alpha}\right)
\end{aligned}
\qquad (4.1.2)
$$

Since the model in (4.1.1) does not present the BCF, we need to find a new state vector $\mathbf{x}_k$ that presents this form and then apply the transformation process

$$\mathbf{z}_k = \varphi(\mathbf{x}_k) \quad \varphi = (\varphi_1, \ldots, \varphi_r)^T \tag{4.1.3}$$

Let us define the control error states as

$$\begin{aligned} \mathbf{x}_k^1 &= \begin{bmatrix} x_k^1 \\ x_k^2 \end{bmatrix} = \begin{bmatrix} \omega_k - \omega_k^r \\ \psi_k - \psi_k^r \end{bmatrix} \\ \mathbf{x}_k^2 &= \begin{bmatrix} x_k^3 \\ x_k^4 \end{bmatrix} = \begin{bmatrix} i_k^\alpha \\ i_k^\beta \end{bmatrix} \end{aligned} \tag{4.1.4}$$

where ψ_k is the rotor flux magnitude modulus, ω_k^r and ψ_k^r are reference signals. Then the system involving states in (4.1.4) can be represented in the BCF consisting of two blocks

$$\begin{aligned} \mathbf{x}_{k+1}^1 &= \mathbf{f}_k^1(\mathbf{x}_k^1) + \mathbf{B}_1(\mathbf{x}_k^1)\mathbf{x}_k^2 \\ \mathbf{x}_{k+1}^2 &= \mathbf{f}_k^2(\mathbf{x}_k^1, \mathbf{x}_k^2) + \mathbf{B}_2\mathbf{u}_k \\ \mathbf{y}_k &= \mathbf{x}_k^1 \end{aligned} \tag{4.1.5}$$

It can be easily seen that the dynamical current equations in (4.1.1) adopt the form of the second block. The structure of the first block will be revealed next.

4.2 DISCRETE-TIME SLIDING MODE WITH BLOCK CONTROL

4.2.1 Master control law

To begin, we define the z_k^1 variable as

$$z_k^1 = x_k^1 = \omega_k - \omega_k^r \tag{4.2.1.1}$$

where ω_k^r is the reference signal to be tracked, and can be generated by an exosystem as seen in the previous chapter. Taking the next step of (4.2.1.1), we have

$$z_{k+1}^1 = \omega_{k+1} - \omega_{k+1}^r = \omega_k + \frac{\mu}{\alpha}(1-a)M\left(i_k^\beta \psi_k^\alpha - i_k^\alpha \psi_k^\beta\right) - \left(\frac{T}{J}\right)T_{Lk} - \omega_{k+1}^r \tag{4.2.1.2}$$

If we define the following variable and constant to simplify (4.2.1.2)

$$\begin{aligned} f_k^1 &= \omega_k - \left(\frac{T}{J}\right)T_{Lk} - \omega_{k+1}^r \\ c_1 &= \frac{\mu}{\alpha}(1-a)M \end{aligned} \tag{4.2.1.3}$$

yielding then following compact description of (4.2.1.2)

$$z_{k+1}^1 = f_k^1 + c_1\left(i_k^\beta \psi_k^\alpha - i_k^\alpha \psi_k^\beta\right) \tag{4.2.1.4}$$

Next, we define the z_k^2 variable as

$$z_k^2 = x_k^2 = \psi_k - \psi_k^r \tag{4.2.1.5}$$

Where ψ_k^r is the reference signal to be tracked, and ψ_k is defined as follows

$$\psi_k = \|\psi\|_2^2 = \psi_k^{\alpha 2} + \psi_k^{\beta 2} \tag{4.2.1.6}$$

Taking one step ahead of (4.2.1.5)

$$z_{k+1}^2 = \psi_{k+1}^{\alpha\ 2} + \psi_{k+1}^{\beta\ 2} - \psi_{k+1}^r \tag{4.2.1.7}$$

Next, we separately compute the squared flux summation

$$\begin{aligned}\psi_{k+1}^{\alpha\ 2} &= [\cos(np\,\theta_{k+1})\rho_1 - sin(np\,\theta_{k+1})\rho_2]^2 = \\ &= \cos^2(np\,\theta_{k+1})\rho_1^{\ 2} - 2\cos(np\,\theta_{k+1})\rho_1 sin(np\,\theta_{k+1})\rho_2 + sin^2(np\,\theta_{k+1})\rho_2^{\ 2}\end{aligned}$$

$$\begin{aligned}\psi_{k+1}^{\beta\ 2} &= [sin(np\,\theta_{k+1})\rho_1 + \cos(np\,\theta_{k+1})\rho_2]^2 = \\ &= sin^2(np\,\theta_{k+1})\rho_1^{\ 2} + 2\cos(np\,\theta_{k+1})\rho_1 sin(np\,\theta_{k+1})\rho_2 + \cos^2(np\,\theta_{k+1})\rho_2^{\ 2}\end{aligned}$$

$$\psi_{k+1}^{\alpha\ 2} + \psi_{k+1}^{\beta\ 2} = \rho_1^{\ 2} + \rho_2^{\ 2}$$

With the last result we can redefine the flux amplitude tracking error dynamics

$$z_{k+1}^2 = \rho_1^{\ 2} + \rho_2^{\ 2} - \psi_{k+1}^r \tag{4.2.1.8}$$

Continuing in the same way, we perform the squared ρ function summation; defined in (4.1.2). For sake of simplicity, we define the following dummy variables

$$\begin{aligned}\lambda 1 &= \cos(np\,\theta_k)\psi_k^{\alpha} + sin(np\,\theta_k)\psi_k^{\beta} \\ \lambda 2 &= \cos(np\,\theta_k)i_k^{\alpha} + sin(np\,\theta_k)i_k^{\beta} \\ \phi 1 &= \cos(np\,\theta_k)\psi_k^{\beta} - sin(np\,\theta_k)\psi_k^{\alpha} \\ \phi 2 &= \cos(np\,\theta_k)i_k^{\beta} - sin(np\,\theta_k)i_k^{\alpha}\end{aligned} \tag{4.2.1.9}$$

Rewriting the ρ functions (4.1.2) with the dummy variables (4.2.1.9)

$$\begin{aligned}\rho_k^1 &= a(\lambda 1)+(1-a)M(\lambda 2)\\ \rho_k^2 &= a(\phi 1)+(1-a)M(\phi 2)\end{aligned} \qquad (4.2.1.10)$$

The summation of the ρ functions of (4.2.1.10) elevated to the power of two is shown as follows

$$\begin{aligned}\rho_1{}^2 &= a^2(\lambda 1)^2+2a(1-a)M(\lambda 1)(\lambda 2)+(1-a)^2M^2(\lambda 2)^2\\ \rho_2{}^2 &= a^2(\phi 1)^2+2a(1-a)M(\phi 1)(\phi 2)+(1-a)^2M^2(\phi 2)^2\end{aligned} \qquad (4.2.1.11)$$

$$\rho_1{}^2+\rho_2{}^2 = a^2\left(\lambda 1^2+\phi 1^2\right)+2a(1-a)M(\lambda 1\lambda 2+\phi 1\phi 2)+(1-a)^2M^2\left(\lambda 2^2+\phi 2^2\right)$$

Computing each operation separately

$$\begin{aligned}\lambda 1^2 &= \left[\cos(np\,\theta_k)\psi_k^{\alpha}+\sin(np\,\theta_k)\psi_k^{\beta}\right]^2 =\\ &= \cos^2(np\,\theta_k)\psi_k^{\alpha\,2}+2\cos(np\,\theta_k)\psi_k^{\alpha}\sin(np\,\theta_k)\psi_k^{\beta}+\sin^2(np\,\theta_k)\psi_k^{\beta\,2}\\ \phi 1^2 &= \left[\cos(np\,\theta_k)\psi_k^{\beta}-\sin(np\,\theta_k)\psi_k^{\alpha}\right]^2 =\\ &= \cos^2(np\,\theta_k)\psi_k^{\beta\,2}-2\cos(np\,\theta_k)\psi_k^{\alpha}\sin(np\,\theta_k)\psi_k^{\beta}+\sin^2(np\,\theta_k)\psi_k^{\alpha\,2}\end{aligned}$$

$$\lambda 1^2+\phi 1^2 = \psi_k^{\alpha\,2}+\psi_k^{\beta\,2} = \psi_k \Rightarrow \lambda 2^2+\phi 2^2 = i_k^{\alpha\,2}+i_k^{\beta\,2}$$

$$\begin{aligned}\lambda 1\lambda 2 &= \cos^2(np\,\theta_k)\psi_k^{\alpha}i_k^{\alpha}+\cos(np\,\theta_k)\sin(np\,\theta_k)\psi_k^{\beta}i_k^{\alpha}+\\ &\quad+\cos(np\,\theta_k)\sin(np\,\theta_k)\psi_k^{\alpha}i_k^{\beta}+\sin^2(np\,\theta_k)\psi_k^{\beta}i_k^{\beta}\\ \phi 1\phi 2 &= \cos^2(np\,\theta_k)\psi_k^{\beta}i_k^{\beta}-\cos(np\,\theta_k)\sin(np\,\theta_k)\psi_k^{\alpha}i_k^{\beta}+\\ &\quad-\cos(np\,\theta_k)\sin(np\,\theta_k)\psi_k^{\beta}i_k^{\alpha}+\sin^2(np\,\theta_k)\psi_k^{\alpha}i_k^{\alpha}\end{aligned}$$

$$\lambda 1\lambda 2+\phi 1\phi 2 = \psi_k^{\alpha}i_k^{\alpha}+\psi_k^{\beta}i_k^{\beta}$$

With the new computations we rewrite equation (4.2.1.11) in the following form

$$\rho_1^2 + \rho_2^2 = a^2(\psi_k) + c_2\left(\psi_k^{\alpha} i_k^{\alpha} + \psi_k^{\beta} i_k^{\beta}\right) + (1-a)^2 M^2\left(i_k^{\alpha 2} + i_k^{\beta 2}\right) \qquad (4.2.1.12)$$

where c_2 is defined as

$$c_2 = 2a(1-a)M \qquad (4.2.1.13)$$

Because, i_k^{α} and i_k^{β} are sinusoidal shape signals, with a 90 degree phase of difference between them, we can easily see that

$$i_k^{\alpha 2} + i_k^{\beta 2} = \mathrm{Im}_k^2 \, sin^2(*) + \mathrm{Im}_k^2 \cos^2(*) = \mathrm{Im}_k^2 \qquad (4.2.1.14)$$

where Im is the peak value of the sinusoidal currents; and taking into consideration the last assumption, we have that

$$\rho_k^{1\,2} + \rho_k^{2\,2} = a^2(\psi_k) + c_2\left(\psi_k^{\alpha} i_k^{\alpha} + \psi_k^{\beta} i_k^{\beta}\right) + (1-a)^2 M^2\left(\mathrm{Im}_k^2\right) \qquad (4.2.1.15)$$

Finally equation (4.2.1.7) is

$$z^2{}_{k+1} = a^2(\psi_k) + c_2\left(\psi_k^{\alpha} i_k^{\alpha} + \psi_k^{\beta} i_k^{\beta}\right) + (1-a)^2 M^2\left(\mathrm{Im}_k^2\right) - \psi_{k+1}^r \qquad (4.2.1.16)$$

Defining the following variable

$$f_k^2 = a^2(\psi_k) + (1-a)^2 M^2\left(\mathrm{Im}_k^2\right) - \psi_{k+1}^r \qquad (4.2.1.17)$$

We simplify the flux amplitude tracking error dynamics shown in (4.2.1.16) as follows

$$z_{k+1}^2 = f_k^2 + c_2\left(\psi_k^\alpha i_k^\alpha + \psi_k^\beta i_k^\beta\right) \tag{4.2.1.18}$$

Now, if we define an error vector as

$$\mathbf{z}_k^1 = \begin{bmatrix} z_k^1 \\ z_k^2 \end{bmatrix} = \mathbf{x}_k^1 \tag{4.2.1.19}$$

equations (4.2.1.4) and (4.2.1.20) are shown in matrix form

$$\begin{bmatrix} z_{k+1}^1 \\ z_{k+1}^2 \end{bmatrix} = \begin{bmatrix} f_k^1 \\ f_k^2 \end{bmatrix} + \begin{bmatrix} c_1 & 0 \\ 0 & c_2 \end{bmatrix} \begin{bmatrix} -\psi_k^\beta & \psi_k^\alpha \\ \psi_k^\alpha & \psi_k^\beta \end{bmatrix} \begin{bmatrix} i_k^\alpha \\ i_k^\beta \end{bmatrix} \tag{4.2.1.20}$$

A more compact description of (4.2.1.22) is

$$\mathbf{z}_{k+1}^1 = \mathbf{f}_k^1 + \mathbf{C}\mathbf{B}_k \mathbf{i}_k^d \tag{4.2.1.21}$$

from (4.2.1.21) we found the relations of the first block of (4.1.5) as $\mathbf{f}_k^1(\mathbf{x}_k^1) = \mathbf{f}_k^1$, $\mathbf{B}_1(\mathbf{x}_k^1) = \mathbf{C}\mathbf{B}_k$ and $\mathbf{x}_k^2 = \mathbf{i}_k$. The reason we named the vector current with the upper-index 'd' is that these currents are desired ones, capable of make the dynamical error equations stable. Then we can view these currents as a "pseudo-control", so, if we desire that the dynamical error equation to decay asymptotically to zero, we can force the dynamics to be

$$\mathbf{z}_{k+1}^1 = \mathbf{f}_k^1 + \mathbf{C}\mathbf{B}_k \mathbf{i}_k^d = \mathbf{K}^1 \mathbf{z}_k^1 \tag{4.2.1.22}$$

where

$$\mathbf{K}^1 = \begin{bmatrix} k_1 & 0 \\ 0 & k_2 \end{bmatrix}$$
$$|k_1| < 1 \qquad (4.2.1.23)$$
$$|k_2| < 1$$

These constants will guarantee asymptotic stability, and in order to accomplish it, we calculate the vectorial current from the equation (4.2.1.22) as

$$\mathbf{i}_k^d = \mathbf{B}_k^{-1}\mathbf{C}^{-1}\left[\mathbf{K}^1\mathbf{z}_k^1 - \mathbf{f}_k^1\right] \qquad (4.2.1.24)$$

this vectorial current indicates the desired behavior of the state variables i_k^α and i_k^β in order to satisfy the speed and flux amplitude tracking requirements.

4.2.2 Slave control law

Proceeding in the same way, we now need that the real currents, i_k^α and i_k^β, can track the desired ones, so we define the following two error signals

$$z_k^3 = i_k^{\alpha d} - i_k^\alpha$$
$$z_k^4 = i_k^{\beta d} - i_k^\beta \qquad (4.2.2.1)$$

Now (4.2.2.1) is shown in vector form

$$\mathbf{z}_k^2 = \begin{bmatrix} z_k^3 \\ z_k^4 \end{bmatrix} \qquad (4.2.2.2)$$
$$\mathbf{z}_k^2 = \mathbf{i}_k^d - \mathbf{i}_k = \mathbf{B}_k^{-1}\mathbf{C}^{-1}\left[\mathbf{K}^1\mathbf{z}_k^1 - \mathbf{f}_k^1\right] - \mathbf{i}_k$$

Taking one step ahead

$$\mathbf{z}_{k+1}^2 = \mathbf{i}_{k+1}^d - \mathbf{i}_{k+1} = \mathbf{B}_{k+1}^{-1}\mathbf{C}^{-1}\left[\mathbf{K}^1\mathbf{z}_{k+1}^1 - \mathbf{f}_{k+1}^1\right] - \varphi_k - \frac{T}{\sigma}\mathbf{u}_k$$

$$\mathbf{z}_{k+1}^2 = \mathbf{f}_k^2 - \frac{T}{\sigma}\mathbf{u}_k \qquad (4.2.2.3)$$

where

$$\mathbf{f}_k^2 = \mathbf{B}^{-1}{}_{k+1}\mathbf{C}^{-1}\left[\mathbf{K}^1\mathbf{z}_{k+1}^1 - \mathbf{f}_{k+1}^1\right] - \varphi_k \qquad (4.2.2.4)$$

Finally, the open-loop error dynamical equations are

$$\begin{aligned}\mathbf{z}_{k+1}^1 &= \mathbf{K}^1\mathbf{z}_k^1 + \mathbf{C}\mathbf{B}_k\mathbf{z}_k^2 \\ \mathbf{z}_{k+1}^2 &= \mathbf{f}_k^2 - \frac{T}{\sigma}\mathbf{u}_k\end{aligned} \qquad (4.2.2.5)$$

If we choose control such that $\mathbf{z}_k^2 = \mathbf{0}$, this will imply that $\mathbf{i}_k = \mathbf{i}_k^d$, making possible the control tracking objectives, that is

$$\mathbf{z}_k^2 = \mathbf{0} \Rightarrow \lim_{kT \to \infty}\left(\mathbf{z}_k^1\right) = \mathbf{0} \qquad (4.2.2.6)$$

It's an obvious fact that control $\mathbf{u}_k$ will depend on $\mathbf{f}_k^2$ in order to eliminate old dynamics, but this function depends of control $\mathbf{u}_k$ squared, through $\mathbf{f}_{k+1}^1$. This means that there is an algebraic loop that makes the system unsolvable. The problem comes when we take one step ahead of function Im_k shown in (4.2.1.14). To overcome this problem we design an observer for Im_k only with current measurements. We assume that Im_k is constant, i.e.

$$\mathrm{Im}_{k+1} = \mathrm{Im}_k \qquad (4.2.2.7)$$

and define the observer as the original plant plus a tracking error

$$\hat{\mathrm{Im}}_{k+1} = \hat{\mathrm{Im}}_k + g e_k^I \tag{4.2.2.8}$$

where

$$\begin{aligned} e_k^I &= \mathrm{Im}_k - \hat{\mathrm{Im}}_k \\ \mathrm{Im}_k &= \sqrt{i_k^{\alpha 2} + i_k^{\beta 2}} \end{aligned} \tag{4.2.2.9}$$

taking one step ahead , we obtain the error dynamics

$$\begin{aligned} e_{k+1}^I &= \mathrm{Im}_{k+1} - \hat{\mathrm{Im}}_{k+1} \\ e_{k+1}^I &= \mathrm{Im}_k - \hat{\mathrm{Im}}_k - g e_k^I \\ e_{k+1}^I &= e_k^I - g e_k^I = (1-g) e_{k+1}^I \end{aligned} \tag{4.2.2.10}$$

It's easy to see that with the following condition the dynamical error equation will decay asymptotically to zero

$$2 > g > 0 \tag{4.2.2.11}$$

and the observer will asymptotically track Im_k, also will avoid the dependency of $\mathbf{u}_k$ squared. Figure 4.2 shows a simulation of the observer.

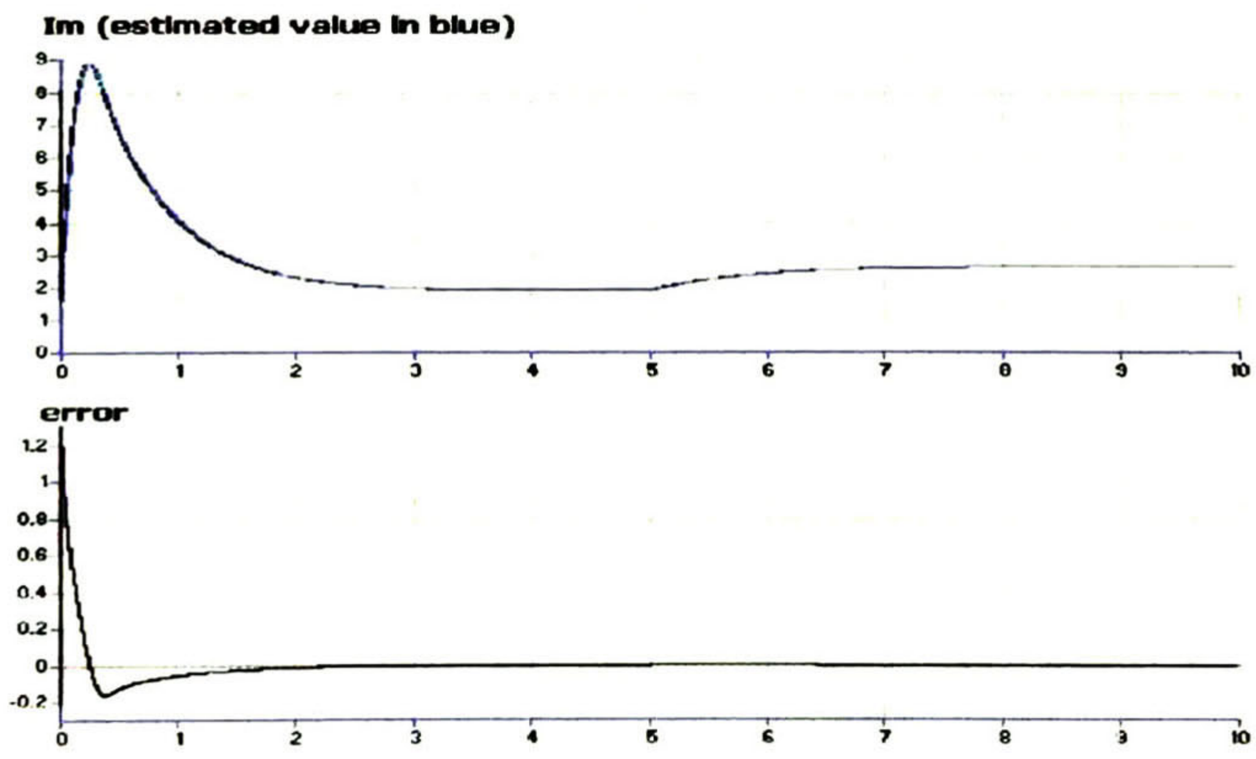

Figure 4.2. Graph of Im vs $\hat{\mathrm{Im}}$ and its tracking error.

4.2.3 Sliding mode control

We are ready to design the control law from the last results. The first step is to choose a surface, and a good approach is

$$\mathbf{S}_k = \mathbf{z}_k^2 = \mathbf{0} \tag{4.2.3.1}$$

This surface will be zeroing as the state trajectories reach the surface and we will get the control objectives accomplished as can be seen in (4.2.2.6). The system in (4.2.2.5) is redefined as

$$\begin{aligned} \mathbf{z}_{k+1}^1 &= \mathbf{K}^1 \mathbf{z}_k^1 + \mathbf{C}\mathbf{B}_k \mathbf{z}_k^2 \\ \mathbf{S}_{k+1} &= \mathbf{f}_k^2 - \frac{T}{\sigma}\mathbf{u}_k \end{aligned} \tag{4.2.3.2}$$

The next step is the design of control $\mathbf{u}_k$, but we really have two choices for $\mathbf{u}_k$. The discrete-time version of sliding mode results in a continuos function, that can not be implemented to the discontinuous inputs of the electronic device (IGBT) that drive the motor, rather, it is necessary to implement a PWM to drive this device. The other option for $\mathbf{u}_k$ is to implement it as in continuos-time that is, control $\mathbf{u}_k$ depends on the sign of the surface. This has the advantage that the control results in a discontinuous function that can be implemented in a straightforward manner to the discontinuous inputs of the electronic device that drive the motor, avoiding the use of PWM. Both cases will be analyzed.

4.2.3.1 Sliding mode control as a continuous function of states

As seen in section 3.3, a discrete-time sliding mode version is implemented with the following control

$$\mathbf{u}_k = \begin{cases} \mathbf{u}_{keq} & for \quad \|\mathbf{u}_{keq}\| \le u_0 \\ u_0 \dfrac{\mathbf{u}_{keq}}{\|\mathbf{u}_{keq}\|} & for \quad \|\mathbf{u}_{keq}\| > u_0 \end{cases} \tag{4.2.3.1.1}$$

where $\mathbf{u}_{keq}$ is calculated from $\mathbf{S}_{k+1} = \mathbf{0}$

$$\mathbf{u}_{keq} = \frac{\sigma}{T}\left[\mathbf{B}_{k+1}^{-1}\mathbf{C}^{-1}\left[\mathbf{K}^1\mathbf{z}^1{}_{k+1} - \mathbf{f}^1{}_{k+1}\right] - \varphi_k\right] = \frac{\sigma}{T}\mathbf{f}_k^2 \qquad (4.2.3.1.2)$$

and u_0 is the control resources that bound the control.

Proceeding with a stability analysis, we first verify stability for $\left\|\mathbf{u}_{keq}\right\| \le u_0$. To reveal the structure of $\mathbf{u}_{keq}$, let us represent it as the sum of two linear functions

$$\mathbf{u}_{keq} = \frac{\sigma}{T}\left(\mathbf{f}_k^2 + \mathbf{S}_k - \mathbf{i}_k^d + \mathbf{i}_k\right) \qquad (4.2.3.1.3)$$

and

$$\mathbf{S}_{k+1} = \mathbf{S}_k + \mathbf{f}_k^2 - \mathbf{i}_k^d + \mathbf{i}_k - \frac{T}{\sigma}\mathbf{u}_k \qquad (4.2.3.1.4)$$

$\|\mathbf{S}_k\|$ in order to decrease monotonically to zero, we need to satisfy $\mathbf{S}_{k+1} - \mathbf{S}_k \le 0$ and using the fact that control can vary within $\left\|\mathbf{u}_{keq}\right\| \le u_0$ we found the condition that guarantees stability on the surface is

$$\left\|\frac{\sigma}{T}\left(\mathbf{f}_k^2 - \mathbf{i}_k^d + \mathbf{i}_k\right)\right\| \le u_0 \qquad (4.2.3.1.5)$$

Note that otherwise, the control resources are insufficient to stabilize the system.

Let us turn to the case in $\left\|\mathbf{u}_{keq}\right\| > u_0$. Replacing $\mathbf{u}_k = u_0 \dfrac{\mathbf{u}_{keq}}{\left\|\mathbf{u}_{keq}\right\|}$ in (4.2.3.1.4) and with few computations we obtain

$$\mathbf{S}_{k+1} = \left(\mathbf{S}_k + \mathbf{f}_k^2 - \mathbf{i}_k^d + \mathbf{i}_k\right)\left(1 - \frac{u_0}{\left\|\mathbf{u}_{keq}\right\|}\right) \qquad (4.2.3.1.6)$$

Yielding to

$$\|\mathbf{S}_{k+1}\| = \left\|\mathbf{S}_k + \mathbf{f}_k^2 - \mathbf{i}_k^d + \mathbf{i}_k\right\| \left(1 - \frac{u_0}{\|\mathbf{u}_{keq}\|}\right)$$

$$\|\mathbf{S}_{k+1}\| \leq \|\mathbf{S}_k\| + \left\|\mathbf{f}_k^2 - \mathbf{i}_k^d + \mathbf{i}_k\right\| - \frac{u_0}{\left|\frac{\sigma}{T}\right|} \qquad (4.2.3.1.7)$$

$$\|\mathbf{S}_{k+1}\| < \|\mathbf{S}_k\|$$

due to (4.2.3.1.5). Hence $\|\mathbf{S}_k\|$ decreases monotonically to zero and after a finite number of steps, $\|\mathbf{u}_k\| \leq u_0$ is achieved. Discrete-time sliding mode will take place from the next sampling point onwards and is modeled by the following reduced order system

$$\mathbf{z}_{k+1}^1 = \mathbf{K}^1 \mathbf{z}_k^1 \qquad (4.2.3.1.8)$$

4.2.3.2 Sliding mode control as a discontinuous function of states

We propose the following discontinuous control law

$$\mathbf{u}_k = u_0 sign(\mathbf{S}_k) \qquad (4.2.3.2.1)$$

Once again the control resources are delimited by the natural bound u_0. A stability analysis will help us to determine this bound. Satisfying the stability condition $\mathbf{S}_{k+1} - \mathbf{S}_k \leq 0$, we easily found a bound for u_0

$$\frac{\sigma}{T}\left\|\mathbf{f}_k^2 - \mathbf{i}_k^d + \mathbf{i}_k\right\| \leq u_0 \qquad (4.2.3.2.2)$$

4.3 REDUCED ORDER OBSERVER

The last control algorithm works with the full state and parameters measurement assumption. But actually the rotor fluxes and torque measurement is a difficult task. Here we design a reduced order nonlinear observer for fluxes and load, with rotor speed and currents measurements only.

Based on the results of chapter 3, and making analogies with system (3.5.4), we found that

$$\mathbf{y}_k^1 = [\omega_k],\ \mathbf{y}_k^2 = \left[i_k^\alpha, i_k^\beta\right]^T,\ \mathbf{x}_k = \left[\psi_k^\alpha, \psi_k^\beta\right]^T \text{ and } \boldsymbol{\omega}_k = [T_{Lk}]$$

We present the plant to be observed with the same structure of (3.5.4)

$$\begin{aligned} \omega_{k+1} &= \omega_k + \mathbf{i}_k^T \Im \Psi_k - \left(\frac{T}{J}\right) T_{Lk} \\ \mathbf{i}_{k+1} &= \varphi_k + \frac{T}{\sigma}\mathbf{u}_k \\ \Psi_{k+1} &= a\mathbf{G}_k \boldsymbol{\Psi}_k + (1-a)M\mathbf{G}_k \mathbf{i}_k \end{aligned} \tag{4.3.1}$$

where $\Im$ is defined in (2.3.4), the elements of the vector φ_k are defined in (2.3.26) and $\mathbf{G}_k$ is defined as

$$\mathbf{G}_k = \begin{bmatrix} \cos\left(np(\theta_{k+1} - \theta_k)\right) & -sin\left(np(\theta_{k+1} - \theta_k)\right) \\ sin\left(np(\theta_{k+1} - \theta_k)\right) & \cos\left(np(\theta_{k+1} - \theta_k)\right) \end{bmatrix} \tag{4.3.2}$$

it is convenient to describe (4.3.2) in terms of measurable variables as ω_k

$$\mathbf{G}_k = \begin{bmatrix} \cos\left(npT\omega_k\right) & -sin\left(npT\omega_k\right) \\ sin\left(npT\omega_k\right) & \cos\left(npT\omega_k\right) \end{bmatrix} \tag{4.3.3}$$

Next, we show the observer as in (3.5.5).

$$\begin{aligned}
\hat{\omega}_{k+1} &= \omega_k + \mathbf{i}_k^T \Im \hat{\boldsymbol{\psi}}_k - \left(\frac{T}{J}\right)\hat{T}_{Lk} + l_1(\omega_k - \hat{\omega}_k) \\
\hat{T}_{Lk+1} &= \hat{T}_{Lk} + l_2(\omega_k - \hat{\omega}_k) \\
\hat{\boldsymbol{\psi}}_{k+1} &= a\mathbf{G}_k \hat{\boldsymbol{\Psi}}_k + (1-a)M\mathbf{G}_k \mathbf{i}_k
\end{aligned} \tag{4.3.4}$$

Let e_k^{ω} be the difference between the measured rotor speed and the estimated one

$$e_k^{\omega} = \omega_k - \hat{\omega}_k \tag{4.3.5}$$

e_k^L the difference between the real load and the estimated one

$$e_k^L = T_{Lk} - \hat{T}_{Lk} \tag{4.3.6}$$

and the difference between real flux vector and the estimated one as

$$\mathbf{e}_k^{\psi} = \boldsymbol{\psi}_k - \hat{\boldsymbol{\psi}}_k \tag{4.3.7}$$

Taking one step ahead of equations (4.3.5), (4.3.6) and (4.3.7) we found the dynamical error equations, just as in (3.5.7)

$$\begin{aligned}
\begin{bmatrix} e_{k+1}^{\omega} \\ e_{k+1}^{L} \end{bmatrix} &= \begin{bmatrix} -l_1 & -\dfrac{T}{J} \\ -l_2 & 1 \end{bmatrix} \begin{bmatrix} e_k^{\omega} \\ e_k^{L} \end{bmatrix} + \mathbf{i}_k^T \Im \mathbf{e}_k^{\psi} \\
\mathbf{e}_{k+1}^{\psi} &= a\mathbf{G}_k \mathbf{e}_k^{\psi}
\end{aligned} \tag{4.3.8}$$

A Lyapunov function can be used to proof stability of $\mathbf{e}_k^{\psi}$

$$\mathbf{V}_k = \mathbf{e}_k^{\Psi^T} \mathbf{e}_k^{\Psi} \tag{4.3.9}$$

Taking one step ahead of (4.3.9)

$$\mathbf{V}_{k+1} = \mathbf{e}_k^{\Psi^T} a^2 \mathbf{G}_k^T \mathbf{G}_k \mathbf{e}_k^{\Psi} \tag{4.3.10}$$

The increment of the Lyapunov function should be negative, and is expressed as

$$\Delta \mathbf{V}_k = \mathbf{e}_k^{\Psi^T} \left(a^2 \mathbf{G}_k^T \mathbf{G}_k - \mathbf{I}_{2x2} \right) \mathbf{e}_k^{\Psi} < 0 \tag{4.3.11}$$

where

$$\left(a^2 \mathbf{G}_k^T \mathbf{G}_k - \mathbf{I}_{2x2} \right) < 0 \tag{4.3.12}$$

or

$$a^2 \mathbf{G}_k^T \mathbf{G}_k < \mathbf{I}_{2x2}$$

With some basic manipulations we found that

$$\begin{bmatrix} a^2 & 0 \\ 0 & a^2 \end{bmatrix} < \begin{bmatrix} 1 & 0 \\ 0 & 1 \end{bmatrix} \Rightarrow a < 1 \tag{4.3.13}$$

where $a = e^{-\alpha T}$ The condition (4.3.13) is satisfied due to the fact that T and α are always positive. So, the increment of the Lyapunov function is negative implying that the tracking error tends asymptotically to zero, i.e.

$$\lim_{k \to \infty} \hat{\mathbf{\Psi}}_k = \mathbf{\Psi}_k \tag{4.3.14}$$

Since $\mathbf{i}_k^T \mathfrak{I}$ is bounded, (4.3.8) is reduced to

$$\begin{bmatrix} e_{k+1}^{\omega} \\ e_{k+1}^{L} \end{bmatrix} = \begin{bmatrix} -l_1 & -\frac{T}{J} \\ -l_2 & 1 \end{bmatrix} \begin{bmatrix} e_k^{\omega} \\ e_k^{L} \end{bmatrix} \tag{4.3.15}$$

Finding suitable l_1 and l_2 constants, the system (4.3.15) will be asymptotically stable and the observer (4.3.4) will asymptotically track the plant. A well known Jury's stability test [1] criterion for a second order system will help to find l_1 and l_2.

The characteristic equation of (4.3.15) is

$$z^2 + (l_1 - 1)z + (-l_1 - \frac{T}{J} l_2) = 0 \tag{4.3.16}$$

Comparing (4.3.16) with an algebraic second order equation

$$z^2 + a_1 z + a_2 = 0$$

$$\begin{aligned} a_1 &= (l_1 - 1) \\ a_2 &= (-l_1 - \frac{T}{J} l_2) \end{aligned} \tag{4.3.17}$$

The Jury's stability test establishes for a second order system the following conditions

$$\begin{aligned} &a_1 < 1 \\ &a_2 > -1 + a_1 \\ &a_2 > -1 - a_1 \end{aligned} \tag{4.3.18}$$

and with some computations we obtain the following conditions that make the observer a stable system

$$\begin{aligned} &1 < l_1 < 2 \\ &l_2 < 0 \end{aligned} \tag{4.3.19}$$

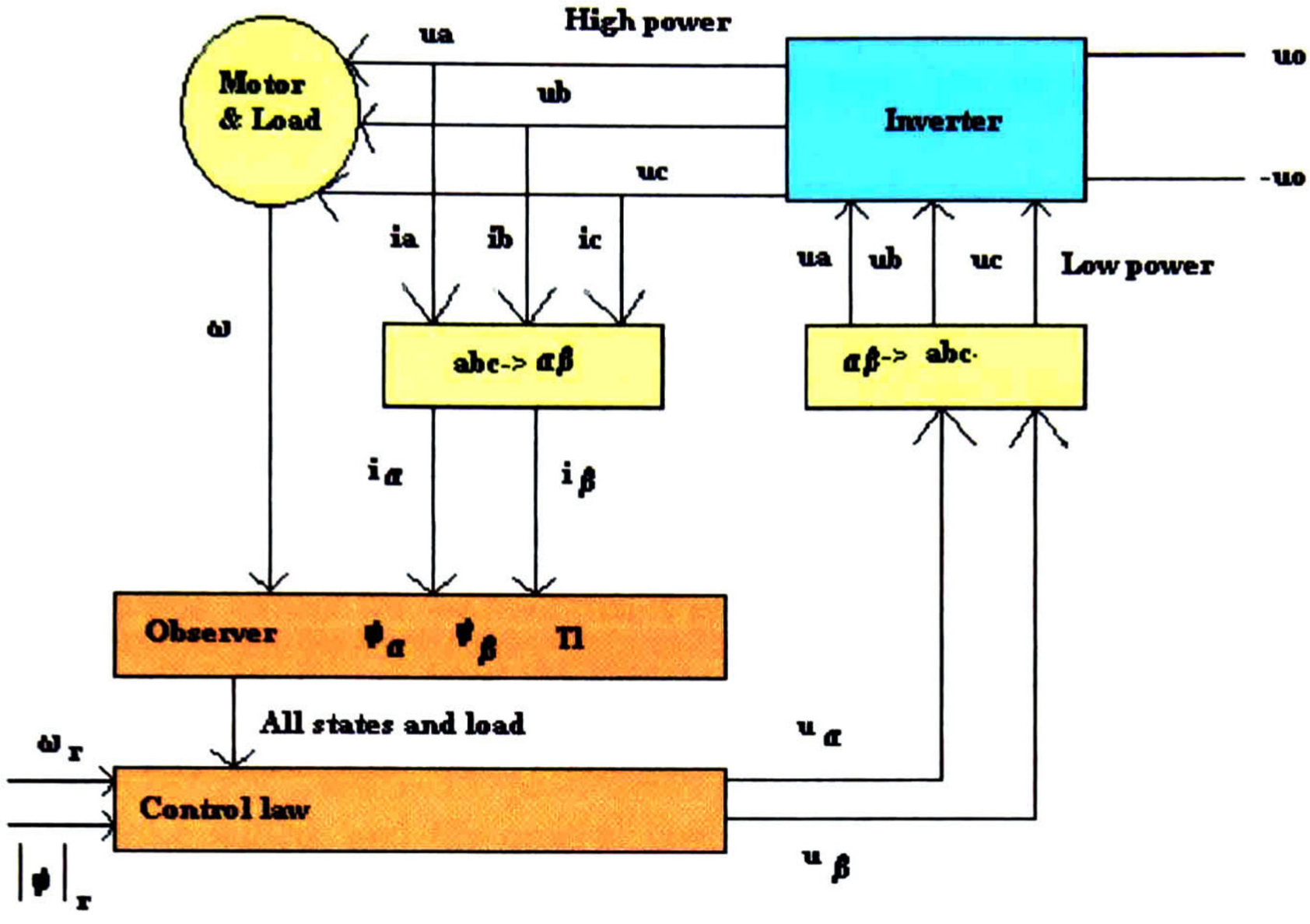

Figure 4.3. System configuration diagram.

Finally, Figure 4.3 shows a detailed view of the manipulated variables. We observe that the speed and currents are measurable from the motor. The blocks with labels $abc \rightarrow \alpha\beta$ and $\alpha\beta \rightarrow abc$ transforms the variables from a,b,c to α,β and α,β to a,b,c respectively depending on the direction of the signals. We also note the block named '*inverter*' transform the low power control signals coming out the computer to high power signals capable of driving the motor. The fluxes and load are estimated with speed and current measurements. All the state information is fed to the control law block and the reference signals as well. In chapter six we will deal with details about transformations and the inverter device, and how to implement the whole system.

Chapter five

Results

5.1 INTRODUCTION

Simulations are carried out in SIMNON to demonstrate the effectiveness of the above discrete-time sliding mode and observers. All reference signals are generated from second-order exosystems, except for the load that is generated from a first-order exosystem. The flux magnitude reference is simulated always constant, the speed reference is simulated constant and with a sinusoidal reference. The load is simulated constant and as a square shape signal with noise added, and the control law is simulated as a discontinuous and continuos sliding mode, making a total of eight different simulations. Then, the control law combined with an observer is simulated to track a constant signal. The load is considered as a square shape noisy signal and the rotor fluxes is simulated as well.

5.2 CONTROL LAW SIMULATIONS

In the following table are shown all the induction motor and control law parameters:

PARAMETER	VALUE	DESCRIPTION
Rs	14 ohms	Stator Resistance
Ls	400 Mh	Stator Inductance
M	377 Mh	Mutual Inductance
Rr	10.1 ohms	Rotor Resistance
Lr	412.8 mH	Rotor Inductance
n_p	2	Number of Pole Pairs
J	0.01Kgm^2	Moment of Inertia
ω_n	168.5 rad/sec	Nominal speed

PARAMETER	VALUE	DESCRIPTION
T_{Ln}	1.1 Nm	Nominal Load Torque
T	0.001 sec	Sampling Period
u_o	330	Voltage bound
k_1	0.9	Control law gain
k_2	0.9	Control law gain
l_1	0.5	Observer gain
l_2	-0.5	Observer gain
$\psi_k^{\alpha}(0)$	0.001	ψ_k^{α} initial condition
$\psi_k^{\beta}(0)$	0.001	ψ_k^{β} initial condition
$z_k^3(0)$	-0.5	z_k^3 initial condition
$z_k^4(0)$	0.5	z_k^4 initial condition

Other initial conditions are zero.

5.2.1 Continuos sliding mode simulations

We set the speed tracking reference signal as a constant signal at the nominal value. The flux amplitude tracks a constant signal at $0.2wb^2$ for all simulations, and the load is considered as a constant signal at $0.7Nm$ and in time $t = 5\,\text{sec}$ raises to the nominal load as shown in Figure 5.1. The time axis in all the graphics are in seconds.

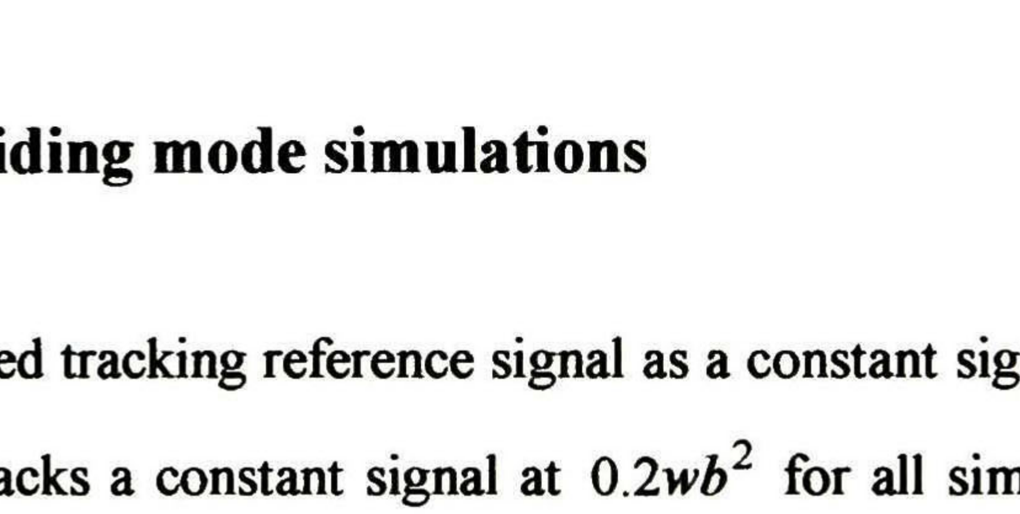

Figure 5.1 Load affecting the motor.

Figure 5.2 shows the output signals with their references. We observe that the output signals exactly tracks the reference signals, and that the load change does not affect the outputs due to the robustness of sliding mode.

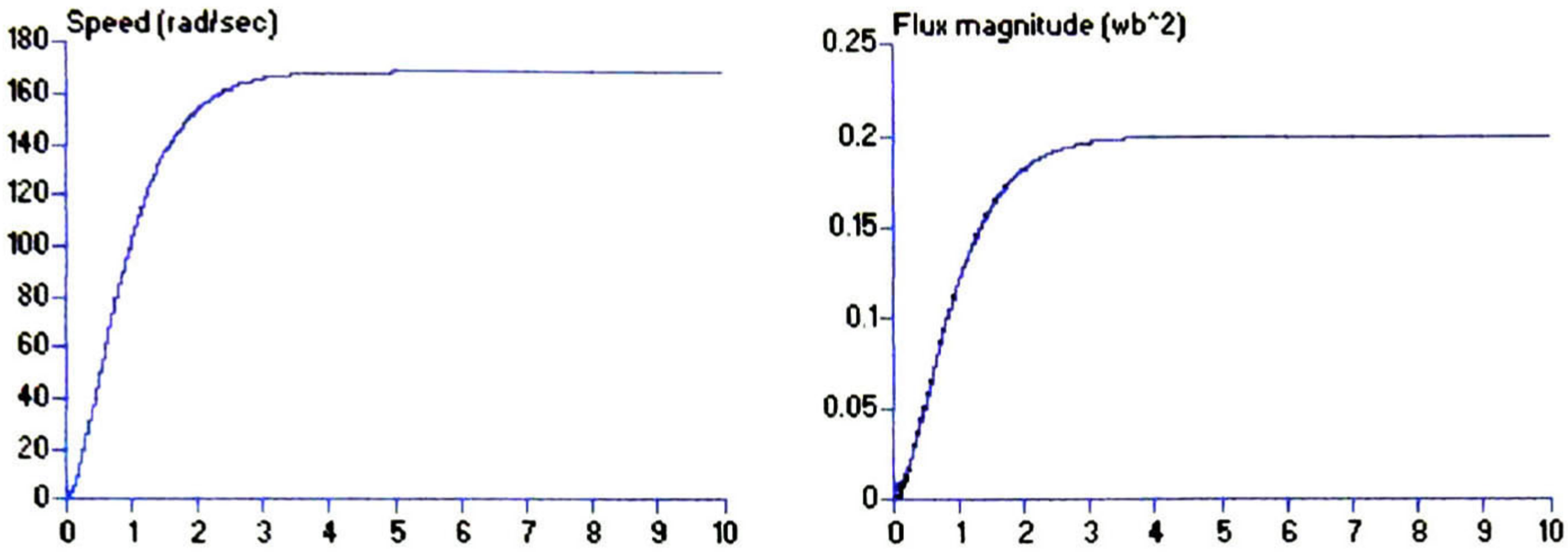

Figure 5.2. Output signals with their references in black.

In Figure 5.3 we found the tracking error signals. We observe that errors z_k^3 and z_k^4 decay in finite time due the sliding mode, actually it just took one step to tend to zero. On the other hand the errors z_k^1 and z_k^2 decay asymptotically to zero.

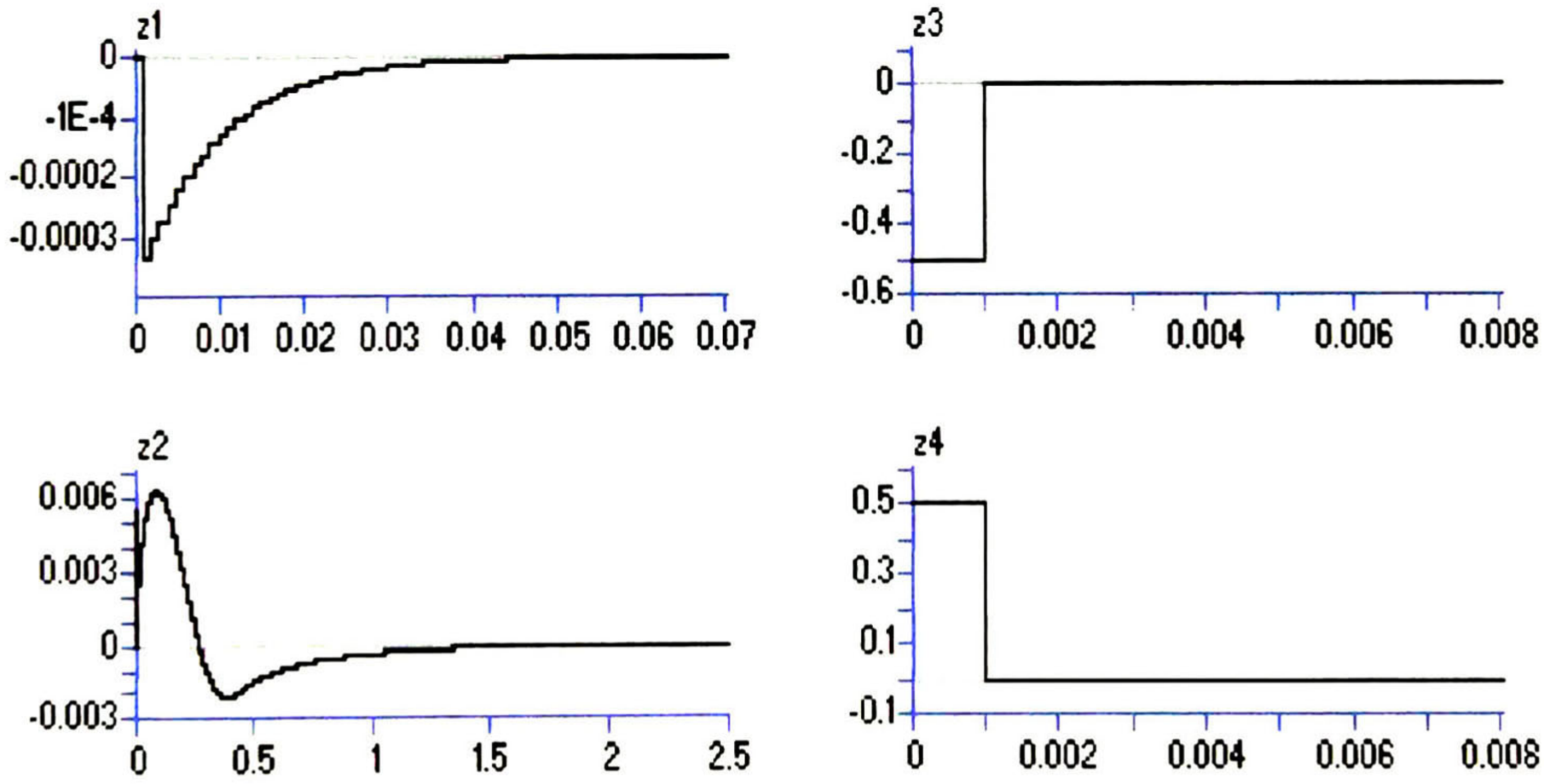

Figure 5.3. Tracking error signals.

Figure 5.4 illustrates the voltages, currents and fluxes flowing through the motor. We note how the voltages and currents increase their values at $t = 5\,\text{sec}$ just when the load increases, but the fluxes are not affected by the load change.

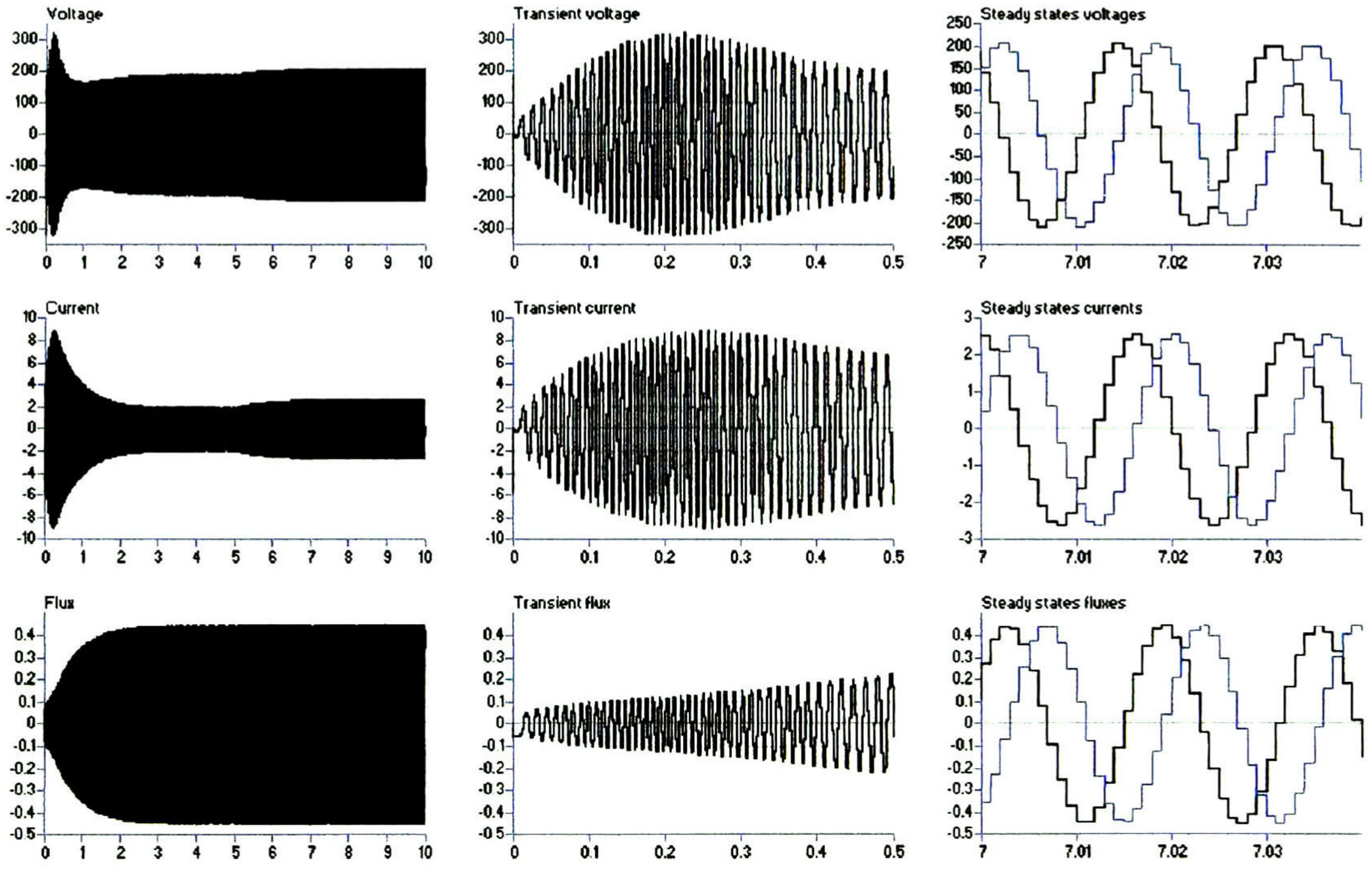

Figure 5.4. Voltages, currents and fluxes signal.

From the last scenario, we only change the reference signal for speed tracking to a sinusoidal signal with a peak value of 70 *volts* and a frequency of 3 $\frac{rad}{\text{sec}}$. Figure 5.5 shows the output signals. We observe that the speed tracks exactly the reference signal and the flux magnitude tracks the reference with a slight amount of error. Figure 5.6 shows the tracking error signals where we observe that error z_k^1 decay asymptotically to zero and z_k^2 oscillate a little bit around zero. z_k^3 and z_k^4 decay in finite time to zero. Figure 5.7 illustrates the voltages, currents and fluxes of the motor. We observe the rich dynamics responses due to sinusoidal speed.

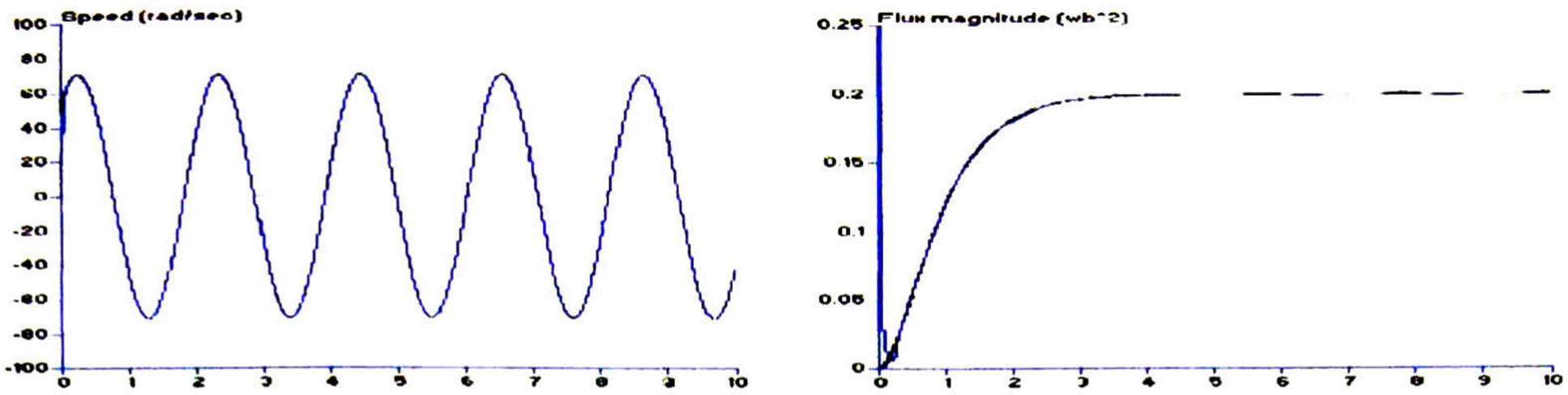

Figure 5.5. Output signals in the second scenario with their references in black.

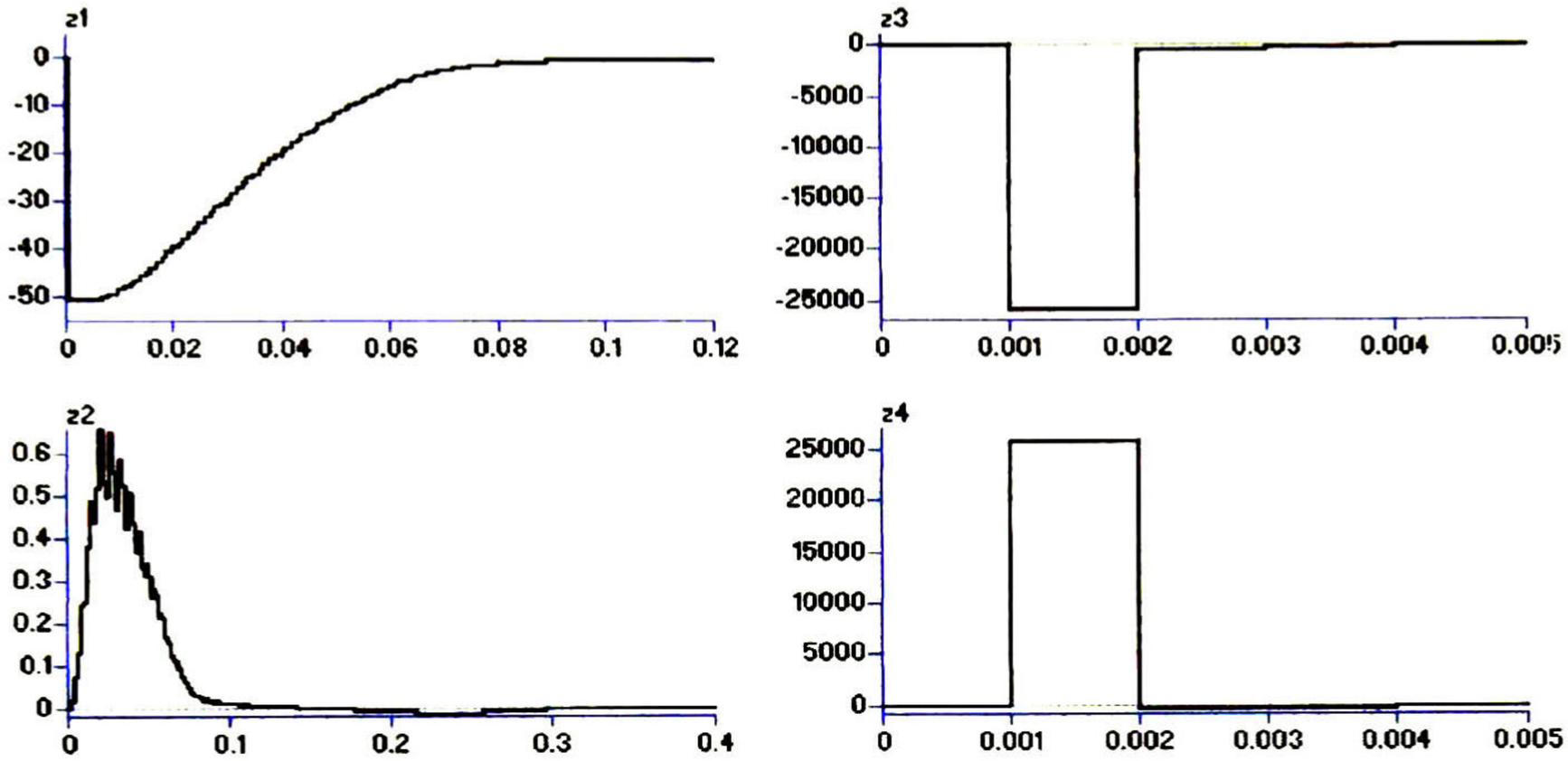

Figure 5.6. Tracking error signals in the second scenario.

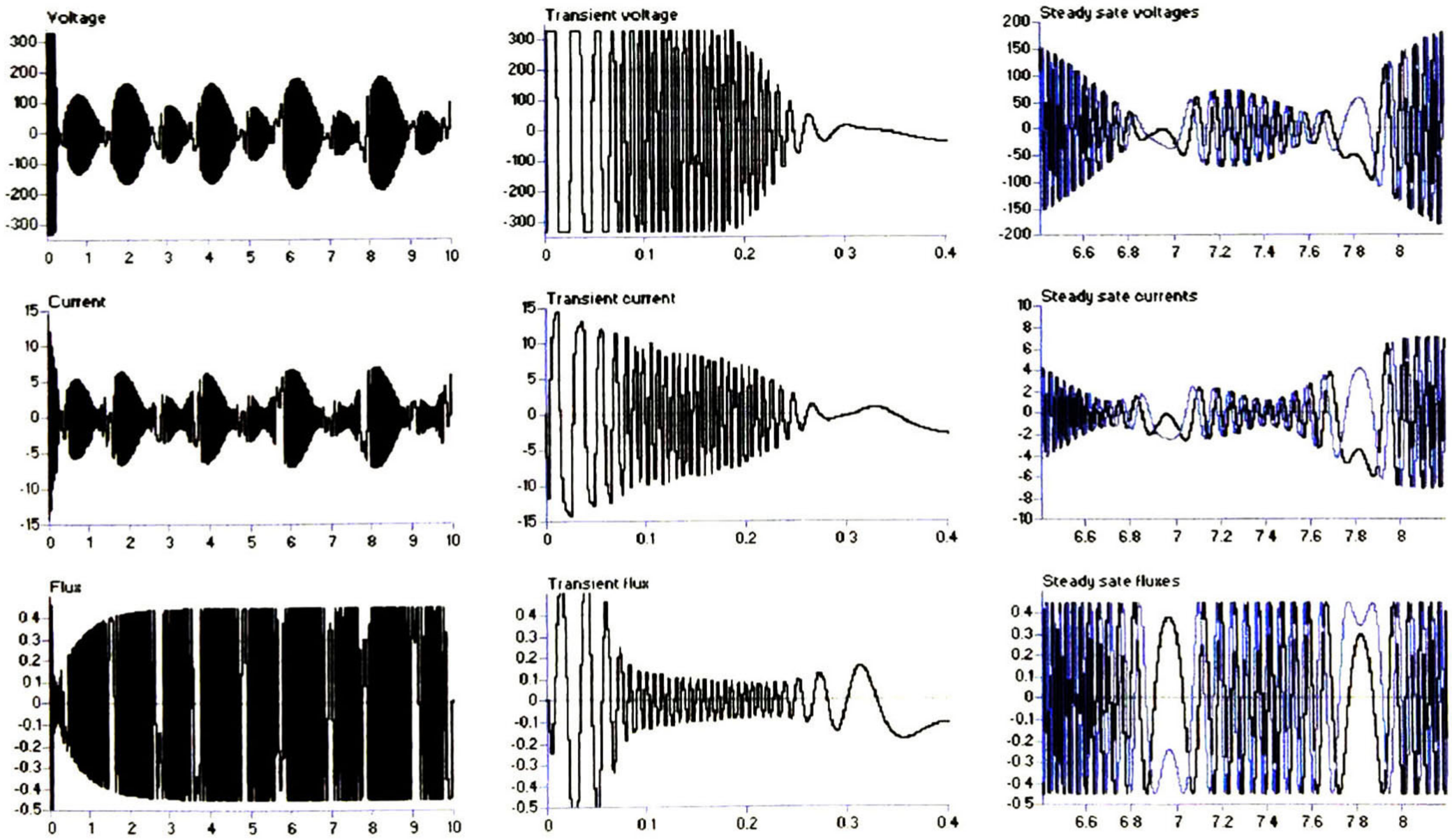

Figure 5.7. Voltages, currents and fluxes from the second case.

Now we show the simulation results with constant speed reference signal at the nominal value and a square shape load with noise as seen in Figure 5.8.

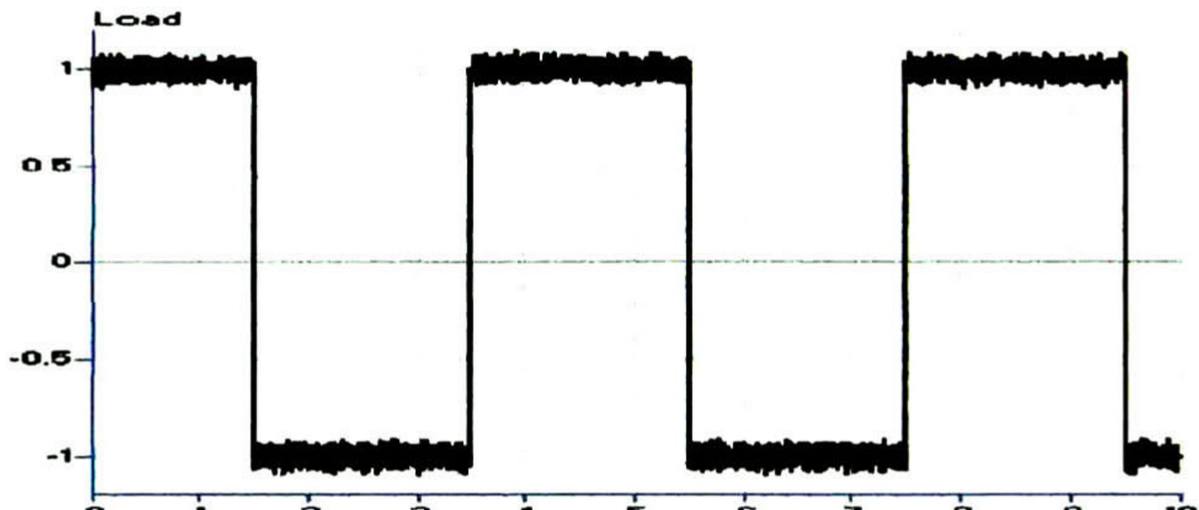

Figure 5.8. Square shape load.

Figure 5.9 illustrates the output signals, and Figure 5.10 illustrates the error signals.

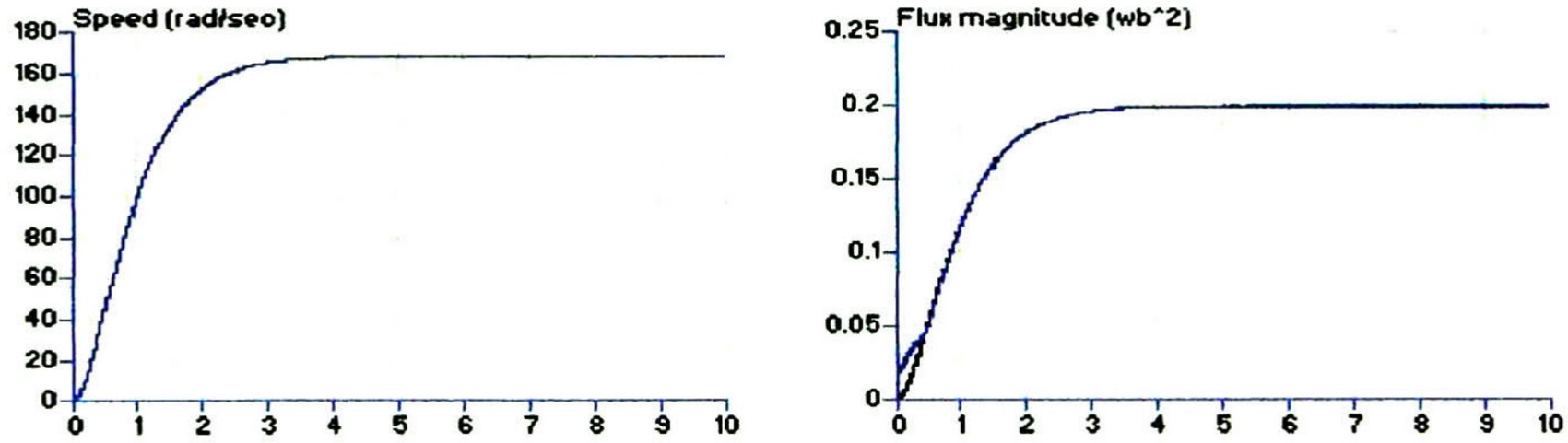

Figure 5.9. Output signals with the load of Figure 5.8.

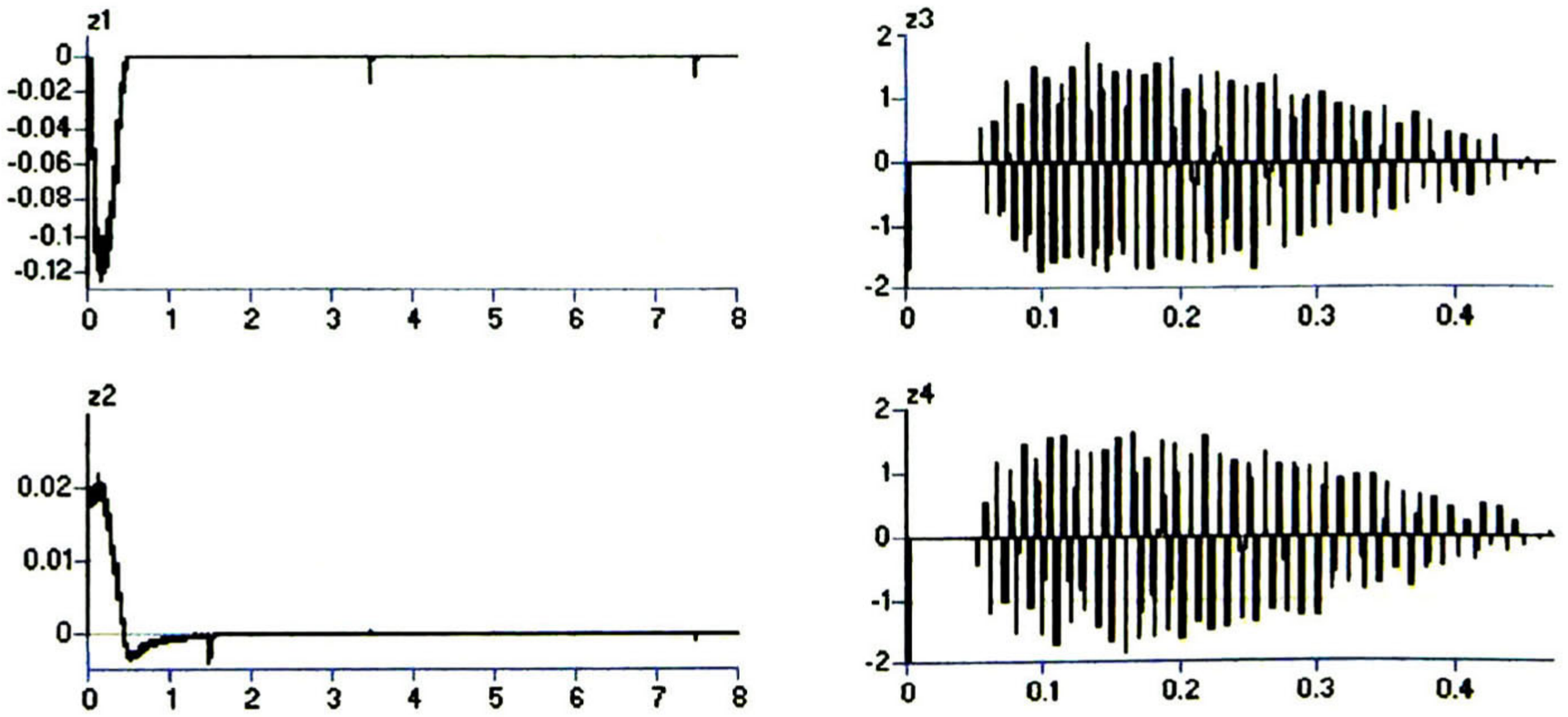

Figure 5.10. Error tracking signals.

Figure 5.11 shows the voltages, currents and fluxes. We observe that the voltage change its magnitude to get ride of the load.

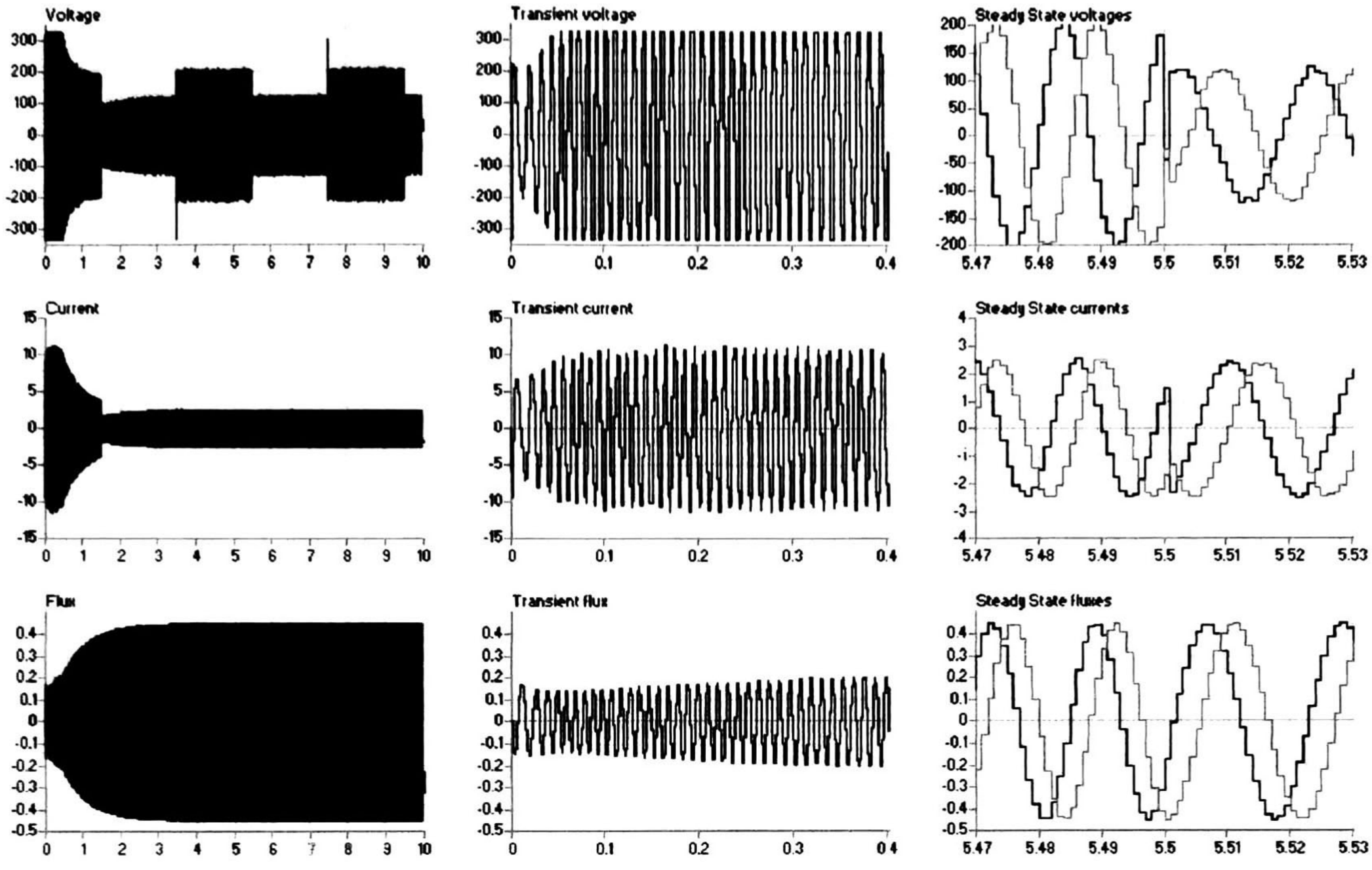

Figure 5.11. Voltages, currents, fluxes signal.

Here we present the worst case scenario, compound by the square shape load with noise and the sinusoidal speed reference. Figure 5.12 shows the output signals.

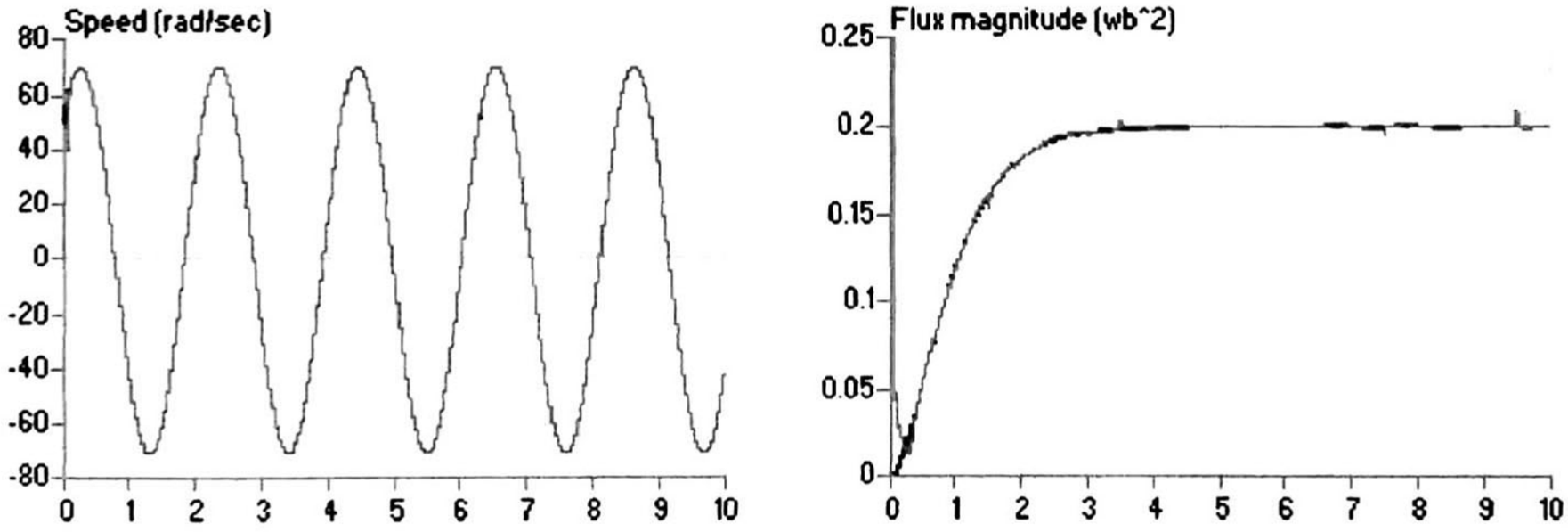

Figure 5.12. Output signals.

Figure 5.13 shows the tracking error signals.

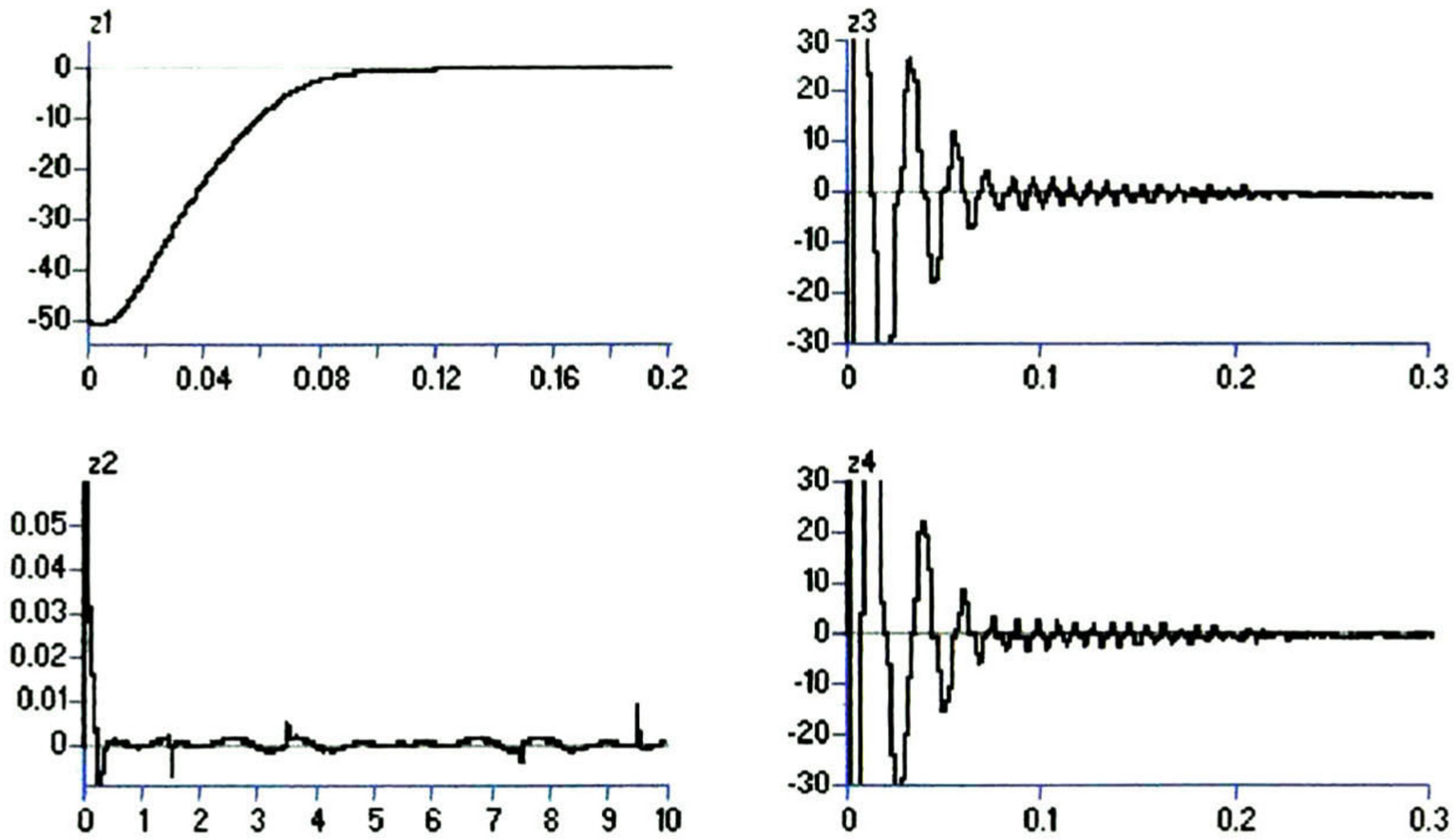

Figure 5.13. Error signals.

Figure 5.14 illustrates the voltages, currents and fluxes that we found inside the motor.

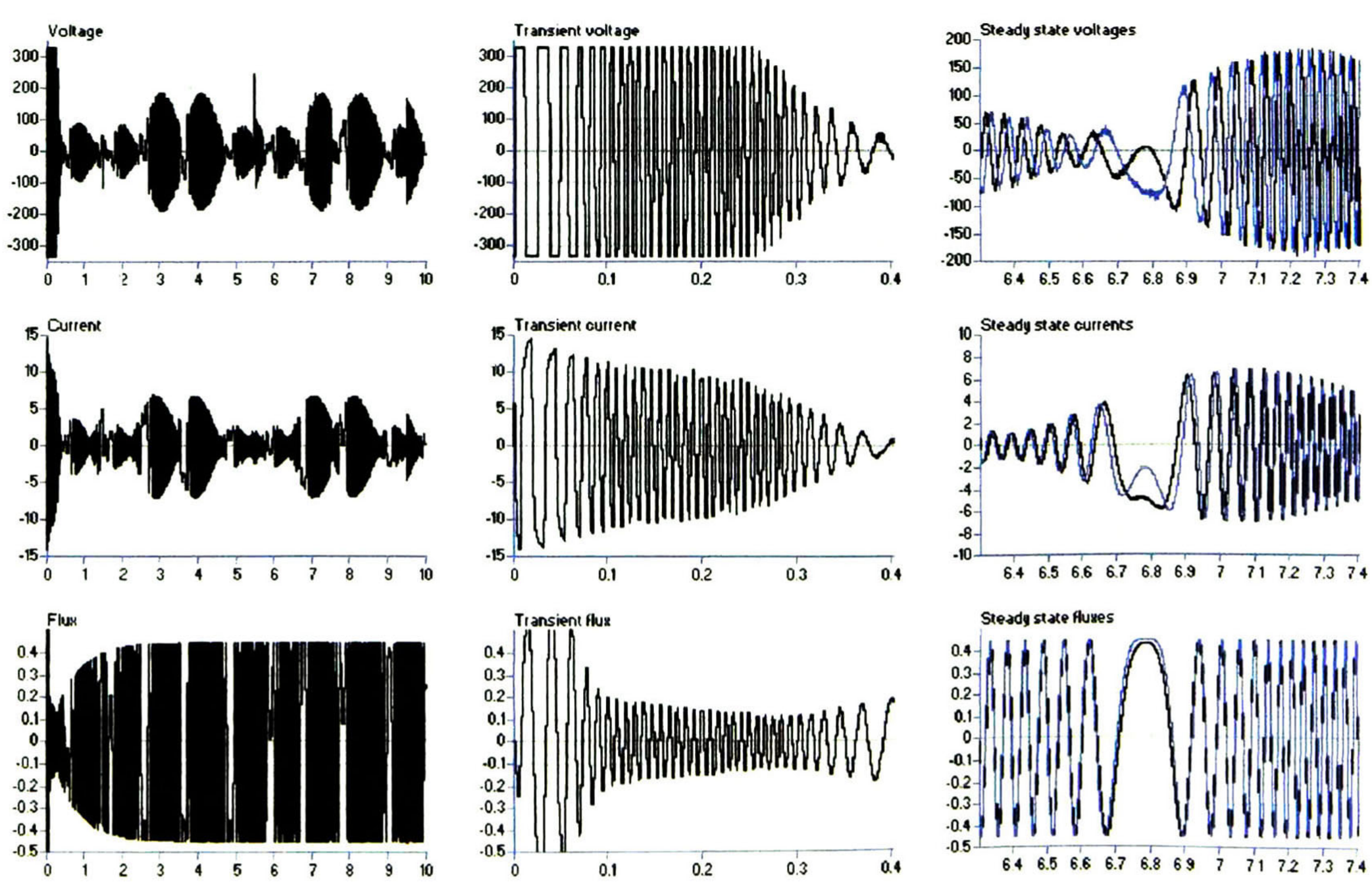

Figure 5.14. Voltages, currents and fluxes in the worst case scenario.

We conclude from all the simulations with the continuous sliding mode control law, that the voltage changes according load and speed variations. We observe that the fluxes always preserve the same magnitude due to the constant flux magnitude control. The error signals always decays to zero or stay nearby. In general, the control law acceptably achieves our control objectives.

5.2.2 Discontinuous sliding mode simulations

We will show only one simulation just to compare what control performs the best. Taking into consideration the simplest case with a constant reference for speed and flux magnitude and a constant load. Figure 5.15 shows the output signals. We observe that the speed is well tracked and the flux magnitude has a considerable amount of noise around the set point. From this facts we conclude that the continuos controller performs better than the discontinuous one.

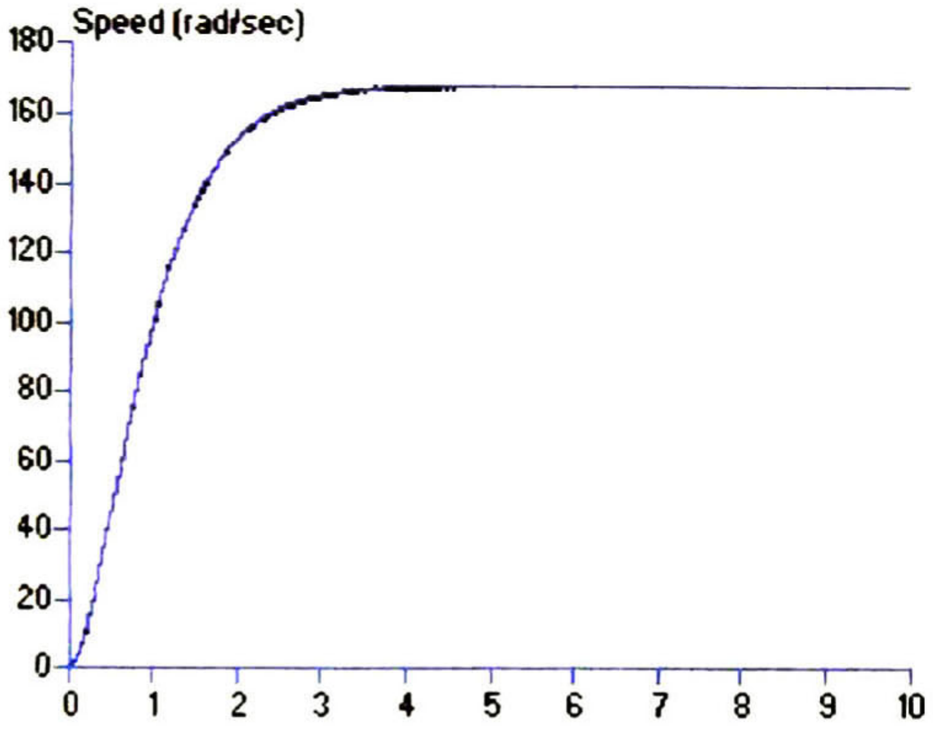

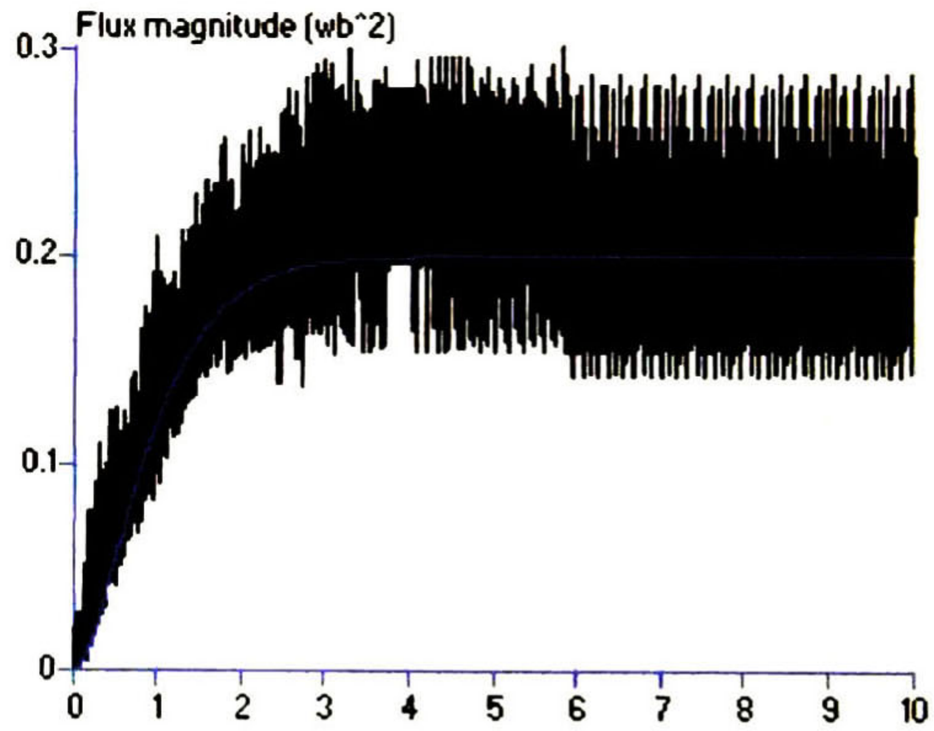

Figure 5.15. Outputs signals.

Figure 5.16 shows the tracking error signals. We observe that the speed error tracking is not zero by a relatively small amount of error. z_k^3 and z_k^4 does not perform the sliding mode principle, instead of that they perform a lot of noise around zero.

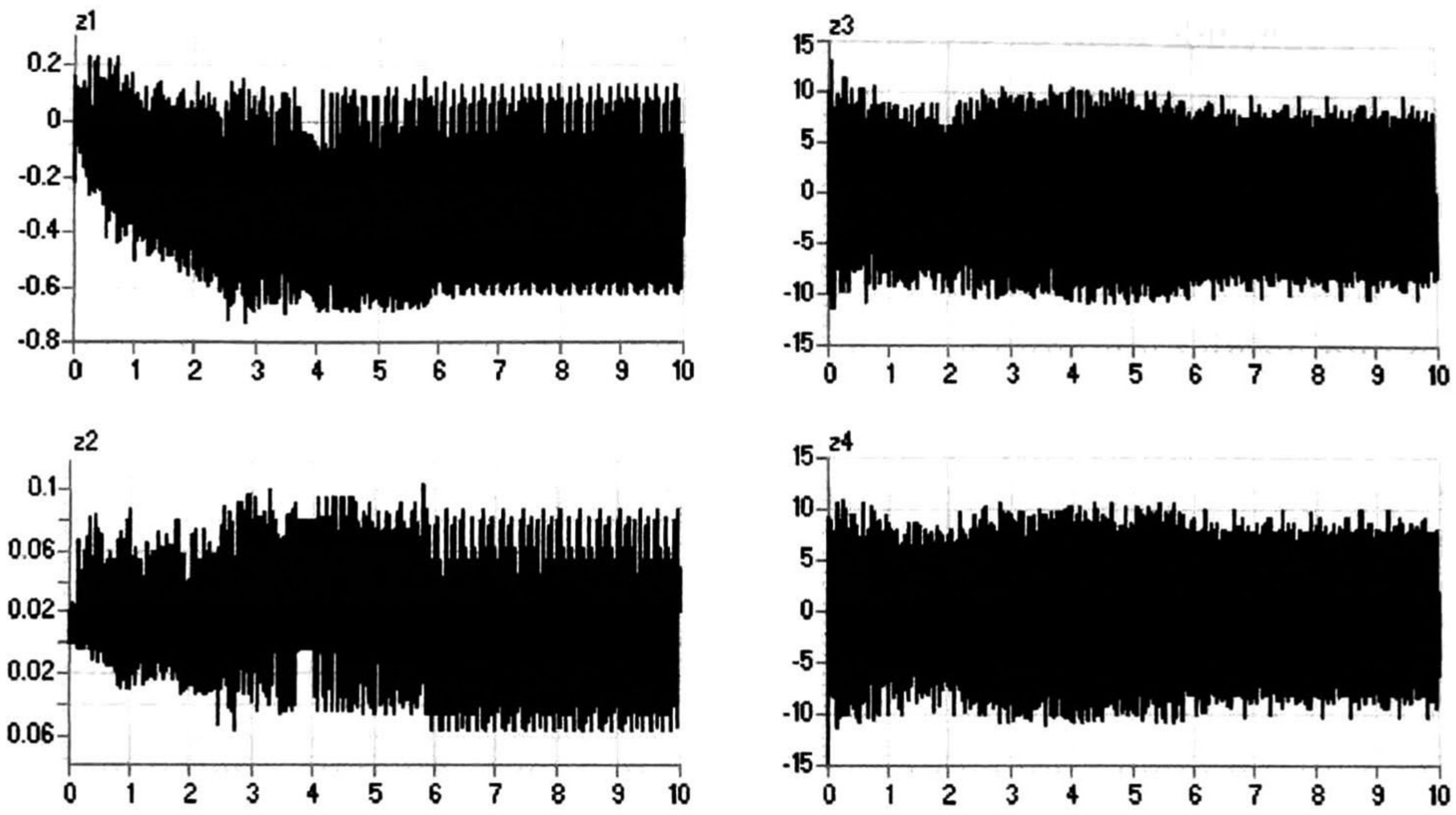

Figure 5.16. Error signals.

Finally Figure 5.17 illustrates the voltages, currents and fluxes interacting in the motor.

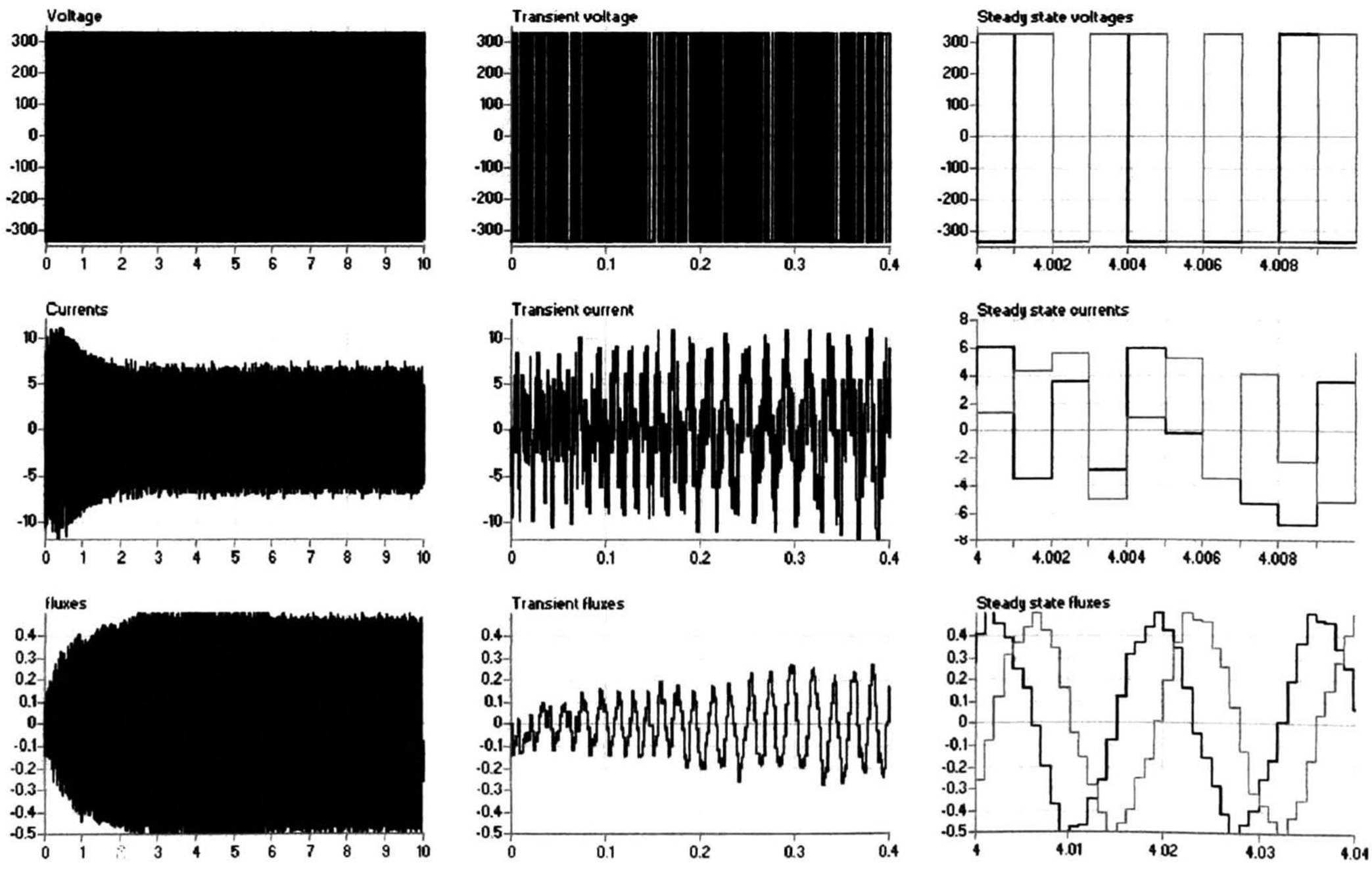

Figure 5.17. Voltages, currents and fluxes signal.

We note that the voltages are pulses (discontinuous voltage) that can be applied directly to a device with discontinuous inputs like an IGBT to drive the motor. The currents remain with the same amplitude but the sinusoidal form is lost. The fluxes are almost the same but just with a little bit of distortion.

5.3 OBSERVER SIMULATIONS

The observer was simulated with a constant reference for speed and flux magnitude, and with a noisy square shape load. Figure 5.18 illustrates the fluxes of the rotor with its observed fluxes (in blue).

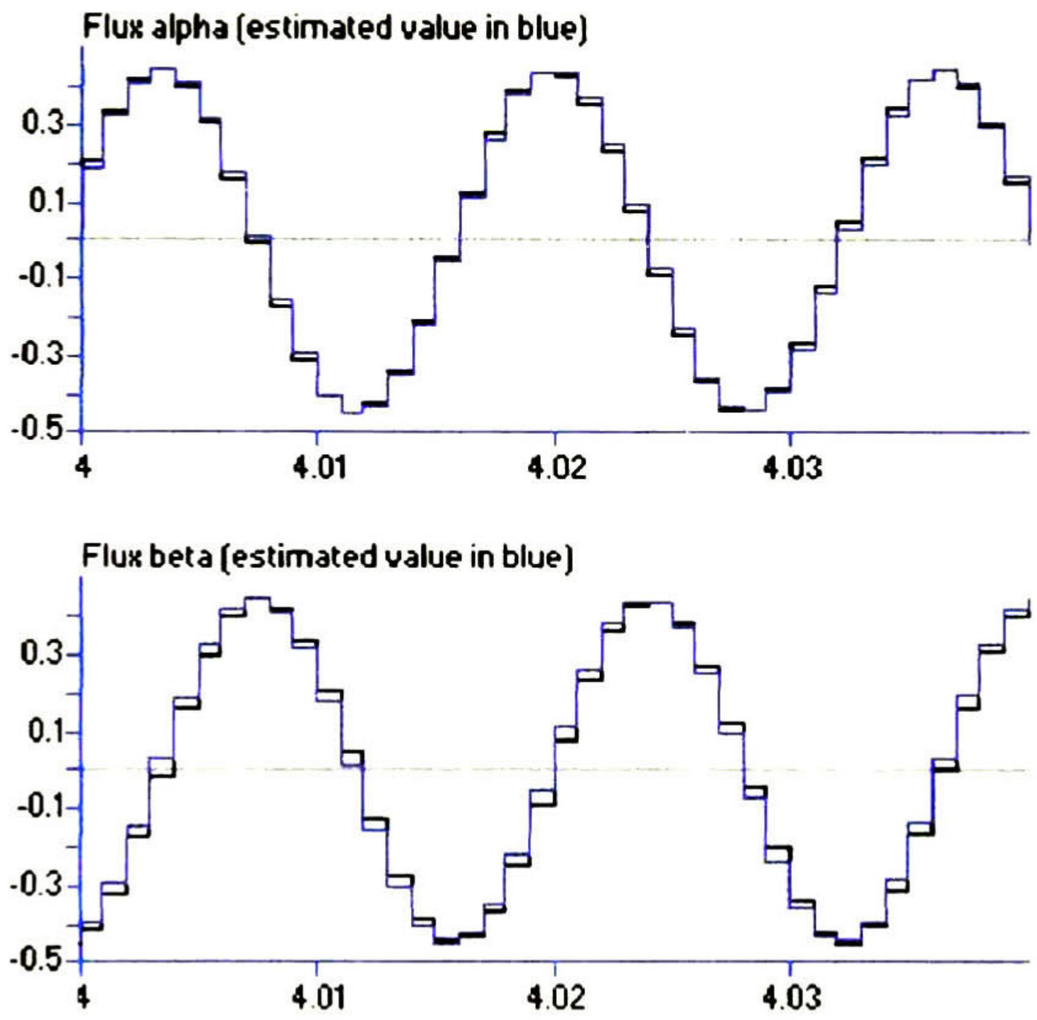

Figure 5.18. Simulated plant and observed fluxes.

We appreciate that the fluxes are well tracked by the observer, due to the stable flux dynamics. Figure 5.19 illustrates the load observation results

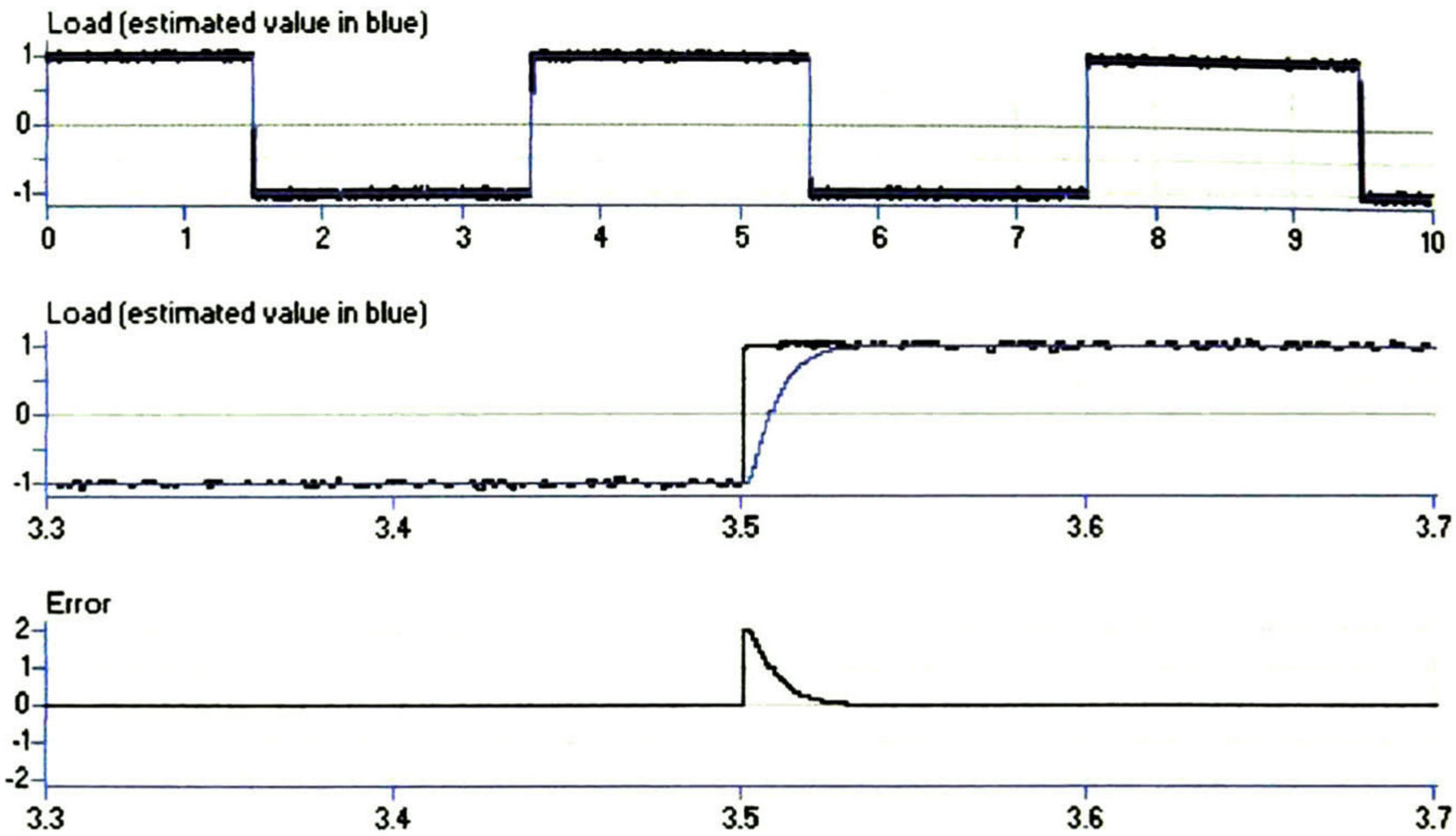

Figure 5.19. Observed load and tracking error.

Despite that the observer models the load as a constant load, it tracks so fine a square shape signal. Note when the load change of value, the observer response is fast. Figure 5.20 shows the output signals.

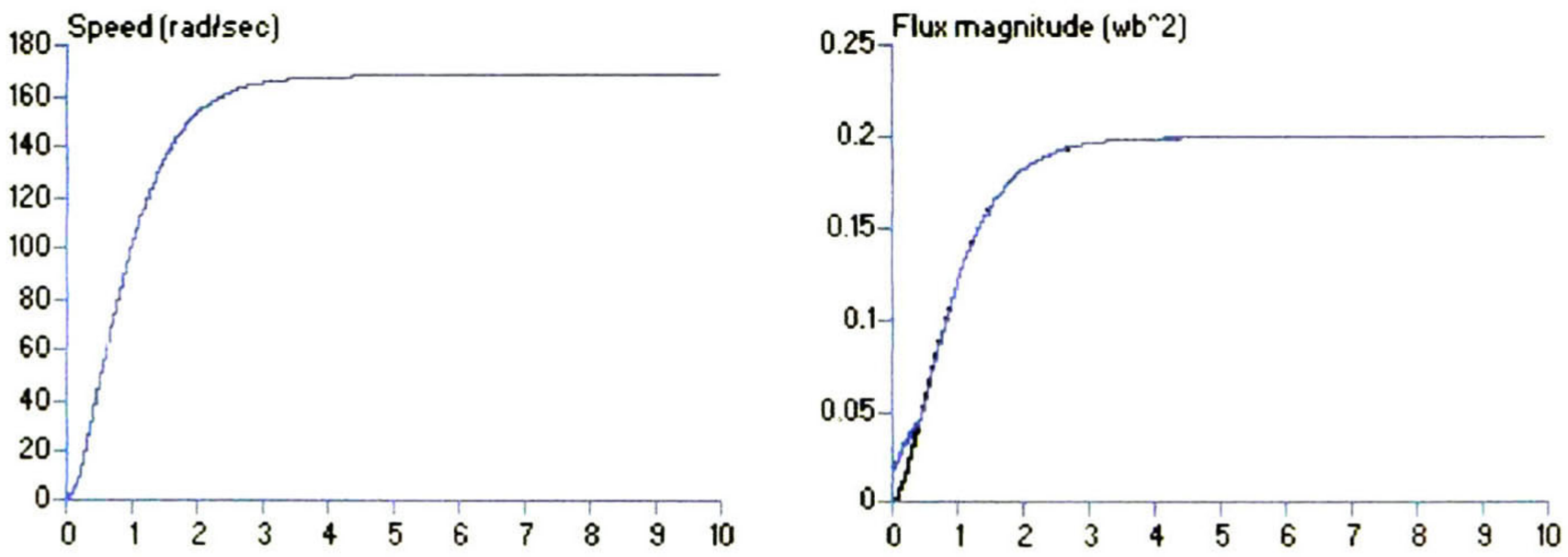

Figure 5.20. Output signals with its references in black.

We can appreciate that the output signals exactly tracks the references, it looks like the non-observer based simulations. The observer brings the non-accessible information to accomplish a real time implementation.

Chapter six

Practical aspects for a real time future implementation

6.1 INTRODUCTION

The last chapters review all the theoretical aspects of the induction motor. In chapter two, a compact induction motor model has been presented with the help of transformation variables [9] moreover, a discrete-time version of this model has been developed for a real time future implementation. Then in chapter three we revisit basic concepts of control theory, like exosystems and sliding modes, and developed block control and sliding mode technique for discrete-time nonlinear systems. Chapter four is an application of the concepts developed in chapter three to the discrete-time version model found in chapter two. Chapter 5 illustrates all the simulations to prove all the results found in chapter four. Now it is time to view some practical aspects for a real time future implementation. Figure 6.1 will serve as a guide for this section.

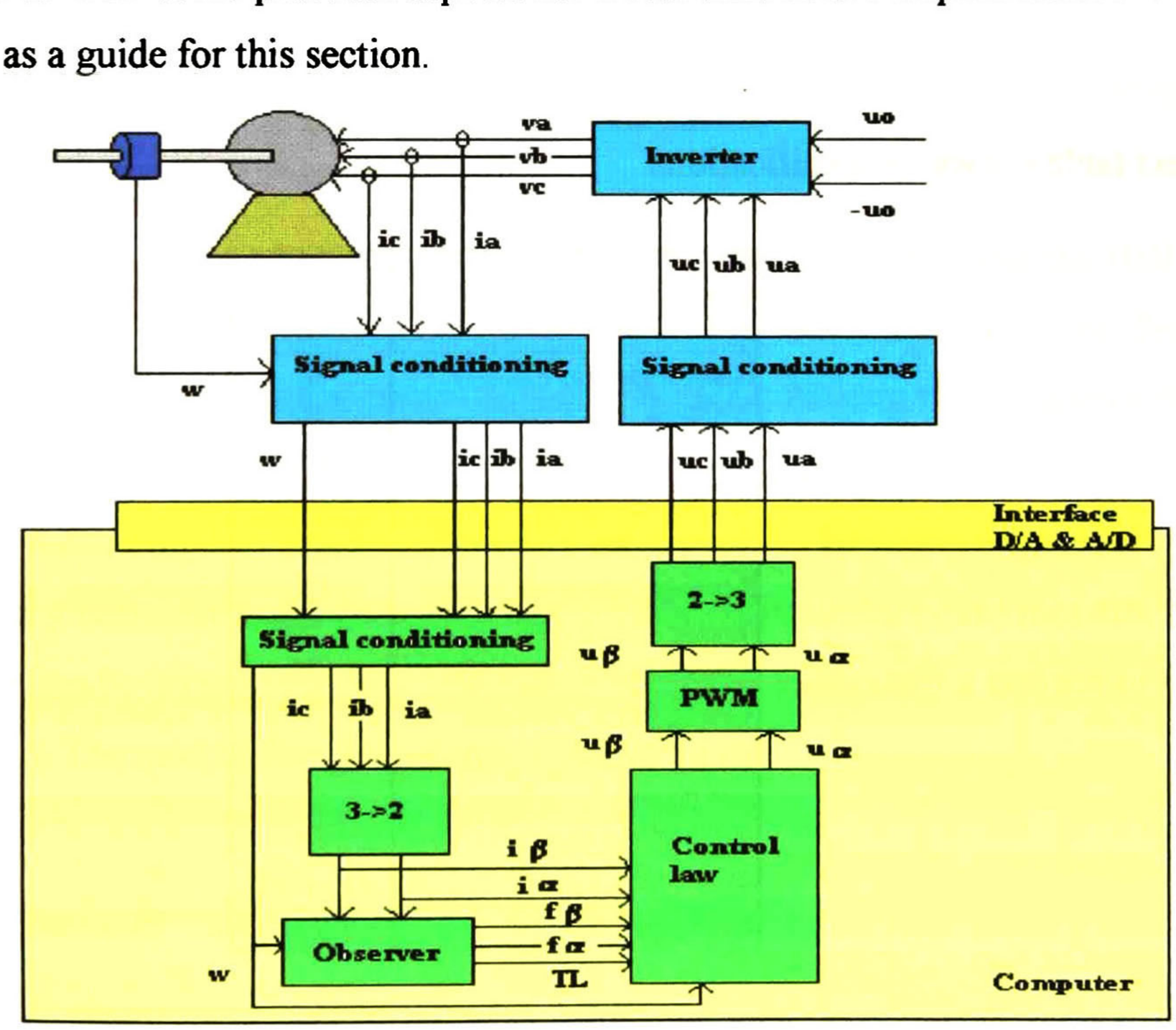

Figure 6.1. Block diagram for a real time implementation of the induction motor.

6.2 SENSORS

6.2.1 Speed sensor

To determine the angular velocity of the rotor, a shaft coupled tach generator can be used. For example, the tach generator BTG 1000, manufactured by BALDOR ELECTRIC CO., is shown in Figure 6.2

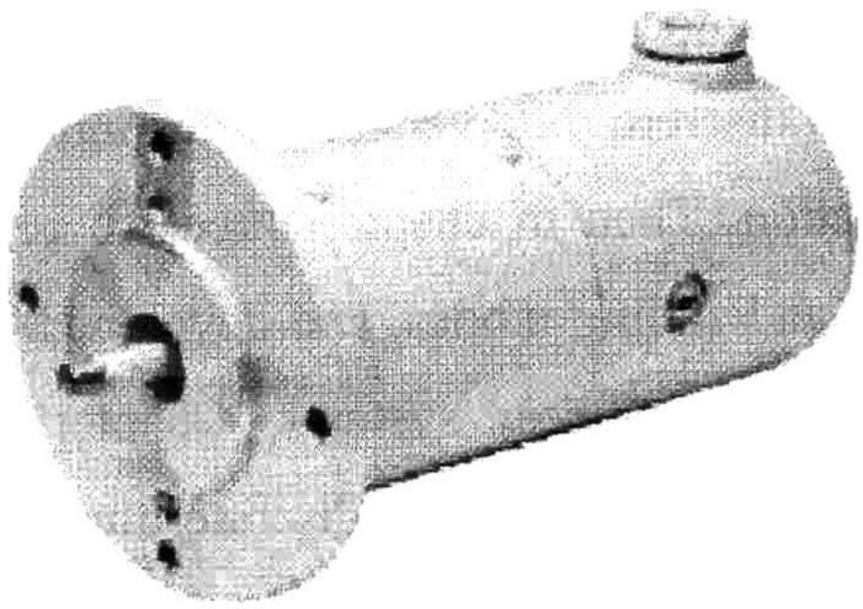

Figure 6.2. Picture of the tach generator BTG 1000 by BALDOR ELECTRIC CO.

The next table shows its specifications.

Specification	Type BTG1000
Voltage Gradient (V/1000rpm)	50
RMS Ripple	8%
Maximum Speed (rpm)	5000
Maximum Current (mA)	400
Armature Resistance (at 25°C)	52Ω
Armature Inductance (mH)	124
Armature Inertia ($kg.cm^2$)	1.175
Maximum Terminal Voltage (Vdc)	250
Reversing Error	2%
Min. Load Resistance for 1% Linearity	—
Shaft Diameter	⅜"
Mounting Spigot Diameter	2"
Mounting Holes & PCD	4 @ 4" PCD
Weight approx. (kg)	2.7

This dc tachometer supplies a dc voltage that is proportional to the motor rpm, and the polarity is changed with the direction of rotation. This type is suitable for regulation within a very wide range of armature speeds. It also has the advantage of generating a very low ripple-voltage, which results in good regulation at low motor rpm.

6.2.2 Current sensor

To measure the currents that flow to the stator of the motor we can use a current transducer. For example, the RS 286-327 manufactured by RS is shown in Figure 6.3

Figure 6.3. Current transducer.

This is a fast response PCB mountable current transducer employing the Hall effect principle to accurately measure ac, and dc currents. The transducer uses the feedback operating technique and has high accuracy analogue outputs. Passing the conductor through a 10mm diameter hole senses the primary current. An increase in sensitivity can be achieved when measuring lower currents than the nominal 50A by increasing the number of times the primary current conductor passes through the center hole, i.e. to measure 5A, 10 passes of cable can be arranged giving 50 ampere turns and a full output current or voltage signal is derived. The next table shows its specifications

RS stock no.	**286-327**
Nominal current I_N	50A rms
Output modes	
1. Current output	1mA/A
Measuring range	0 to ±160A (Supply voltage ±15V; Rmeas = 50Ω)
Overall accuracy at +25°C	±0.5% of I_N
2. Voltage output	100mV/A
Measuring range	∿ to ±50A
Overall accuracy at +25°C	±1.0 of I_N
Turns ratio	1:1000
Supply voltage	±15V (±5%)
Dielectric strength	3kVrms/50Hz/1 min

6.3 SIGNAL CONDITIONING

Electrical signals can be generated by transducers to measure physical phenomena such speed, currents, temperature, sound, force, etc. To measure a signal from transducers, you must convert them into a form that the computer interface can accept. For example, the output current of the current transducer is very large. Therefore you may convert it to voltage, then lower the output and isolating before digitizing. The manipulation of signals to prepare them for digitizing is called *signal conditioning*. The following are some common types of signal conditioning

- Amplification
- Isolation
- Filtering
- Transducer excitation
- Linearization

In the case of the tachometer, in order to use the output of this device, it is required that its voltage output level must be acceptable, for example, if at 1800 rpm we need an output

of 5V, then we apply a voltage divider with a gain of $5.5556x10^{-2}$. The main inconvenient of using a tachometer is noise level in its output, so, a low pass filter is needed.

The current sensor can operate in two different output modes, current and voltage output. Figure 6.4 shows such configurations

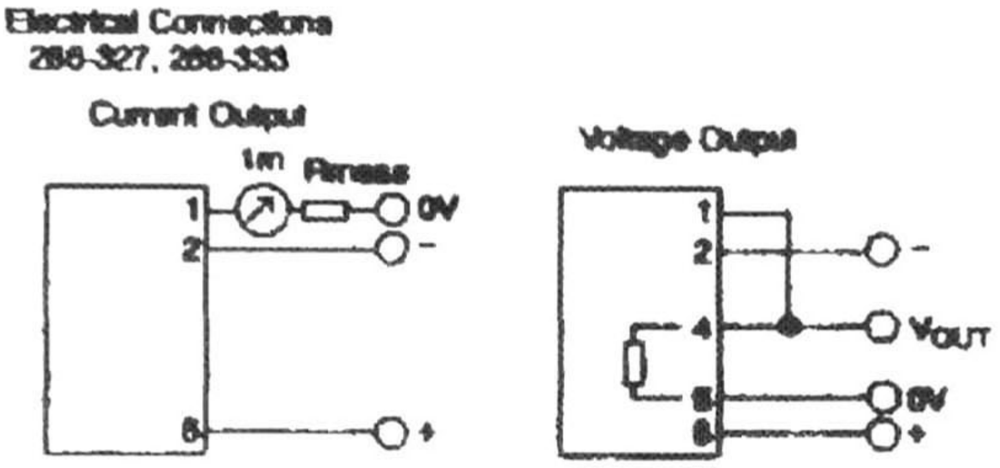

Figure 6.4. Electrical connections of RS 286-327.

Suppose that we want to work with the current output configuration, then the Rmeas resistance is choose to get the desired voltage level.

To isolate the signal ground reference of the incoming signals to the computer in order to avoid a short-circuit if something fails outside of this. It is necessary to dispose of isolation amplifiers. For example the ISO122 manufactured by BURR-BROWN is a precision isolation amplifier incorporating a novel duty cycle modulation-demodulation technique. The signal is transmitted digitally across a 2pF differential capacitive barrier. With digital modulation the barrier characteristics do not affect signal integrity, resulting in excellent reliability and good high frequency transient immunity across the barrier. Both barrier capacitors are inbedded in the plastic body of the package. Figure 6.5 shows a picture of the isolation amplifier and a schematic diagram.

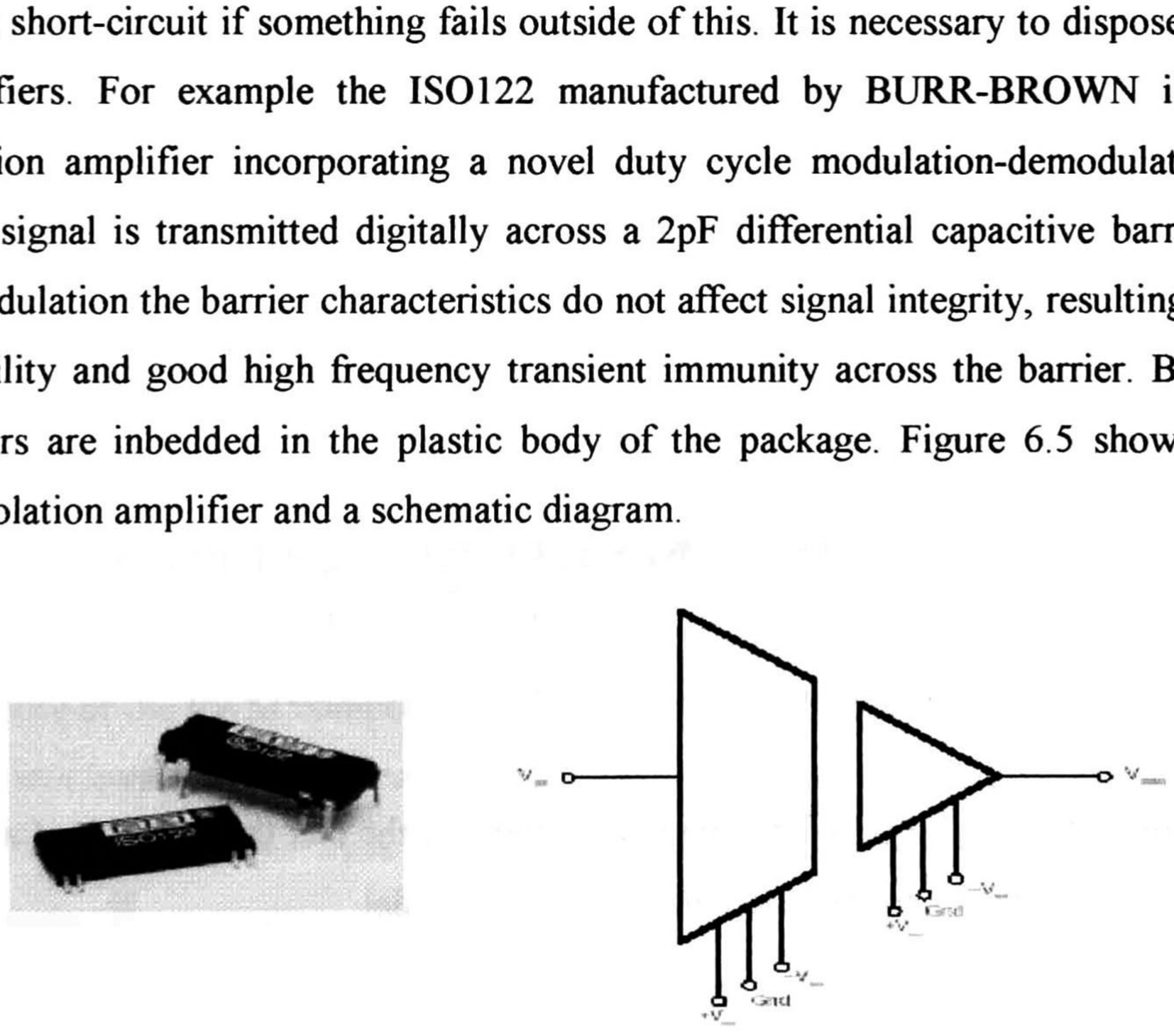

Figure 6.5. Schematic diagram and picture of ISO122.

The ISO122 is easy to use. No external components are required for operation. The specifications are 0.020% max nonlinearity, 50 kHz of bandwidth, and $200\mu V/^{o}C$ V_{os} drift. A power supply range of ±4.5V to ±18V.

Once the input signals (currents and speed) are conditioned, they enter the computer through the A/D converter. The software manipulates these signals to produce the control law. The first thing to do is to return this signals to the original levels, that is the reason for the block named 'signal conditioning' inside the computer.

As we will see later, the computer sends digital pulses that drive the IGBT. These pulses are also isolated in order to avoid computer damage. For example the optocoupler 4N25 is a very common device for digital signal isolation.

6.4 CURRENT TRANSFORMATION

We continue with the signal paths inside the computer, i.e. software execution. The stator currents are transformed to α,β currents using equation (2.2.5.3). The matrix $\mathbf{K}_s$ defined in (2.2.5.4) depends on the angular position of the rotating d,q axis, but this axis has been fixed to the stator, i.e. $\theta = 0$, yielding the next matrix

$$\mathbf{K}_s = \frac{2}{3}\begin{bmatrix} 1 & \frac{-1}{2} & \frac{-1}{2} \\ 0 & \frac{\sqrt{3}}{2} & -\frac{\sqrt{3}}{2} \\ \frac{1}{2} & \frac{\sqrt{3}}{2} & \frac{\sqrt{3}}{2} \end{bmatrix} \tag{6.4.1}$$

Using (6.4.1) in (2.2.5.3) for current variables and the fact that the sum of all three currents equals zero, we found these signals in the α,β model

$$
\begin{aligned}
i_\alpha &= i_a \\
i_\beta &= \frac{1}{\sqrt{3}}(i_a + 2i_b)
\end{aligned}
\tag{6.3.2}
$$

The voltage of the stator in α,β are transformed into a,b,c variables and if we substitute i by u in (6.4.2) and solve for a,b,c and using the fact that the sum of the voltages equals zero, we yield to the next set of equations

$$
\begin{aligned}
u_a &= u_\alpha \\
u_b &= -\frac{1}{2}u_\alpha + \frac{\sqrt{3}}{2}u_\beta \\
u_c &= -u_a - u_b
\end{aligned}
\tag{6.3.3}
$$

Then the signal path continues with the observer and the control law. These parts have been analyzed in chapter four. It is worth to mention that the exosystems are included in the control law block. As mentioned in an early chapter, a continuous control will depend on a PWM, but a discontinuous control will not. If we decide to apply a discontinuous control we can get rid of the PWM block. The discontinuous voltages coming from the PWM or the discontinuous control are transformed to a,b,c discontinuous voltages, where each variable can be -1 or 1, but in order to be considered as digital control signals, each of them should be 0 instead of -1.

6.5 PULSE WIDTH MODULATION

The purpose of the PWM component of the controller [2], is to generate pulses that trigger the transistor switches of the inverter. The pulse-width-modulated signal is created by comparing a fundamental sine wave from a sine-wave generator with a carrier triangle wave from a triangle wave generator as in Figure 6.6.

The variable width pulses from the PWM drives the gates of the switching transistors in the inverter and controls the duration and frequency that these switches turn

on and off. The frequency of the fundamental sine wave of the PWM determines the frequency of the output voltage of the inverter. The frequency of the carrier triangle wave of the PWM determines the frequency of the transistor switches and the resulting number of square notches in the output waveform of the inverter.

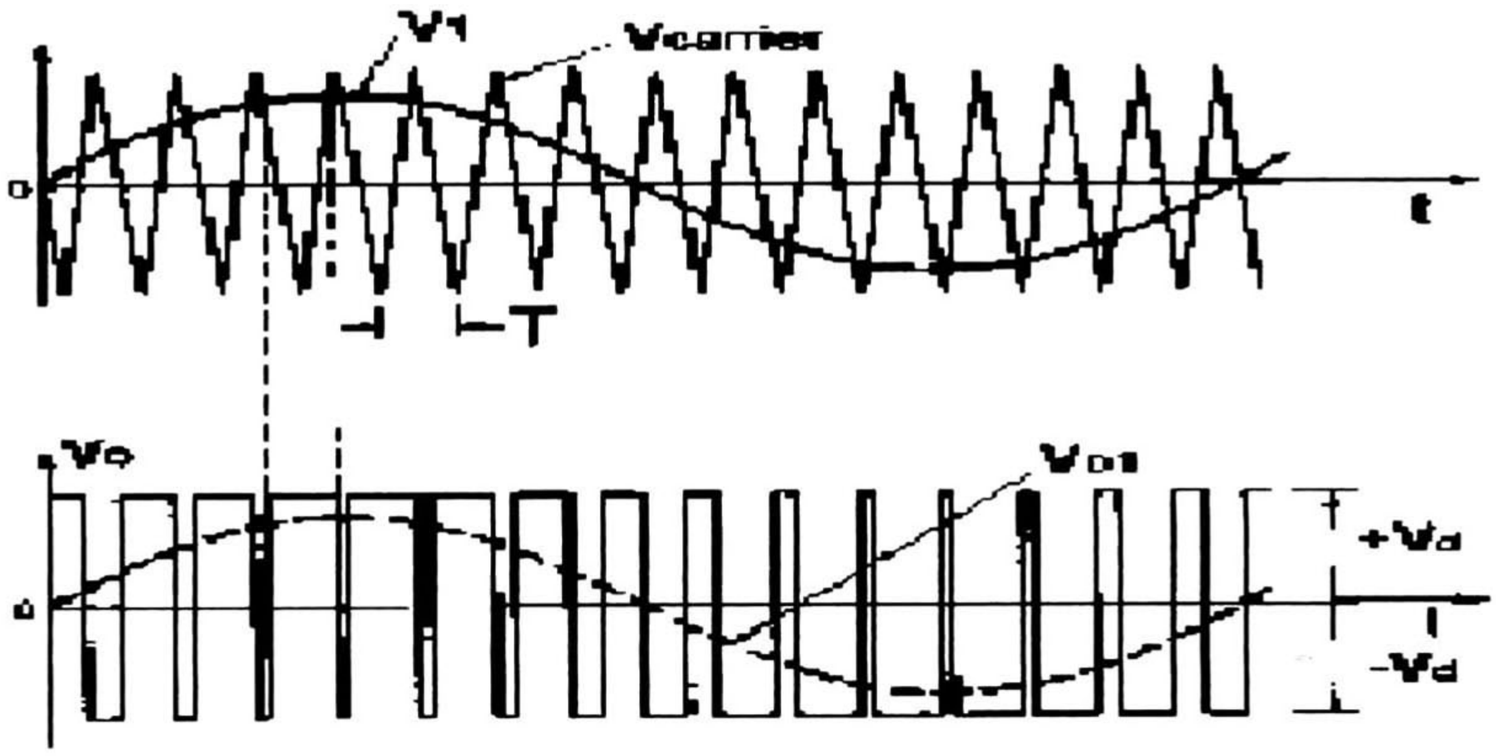

Figure 6.6. PWM operation. V1 is compared to Vcarrier. For each time period, T, a square pulse operates the switch of the inverter to output the fundamental waveform Vo1.

A graph of the PWM waveforms together with the resulting pulse is shown below in Figure 6.7.

Figure 6.7. PWM operation. The square pulse from the PWM is superimposed on the sine and triangle waves as shown in this Figure. The pulse is high during the interval when the sine wave is greater than the triangle wave.

In this case the aforementioned sine waves are the waves generated by the continuos control. Do not forget that the pulses can only be 0 or 1 for digital purposes. These pulses are available at the computer interface with the common TTL voltage levels.

As mentioned in sub-chapter 6.3, these pulses are isolated with optocouplers, i.e. digital isolators.

6.6 INVERTER

The purpose of the inverter is to convert the dc signal into a three-phase ac signal with a variable frequency. The output waveform from the inverter is a series of square waves that the motor 'sees' as a sine wave because the inductance of the motor smoothes out this 'chopped' waveform. The amplitude of the synthesized sine wave is determined by the widths of these square waves. The relative widths of these square waves represent the applied voltage. The wider the widths and the narrower the notches between the widths, the higher the amplitude of the synthesized sine wave because more voltage is being applied.

With the help of Figure 6.8, we will obtain a mathematical model for the inverter to proof the ability to generate sinusoidal like signals.

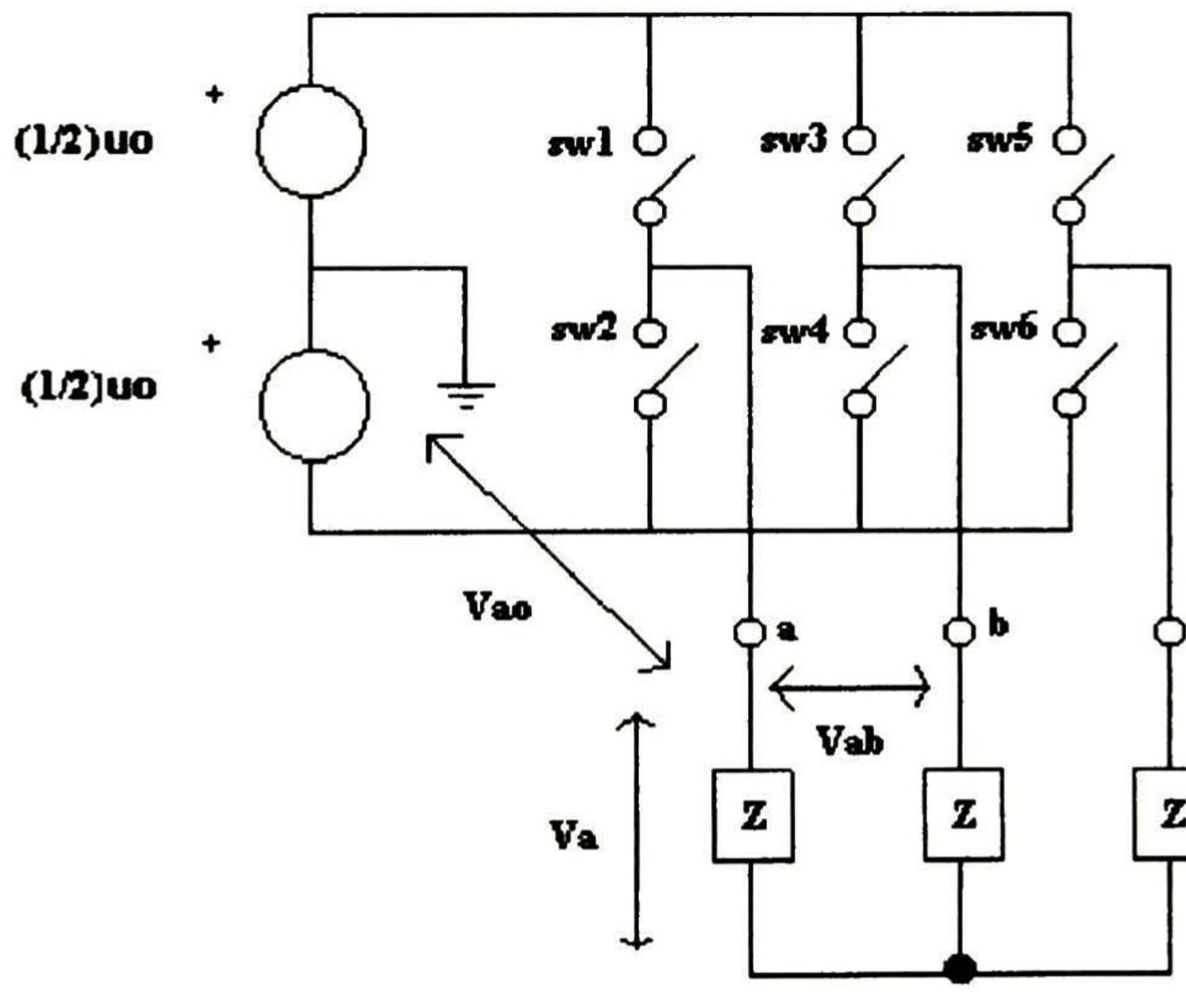

Figure 6.8. Inverter scheme. The switches represent the IGBT and the 'Z' blocks represents the stator load of the motor.

We redefine the sliding mode control variables as $X_1(sw1)$, $X_2(sw3)$ and $X_3(sw5)$, where

$$X_i \in \{0,1\}$$
$$i = 1,2,3$$

These variables determine the states of the inverter upper switches. The lower switches follows the next relations

$$\begin{aligned} sw2 &= 1 - sw1 \\ sw4 &= 1 - sw3 \\ sw6 &= 1 - sw5 \end{aligned} \tag{6.4.1}$$

This means when one upper switch is on, the corresponding lower switch is off and vice-versa. If the states of the upper inverter switches are marked as 1 for switch-on state and 0 for switch-off state then fictitious voltage related to the center of dc supply u_0 can be computed from equations (6.4.2). Line to line voltage and motor phase voltages are determined as described by the set of equations (6.4.3) and (6.4.4), if the system is symmetrical with isolated center.

$$\begin{aligned} V_{ao} &= u_0\left(-\frac{1}{2} + X_1\right) \\ V_{bo} &= u_0\left(-\frac{1}{2} + X_2\right) \\ V_{co} &= u_0\left(-\frac{1}{2} + X_3\right) \end{aligned} \tag{6.4.2}$$

$$\begin{aligned} V_{ab} &= V_{ao} - V_{bo} \\ V_{bc} &= V_{bo} - V_{co} \\ V_{ca} &= V_{co} - V_{ao} \end{aligned} \tag{6.4.3}$$

$$V_a = -\frac{1}{3}(V_{ca} - V_{ab})$$
$$V_b = -\frac{1}{3}(V_{ab} - V_{bc}) \qquad (6.4.4)$$
$$V_c = -\frac{1}{3}(V_{bc} - V_{ca})$$

If we substitute (6.4.2) into (6.4.3) and (6.4.3) into (6.4.4), we yield to a direct relation between the input and output of the inverter, i.e. a relation between the sliding mode control variables and the motor phase voltages, as shown in the next expression

$$\begin{bmatrix} V_a \\ V_b \\ V_c \end{bmatrix} = \frac{u_0}{3}\begin{bmatrix} 2 & -1 & -1 \\ -1 & 2 & -1 \\ -1 & -1 & 2 \end{bmatrix}\begin{bmatrix} X_1 \\ X_2 \\ X_3 \end{bmatrix} \qquad (6.4.5)$$

The output control signals will intrinsically generate sinusoidal shape signals at the output of the inverter, but, to proof this feature, we propose a sequence of fired switches in the next table

Step sequence	**Fired sequence**
Step 1	sw1 sw4 sw5
Step 2	sw1 sw4 sw6
Step 3	sw1 sw3 sw6
Step 4	sw2 sw3 sw6
Step 5	sw2 sw3 sw5
Step 6	sw2 sw4 sw5

The fired sequences or fired switches accomplishes that in any step sequence there are only three active switches, one in each phase of the inverter, but, two upper switches and one of the bottom, or vice-versa. This implies that a complete cycle will be accomplished in six steps. Figure 6.9 shows the graphics of the voltages in (6.4.2), (6.4.3) and (6.4.4). We observe that the motor phase voltages are really sinusoidal like signals.

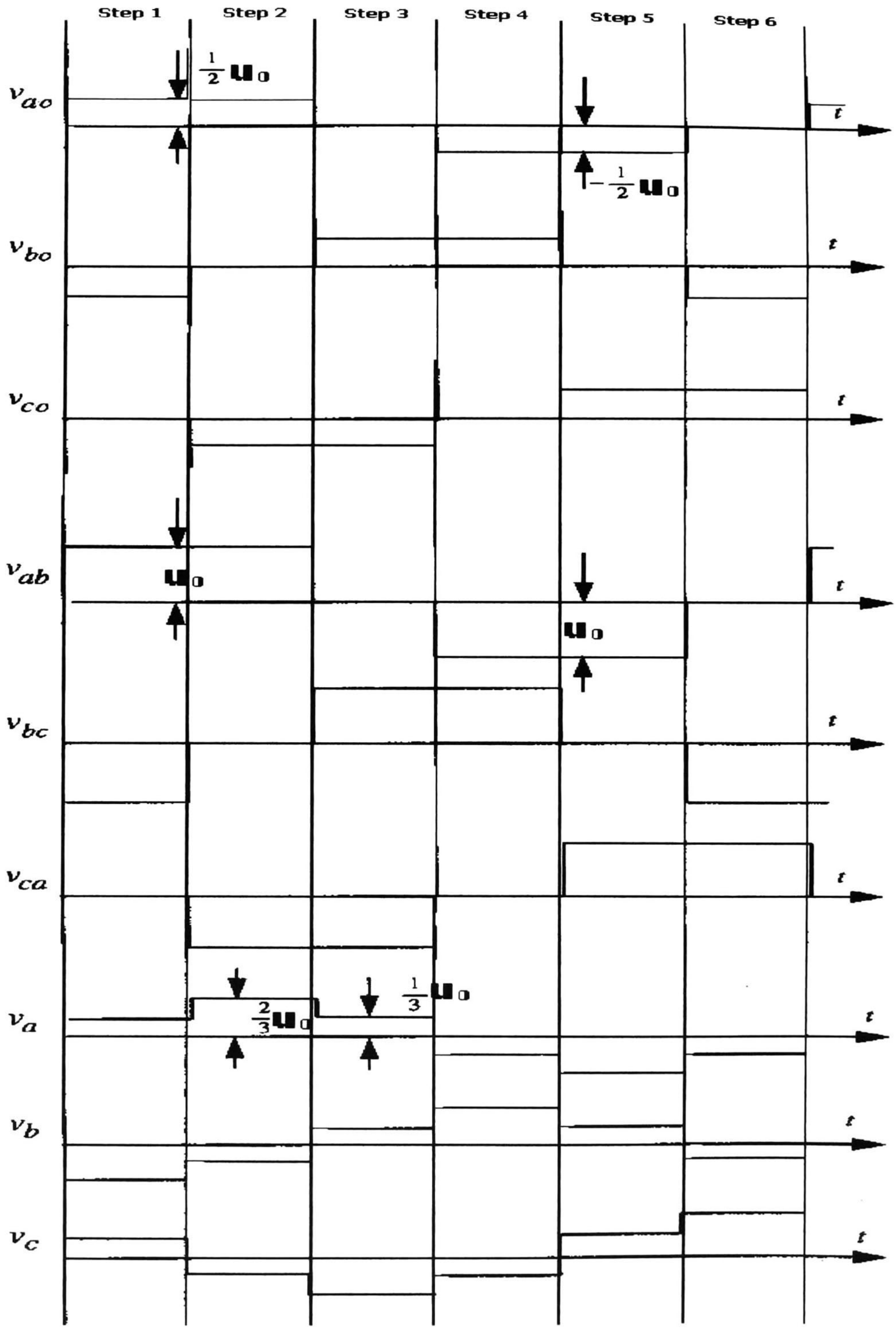

Figure 6.9. Fictitious voltages, line to line voltages and motor phase voltages when operating from a six step voltage inverter.

A common IGBT module is the 6MBI10GS-060 model manufactured by FUJI Electric. Figure 6.10 shows a photo and a schematic diagram of this device

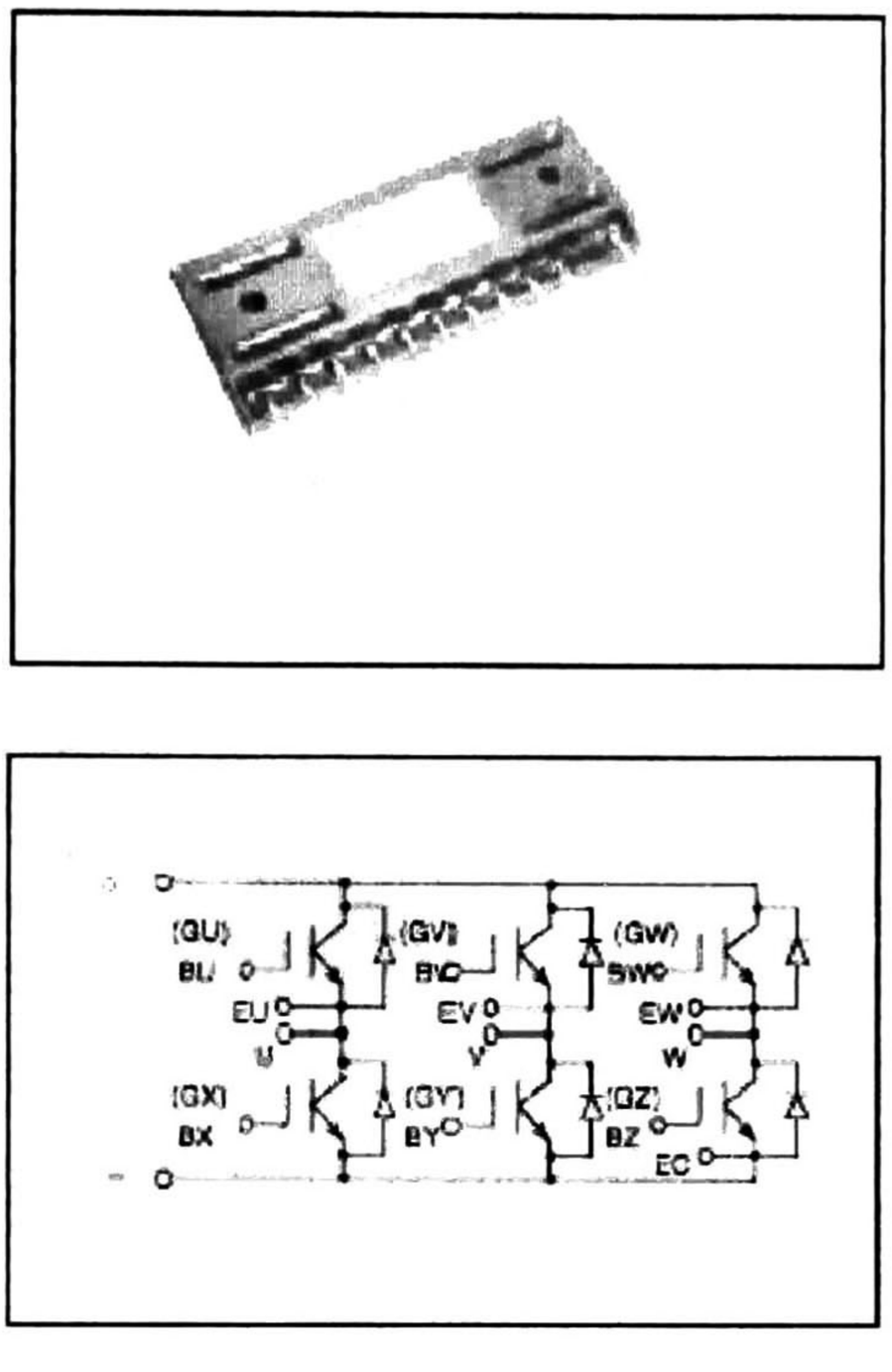

Figure 6.10. Photo and schematic diagram of 6MBI10GS-060 module.

The next table shows the maximum ratings and characteristics of this device.

● **Absolute maximum ratings (at Tc=25°C unless otherwise specified)**

Item		Symbol	Rating	Unit
Collector-Emitter voltage		V_{CES}	600	V
Gate-Emitter voltage		V_{GES}	±20	V
Collector current	Continuous	Ic	10	A
	1ms	Ic pulse	20	A
		-Ic	10	A
	1ms	-Ic pulse	20	A
Max. power dissipation		Pc	46	W
Operating temperature		T_j	+150	°C
Storage temperature		T_{stg}	-40 to +125	°C
Isolation voltage		V_{is}	AC 2000 (1min.)	V
Screw torque		Mounting *1	1.7	N·m

*1 Recommendable value : 1.3 to 1.7 N·m (M4)

The output of the PWM or the discontinuous control can not drive the input gates of the IGBT, instead, signal conditioning is needed in order to guarantee the turn-on and turn-off of the IGBT with proper current and voltage levels. This can be achieved with a three-phase bridge driver. A common device that can do the job is the IR2130 model from International Rectifier. This device is a high voltage, high speed power MOSFET and IGBT driver with three independent high and low side referenced output channels. Figure 6.11 shows three typical packages of this device and Figure 6.12 shows a typical connection of this device as well.

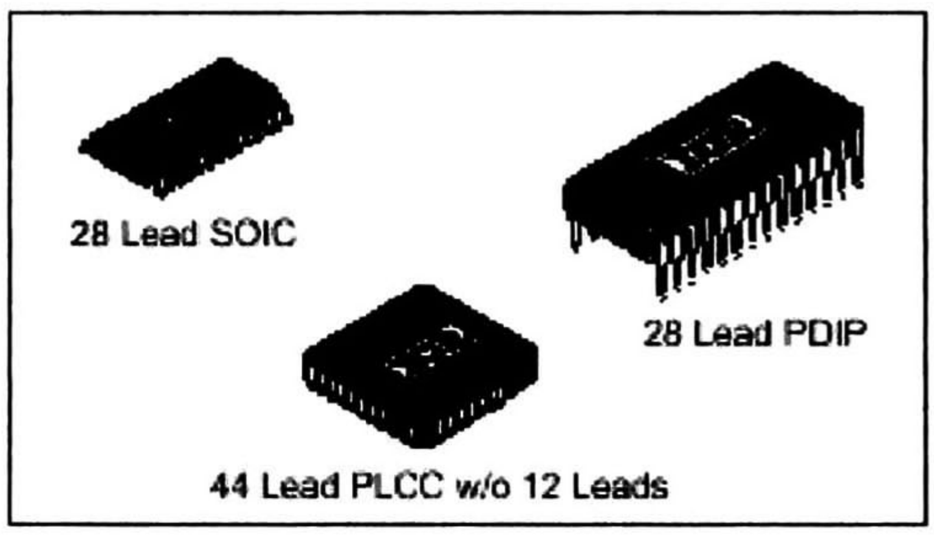

Figure 6.11. Different packages of the IR2130 device.

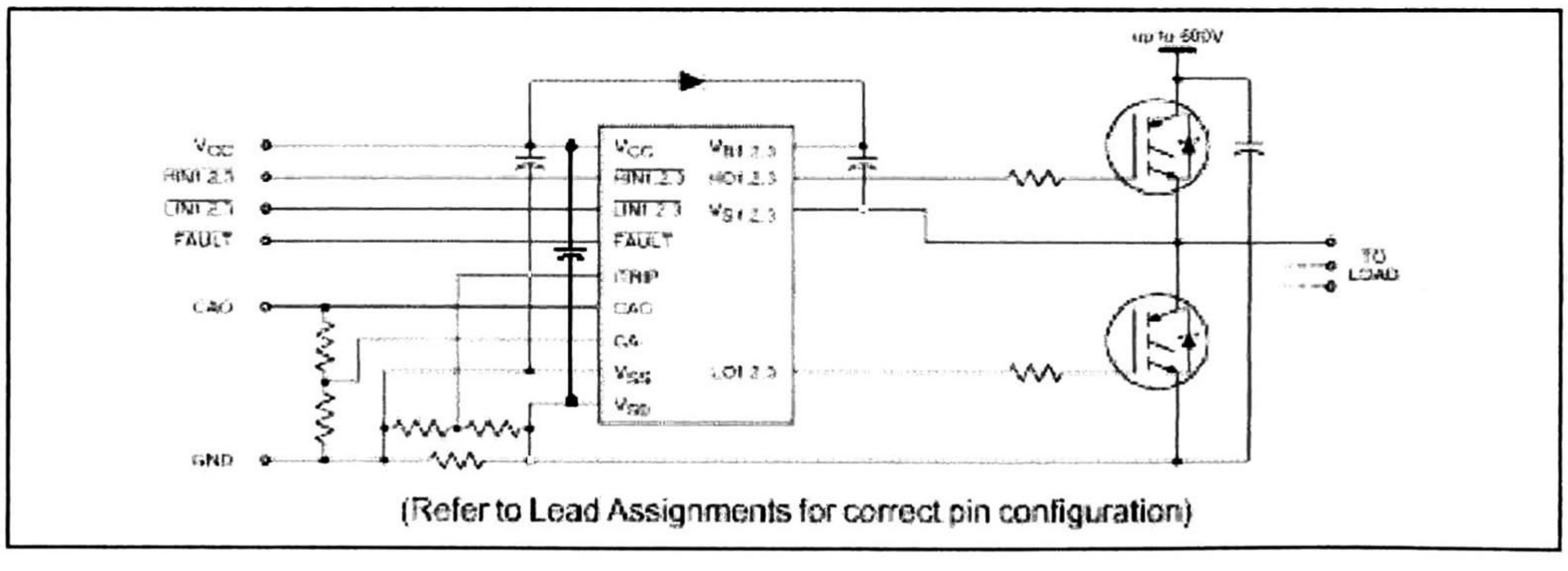

Figure 6.12. Typical connection of the IR2130 device.

Chapter seven

Conclusions and future work

7.1 CONCLUSIONS

This work has shown the three-phase induction motor modelling. The obtained model is nonlinear and time-variant due to the mutual inductance rotor position dependency [9]. Dealing with a time-variant system is a difficult task. To overcome this problem, a transformation reference frame was proposed, i.e., all the induction motor variables involved were represented with respect to an arbitrary spinning reference frame, where the velocity of the reference frame is open. In this work we consider the fixed reference frame, i.e., the reference frame is not spinning, and the induction motor model becomes time-invariant, even the model order has reduced. Since the objective of this work is to make possible a future real-time implementation in a digital device, it was necessary to discretize the continuos-time model. The fifth order model solution is difficult to obtain, but the current fed model (third order model) is easier. So, the current fed model was exactly discretized and the dynamical current equations were discretize trough a first-order Taylor series.

Due to the tracking control objectives, it is very common to prescribe the reference signals as constants. This work proposes reference signals that are generated in an exosystem. This has the advantage that the output signals are totally prescribed.

The principles of continuous-time sliding mode were revisited, and from the revealed properties, a discrete-time sliding mode concept was developed. A discrete-time sliding mode is necessary in order to avoid chattering in the discrete-time implementation of the continuos-time sliding mode controller.

A novel block control technique was design for discrete-time nonlinear systems. This technique consists of a step-by-step interconnected process where the system is transformed into an error dynamical system, this is of great help due that error states are good candidates for a sliding mode surface.

A discrete-time nonlinear observer was developed for electromechanical systems. The tracking error dynamical equation was analyzed with a discrete-time Lyapunov approach, in order to investigate the stability of the observer.

The control law design was carried out with the block control technique applied to the discrete-time system, where we obtained a surface for a discrete-time sliding mode. Continuos-time sliding mode control is a discontinuous control function, but discrete-time sliding mode control results in a continuous function, because this control is based in equivalent control, so, a discrete-time sliding mode discontinuous control was also proposed with the classical sign function, for later simulation comparison.

The observer considered a constant load for practical reasons. The autonomous flux tracking error difference equations are analyzed with a discrete-time Lyapunov approach, that revealed that the flux dynamical equations are stable itself. The other part of the observer was analyzed with Jury's stability criterion.

Simulations were carried out in Simnon. These were done for various reference signals, load signals and for continuous and discontinuous sliding mode controls. The continuous control law performed better than the discontinuous control law, but the continuous control law has the disadvantage of a PWM requirement in order to drive an inverter device, and the discontinuous control law has the advantage of driving directly the inverter module.

For a future real time implementation is considered a personal computer as the digital device to implement the discrete-time control law. The measurement of the variables of the motor and how to feed them into the computer was considered. The PWM technique was explained, and was shown that can be implemented in software. The mathematical foundation of the inverter module revealed the capability of generating a sinusoidal shape signal and that the inductances of the stator smooth this signal.

In general, we conclude that sliding mode control is a powerful tool for nonlinear dynamical systems, and in particular for systems with discontinuous inputs just like the induction motor that is driven with the inverter module that have discontinuous inputs. This gives the opportunity to the induction motor to perform high precision position control with appropriate sensors and can replace the expensive d.c. brushless motor in any application.

A drawn paper from this thesis, was submitted to IFAC 2002 in Barcelona, Spain.

7.2 FUTURE WORK

Let us consider as an extension for this work

- The development of a discrete-time adaptive controller for parameter uncertainties.
- The design of a discrete-time sliding mode controller for the d,q model, i.e., $\omega = \omega_r$.
- The design of a discrete-time sliding mode controller for the transformed system (2.3.21).
- The simulation of the continuous plant and the inverter with the discrete-time sliding mode control law.
- And to perform a real time implementation.

REFERENCES

[1] Åström, K. J. & Wittenmark, B. **Computer-Controlled Systems,** Prentice Hall, 1997.

[2] Bose, B.K. **Power Electronics and Variable Frequency Drives,** IEEE Press, 1997.

[3] Chapman, S.J. **MAQUINAS ELECTRICAS,** Mc Graw Hill, 1994.

[4] Kazantzis, N. and Kravaris C. **Time-discretization of nonlinear control systems via Taylor methods,** Computer and Chemical Engineering 23 (1999) 763-784.

[5] Loukianov, G.A., Cañedo, J.M., Serrano, O. Utkin, I.V. and Celikovsky, S. **ADAPTIVE SLIDING MODE BLOCK CONTROL OF INDUCTION MOTORS,** Mc Graw Hill, 1999.

[6] Khalil, H. K. **NONLINEAR SYSTEMS,** Mac Millan, 1992.

[7] Marino, R. and Tomei, P. **Nonlinear Control Design,** Prentice Hall, 1995.

[8] Maloney, T.J. **Electrónica Industrial,** Prentice Hall, 1983.

[9] Novotny, D. W. and Lipo, T. A. **VECTOR CONTROL AND DYNAMICS OF AC DRIVES,** Oxford Univerty Press, 1998.

[10] Ortega, R. and Taoutaou, D. **A globally stable discrete-time controller for current-fed induction motors,** Systems & Control Letters (1996) 123-128.

[11] Ortega, R., Nicklasson, P.J. and Epinosa-Pérez, G. **On Speed Control of Induction Motors,** Automatica, Vol. 32, No. 3, 455-460, 1996.

[12] Proakis, J.G. and Manolakis, D.G. **DIGITAL SIGNAL PROCESSING**, Prentice Hall, 1996.

[13] Tan, H. and Chang, J. **Adaptive Backstepping Control of Induction Motor with Uncertainties,** Proceedings of the American Control Conference. San Diego, California. June 1999.

[14] Taoutaou, D., Puerto, R., Ortega R. and Loron L. **A NEW FIELD ORIENTED DISCRETE-TIME CONTROLLER FOR CURRENT-FED INDUCTION MOTORS,** Supported in part by the Commission of European Communities under contract ERB CHRX CT 93-0380 and by the DIVA project of the Picardie region.

[15] Utkin, V. I. **Sliding Modes in Control and Optimization,** Springer-Verlag, 1993.

[16] Utkin, V. I., Guldner, J. and Shi, J. **Sliding Mode Control in Electromechanical Systems,** Taylor & Francis, 1999.

[17] Vittek, J., Utkin, V. A. and Dodds, S. J. **Self Oscillating, Sensorless Induction Motor Drive Control System with Prescribed Closed-Loop and Rotor Flux Dynamics.**

Subject: IFAC'2002: paper registered
Date: Sat, 22 Sep 2001 23:29:21 +0200
From: "IFAC'2002 Secretariat" <secretariatipc@b02.ifac2002.org>
To: louk@gdl.cinvestav.mx
CC: secretariatipc@b02.ifac2002.org

Your paper has been registered in the IFAC'2002 database.

Paper number:	2693
Title:	DISCRETE-TIME SLIDING MODE CONTROL OF AN IN
Authors:	Alexader G. Loukianov, Jorge Rivera and Jos
Contact:	Alexander Loukianov
Presentation:	oral
On-line demo:	no
Technical area:	2a. Control Design
Axis:	scientific
Proposed for pre-discussion:	no
Proposed for Young Author Prize:	no
Proposed for Application Paper Prize:	yes

Keep the paper number for future inquiries.

A confirmation will be sent to you when the paper has been printed
and validated, and the copyright transfer form has been received.

IFAC'2002 IPC Secretariat
secretariatipc@b02.ifac2002.org

DISCRETE-TIME SLIDING MODE CONTROL OF AN INDUCTION MOTOR

Alexader G. Loukianov, Jorge Rivera and José M. Cañedo

CINVESTAV del IPN, Automatic Control Department,
López Mateos Sur 519, Guadalajara, Jalisco 45090, MEXICO
(louk@gdl.cinvestav.mx),(jorger@gdl.cinvestav.mx), (canedoj@gdl.cinvestav.mx)

Abstract: A discrete-time sliding mode with block control aided design is applied to a nonlinear discrete-time induction motor model where the load torque is considered as unknown perturbation. With full state measurements, both rotor speed and rotor flux amplitude tracking objectives are satisfied. Then, a reduced order observer is implemented where speed and current measurements provide the observation for the unreachable fluxes and load torque. The simulations predict the system to be robust with respect to external load torques. *Copyright © 2002 IFAC*

Keywords: Inductions motors, discrete-time systems, sliding mode control, observer.

1. INTRODUCTION

Induction motor is one of the most used actuator for industrial applications due to its reliability, ruggedness and relatively low cost. The control of induction motor is challenging, since the dynamical system is multivariable, coupled, and highly nonlinear. A classical technique for induction motor control is field oriented control (Blaschke, 1972), which involves nonlinear state transformation and feedback for asymptotic decoupling of the rotor speed and rotor flux, and applying linear control methods such as PID. More recently, various nonlinear control design approaches have been applied to the induction motor control problem for better performance, like backstepping (Tan, and Chang; 1999), passivity (Ortega, *et al.*, 1996), adaptive input-output linearization (Marino, and Tomei, 1995), and sliding modes (Utkin, *et al.*, 1999).

All of these approaches are based on the continuous-time model of the plant, and for practical implementation in a digital device, is necessary to design the controller for a discrete-time model of the plant.

This research work is based on a digital sliding mode (Utkin, et al., 1999) with block control aided design approach to achieve rotor speed and rotor flux amplitude tracking objectives for the fixed reference frame model. The uncertainty accounted for is an unknown load torque

The paper is organized as follows. Section 2 briefly reviews the continuous-time induction motor model and using the solution of the mechanical and rotor flux dynamics systems, this model is discretized. The main results are presented in Section 3, where the discrete-time sliding mode block control and the rotor flux and load torque observer, are designed. Section 4 deals with the proposed control law and observer simulations. Finally, in Section 5 are some concluding remarks drawn from simulations and control technique.

2. DISCRETIZATION OF THE CONTINUOS-TIME INDUCTION MOTOR MODEL

In this section, it is developed another representation of the induction motor model, called *discrete-time* induction motor model. Under the assumptions of equal mutual inductance and a linear magnetic circuit, a fifth-order induction motor model is given as

$$\frac{d\omega}{dt} = \mu \mathbf{I}^{\mathrm{T}} \mathfrak{J} \Psi - \frac{T_L}{J}$$
$$\frac{d\Psi}{dt} = -\alpha \Psi + n_p \omega \mathfrak{J} \Psi + \alpha M \mathbf{I}$$
$$\frac{d\mathbf{I}}{dt} = \varphi + \frac{1}{\sigma}\mathbf{u}$$

where

$$\mathfrak{J} = \begin{bmatrix} 0 & -1 \\ 1 & 0 \end{bmatrix}$$

is the skew matrix, and has the following property: $\mathbf{z}^T \mathfrak{J} \mathbf{z} = \mathbf{0}$; the other variables and parameters have the following definitions: $\Psi \in \mathbf{R}^2$ is the rotor flux vector, $\mathbf{I} \in \mathbf{R}^2$ is the stator current vector, which in current-fed motors is the control input, $\mathbf{u} \in \mathbf{R}^2$ is the control input voltage vector, ω is the rotor angular velocity, T_L is the load torque, J is the rotor moment of inertia, and

$$\varphi = \begin{bmatrix} \alpha\beta\psi_\alpha + n_p\beta\omega\psi_\beta - \gamma i_\alpha \\ \alpha\beta\psi_\beta - n_p\beta\omega\psi_\alpha - \gamma i_\beta \end{bmatrix}$$

$$\alpha = \frac{R_r}{L_r} = \frac{1}{T_r}, \quad \beta = \frac{M}{\sigma L_r}, \quad \gamma = \frac{M^2 R_r}{\sigma L_r^2} + \frac{Rs}{\sigma},$$
$$\sigma = L_s - \frac{M^2}{L_r}, \quad \mu = \frac{3}{2}\frac{M n_p}{J L_r},$$

L_s, L_r and M are the stator, rotor and mutual inductance respectively, R_s, R_r are the stator and rotor resistances respectively, and n_p is the number of pole pairs.

To face the problem of discretization it is necessary to found the solution of the system, but this system has no analytic solution at all. To overcome this problem, the model is divided in a current-fed induction motor third-order model, where the current inputs are considered as pseudo-inputs, and a second-order subsystem that only models the currents of the stator with voltages as inputs. The current-fed model will be exactly discretized by solving the set of differential equations and the other subsystem will be discretized by a first-order Taylor series (Kazantzis and Kravaris; 1999). Making use of the following globally defined change of coordinate

$$\mathbf{Y} = e^{-np\theta\mathfrak{J}}\Psi \quad \mathbf{X} = e^{-np\theta\mathfrak{J}}\mathbf{I} \tag{1}$$

where $\dot{\theta} = \omega$, yields the following bilinear model

$$\frac{d\omega}{dt} = \mu \mathbf{X}^{\mathrm{T}} \mathfrak{J} \mathbf{Y} - \frac{T_L}{J} \tag{2}$$
$$\frac{d\Psi}{dt} = -\alpha \mathbf{Y} + \alpha M \mathbf{X}$$

Founding a solution to (2) involves integral operations, where it is assumed that control is applied in a piecewise constant fashion. So, the control is constant over the integration time interval $[kT, (k+1)T]$, $k = 0,1,2,...,$ where $T > 0$ is the *sampling time*. The solution to (2) in this time interval is

$$\omega((k+1)T) = \omega(kT) + \frac{\mu}{\alpha}\left(1 - e^{-\alpha T}\right)\mathbf{X}^T(kT)\mathfrak{J}\mathbf{Y}(kT) - \frac{T_{Lk}}{J}T$$
$$\mathbf{Y}((k+1)T) = e^{-\alpha T}\mathbf{Y}(kT) + M\left[1 - e^{-\alpha T}\right]\mathbf{X}(kT)$$

Defining a common notation $\mathbf{x}_k = \mathbf{x}(kT)$, yields

$$\omega_{k+1} = \omega_k + \frac{\mu}{\alpha}\left(1 - e^{-\alpha T}\right)\mathbf{X}_k^T \mathfrak{J} \mathbf{Y}_k - \frac{T_{Lk}}{J}T \tag{3}$$
$$\mathbf{Y}_{k+1} = e^{-\alpha T}\mathbf{Y}_k + M\left[1 - e^{-\alpha T}\right]\mathbf{X}_k$$

Taking (3) to the original states with a inverse transformation of (1), finally yields

$$\omega_{k+1} = \omega_k + \frac{\mu}{\alpha}(1-a)M\left(i_k^\beta \psi_k^\alpha - i_k^\alpha \psi_k^\beta\right) - \left(\frac{T}{J}\right)T_{Lk}$$
$$\psi_{k+1}^\alpha = \cos(n_p\theta_{k+1})\rho_1 - \sin(n_p\theta_{k+1})\rho_2$$
$$\psi_{k+1}^\beta = \sin(n_p\theta_{k+1})\rho_1 + \cos(n_p\theta_{k+1})\rho_2$$

where

$$\rho_1 = a\left(\cos(n_p\theta_k)\psi_k^\alpha + \sin(n_p\theta_k)\psi_k^\beta\right) + (1-a)M\left(\cos(n_p\theta_k)i_k^\alpha + \sin(n_p\theta_k)i_k^\beta\right)$$
$$\rho_2 = a\left(\cos(n_p\theta_k)\psi_k^\beta - \sin(n_p\theta_k)\psi_k^\alpha\right) + (1-a)M\left(\cos(n_p\theta_k)i_k^\beta - \sin(n_p\theta_k)i_k^\alpha\right)$$

The rotor position is calculated from $\dot{\theta} = \omega$, in the same way, yielding

$$\theta_{k+1} = \theta_k + \omega_k T + \frac{\mu}{\alpha}\left[T - \frac{1}{\alpha}(1-a)\right]M(i_k^\beta \psi_k^\alpha - i_k^\alpha \psi_k^\beta) - \frac{T_{Lk}}{2J}T^2$$

There are left two differential current equations to discretize, by a first order Taylor series

$$i_{k+1}^\alpha = \varphi_k^\alpha + \frac{T}{\sigma}u_k^\alpha$$
$$i_{k+1}^\beta = \varphi_k^\beta + \frac{T}{\sigma}u_k^\beta$$

where $a = e^{-\alpha T}$ and

$$\varphi_k^\alpha = i_k^\alpha + \alpha\beta T\psi_k^\alpha + n_p\beta T\omega_k\psi_k^\beta - \gamma T i_k^\alpha$$
$$\varphi_k^\beta = i_k^\beta + \alpha\beta T\psi_k^\beta - n_p\beta T\omega_k\psi_k^\alpha - \gamma T i_k^\beta$$

Finally, putting all together, the discrete-time version of the induction motor model, is feature

$$\omega_{k+1} = \omega_k + \frac{\mu}{\alpha}(1-a)M\left(i_k^\beta \psi_k^\alpha - i_k^\alpha \psi_k^\beta\right) - \left(\frac{T}{J}\right)T_{Lk}$$
$$\psi_{k+1}^\alpha = \cos(n_p\theta_{k+1})\rho_1 - \sin(n_p\theta_{k+1})\rho_2$$
$$\psi_{k+1}^\beta = \sin(n_p\theta_{k+1})\rho_1 + \cos(n_p\theta_{k+1})\rho_2$$
$$i_{k+1}^\alpha = \varphi_k^\alpha + \frac{T}{\sigma}u_k^\alpha$$
$$i_{k+1}^\beta = \varphi_k^\beta + \frac{T}{\sigma}u_k^\beta$$
$$\theta_{k+1} = \theta_k + \omega_k T + \frac{\mu}{\alpha}\left[T - \frac{1}{\alpha}(1-a)\right]M(i_k^\beta \psi_k^\alpha - i_k^\alpha \psi_k^\beta) - \frac{T_{Lk}}{2J}T^2 \tag{4}$$

Fig. 1 compares the open-loop velocity simulation of both models

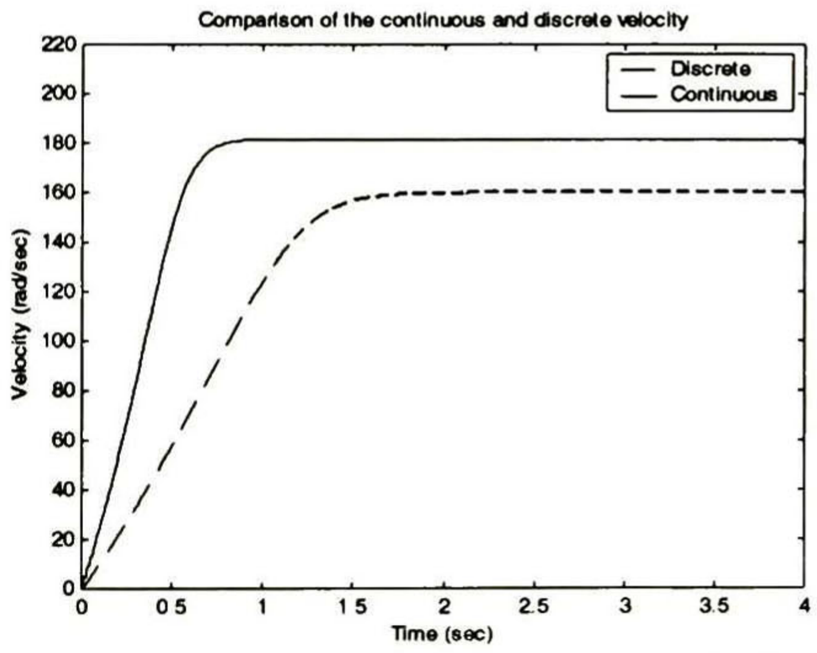

Fig. 1. Comparison of the continuous and discrete velocity.

There is a slight amount of error introduced by the current dynamical equations that were discretized by a first order Taylor series. Since the control input appears in these equations, the error can be eliminated.

3. DISCRETE-TIME SLIDING MODE CONTROL

Given full state measurements, the control objectives are to develop velocity and flux amplitude tracking for the electromechanical dynamics founded in the discrete-time induction motor model (4), using block control and discrete-time sliding mode.

3.1 Control design

Let us define the following states as

$$\mathbf{x}_k^1 = \begin{bmatrix} x_k^1 \\ x_k^2 \end{bmatrix} = \begin{bmatrix} \omega_k - \omega_k^r \\ \psi_k - \psi_k^r \end{bmatrix} \quad \mathbf{x}_k^2 = \begin{bmatrix} x_k^3 \\ x_k^4 \end{bmatrix} = \begin{bmatrix} i_k^\alpha \\ i_k^\beta \end{bmatrix} \tag{5}$$

where $\psi_k = \psi_k^{\alpha\,2} + \psi_k^{\beta\,2}$ is the rotor flux magnitude, ω_k^r and ψ_k^r are reference signals. If the resulting control, drives the state $\mathbf{x}_k^1$ toward zero, then ω_k and ψ_k will track exactly their respective reference signals, accomplishing in that way the control objectives. The system (4) involving (5), can be represented in the Block Controllable Form (BCF) consisting of two blocks

$$\begin{aligned} \mathbf{x}_{k+1}^1 &= \mathbf{f}^1(\mathbf{x}_k^1) + \mathbf{B}_1(\mathbf{x}_k^1)\mathbf{x}_k^2 \\ \mathbf{x}_{k+1}^2 &= \mathbf{f}^2(\mathbf{x}_k^1, \mathbf{x}_k^2) + \mathbf{B}_2\mathbf{u}_k \end{aligned} \tag{6}$$

where

$$\mathbf{f}^1 = \begin{bmatrix} f^1 \\ f^2 \end{bmatrix} = \begin{bmatrix} \omega_k - \left(\frac{T}{J}\right)T_{Lk} - \omega_{k+1}^r \\ a^2(\psi_k) + (1-a)^2 M^2\left(i_k^{\alpha\,2} + i_k^{\beta\,2}\right) - \psi_{k+1}^r \end{bmatrix}$$

$$\mathbf{B}_1 = \begin{bmatrix} c_1 & 0 \\ 0 & c_2 \end{bmatrix}\begin{bmatrix} -\psi_k^\beta & \psi_k^\alpha \\ \psi_k^\alpha & \psi_k^\beta \end{bmatrix} \quad \mathbf{f}^2 = \begin{bmatrix} f^1 \\ f^2 \end{bmatrix} = \begin{bmatrix} \varphi_k^\alpha \\ \varphi_k^\beta \end{bmatrix}$$

$$\mathbf{B}_2 = \begin{bmatrix} \frac{T}{\sigma} & 0 \\ 0 & \frac{T}{\sigma} \end{bmatrix} \quad \mathbf{u}_k = \begin{bmatrix} u_k^\alpha \\ u_k^\beta \end{bmatrix} \quad \begin{aligned} c_1 &= \frac{\mu}{\alpha}(1-a)M \\ c_2 &= 2a(1-a)M \end{aligned}$$

Note that matrices $\mathbf{B}_1$ and $\mathbf{B}_2$ have full rank, that is: $rank(\mathbf{B}_1) = rank(\mathbf{B}_2) = 2$, and

$$\|\mathbf{B}_1\| \le \beta_1 \quad \|\mathbf{B}_2\| \le \beta_2 \tag{7}$$

Applying the block control technique, define an error vector, $\mathbf{z}_k^1$ is defined as $\mathbf{z}_k^1 = \left[z_k^1, \; z_k^2\right]^T = \mathbf{x}_k^1$, then, the error dynamical equation is

$$\mathbf{z}_{k+1}^1 = \mathbf{f}^1(\mathbf{x}_k^1) + \mathbf{B}_1(\mathbf{x}_k^1)\mathbf{x}_k^2 \tag{8}$$

Handling $\mathbf{x}_k^2$ as a fictitious control for (8) and making the error $\mathbf{z}_k^1$ to tends to zero, with the anticipation of its dynamics as follows

$$\mathbf{z}_{k+1}^1 = \mathbf{f}^1(\mathbf{x}_k^1) + \mathbf{B}_1(\mathbf{x}_k^1)\mathbf{x}_k^2 = \mathbf{K}_1\mathbf{z}_k^1 \tag{9}$$

where $\mathbf{K}_1 = diag\{k_1, k_2\}$, with $k_1 > 0$ and $k_2 > 0$; then, the desired value $\mathbf{x}_k^{2d}$ of $\mathbf{x}_k^2$ is calculated from (9) as

$$\mathbf{x}_k^{2d} = \mathbf{B}_1^{-1}(\mathbf{x}_k^1)\left[-\mathbf{f}^1(\mathbf{x}_k^1) + \mathbf{K}_1\mathbf{z}_k^1\right]$$

It is desired that $\mathbf{x}_k^2 = \mathbf{x}_k^{2d}$. In this way, it is defined a second new error vector, $\mathbf{z}_k^2$ as

$$\mathbf{z}_k^2 = \begin{bmatrix} z_k^3 \\ z_k^4 \end{bmatrix} = \mathbf{x}_k^{2d} - \mathbf{x}_k^2$$

The error dynamical equation is

$$\mathbf{z}_{k+1}^2 = \bar{\mathbf{f}}^2 - \mathbf{B}_2\mathbf{u}_k$$

where

$$\bar{\mathbf{f}}^2 = \bar{\mathbf{B}}_1\left[-\bar{\mathbf{f}}^1 + \mathbf{K}_1\mathbf{z}_{k+1}^1\right] - \mathbf{f}^2$$

with

$$\bar{\mathbf{B}}_1 = \left[\begin{bmatrix} c_1 & 0 \\ 0 & c_2 \end{bmatrix}\begin{bmatrix} -\psi_{k+1}^\beta & \psi_{k+1}^\alpha \\ \psi_{k+1}^\alpha & \psi_{k+1}^\beta \end{bmatrix}\right]^{-1}$$

and

$$\bar{\mathbf{f}}^1 = \begin{bmatrix} \omega_{k+1} - \left(\frac{T}{J}\right)T_{Lk+1} - \omega_{k+2}^r \\ a^2(\psi_{k+1}) + (1-a)^2 M^2\left(i_{k+1}^{\alpha\,2} + i_{k+1}^{\beta\,2}\right) - \psi_{k+2}^r \end{bmatrix}$$

Since all the states variable are measurable at time 'kT', the states variables at time '$(k+1)T$' are calculated from (4). It is assumed that the load signal is constant, so

$$T_{Lk+1} = T_{Lk}$$

The system (6) in the new coordinates is

$$\begin{aligned} \mathbf{z}_{k+1}^1 &= \mathbf{K}_1\mathbf{z}_k^1 - \mathbf{B}_1\mathbf{z}_k^2 \\ \mathbf{z}_{k+1}^2 &= \bar{\mathbf{f}}^2 - \mathbf{B}_2\mathbf{u}_k \end{aligned} \tag{10}$$

The next step is to design the control law from the last results. The first step in sliding mode control is to choose the surface $\mathbf{S}_k = \mathbf{0}$, and, a smart selection is

$$\mathbf{S}_k = \mathbf{z}_k^2 = \mathbf{0}$$

This surface will be zeroing as the state trajectories reach the surface, and then the control objectives will be accomplished. The transformed system (10) is redefined as

$$\begin{aligned} \mathbf{z}_{k+1}^1 &= \mathbf{K}_1\mathbf{z}_k^1 - \mathbf{B}_1\mathbf{z}_k^2 \\ \mathbf{S}_{k+1} &= \bar{\mathbf{f}}^2 - \mathbf{B}_2\mathbf{u}_k \end{aligned} \tag{11}$$

In order to design a control law, a discrete-time sliding mode version (Utkin, *et al.*, 1999), is implemented as

$$\mathbf{u}_k = \begin{cases} \mathbf{u}_{keq} & for \quad \|\mathbf{u}_{keq}\| \le u_0 \\ u_0 \dfrac{\mathbf{u}_{keq}}{\|\mathbf{u}_{keq}\|} & for \quad \|\mathbf{u}_{keq}\| > u_0 \end{cases}$$

where $\mathbf{u}_{keq}$ is calculated from $\mathbf{S}_{k+1} = \mathbf{0}$ of the form

$$\mathbf{u}_{keq} = \mathbf{B}_2^{-1}\left[\bar{\mathbf{f}}^2\right]$$

and u_0 is the control resources that bound the control. Proceeding with a stability analysis, where the case $\|\mathbf{u}_{keq}\| \le u_0$ is first analyzed. To reveal the structure of $\mathbf{u}_{keq}$ and $\mathbf{S}_{k+1}$, let us represent them as the following functions:

$$\mathbf{u}_{keq} = \mathbf{B}_2^{-1}\left[\bar{\mathbf{f}}^2 + \mathbf{S}_k - \mathbf{x}_k^{2d} + \mathbf{x}_k^2\right]$$

and

$$\mathbf{S}_{k+1} = \mathbf{S}_k + \bar{\mathbf{f}}^2 - \mathbf{x}_k^{2d} + \mathbf{x}_k^2 - \mathbf{B}_2\mathbf{u}_k \tag{12}$$

In order to decrease $\|\mathbf{S}_k\|$ monotonically to zero, it is

necessary to satisfy $\mathbf{S}_{k+1} - \mathbf{S}_k \le 0$, and using the fact that control can vary within $\|\mathbf{u}_{keq}\| \le u_0$, then, the condition that guarantees sliding mode stability, is calculated as

$$\left\|\mathbf{B}_2^{-1}\left(\bar{\mathbf{f}}^2 - \mathbf{x}_k^{2^d} + \mathbf{x}_k^2\right)\right\| \le u_0 \qquad (13)$$

Note that otherwise, the control resources are insufficient to stabilize the system. Let us turn to the case when $\|\mathbf{u}_{keq}\| \le u_0$. Replacing $\mathbf{u}_k = u_0 \dfrac{\mathbf{u}_{keq}}{\|\mathbf{u}_{keq}\|}$ in (12) yields

$$\mathbf{S}_{k+1} = \left(\mathbf{S}_k + \bar{\mathbf{f}}^2 - \mathbf{x}_k^{2^d} + \mathbf{x}_k^2\right)\left(1 - \frac{u_0}{\|\mathbf{u}_{keq}\|}\right)$$

$$|\mathbf{S}_{k+1}| \le |\mathbf{S}_k| + \left|\bar{\mathbf{f}}^2 - \mathbf{x}_k^{2^d} + \mathbf{x}_k^2\right| - \frac{u_0}{\|B_2^{-1}\|}$$

$$|\mathbf{S}_{k+1}| < |\mathbf{S}_k|$$

due to (13). Hence $\|\mathbf{S}_k\|$ decreases monotonically to zero, and, after a finite number of steps, $\|\mathbf{u}_k\| \le u_0$ is achieved, i.e.

$$\mathbf{S}_k = \mathbf{z}_k^2 = \mathbf{0} \Rightarrow \mathbf{x}_k^2 = \mathbf{x}_k^{2^d}$$

Discrete-time sliding mode will take place from the following sampling point onwards. Under the condition (7), the transformed system (11) of order 4, reduces its order to 2, and it is modeled by

$$\mathbf{z}_{k+1}^1 = \mathbf{K}_1 \mathbf{z}_k^1$$

This system represents the sliding mode dynamics which achieves the control objectives.

It is an obvious fact that the proposed control $\mathbf{u}_k$ depends on $\bar{\mathbf{f}}^2$ in order to eliminate old dynamics, but this function depends of control $\mathbf{u}_k$ squared, due to term $i_{k+1}^{\alpha\,2} + i_{k+1}^{\beta\,2}$, that appears in $\bar{\mathbf{f}}^1$, making the system in that way, unsolvable. To overcome this problem it is designed an observer only with current measurements, for the new variable Im_k, defined as follows

$$\mathrm{Im}_k = \sqrt{i_k^{\alpha\,2} + i_k^{\beta\,2}}$$

It is assumed that Im_k is constant, i.e.

$$\mathrm{Im}_{k+1} = \mathrm{Im}_k$$

then the observer is presented as the original plant plus a tracking error

$$\hat{\mathrm{Im}}_{k+1} = \hat{\mathrm{Im}}_k + g e_k^I$$

where $e_k^I = \mathrm{Im}_k - \hat{\mathrm{Im}}_k$ is the tracking error. Taking one step ahead

$$e_{k+1}^I = (1-g) e_k^I$$

it is easy to see that with the following condition

$$2 > g > 0$$

the observer error will tends asymptotically to zero, and the estimation $\hat{\mathrm{Im}}_k$ will track the real value Im_k, Avoiding the control dependency of $\mathbf{u}_k$ squared. Fig. 2 shows a simulation of the observer.

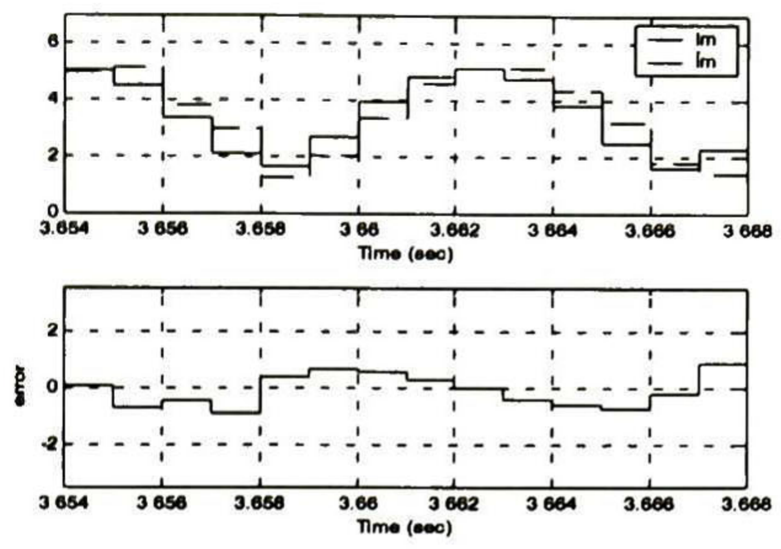

Fig. 2. (1) Comparison of Im_k with $\hat{\mathrm{Im}}_k$.
(2) The tracking error.

Again, there is an error that can be eliminated by the control action.

3.2 Reduced order nonlinear observer

The last control algorithm works with the full state and parameters measurement assumption. But in reality, the rotor fluxes and torque measurement is a difficult task. Here, it is design a reduced order nonlinear observer for fluxes and load, with the rotor speed and currents measurements only. System (4) is written as

$$\begin{aligned}
\omega_{k+1} &= \omega_k + \mathbf{I}_k \Im \Psi_k - (T/J) T_{Lk} \\
\mathbf{I}_{k+1} &= \varphi_k + (T/\sigma)\mathbf{u}_k \qquad (14) \\
\Psi_{k+1} &= a\mathbf{G}_k \Psi_k + (1-a) M \mathbf{G}_k \mathbf{I}_k
\end{aligned}$$

where $\mathbf{G}_k$ is defined as

$$\mathbf{G}_k = \begin{bmatrix} \cos(npT\omega_k) & -\sin(npT\omega_k) \\ \sin(npT\omega_k) & \cos(npT\omega_k) \end{bmatrix}$$

The proposed observer for the system (14), assumes the speed and current measurements, and an unknown constant load

$$\begin{aligned}
\hat{\omega}_{k+1} &= \omega_k + \mathbf{I}\Im\hat{\Psi}_k - \left(\frac{T}{J}\right)\hat{T}_{Lk} + l_1(\omega_k - \hat{\omega}_k) \qquad (15) \\
\hat{T}_{Lk+1} &= \hat{T}_{Lk} + l_2(\omega_k - \hat{\omega}_k) \\
\hat{\Psi}_{k+1} &= a\mathbf{G}_k \hat{\Psi}_k + (1-a) M \mathbf{G}_k \mathbf{I}_k
\end{aligned}$$

Let e_k^ω, be the difference between the measured rotor speed and the estimated one, i.e

$$e_k^\omega = \omega_k - \hat{\omega}_k$$

then the following error definition is e_k^L, and represents the difference between the real and the estimated load

$$e_k^L = T_{Lk} - \hat{T}_{Lk}$$

and the difference between real flux vector and the estimated one is as follows

$$\mathbf{e}_k^\psi = \Psi_k - \hat{\Psi}_k$$

Taking one step ahead of the three error equations, it yields to the dynamical error equations

$$\begin{aligned}
\begin{bmatrix} e_{k+1}^\omega \\ e_{k+1}^L \end{bmatrix} &= \begin{bmatrix} -l_1 & -\dfrac{T}{J} \\ -l_2 & 1 \end{bmatrix} \begin{bmatrix} e_k^\omega \\ e_k^L \end{bmatrix} + \mathbf{i}_k \Im \mathbf{e}_k^\psi \qquad (16) \\
\mathbf{e}_{k+1}^\psi &= a\mathbf{G}_k \mathbf{e}_k^\psi
\end{aligned}$$

A Lyapunov function can be used to proof stability of $\mathbf{e}_k^{\Psi}$

$$\mathbf{V}_k = \mathbf{e}_k^{\Psi^T} \mathbf{e}_k^{\Psi}$$

Taking one step ahead of the Lyapunov function

$$\mathbf{V}_{k+1} = \mathbf{e}_k^{\Psi^T} a^2 \mathbf{G}_k^T \mathbf{G}_k \mathbf{e}_k^{\Psi}$$

The increment of the Lyapunov function should be negative, and is expressed as

$$\Delta \mathbf{V}_k = \mathbf{e}_k^{\Psi^T} \left(a^2 \mathbf{G}_k^T \mathbf{G}_k - \mathbf{I}_{2x2} \right) \mathbf{e}_k^{\Psi} < 0$$

where

$$\left(a^2 \mathbf{G}_k^T \mathbf{G}_k - \mathbf{I}_{2x2} \right) < 0$$

or

$$a^2 \mathbf{G}_k^T \mathbf{G}_k < \mathbf{I}_{2x2}$$

With some basic manipulations yields

$$\begin{bmatrix} a^2 & 0 \\ 0 & a^2 \end{bmatrix} < \begin{bmatrix} 1 & 0 \\ 0 & 1 \end{bmatrix} \Rightarrow a < 1 \qquad (17)$$

where $a = e^{-\alpha T}$ The condition (17) is satisfied due to the fact that T and α are always positive. So, the increment of the Lyapunov function is negative implying that the tracking error tends asymptotically to zero, i.e.

$$lim \hat{\Psi}_k = \Psi_k$$
$$k \to \infty$$

Since $\mathbf{i}_k^T \Im$ is bounded, (16) is reduced to

$$\begin{bmatrix} e_{k+1}^{\omega} \\ e_{k+1}^{L} \end{bmatrix} = \begin{bmatrix} -l_1 & -\frac{T}{J} \\ -l_2 & 1 \end{bmatrix} \begin{bmatrix} e_k^{\omega} \\ e_k^{L} \end{bmatrix} \qquad (18)$$

Finding suitable l_1 and l_2 constants, the system (18) will be asymptotically stable and the observer (15) will asymptotically track the plant. A well known Jury's stability test (Åström and Wittenmark; 1997) criterion for a second order system will help to find l_1 and l_2. The characteristic equation of (17) is

$$z^2 + (l_1 - 1)z + (-l_1 - \frac{T}{J} l_2) = 0 \qquad (19)$$

Comparing (19) with an algebraic second order equation, yields

$$z^2 + a_1 z + a_2 = 0$$
$$a_1 = (l_1 - 1)$$
$$a_2 = (-l_1 - \frac{T}{J} l_2)$$

The Jury's stability test establishes for a second order system the following conditions

$$a_1 < 1$$
$$a_2 > -1 + a_1$$
$$a_2 > -1 - a_1$$

and with some computations the conditions that make the observer a stable system, are

$$1 < l_1 < 2$$
$$l_2 < 0$$

4. CONTROL LAW SIMULATIONS

Simulations are carried out to demonstrate the effectiveness of the above discrete-time sliding mode control and observers. The worst case scenario is simulated, i.e., the flux magnitude tracks an exponential signal and the speed tracks a sinusoidal shape signal. The unknown load torque is proposed as a noisy square shape signal that goes from minus nominal torque to positive nominal torque. Table 1 shows the induction motor parameters and Table 2 shows the control law parameters.

Table 1. Parameters of the induction motor. It is considered a three-phase, two-pole machine, with a stator-referred rotor.

Parameter	Value	Description
Rs	14 ohms	Stator Resistance
Ls	400 Mh	Stator Inductance
M	377 Mh	Mutual Inductance
Rr	10.1 ohms	Rotor Resistance
Lr	412.8 mH	Rotor Inductance
n_p	2	Number of Pole Pairs
J	0.01 Kgm^2	Moment of Inertia
ω_n	168.5 rad/sec	Nominal speed
T_{Ln}	1.1 Nm	Nominal Load

Table 2. Parameters used in the control law and the observer.

Parameter	Value	Description
T	0.001 sec	Sampling Period
u_o	330 Volts	Voltage bound
k_1	0.9	Control law gain
k_2	0.9	Control law gain
l_1	0.5	Observer gain
l_2	-0.5	Observer gain
G	1.9	Observer gain
$\hat{\psi}_k^{\alpha}(0)$	0.001 wb	Initial condition
$\hat{\psi}_k^{\beta}(0)$	0.001 wb	Initial condition
$z_k^3(0)$	-0.5	Initial condition
$z_k^4(0)$	0.5	Initial condition

The flux amplitude tracks an exponential signal at $0.2wb^2$. The rotor velocity tracks a sinusoidal signal with peak value of 70 *volts* and frequency of 3 *rad/sec*. The load torque is considered as a noisy square shape signal. Fig. 3 shows this load signal.

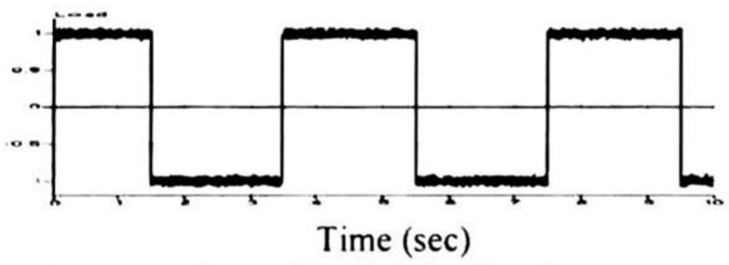

Fig. 3. Square shape load. The load torque goes from −1.1Nm to 1.1Nm.

Fig. 4 illustrates the speed output signal and its references, and Fig. 5 shows the tracking error.

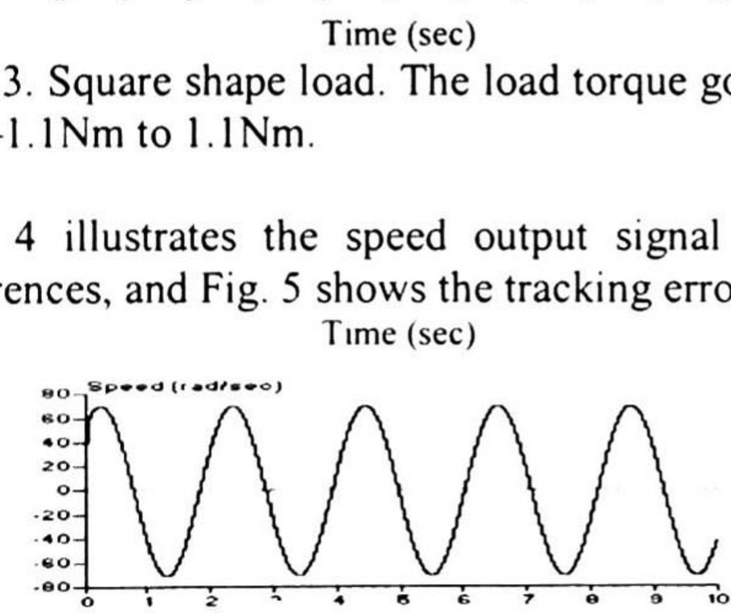

Fig. 4. Speed output signal and its reference. Note that the output exactly tracks its reference.

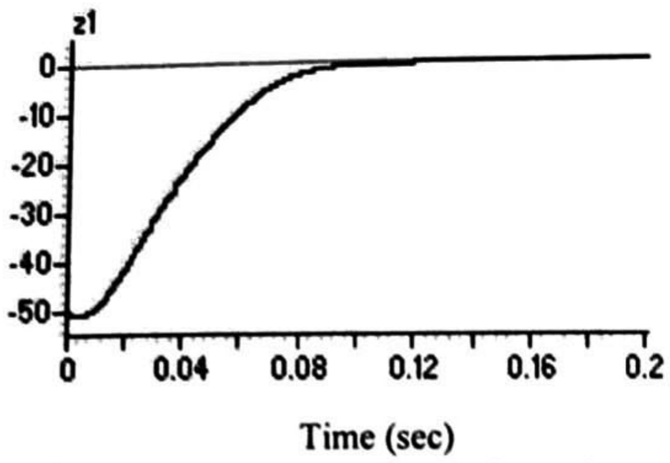

Fig. 5. Tracking error. Note that the error tends asymptotically to zero.

Fig. 6 shows the flux amplitude output and its reference signal as well. And Fig. 7 shows the tracking error signal.

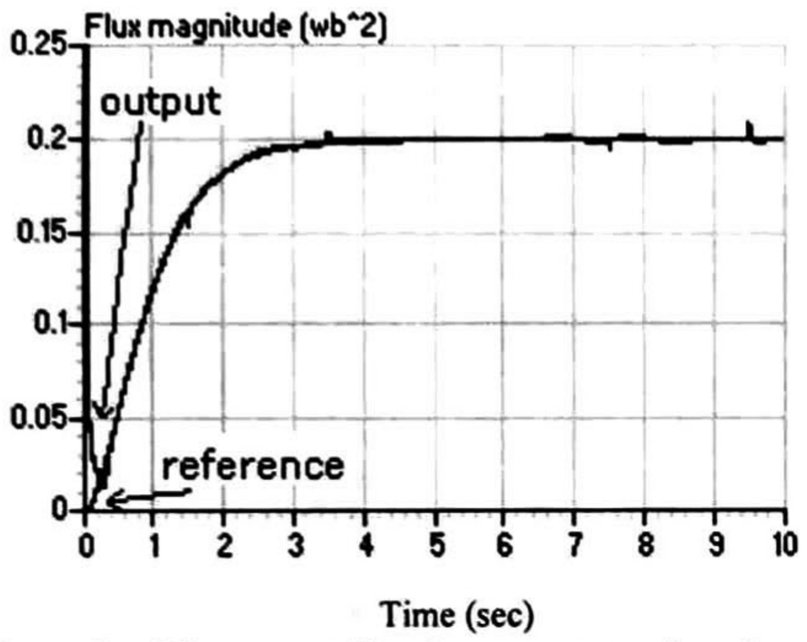

Fig. 6. Flux amplitude output signal and its reference. Note that the output tracks its reference with a slight amount of error .

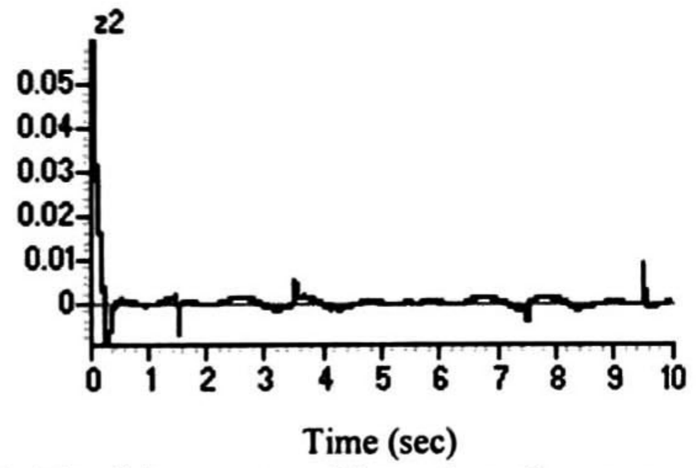

Fig. 7. Tracking error. Note that the error oscillates around zero.

Fig. 8 shows the flux observer results

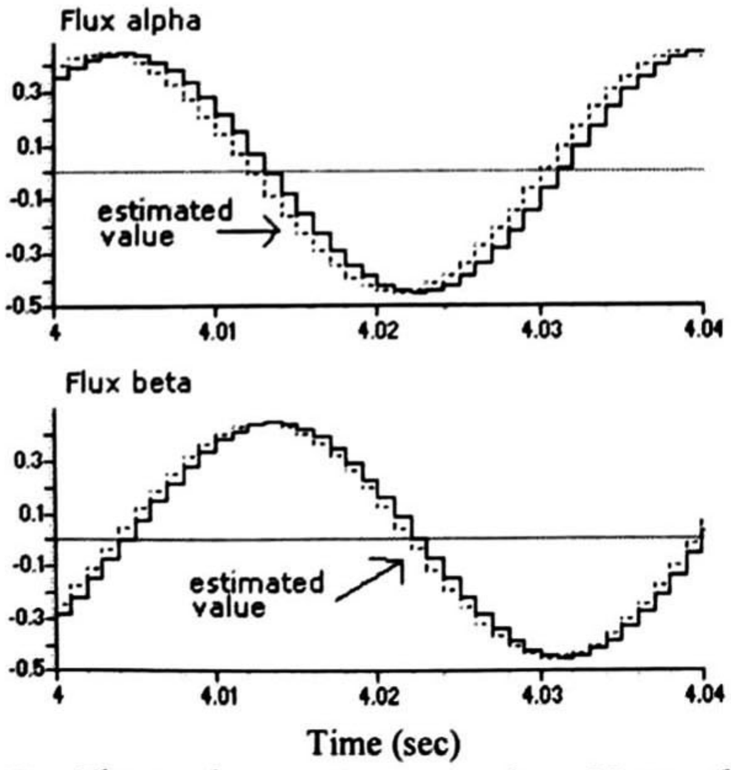

Fig. 8. Flux observation graphs. Note that the amplitude is well tracked, but, the phase angle differs a little bit.

Fig. 9 illustrates the load observation results. Despite that the observer models the load as constant load , it tracks so fine a square shape signal.

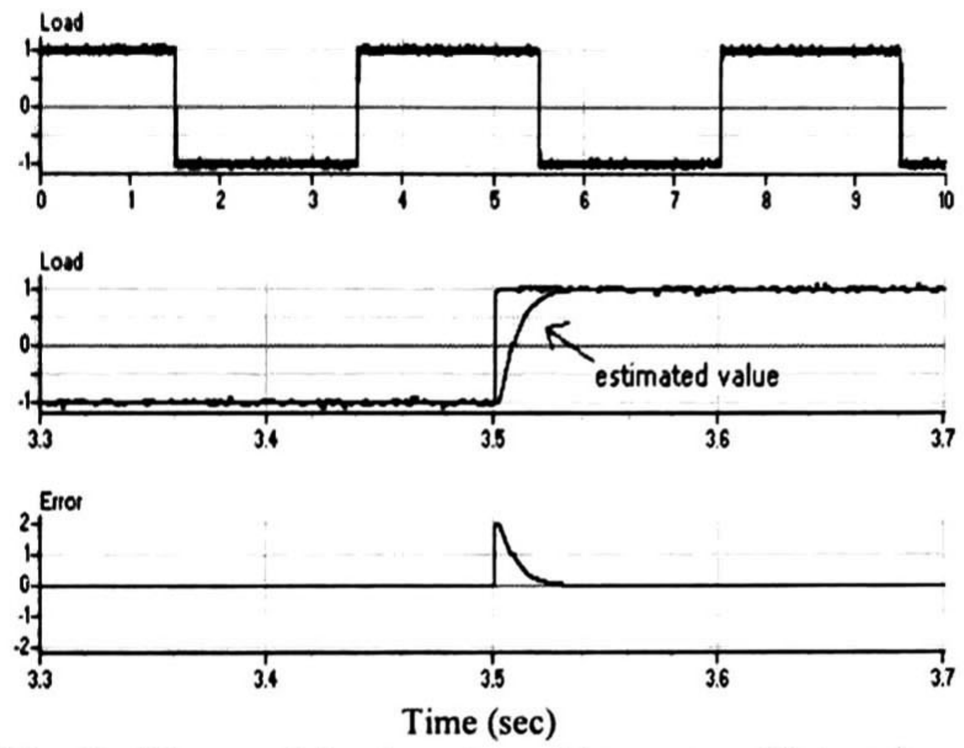

Fig. 9. Observed load and tracking error. Note when the load change its value, the observer response is fast.

5. CONCLUSIONS

The contributions of this paper can be stated as follows. The combination of sliding mode and block control results in a control law that achieves an excellent performance in the worst case scenario. With the flux observer it was demonstrated that its dynamics are stable. The load torque observer performs well..

REFERENCES

Åström, K. J. and Wittenmark, B. (1997). *Computer-Controlled Systems.* Prentice Hall, New Jersey.

Blaschke, F. (1972). The principle of field orientation applied to the new transvector closed-loop control system for rotating field machines. *Siemens-rev,vol. 39, 217-220.*

Kazantzis, N. and Kravaris C. (1999). Time-discretization of nonlinear control systems via Taylor methods. *Computer and Chemical Engineering,* Vol. 23, 763-784.

Marino, R. and Tomei, P. (1995). *Nonlinear Control Design*. Prentice Hall, United Kingdom.

Ortega, R., Nicklasson, P.J. and Epinoza-Pérez. (1996). On-Speed Control of Induction Motors. *Automatica,* Vol. 32, No. 3, 455-460.

Tan, H. and Chang, J. (1999). Adaptive Backstepping Control of Induction Motor with Uncertainties. *Proceedings of the American Control Conference.* San Diego, California.

Utkin, V. I., Guldner, J. and Shi, J. (1999). *Sliding Mode Control in Electromechanical Systems*. Taylor & Francis, United Kingdom.

ANIVERSARIO
Cinvestav

Centro de Investigación y de Estudios Avanzados del IPN

Unidad Guadalajara

El Jurado designado por la Unidad Guadalajara del Centro de Investigación y de Estudios Avanzados del Instituto Politécnico Nacional, aprobó la tesis: CONTROL DISCRETO DE MODOS DESLIZANTES DE UN MOTOR DE INDUCCIÓN del(a) C. Jorge RIVERA DOMINGUEZ el día 17 de Diciembre de 2001

Dr. Bernardino Castillo
Toledo
Investigador Cinvestav 3A
CINVESTAV GDL
Zapopan

Dr. Ofelia Begovich
Mendoza
Investigador Cinvestav 3A
CINVESTAV GDL
Guadalajara

Dr. Alexander Georgievich
Loukianov
Investigador Cinvestav 3A
CINVESTAV GDL
Guadalajara

Dr. Juan Manuel Ramírez
Arredondo
Investigador Cinvestav 3A
CINVESTAV GDL
Guadalajara

Dr. José Manuel Cañedo
Castañeda
Investigador Cinvestav 2C
CINVESTAV GDL
Guadalajara

CINVESTAV
BIBLIOTECA CENTRAL
SSIT000003920